

# Physics at Super $B$ Factory

A. G. Akeroyd,<sup>7</sup> W. Bartel,<sup>3</sup> A. Bondar,<sup>1</sup> T. E. Browder,<sup>4</sup> A. Drutskoy,<sup>2</sup>  
 Y. Enari,<sup>10</sup> T. Gershon,<sup>7</sup> T. Goto,<sup>17</sup> F. Handa,<sup>14</sup> K. Hara,<sup>7</sup>  
 S. Hashimoto,<sup>7</sup> H. Hayashii,<sup>11</sup> M. Hazumi,<sup>7</sup> T. Higuchi,<sup>7</sup> J. Hisano,<sup>6</sup>  
 T. Iijima,<sup>10</sup> K. Inami,<sup>10</sup> R. Itoh,<sup>7</sup> N. Katayama,<sup>7</sup> Y. Y. Keum,<sup>10</sup>  
 E. Kou,<sup>8</sup> T. Kurimoto,<sup>15</sup> Y. Kwon,<sup>16</sup> T. Matsumoto,<sup>13</sup> T. Morozumi,<sup>5</sup>  
 M. Nakao,<sup>7</sup> S. Nishida,<sup>7</sup> T. Ohshima,<sup>10</sup> Y. Okada,<sup>7</sup> S. L. Olsen,<sup>4</sup>  
 T. Onogi,<sup>17</sup> A. Poluektov,<sup>1</sup> S. Recksiegel,<sup>9</sup> H. Sagawa,<sup>7</sup> M. Saigo,<sup>14</sup>  
 Y. Sakai,<sup>7</sup> A. I. Sanda,<sup>10</sup> K. Senyo,<sup>10</sup> Y. Shimizu,<sup>10</sup> T. Shindou,<sup>7</sup>  
 K. Sumisawa,<sup>12</sup> M. Tanaka,<sup>12</sup> H. Yamamoto,<sup>14</sup> M. Yamauchi<sup>7</sup>

(The SuperKEKB Physics Working Group)

<sup>1</sup> *Budker Institute of Nuclear Physics, Novosibirsk, Russia*

<sup>2</sup> *University of Cincinnati, Cincinnati, Ohio 45221, USA*

<sup>3</sup> *DESY, Hamburg, Germany*

<sup>4</sup> *University of Hawaii, Honolulu, Hawaii 96822, USA*

<sup>5</sup> *Graduate School of Science, Hiroshima University,  
Higashi-Hiroshima, 739-8526, Japan*

<sup>6</sup> *ICRR, University of Tokyo, Kashiwa 277-8582, Japan*

<sup>7</sup> *High Energy Accelerator Research Organization (KEK), Tsukuba, Japan*

<sup>8</sup> *Institut de Physique Théorique, Université Catholique de Louvain,  
B-1348 Louvain-la-Neuve, Belgium*

<sup>9</sup> *Technische Universität München, D-85748 Garching, Germany*

<sup>10</sup> *Nagoya University, Nagoya, Japan*

<sup>11</sup> *Nara Women's University, Nara, Japan*

<sup>12</sup> *Osaka University, Osaka, Japan*

<sup>13</sup> *Tokyo Metropolitan University, Tokyo, Japan*

<sup>14</sup> *Tohoku University, Sendai, Japan*

<sup>15</sup> *Toyama University, Toyama, Japan*

<sup>16</sup> *Yonsei University, Seoul, Korea*

<sup>17</sup> *YITP, Kyoto University, Kyoto 606-8502, Japan*

February 7, 2008

## Abstract

This report presents the results of studies that investigate the physics reach at a Super  $B$  factory, an asymmetric-energy  $e^+e^-$  collider with a design luminosity of  $5 \times 10^{35} \text{ cm}^{-2}\text{s}^{-1}$ , which is around 40 times as large as the peak luminosity achieved by the KEKB collider. The studies focus on flavor physics and  $CP$  violation measurements that could be carried out in the LHC era. The physics motivation, key observables, measurement methods and expected precisions are presented. The sensitivity studies are a part of the activities associated with the preparation of a Letter of Intent for SuperKEKB, which has been submitted recently <sup>1</sup>.

---

<sup>1</sup>KEK Report 04-4 “Letter of Intent for KEK Super  $B$  Factory”, available from <http://belle.kek.jp/superb/loi/>.

# Contents

<b>1</b>	<b>Introduction</b>	<b>4</b>
1.1	Motivation for the Higher Luminosity $B$ Factory . . . . .	4
1.2	Belle Status and Prospects . . . . .	6
1.2.1	Status of $CP$ -Violation in $b \rightarrow c\bar{c}s$ Processes . . . . .	6
1.2.2	Status of $CP$ -Violation in $b \rightarrow sq\bar{q}$ Penguin Processes . . . . .	9
1.2.3	Radiative $B$ decays . . . . .	11
1.2.4	Electroweak Rare $B$ Decays . . . . .	15
1.2.5	Prospects . . . . .	19
<b>2</b>	<b>Flavor Structure of the Standard Model</b>	<b>20</b>
2.1	Flavor Structure of the Standard Model . . . . .	20
2.2	Low Energy Effective Hamiltonians . . . . .	22
2.3	$B - \bar{B}$ Mixing . . . . .	25
2.4	Time-dependent Asymmetries . . . . .	26
2.4.1	Measurement of $\sin 2\phi_1$ . . . . .	27
2.4.2	Measurement of $\phi_2$ . . . . .	28
2.5	Theoretical Methods . . . . .	29
2.5.1	Heavy Quark Symmetry . . . . .	29
2.5.2	Heavy Quark Expansion . . . . .	30
2.5.3	Perturbative Methods . . . . .	30
2.5.4	Lattice QCD . . . . .	31
<b>3</b>	<b>Flavor Structure of the Physics beyond the Standard Model</b>	<b>34</b>
3.1	Motivation for New Physics . . . . .	34
3.2	New physics scenarios . . . . .	35
3.3	Supersymmetric models . . . . .	35
3.4	SUSY effect on $b \rightarrow s$ transitions . . . . .	37
3.5	Model independent study of $b \rightarrow s\gamma$ and $b \rightarrow s\ell^+\ell^-$ processes . . . . .	42
3.6	Lepton Flavor Violation . . . . .	44
3.6.1	LFV in the Supersymmetric Models . . . . .	45
3.6.2	SUSY Seesaw Mechanism and SUSY GUTs . . . . .	48
3.6.3	Other Theoretical Models . . . . .	50
<b>4</b>	<b>Sensitivity at SuperKEKB</b>	<b>51</b>
4.1	Overview . . . . .	51
4.1.1	Goals of sensitivity studies . . . . .	51
4.1.2	Time-dependent $CP$ asymmetries . . . . .	52
4.1.3	$B$ tagging with full reconstruction . . . . .	54

4.2	New $CP$ -violating phase in $b \rightarrow s\bar{q}q$ . . . . .	57
4.2.1	Introduction . . . . .	57
4.2.2	$B^0 \rightarrow \phi K_S^0, \eta' K_S^0$ and $K^+ K^- K_S^0$ . . . . .	57
4.2.3	$B^0 \rightarrow K_S^0 K_S^0 K_S^0$ and $\pi^0 K_S^0$ . . . . .	61
4.2.4	$B^\pm \rightarrow \phi \phi X_s^\pm$ . . . . .	64
4.2.5	Discussion . . . . .	67
4.3	$b \rightarrow s\gamma$ and $b \rightarrow s\ell^+\ell^-$ . . . . .	70
4.3.1	Introduction . . . . .	70
4.3.2	$B \rightarrow X_s\gamma$ branching fraction . . . . .	71
4.3.3	$B \rightarrow K^*\ell^+\ell^-$ forward-backward asymmetry . . . . .	72
4.3.4	$B \rightarrow K\mu^+\mu^-$ versus $B \rightarrow Ke^+e^-$ . . . . .	74
4.3.5	Mixing induced $CP$ asymmetry in $B \rightarrow K^*\gamma$ . . . . .	74
4.3.6	$B \rightarrow X_s\gamma$ direct $CP$ asymmetry . . . . .	77
4.3.7	$b \rightarrow d\gamma$ and $b \rightarrow d\ell^+\ell^-$ . . . . .	77
4.3.8	Summary . . . . .	78
4.4	More than one neutrino I: $B \rightarrow K^{(*)}\nu\bar{\nu}$ and $B \rightarrow \tau\nu$ . . . . .	79
4.4.1	Introduction . . . . .	79
4.4.2	Estimation of signal and background . . . . .	80
4.4.3	Discussion . . . . .	81
4.5	More than one neutrino II: $B \rightarrow \bar{D}\tau^+\nu_\tau$ . . . . .	85
4.5.1	Introduction . . . . .	85
4.5.2	$B \rightarrow \bar{D}\tau^+\nu_\tau$ Reconstruction . . . . .	85
4.5.3	Kinematic Event Selection . . . . .	87
4.5.4	Background Components . . . . .	91
4.5.5	Statistical Significance . . . . .	91
4.5.6	Systematic Uncertainty . . . . .	91
4.5.7	Constraints on the Charged Higgs Mass . . . . .	92
4.5.8	Summary . . . . .	93
4.6	$\sin 2\phi_1$ . . . . .	94
4.7	$\phi_2$ . . . . .	97
4.7.1	Status of the $B^0 \rightarrow \pi^+\pi^-$ analysis . . . . .	97
4.7.2	Isospin analysis for $B \rightarrow \pi\pi$ . . . . .	97
4.7.3	Status of the $B^0 \rightarrow \rho\pi$ analysis . . . . .	100
4.7.4	Dalitz plot analysis of $B^0 \rightarrow \rho\pi$ . . . . .	101
4.8	$\phi_3$ . . . . .	104
4.8.1	Introduction . . . . .	104
4.8.2	$D^{(*)-}\pi^+$ modes . . . . .	104
4.8.3	$B^\pm \rightarrow DK^{*\pm}$ (ADS method) . . . . .	108
4.8.4	$B^\pm \rightarrow DK^\pm$ (Dalitz analysis) . . . . .	110
4.9	$ V_{ub} $ . . . . .	116
4.9.1	Introduction . . . . .	116
4.9.2	Theoretical formalisms for the semileptonic $B$ decays . . . . .	116
4.9.3	Measurement of inclusive $b \rightarrow u$ semileptonic decays . . . . .	122
4.9.4	Measurement of exclusive $b \rightarrow u$ semileptonic decays . . . . .	125
4.10	Tau decays . . . . .	128
4.10.1	Introduction . . . . .	128
4.10.2	Present experimental status . . . . .	128
4.10.3	Achievable sensitivity at SuperKEKB and physics reaches . . . . .	129

4.10.4	Summary . . . . .	135
4.11	Diversity of physics at Super-KEKB–other possibilities . . . . .	137
4.11.1	Charm physics . . . . .	137
4.11.2	Electroweak physics . . . . .	138
4.11.3	Charmonium physics . . . . .	141
4.11.4	Physics potential at $\Upsilon(5S)$ . . . . .	145
4.12	Summary . . . . .	148
<b>5</b>	<b>Study of New Physics Scenarios at SuperKEKB</b>	<b>149</b>
5.1	New physics case study . . . . .	149
5.2	Model independent approaches . . . . .	150
5.3	The CKM fit . . . . .	156
<b>6</b>	<b>Summary</b>	<b>162</b>

# Chapter 1

## Introduction

### 1.1 Motivation for the Higher Luminosity $B$ Factory

What are the most fundamental elements of the Universe? What is the law which governs their interactions? These are the questions that theoretical and experimental particle physicists have been working hard to answer for more than a century, and it was about thirty years ago that they arrived at the Standard Model of elementary particles. The Standard Model contains three generations of quarks and leptons, and their interactions are mediated by gauge bosons according to the  $SU(3)_C \times SU(2)_L \times U(1)_Y$  gauge field theory. Over the past thirty years the Standard Model has been confirmed by many precise experimental measurements.

Nevertheless, there are several reasons why the Standard Model is not completely satisfactory as *the* theory of elementary particles. First of all, it includes many parameters, *i.e.* the masses and mixing of the quarks and leptons, all of which are a priori unknown. The hierarchy of quark and lepton masses and the flavor mixing matrices suggest that some hidden mechanism occurring at a higher energy scale governs their pattern. Secondly, due to quadratically divergent radiative corrections, the Higgs mass is naturally of the same order as its cutoff scale; this implies that some new physics exists not far above the electroweak scale. From a cosmological viewpoint, there is a serious problem with the matter-antimatter asymmetry in the universe. This cannot be explained solely by the  $CP$  violation that occurs in the Standard Model, which originates from quark-flavor mixing. These reasons lead us to believe that new physics exists, and is most likely at the TeV energy scale.

The most direct way to discover the new physics is to construct energy frontier machines, such as the Large Hadron Collider (LHC) or the Global Linear Collider (GLC), to realize TeV energy scale collisions in which new heavy particles may be produced. The history of particle physics implies, however, that this is not the only way. In fact, before its discovery, the existence of the charm quark was postulated to explain the smallness of strangeness-changing neutral currents (the Glashow-Illiopolous-Maiani (GIM) mechanism [1]). The third family of quarks and leptons was predicted by Kobayashi and Maskawa to explain the small  $CP$  violation seen in kaon mixing [2]. These are examples of Flavor Changing Neutral Current (FCNC) processes, with which one can investigate the effect of heavier particles appearing only in quantum loop corrections.

The mechanism to suppress FCNC processes should also be present in new physics models if the new physics lies at the TeV energy scale, because otherwise such FCNC processes would violate current experimental limits. Information obtained from flavor physics experiments are thus essential to uncover the details of the physics beyond the Standard Model, even after energy frontier machines discover new particles.

A natural place to investigate a wide range of FCNC processes is in  $B$  meson decays. This is because the bottom quark belongs to the third generation and, hence, its decays involve all existing generations of quarks. In addition to  $B^0 - \bar{B}^0$  mixing, which is an analog of the traditional  $K^0 - \bar{K}^0$  mixing, there are many FCNC decay processes induced by so-called penguin diagrams, such as the radiative decay  $b \rightarrow s\gamma$ , the semileptonic decay  $b \rightarrow s\ell^+\ell^-$ , and the hadronic decays  $b \rightarrow dq\bar{q}$  and  $b \rightarrow sq\bar{q}$ . All of these processes are suppressed in the Standard Model by the GIM mechanism, and, therefore, the effect of new physics may be relatively enhanced. The Higher Luminosity B Factory is a machine designed to explore such interesting  $B$  decay processes.

In the summer of 2001 the presence of  $CP$  violation in the  $B$  meson system was established by the Belle collaboration [3,4,5,6] (and simultaneously by the BaBar collaboration [7,8,9,10]) through the measurement of the time dependent asymmetry in the decay process  $B^0(\bar{B}^0) \rightarrow J/\psi K_S^0$ . This measurement was the main target of the present asymmetric  $e^+e^-$   $B$  Factories, and it was achieved as originally planned. The experimental data indicated that the Kobayashi-Maskawa mechanism, which is now a part of the Standard Model of elementary particles, is indeed the dominant source of observed  $CP$  violation in Nature.

The Belle experiment also proved its ability to measure a number of decay modes of the  $B$  meson and to extract Cabibbo-Kobayashi-Maskawa (CKM) matrix elements and other interesting observables. For instance, the precision of the measurement of the angle  $\phi_1$  of the unitarity triangle through the  $B^0 \rightarrow J/\psi K_S^0$  time-dependent asymmetry reached the 10% level [11]; a  $CP$  asymmetry was also observed in  $B^0 \rightarrow \pi^+\pi^-$  decay, from which one can extract the angle  $\phi_2$  [12,13,14]; the angle  $\phi_3$  could also be measured through the processes  $B \rightarrow DK$  and  $D\pi$  [15,16,17]; the semi-leptonic FCNC processes  $B \rightarrow K\ell^+\ell^-$  [18],  $B \rightarrow K^*\ell^+\ell^-$  [19], and even the corresponding inclusive decay  $B \rightarrow X_s\ell^+\ell^-$  [20] were observed. Furthermore, the recently observed disagreement between the values of the angle  $\phi_1$  measured in the penguin process  $B \rightarrow \phi K_S^0$  and the precisely measured value in  $B \rightarrow J/\psi K_S^0$  suggests the existence of a new  $CP$  phase in the penguin process  $b \rightarrow sq\bar{q}$  [21]. By collecting many such observations we may probe new physics, and, once its existence is established, these measurements will determine the properties of the new physics. This is only possible if KEKB's luminosity is upgraded by a substantial amount. As we discuss in the following sections, a factor of 50 improvement will greatly enhance the possibility to discover new physics.

In the program of quark flavor physics, one way to explore physics beyond the Standard Model is to improve substantially the measurement precision of the CKM matrix elements. This can be done in many different ways, and any inconsistency with the Standard Model predictions would imply new physics. In this report we discuss the precision we expect to achieve at the higher luminosity B factory for various determinations of the CKM matrix elements. These consist of measurements of the three angles and three sides of the Unitarity Triangle.

Another way to search for the effect of new physics is to look at loop-induced rare processes for which the Standard Model contribution is extremely suppressed. Such processes may provide an immediate signature of new physics that also contributes through loops but in a different manner. We describe several future measurements including the mixing-induced  $b \rightarrow s\gamma$  asymmetry,  $b \rightarrow s\ell^+\ell^-$  forward-backward asymmetry, and flavor changing tau decay  $\tau \rightarrow \mu\gamma$ .

$B$  physics programs are also being pursued at hadron machines, including the ongoing Tevatron experiments [22] and the  $B$  physics programs at the Large Hadron Collider (LHC) [23], which is scheduled to start operation in 2007. Because of the very large  $B\bar{B}$  production cross

section in the hadron environment, some of the quantities we are planning to measure at the  $e^+e^-$  B factory may be measured with better precision at the hadron colliders. The study of  $B_s$  mesons is probably unique to the hadron machines. However, an  $e^+e^-$  machine provides a much cleaner environment, which is essential for important observables that involve  $\gamma$ 's,  $\pi^0$ 's,  $K_L^0$ 's or neutrinos in the final states. On the  $\Upsilon(4S)$  resonance, the  $B\bar{B}$  pair is produced near the threshold and there are no associated particles. This means that one can reconstruct the full energy-momentum vector of a  $B$  ( $\bar{B}$ ) meson from its daughter particles (the full reconstruction technique), from this one can infer the missing momentum in the decay of the other  $\bar{B}$  ( $B$ ) meson. This technique is essential for the measurement of channels including neutrino(s) in the final state. The measurement of the CKM element  $|V_{ub}|$  through the semi-leptonic decay  $b \rightarrow ul\bar{\nu}$ , the search for a charged Higgs effect in  $B \rightarrow D\tau\bar{\nu}$ , and measurements of  $B \rightarrow K\nu\bar{\nu}$ ,  $B \rightarrow \tau\nu$  fall in this class.

## 1.2 Belle Status and Prospects

By the 2003 summer shutdown, Belle had accumulated data with an integrated luminosity of  $140 \text{ fb}^{-1}$  at the  $\Upsilon(4S)$  resonance, corresponding to 152 million  $B\bar{B}$  pairs. With modest improvements expected for the current KEKB accelerator, we expect an integrated luminosity of  $\sim 500 \text{ fb}^{-1}$  in several years.

In this section, the current physics results are briefly reviewed for selected topics in order to give an overview of the present status. The status and future prospects for further topics are presented in the later sections.

### 1.2.1 Status of $CP$ -Violation in $b \rightarrow c\bar{c}s$ Processes

Decays of  $B^0$  to the following  $b \rightarrow c\bar{c}s$   $CP$ -eigenstates are reconstructed:  $J/\psi K_S^0$ ,  $\psi(2S)K_S^0$ ,  $\chi_{c1}K_S^0$ ,  $\eta_c K_S^0$  for  $\xi_f = -1$  and  $J/\psi K_L^0$  for  $\xi_f = +1$ <sup>1</sup>, where  $\xi_f$  denotes  $CP$  parity. The two classes ( $\xi_f = \pm 1$ ) should have  $CP$ -asymmetries that are opposite in sign.  $B^0 \rightarrow J/\psi K^{*0} [\rightarrow K_S^0 \pi^0]$  decays are also used, where the final state is a mixture of even and odd  $CP$ . The  $CP$  content can, however, be determined from an angular analysis of other  $J\psi K^*$  decays. The  $CP$ -odd fraction is found to be small (i.e.  $(19 \pm 4)\%$ ).

The reconstructed samples with  $140 \text{ fb}^{-1}$  used for the  $\sin 2\phi_1$  measurement [11] are shown in Figure 1.1. Table 1.1 lists the numbers of candidates,  $N_{\text{ev}}$ , and the estimated signal purity for each  $f_{CP}$  mode. It is clear that the  $CP$ -eigenstate event samples used for the  $CP$ -violation measurements in  $b \rightarrow c\bar{c}s$  are large and clean.

Figure 1.2 shows the  $\Delta t$  distributions, where a clear shift between  $B^0$  and  $\bar{B}^0$  tags is visible, and the raw asymmetry plots for two ranges of the flavor tagging quality variable  $r$ . For low quality tags ( $0 < r < 0.5$ ), which have a large background dilution, only a modest asymmetry is visible; in the high quality tag sub-sample ( $0.5 < r < 1.0$ ), a very clear asymmetry with a sine-like time modulation is present. The final results are extracted from an unbinned maximum-likelihood fit to the  $\Delta t$  distributions that takes into account resolution, mistagging and background dilution. The result is

$$\sin 2\phi_1 = 0.733 \pm 0.057 \pm 0.028. \quad (1.1)$$

---

<sup>1</sup>The inclusion of the charge conjugate decay mode is implied unless otherwise stated.



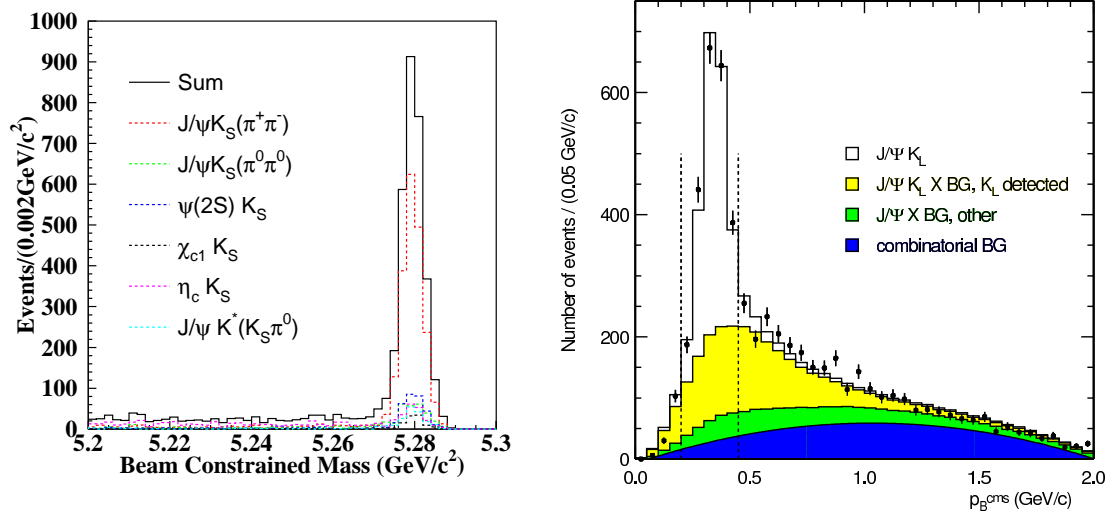


Figure 1.1: (Left) The fully reconstructed  $CP$ -eigenstate sample. (Right) The  $p_B^*$  ( $B$  momentum in the CM frame) distribution for the  $B \rightarrow J/\psi K_L^0$  sample (right). The shaded portions show the contributions of different background components. The vertical dashed lines indicate the signal region.

Table 1.1: The yields for reconstructed  $B \rightarrow f_{CP}$  candidates after flavor tagging and vertex reconstruction,  $N_{ev}$ , and the estimated signal purity,  $p$ , in the signal region for each  $f_{CP}$  mode.  $J/\psi$  mesons are reconstructed in  $J/\psi \rightarrow \mu^+\mu^-$  or  $e^+e^-$  decays. Candidate  $K_S^0$  mesons are reconstructed in  $K_S^0 \rightarrow \pi^+\pi^-$  decays unless explicitly stated otherwise.

Mode	$\xi_f$	$N_{ev}$	$p$
$J/\psi K_S^0$	-1	1997	$0.976 \pm 0.001$
$J/\psi K_S^0(\pi^0\pi^0)$	-1	288	$0.82 \pm 0.02$
$\psi(2S)(\ell^+\ell^-)K_S^0$	-1	145	$0.93 \pm 0.01$
$\psi(2S)(J/\psi\pi^+\pi^-)K_S^0$	-1	163	$0.88 \pm 0.01$
$\chi_{c1}(J/\psi\gamma)K_S^0$	-1	101	$0.92 \pm 0.01$
$\eta_c(K_S^0 K^- \pi^+)K_S^0$	-1	123	$0.72 \pm 0.03$
$\eta_c(K^+ K^- \pi^0)K_S^0$	-1	74	$0.70 \pm 0.04$
$\eta_c(p\bar{p})K_S^0$	-1	20	$0.91 \pm 0.02$
All with $\xi_f = -1$	-1	2911	$0.933 \pm 0.002$
$J/\psi K^{*0}(K_S^0\pi^0)$	+1(81%)	174	$0.93 \pm 0.01$
$J/\psi K_L^0$	+1	2332	$0.60 \pm 0.03$

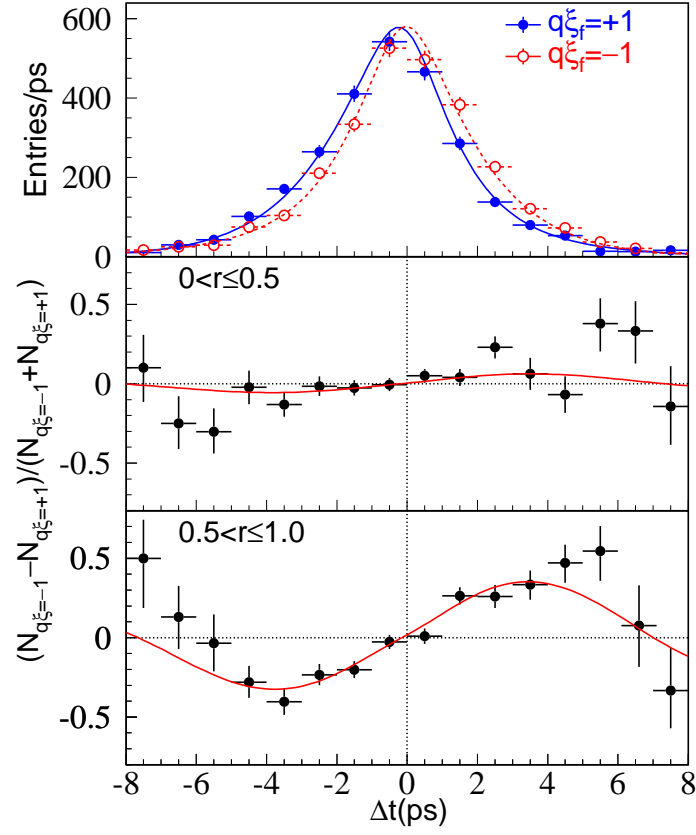


Figure 1.2: (a)  $\Delta t$  distributions for  $B^0$  and  $\bar{B}^0$  tags (b) raw asymmetry for low-quality tags and (c) raw asymmetry for high-quality tags. The smooth curves are projections of the unbinned likelihood fit.

This result may be compared to the BaBar result with  $82 \text{ fb}^{-1}$  of  $\sin 2\phi_1 = 0.741 \pm 0.067 \pm 0.03$  [10]. Both experiments are now in very good agreement; the average of these results is

$$\sin 2\phi_1 = 0.736 \pm 0.049. \quad (1.2)$$

This average can be interpreted as a constraint on the CKM angle  $\phi_1$ . This constraint can be compared with the indirect determinations of the unitarity triangle [24] and is consistent with the hypothesis that the Kobayashi-Maskawa phase is the source of  $CP$  violation. The measurement of  $\sin 2\phi_1$  in  $b \rightarrow c\bar{c}s$  modes, although still statistically limited, is becoming a precision measurement. The systematics are small and well understood.

The presence of an asymmetry with a cosine dependence ( $|\lambda| \neq 1$ ) would indicate direct  $CP$  violation. In order to test for this possibility in  $b \rightarrow c\bar{c}s$  modes, Belle also performed a fit with  $a_{CP} \equiv -\xi_f \text{Im}\lambda/|\lambda|$  and  $|\lambda|$  as free parameters, keeping everything else the same. They obtain

$$|\lambda| = 1.007 \pm 0.041(\text{stat}) \quad \text{and} \quad a_{CP} = 0.733 \pm 0.057(\text{stat}), \quad (1.3)$$

for all the  $b \rightarrow c\bar{c}s$   $CP$  modes combined. This result is consistent with the assumption used in their primary analysis.

### 1.2.2 Status of $CP$ -Violation in $b \rightarrow sq\bar{q}$ Penguin Processes

One of the promising ways to probe additional  $CP$ -violating phases from new physics beyond the Standard Model is to measure the time-dependent  $CP$ -asymmetry in penguin-dominated modes such as  $B^0 \rightarrow \phi K_S^0$ ,  $B^0 \rightarrow \eta' K_S^0$ , where heavy new particles may contribute inside the loop, and compare it with the asymmetry in  $B^0 \rightarrow J/\psi K_S^0$  and related  $b \rightarrow c\bar{c}s$  charmonium modes. Belle has measured  $CP$ -violation in  $B^0 \rightarrow \phi K_S^0$ ,  $\eta' K_S^0$ , and  $K^+ K^- K_S^0$  with  $140 \text{ fb}^{-1}$  [21].

The decay  $B^0 \rightarrow \phi K_S^0$ , which is dominated by the  $b \rightarrow s\bar{s}s$  transition, is an especially unambiguous and sensitive probe of new  $CP$ -violating phases from physics beyond the Standard Model [25]. The Standard Model predicts that measurements of  $CP$ -violation in this mode should yield  $\sin 2\phi_1$  to a very good approximation [26, 27, 28]. A significant deviation in the time-dependent  $CP$ -asymmetry in this mode from what is observed in  $b \rightarrow c\bar{c}s$  decays would be evidence for a new  $CP$ -violating phase.

The  $B \rightarrow \phi K_S^0$  sample is shown in Figure 1.3(a). The signal contains  $68 \pm 11$  events. Figure 1.4(a,b) shows the raw asymmetries in two regions of the flavor-tagging parameter  $r$ .

The observed  $CP$ -asymmetry for  $B^0 \rightarrow \phi K_S^0$  in the region  $0.5 < r \leq 1.0$  (Figure 1.4 (b)) indicates a deviation from the Standard Model expectation (dashed curve). Note that these projections onto the  $\Delta t$  axis do not take into account event-by-event information (such as the signal fraction, the wrong tag fraction and the vertex resolution) that is used in the unbinned maximum likelihood fit. The contamination of  $K^+ K^- K_S^0$  events in the  $\phi K_S^0$  sample ( $7.2 \pm 1.7\%$ ) is small; backgrounds from the decay  $B^0 \rightarrow f_0(980) K_S^0$ , which has the opposite  $CP$ -eigenvalue to  $\phi K_S^0$ , are found to be small ( $1.6_{-1.5}^{+1.9}\%$ ). The influence of these backgrounds is treated as a source of systematic uncertainty.

The likelihood fit gives

$$\sin 2\phi_{1\text{eff}}(B \rightarrow \phi K_S^0) = -0.96 \pm 0.5_{-0.11}^{+0.09}. \quad (1.4)$$

The likelihood function is parabolic and well-behaved. An evaluation of the significance of the result using the Feldman-Cousins method and allowing for systematic uncertainties shows

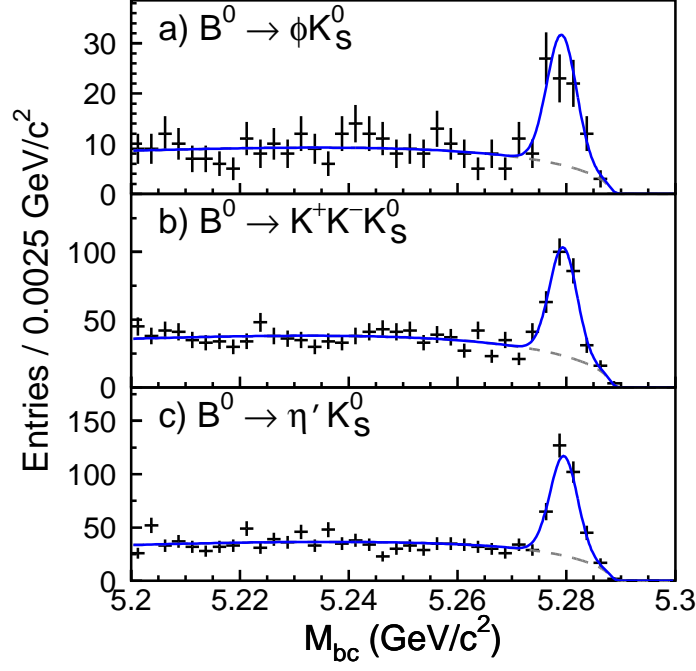


Figure 1.3: The beam-energy constrained mass distributions for (a)  $B^0 \rightarrow \phi K_S^0$ , (b)  $B^0 \rightarrow K^+ K^- K_S^0$ , and (c)  $B^0 \rightarrow \eta' K_S^0$  within the  $\Delta E$  signal region. Solid curves show the fit to signal plus background distributions, and dashed curves show the background contributions. The background for  $B^0 \rightarrow \eta' K_S^0$  decay includes an MC-estimated  $B\bar{B}$  background component.

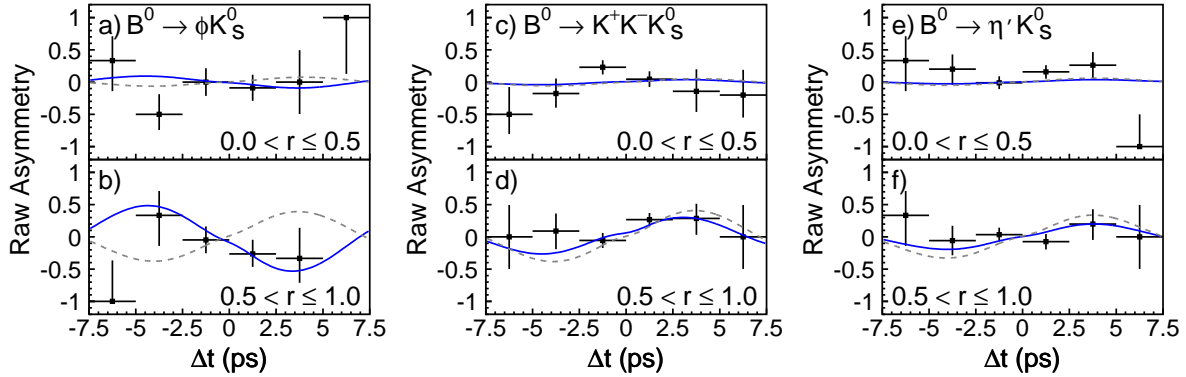


Figure 1.4: (a) The asymmetry,  $A$ , in each  $\Delta t$  bin for  $B^0 \rightarrow \phi K_S^0$  with  $0 < r \leq 0.5$ , (b) with  $0.5 < r \leq 1.0$ , (c) for  $B^0 \rightarrow K^+ K^- K_S^0$  with  $0 < r \leq 0.5$ , (d) with  $0.5 < r \leq 1.0$ , (e) for  $B^0 \rightarrow \eta' K_S^0$  with  $0 < r \leq 0.5$ , and (f) with  $0.5 < r \leq 1.0$ , respectively. The solid curves show the result of the unbinned maximum-likelihood fit. The dashed curves show the Standard Model expectation with  $\sin 2\phi_1 = +0.731$  and  $\mathcal{A} = 0$ .

that this result deviates by  $3.5\sigma$  from the Standard Model expectation [21]. BaBar has analyzed a sample with an integrated luminosity of  $110 \text{ fb}^{-1}$ , containing  $70 \pm 9$  events, and obtain  $\sin 2\phi_{1\text{eff}}(B \rightarrow \phi K_S^0) = 0.45 \pm 0.43 \pm 0.07$  [29]. This result differs from the Belle result by  $2.1\sigma$  and the naive average,  $-0.14 \pm 0.33$ , is still away from the  $\sin 2\phi_1$  world average by  $2.6\sigma$ .

The decay mode  $B \rightarrow K^+ K^- K_S^0$ , where  $K^+ K^-$  combinations consistent with the  $\phi$  have been removed, is found to be dominantly  $CP$ -even [30] and, thus, can be treated as a  $CP$ -eigenstate and used for studies of time-dependent  $CP$ -violation in  $b \rightarrow sq\bar{q}$  processes. The beam constrained mass distribution for the  $B \rightarrow K^+ K^- K_S^0$  sample used by Belle is shown in Figure 1.3(b), where there are  $199 \pm 18$  signal events. The result is

$$\sin 2\phi_{1\text{eff}}(B \rightarrow K^+ K^- K_S^0) = 0.51 \pm 0.26 \pm 0.05_{-0.00}^{+0.18}, \quad (1.5)$$

where the third error is due to the uncertainty in the  $CP$  content of this final state [30]. The results for  $B \rightarrow K^+ K^- K_S^0$  are also consistent with  $b \rightarrow c\bar{c}s$  decays. However, in this decay there is also the possibility of “tree-pollution”, i.e. the contribution of a  $b \rightarrow u\bar{u}s$  tree amplitude that may complicate the interpretation of the results [28].

The mode  $B \rightarrow \eta' K_S^0$  is expected to include contributions from  $b \rightarrow s\bar{u}u$  and  $b \rightarrow s\bar{d}d$  penguin processes. The beam constrained mass distribution for the  $B \rightarrow \eta' K_S^0$  sample shown in Figure 1.3(c) contains  $244 \pm 21$  signal events [31]. The fit gives (Figure 1.4(e,f))

$$\sin 2\phi_{1\text{eff}}(B \rightarrow \eta' K_S^0) = 0.43 \pm 0.27 \pm 0.05. \quad (1.6)$$

The average with the BaBar result ( $0.02 \pm 0.34 \pm 0.03$  with  $82 \text{ fb}^{-1}$ ) [32] is about  $2.2\sigma$  from the  $b \rightarrow c\bar{c}s$  measurement, which is the Standard Model expectation.

### 1.2.3 Radiative $B$ decays

#### Exclusive $B \rightarrow K^* \gamma$

Measurement of the  $B \rightarrow K^* \gamma$  exclusive branching fraction is straightforward, since one can use  $M_{\text{bc}}$ ,  $\Delta E$  and  $K^*$  mass constraints. ( $K^*$  denotes  $K^*(892)$  throughout this section.) The latest Belle branching fraction measurements (Figure 1.5) use  $78 \text{ fb}^{-1}$  of data, and have a total error that is much less than 10% for both  $B^0$  and  $B^+$  decays. The results from CLEO [33], BaBar [34] and Belle [35] are in good agreement and are listed in Table 1.2. The world averages are

$$\mathcal{B}(B^0 \rightarrow K^{*0} \gamma) = (4.17 \pm 0.23) \times 10^{-5}, \quad (1.7)$$

$$\mathcal{B}(B^+ \rightarrow K^{*+} \gamma) = (4.18 \pm 0.32) \times 10^{-5}. \quad (1.8)$$

The corresponding theoretical branching fraction is about  $(7 \pm 2) \times 10^{-5}$ , higher than the measurement but with a large uncertainty [36, 37]. A computation based on PQCD has been just completed [38]:

$$\mathcal{B}(B^0 \rightarrow K^{*0} \gamma) = (4.5_{-1.1}^{+1.5}) \times 10^{-5}, \quad (1.9)$$

$$\mathcal{B}(B^+ \rightarrow K^{*+} \gamma) = (4.3_{-1.1}^{+1.6}) \times 10^{-5}. \quad (1.10)$$

where the errors quoted come from a parameter in the  $B$  meson wave function  $\omega_B$ . The difference in the value of the computed branching ratio compared to the previous computation comes from the fact that PQCD computation of the  $B \rightarrow K^*$  transition form factor is smaller than those of light-cone QCD sum rule and the lattice QCD simulation.

A better approach to exploit the  $B \rightarrow K^* \gamma$  branching fraction measurements is to consider isospin asymmetry [39]. A small difference in the branching fractions between  $B^0 \rightarrow K^{*0} \gamma$  and

Table 1.2: $B \rightarrow K^*\gamma$ branching fractions			
	$B^0 \rightarrow K^{*0}\gamma$	$B^+ \rightarrow K^{*+}\gamma$	
	$[\times 10^{-5}]$	$[\times 10^{-5}]$	
CLEO	$4.55 \pm 0.70 \pm 0.34$	$3.76 \pm 0.86 \pm 0.28$	
BaBar	$4.23 \pm 0.40 \pm 0.22$	$3.83 \pm 0.62 \pm 0.22$	
Belle	$4.09 \pm 0.21 \pm 0.19$	$4.40 \pm 0.33 \pm 0.24$	

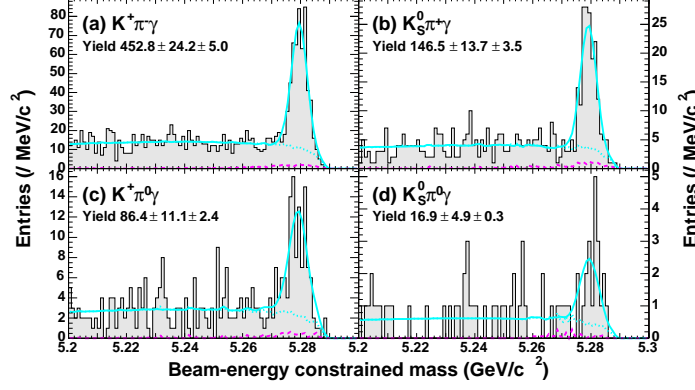


Figure 1.5:  $B \rightarrow K^*\gamma$  signals from Belle.

$B^+ \rightarrow K^{*+}\gamma$  tells us the sign of the combination of the Wilson coefficients,  $C_6/C_7$ . Belle has taken into account correlated systematic errors and obtains

$$\begin{aligned}
\Delta_{+0} &\equiv \frac{(\tau_{B^+}/\tau_{B^0})\mathcal{B}(B^0 \rightarrow K^{*0}\gamma) - \mathcal{B}(B^+ \rightarrow K^{*+}\gamma)}{(\tau_{B^+}/\tau_{B^0})\mathcal{B}(B^0 \rightarrow K^{*0}\gamma) + \mathcal{B}(B^+ \rightarrow K^{*+}\gamma)} \\
&= (+0.003 \pm 0.045 \pm 0.018),
\end{aligned} \tag{1.11}$$

which is consistent with zero. PQCD gives [38]

$$\Delta_{+0} = +0.059^{+0.011}_{-0.012} \tag{1.12}$$

It is extremely interesting to see if nearly 5th PQCD computation based on the standard model is verified.

Here, the lifetime ratio  $\tau_{B^+}/\tau_{B^0} = 1.083 \pm 0.017$  is used, and the  $B^0$  to  $B^+$  production ratio is assumed to be unity. The latter is measured to be  $f_0/f_+ = 1.072 \pm 0.057$  and is included in the systematic error.

### Other Exclusive Radiative Decays

The dominant radiative decay channel  $B \rightarrow K^*\gamma$  covers only 12.5% of the total  $B \rightarrow X_s\gamma$  branching fraction (world average  $(3.34 \pm 0.38) \times 10^{-4}$ ). The remainder has to be accounted for by decays with higher resonances or multi-body decays. Knowledge of these decay modes will eventually be useful to reduce the systematic error for the inclusive measurement.

Belle has extended the analysis into multi-body decay channels in addition to  $B \rightarrow K_2^*(1430)[\rightarrow K\pi]\gamma$  decay [40]. Using  $29 \text{ fb}^{-1}$  of data, the decay  $B^+ \rightarrow K^+\pi^+\pi^-\gamma$  is measured to have a branching fraction of  $(24 \pm 5^{+4}_{-2}) \times 10^{-6}$  for  $M(K\pi\pi) < 2.4 \text{ GeV}$ . The decay is dominated by

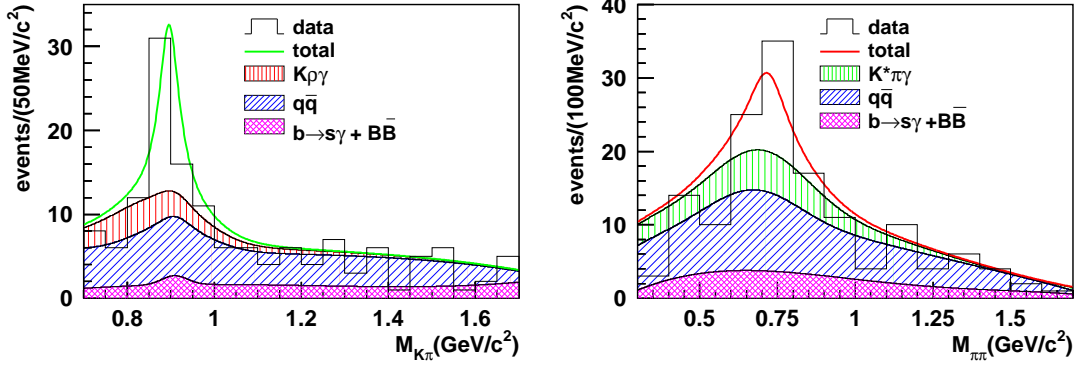


Figure 1.6:  $B^+ \rightarrow K^{*0}\pi^+\gamma$  and  $B \rightarrow K^+\rho^0\gamma$  from Belle.

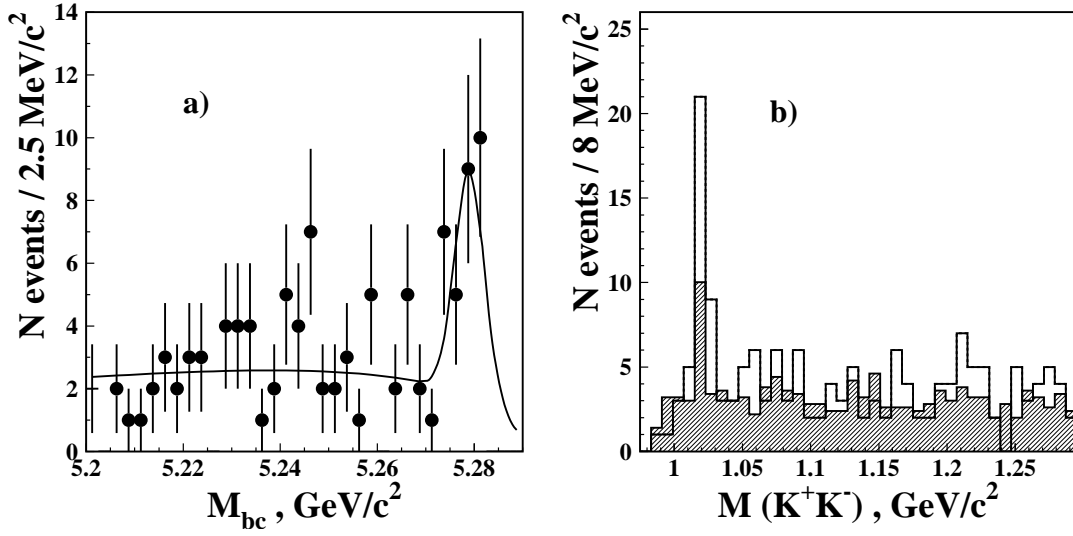


Figure 1.7:  $B^+ \rightarrow K\phi\gamma$  from Belle.

$K^{*0}\pi^+\gamma$  and  $K^+\rho^0\gamma$  final states that overlap each other as shown in Figure 1.6. At this moment, it is not possible to disentangle the resonant states that decay into  $K^*\pi$  or  $K\rho$ , such as  $K_1(1270)$ ,  $K_1(1400)$ ,  $K^*(1650)$ , and so on. A clear  $B^+ \rightarrow K^+\phi\gamma$  ( $5.5\sigma$ ) signal was recently observed by Belle with  $90\text{ fb}^{-1}$  of data (Figure 1.7), together with  $3.3\sigma$  evidence for  $B^0 \rightarrow K_S^0\phi\gamma$ . There is no known  $K\phi$  resonant state. This is the first example of a  $s\bar{s}s\gamma$  final state. The branching fractions for  $B \rightarrow K\phi\gamma$  are measured to be [41]

$$\begin{aligned}
 \mathcal{B}(B^+ \rightarrow K^+\phi\gamma) &= (3.4 \pm 0.9 \pm 0.4) \times 10^{-6}, \\
 \mathcal{B}(B^0 \rightarrow K^0\phi\gamma) &= (4.6 \pm 2.4 \pm 0.4) \times 10^{-6} \\
 &< 8.3 \times 10^{-6} \quad (90\% \text{ CL}).
 \end{aligned}
 \tag{1.13}$$

With more data, one can perform a time-dependent  $CP$ -asymmetry measurement with the  $K_S^0\phi\gamma$  decay channel.

At present,  $(35 \pm 6)\%$  of the total  $B \rightarrow X_s\gamma$  rate is measured to be either  $B \rightarrow K^*\gamma$  (12.5%),  $B \rightarrow K_2^*(1430)\gamma$  (4% after excluding  $K\pi\pi\gamma$ ),  $B \rightarrow K^*\pi\gamma$  (9%),  $B \rightarrow K\rho\gamma$  (9%) or  $B \rightarrow K\phi\gamma$  (1%). The remaining  $(65 \pm 6)\%$  may be accounted for by decays with multi-body final states, baryonic decays, modes with  $\eta$  and  $\eta'$ , multi-kaon final states other than  $K\phi\gamma$  or in the large

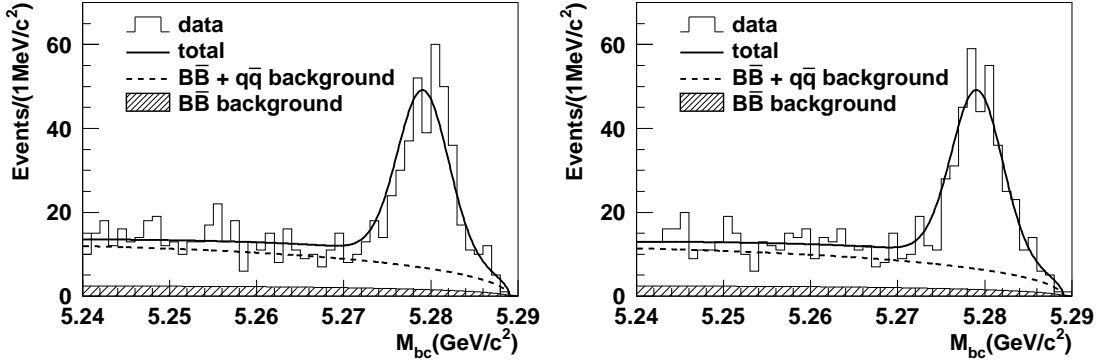


Figure 1.8:  $\overline{B}$ -tagged (top-left),  $B$ -tagged (top-right)  $B \rightarrow X_s \gamma$  signals from Belle.

$X_s$  mass range.

### Search for Direct $CP$ -Asymmetry

In the Standard Model, the direct  $CP$ -asymmetry in  $B \rightarrow X_s \gamma$  is predicted to be 0.6% with a small error [42, 43]. A large  $CP$ -asymmetry would be a clear sign of new physics.

An  $A_{CP}(B \rightarrow X_s \gamma)$  measurement was performed by Belle [44], by summing up the exclusive modes of one kaon plus up to four pions and modes with three kaon plus up to one pion. This result eliminates  $B \rightarrow X_d \gamma$  by exploiting particle identification devices for the tagged hadronic recoil system.  $M(X_s) < 2.1$  GeV is required, which roughly corresponds to  $E_\gamma^{\min} \sim 2.25$  GeV. Events are self-tagged as  $B$  candidates ( $B^0$  or  $B^+$ ) or  $\overline{B}$  candidates ( $\overline{B}^0$  or  $B^-$ ), except for ambiguous modes with a  $K_S^0$  and zero net charge. In order to correct the imperfect knowledge of the hadronic final state, the signal yields for each exclusive mode are used to correct the Monte Carlo multiplicity distribution. The resulting  $\overline{B}$ -tagged ( $342 \pm 23^{+7}_{-14}$  events),  $B$ -tagged ( $349 \pm 23^{+7}_{-14}$  events) signals are shown in Figure 1.8. Using the wrong-tag fractions of  $0.019 \pm 0.014$  between  $B$ - and  $\overline{B}$ -tagged,  $0.240 \pm 0.192$  from ambiguous to  $B$ - or  $\overline{B}$ -tagged, and  $0.0075 \pm 0.0079$  from  $B$ - or  $\overline{B}$ -tagged to ambiguous samples, the asymmetry is measured to be

$$A_{CP}(B \rightarrow X_s \gamma) = 0.004 \pm 0.051 \pm 0.038. \quad (1.14)$$

The result corresponds to a 90% confidence level limit of  $-0.107 < A_{CP}(B \rightarrow X_s \gamma) < 0.099$ , and therefore already constrains part of the new physics parameter space.

For exclusive radiative decays, it is straightforward to extend the analysis to search for a direct  $CP$ -asymmetry [33, 34, 35]. Particle identification devices at Belle and BaBar resolve the possible ambiguity between  $K^{*0} \rightarrow K^+ \pi^-$  and  $\overline{K}^{*0} \rightarrow K^- \pi^+$  to an almost negligible level with a reliable estimation of the wrong-tag fraction (0.9% for Belle). The results of the asymmetry measurements are listed in Table 1.3, whose average is

$$A_{CP}(B \rightarrow K^* \gamma) = (-0.5 \pm 3.7) \times 10^{-2}. \quad (1.15)$$

It is usually thought that large  $CP$ -violation in  $B \rightarrow K^* \gamma$  is not allowed in the Standard Model and the above result may be used to constrain new physics. However, since the involved strong phase difference may not be reliably calculated for exclusive decays, the interpretation may be model dependent.



Table 1.3: $B \rightarrow K^*\gamma$ direct $CP$ -asymmetry	
CLEO ( $9.1 \text{ fb}^{-1}$ )	$(8 \pm 13 \pm 3) \times 10^{-2}$
BaBar ( $20.7 \text{ fb}^{-1}$ )	$(-4.4 \pm 7.6 \pm 1.2) \times 10^{-2}$
Belle ( $78 \text{ fb}^{-1}$ )	$(-0.1 \pm 4.4 \pm 0.8) \times 10^{-2}$

Table 1.4: 90% confidence level upper limits on the  $B \rightarrow \rho\gamma$  and  $\omega\gamma$  branching fractions.

	$\rho^+\gamma$	$\rho^0\gamma$	$\omega\gamma$
CLEO ( $9.1 \text{ fb}^{-1}$ )	$13 \times 10^{-6}$	$17 \times 10^{-6}$	$9.2 \times 10^{-6}$
Belle ( $78 \text{ fb}^{-1}$ )	$2.7 \times 10^{-6}$	$2.6 \times 10^{-6}$	$4.4 \times 10^{-6}$
BaBar ( $78 \text{ fb}^{-1}$ )	$2.1 \times 10^{-6}$	$1.2 \times 10^{-6}$	$1.0 \times 10^{-6}$

### Search for $b \rightarrow d\gamma$ Final States

There are various interesting aspects to the  $b \rightarrow d\gamma$  transition. Within the Standard Model, most of the diagrams are the same as those for  $b \rightarrow s\gamma$ , except for the replacement of the CKM matrix element  $V_{ts}$  with  $V_{td}$ . A measurement of the  $b \rightarrow d\gamma$  process will therefore provide the ratio  $|V_{td}/V_{ts}|$  without large model-dependent uncertainties. This mode is also one where a large direct  $CP$ -asymmetry is predicted both within and beyond the Standard Model.

The search for the exclusive decay  $B \rightarrow \rho\gamma$  is as straightforward as the measurement of  $B \rightarrow K^*\gamma$ , except for its small branching fraction, the enormous combinatorial background from copious  $\rho$  mesons and random pions, and the huge  $B \rightarrow K^*\gamma$  background that overlaps with the  $B \rightarrow \rho\gamma$  signal window.  $B \rightarrow \omega\gamma$  is not affected by  $B \rightarrow K^*\gamma$  background, but is still unobserved. The upper limits obtained by BaBar [45], Belle [46] and CLEO [33] are summarized in Table 1.4. The upper limits are still about twice as large as the Standard Model predictions [36, 37]  $(9.0 \pm 3.4) \times 10^{-7}$  for  $\rho^+\gamma$ , and  $(4.9 \pm 1.8) \times 10^{-7}$  for  $\rho^0\gamma$  and  $\omega\gamma$ .

From these upper limits the bound  $|V_{td}/V_{ts}| < 0.34$  can be obtained, which is still weaker than the corresponding bound derived from  $\Delta m_s/\Delta m_d$ .

### 1.2.4 Electroweak Rare $B$ Decays

#### Observation of $B \rightarrow K^*\ell^+\ell^-$

The first signal for  $B \rightarrow K\ell^+\ell^-$  was observed by Belle [18] using  $29 \text{ fb}^{-1}$  of data and later confirmed by BaBar [47]; a  $B \rightarrow K^*\ell^+\ell^-$  signal, whose branching fraction is expected to be larger, was not significant in those data samples.

The  $B \rightarrow K^{(*)}\ell^+\ell^-$  signal is identified using  $M_{bc}$ ,  $\Delta E$  (and  $M(K\pi)$  for  $K^*\ell^+\ell^-$ ). Belle updated the analysis using a  $140 \text{ fb}^{-1}$  data sample, and with a number of improvements in the analysis procedure [19]. The most significant improvement was a lower minimum lepton momentum of 0.7 (0.4) GeV for muons (electrons) from 1.0 (0.5) GeV that gained 12% (7%) in the total efficiency. In addition, a  $K^*\ell^+\ell^-$  combinations are removed if there can be an unobserved photon along with one of the leptons that can form a  $B \rightarrow J/\psi K \rightarrow \ell^+\ell^-\gamma K$  decay. As a result, the first  $B \rightarrow K^*\ell^+\ell^-$  signal was observed with a statistical significance of  $5.7\sigma$  from a fit to  $M_{bc}$ , as shown in Figure 1.9; in addition, an improved  $B \rightarrow K\ell^+\ell^-$  signal, with a significance of  $7.4\sigma$ , was obtained.

The obtained branching fractions are summarized in Table 1.5, together with the BaBar results [48]. For the combined  $B \rightarrow K^*\ell^+\ell^-$  results,  $\mathcal{B}(B \rightarrow K^*\ell^+\ell^-) = \mathcal{B}(B \rightarrow K^*\mu^+\mu^-) =$

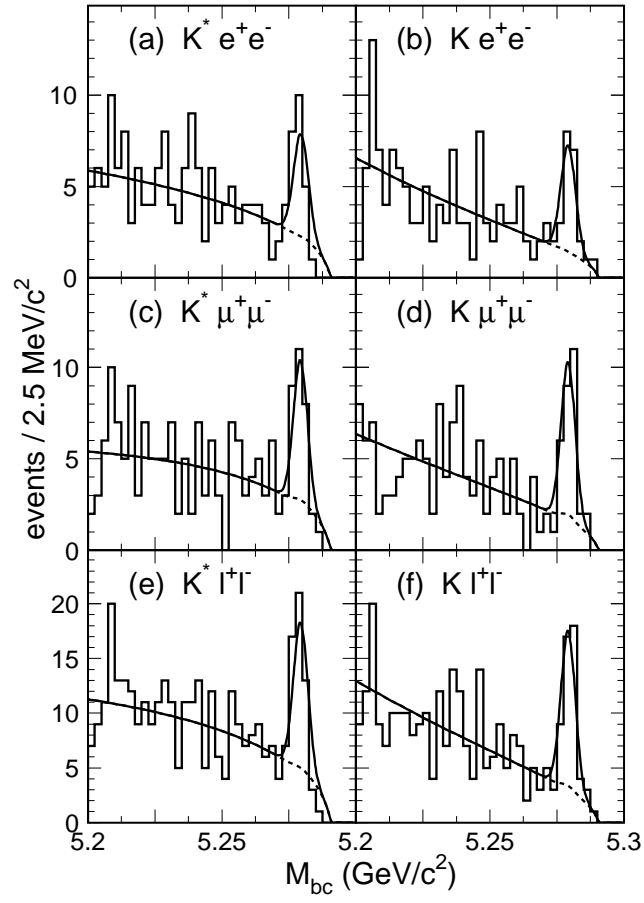


Figure 1.9: The  $B \rightarrow K^{(*)} \ell^+ \ell^-$  signal observed by Belle.

Table 1.5:  $B \rightarrow K^{(*)}\ell^+\ell^-$  branching fractions.

Mode	Belle (140 fb <sup>-1</sup> ) [ $\times 10^{-7}$ ]	BaBar (113 fb <sup>-1</sup> ) [ $\times 10^{-7}$ ]
$B \rightarrow Ke^+e^-$	$4.8^{+1.5}_{-1.3} \pm 0.3 \pm 0.1$	$7.9^{+1.9}_{-1.7} \pm 0.7$
$B \rightarrow K\mu^+\mu^-$	$4.8^{+1.3}_{-1.1} \pm 0.3 \pm 0.2$	$4.8^{+2.5}_{-2.0} \pm 0.4$
$B \rightarrow K\ell^+\ell^-$	$4.8^{+1.0}_{-0.9} \pm 0.3 \pm 0.1$	$6.9^{+1.5}_{-1.3} \pm 0.6$
$B \rightarrow K^*e^+e^-$	$14.9^{+5.2+1.1}_{-4.6-1.3} \pm 0.3$	$10.0^{+5.0}_{-4.2} \pm 1.3$
$B \rightarrow K^*\mu^+\mu^-$	$11.7^{+3.6}_{-3.1} \pm 0.8 \pm 0.6$	$12.8^{+7.8}_{-6.2} \pm 1.7$
$B \rightarrow K^*\ell^+\ell^-$	$11.5^{+2.6}_{-2.4} \pm 0.7 \pm 0.4$	$8.9^{+3.4}_{-2.9} \pm 1.1$

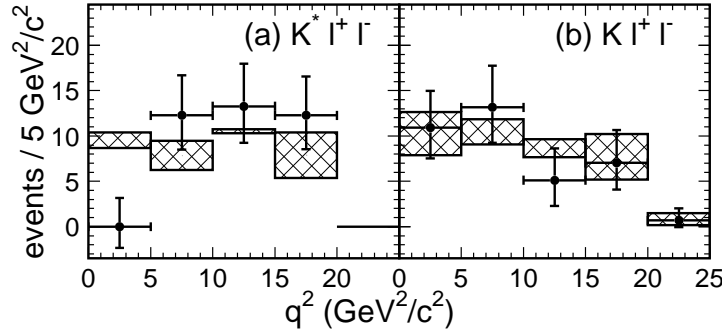


Figure 1.10:  $q^2$  distributions for  $B \rightarrow K^{(*)}\ell^+\ell^-$  from Belle.

$0.75\mathcal{B}(B \rightarrow K^*e^+e^-)$  is assumed which compensates for the enhancement at the  $q^2 = 0$  pole, which is more significant for  $K^*e^+e^-$ , using the expected Standard Model ratio [49]. The measured branching fractions are in agreement with the Standard Model, for example [49, 50]  $(3.5 \pm 1.2) \times 10^{-7}$  for  $B \rightarrow K\ell^+\ell^-$  and  $(11.9 \pm 3.9) \times 10^{-7}$  for  $B \rightarrow K^*\ell^+\ell^-$ . We note that the experimental errors are already much smaller than both the uncertainties in the theoretical predictions of the Standard Model and the variations due to different model-dependent assumptions used to account for the hadronic uncertainties [51, 52, 53, 54, 55].

It is still too early to fit the  $q^2$  distribution to constrain new physics. First attempts by Belle to extract the  $q^2$  distribution using the  $M_{bc}$  signal yields in individual  $q^2$  bins are shown in Figure 1.10.

### Measurement of $B \rightarrow X_s\ell^+\ell^-$

The first measurements of the  $B \rightarrow K^{(*)}\ell^+\ell^-$  branching fractions are consistent with the Standard Model predictions. However since these predictions have uncertainties that are already larger than the measurement errors, the inclusive rate for  $B \rightarrow X_s\ell^+\ell^-$  becomes more important in terms of the search for a deviation from the Standard Model. In contrast to  $B \rightarrow X_s\gamma$ , the lepton pair alone does not provide a sufficient constraint to suppress the largest background from semi-leptonic decays. Therefore, at least for now, it is only possible to use the semi-inclusive method to sum up the exclusive modes for now.

Belle has successfully measured the inclusive  $B \rightarrow X_s\ell^+\ell^-$  branching fraction [20] with a 60 fb<sup>-1</sup> data sample by applying a method that reconstructs the  $X_s$  final state with one kaon

Table 1.6:  $B \rightarrow X_s \ell^+ \ell^-$  branching fractions.

Mode	Belle (60 fb <sup>-1</sup> ) [ $\times 10^{-6}$ ]	BaBar (78 fb <sup>-1</sup> ) [ $\times 10^{-6}$ ]
$X_s e^+ e^-$	$5.0 \pm 2.3^{+1.3}_{-1.1}$	$6.6 \pm 1.9^{+1.9}_{-1.6}$
$X_s \mu^+ \mu^-$	$7.9 \pm 2.1^{+2.1}_{-1.5}$	$5.7 \pm 2.8^{+1.7}_{-1.4}$
$X_s \ell^+ \ell^-$	$6.1 \pm 1.4^{+1.4}_{-1.1}$	$6.3 \pm 1.6^{+1.8}_{-1.5}$

( $K^+$  or  $K_S^0$ ) and up to four pions, of which one pion is allowed to be a  $\pi^0$ . Assuming the  $K_L^0$  contribution is the same as the  $K_S^0$ , this set of final states covers  $82 \pm 2\%$  of the signal. In addition,  $M(X_s)$  is required to be below 2.1 GeV in order to reduce backgrounds. For leptons, a minimum momentum of 0.5 GeV for electrons, 1.0 GeV for muons and  $M(\ell^+ \ell^-) > 0.2$  GeV are required. Background sources and the suppression techniques are similar to those for the exclusive decays. The signal of  $60 \pm 14$  events from Belle with a statistical significance of 5.4 is shown in Figure 1.11. Corresponding branching fractions are given in Table 1.6, together with the BaBar results [56]. The branching fraction results are for the dilepton mass range above  $M(\ell^+ \ell^-) > 0.2$  GeV/ $c^2$  and are interpolated in the  $J/\psi$  and  $\psi'$  regions that are removed from the analysis, assuming no interference with these charmonium states.

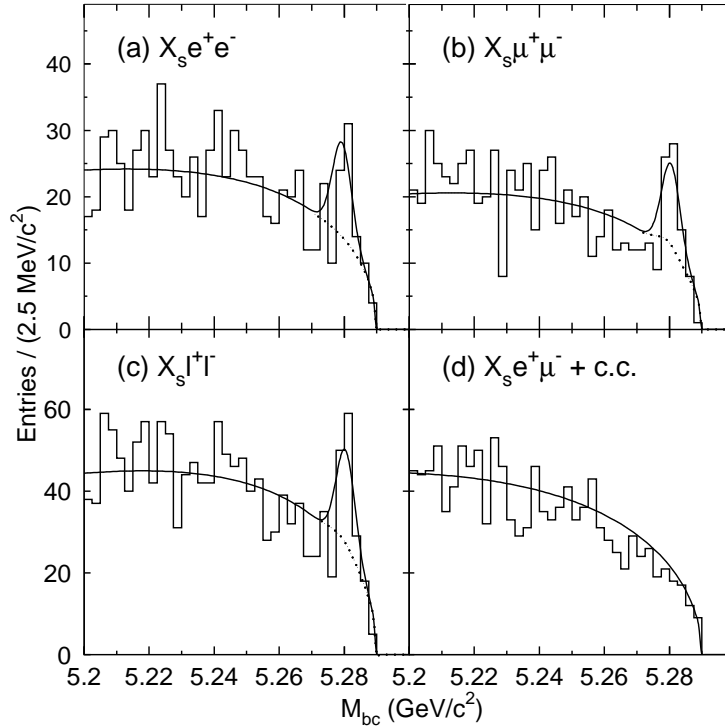


Figure 1.11:  $B \rightarrow X_s \ell^+ \ell^-$  signal measured by Belle. The  $X_s e^+ \mu^-$  sample, which is prohibited in the Standard Model, represents the combinatorial backgrounds.

The results may be compared with the Standard Model prediction [49] of  $(4.2 \pm 0.7) \times 10^{-6}$  integrated over the same dilepton mass range of  $M(\ell^+ \ell^-) > 0.2$  GeV/ $c^2$ . With this requirement, the effect of the  $q^2 = 0$  pole becomes insignificant, giving almost equal branching fractions for

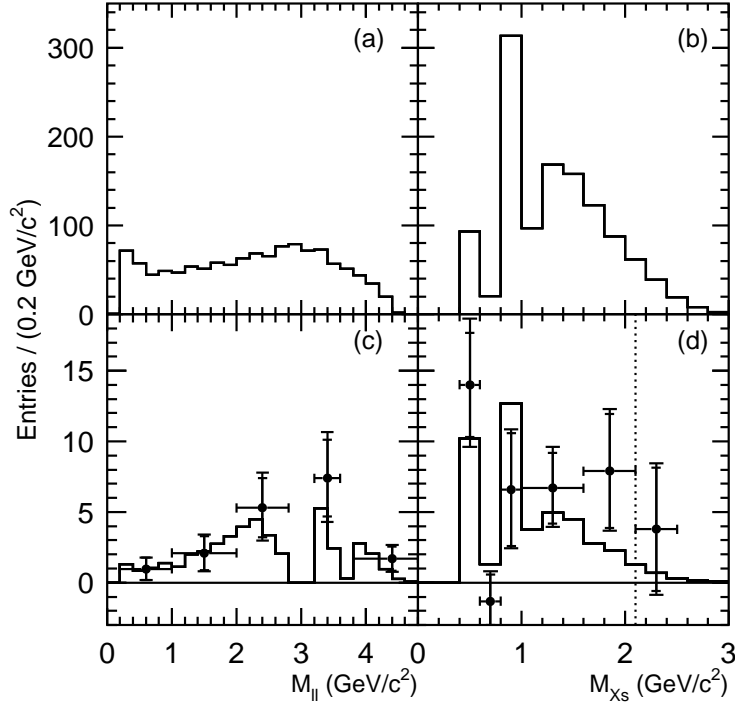


Figure 1.12:  $M(\ell^+\ell^-)$  (left) and  $M(X_s)$  (right) distributions for  $B \rightarrow X_s \ell^+ \ell^-$  from Belle (points with error bars), compared with the Standard Model predictions before (top) and after (bottom) including detector acceptance effects.

the electron and muon modes. The measured branching fractions are in agreement with the Standard Model, considering the large error in the measurement. It should be noted that the large systematic error is dominated by the uncertainty in the  $M(X_s)$  distribution, in particular the fraction of  $B \rightarrow K^{(*)} \ell^+ \ell^-$ , which will be reduced with more statistics. Distributions for  $M(X_s)$  and  $M(\ell^+ \ell^-)$  are shown in Figure 1.12, in which no significant deviation from the Standard Model is observed.

### 1.2.5 Prospects

With a data sample of  $\sim 500 \text{ fb}^{-1}$ , the statistical errors will be reduced to about a half of the present errors. The value of  $\sin 2\phi_1$  will be measured with an accuracy less than 5% using  $b \rightarrow c\bar{c}s$  processes. Though uncertainties will be large,  $\phi_2$  and  $\phi_3$  will also be measured. Together with some improvement in  $|V_{cb}|$  and  $|V_{ub}|$  measurements, the KM scheme for  $CP$ -violation will be further confirmed. Direct  $CP$ -violation will be observed in several decay modes, which also strongly supports the KM scheme.

We expect to obtain results for observables that are sensitive to new physics but have not been measured yet, such as the forward-backward asymmetry of lepton-pairs in  $B \rightarrow K^{(*)} \ell^+ \ell^-$ , time-dependent  $CP$ -violation of radiative decays, *etc.* If the effect of new physics is large, it may be seen; for example, the current indication of the  $CP$ -violation in  $B^0 \rightarrow \phi K_S^0$  decays if its central value remains as currently measured. However, the confirmation of any new physics effect and the understanding its nature will require much larger data samples, which will be the primary goal of the proposed SuperKEKB and upgraded Belle detector.

## Chapter 2

# Flavor Structure of the Standard Model

### 2.1 Flavor Structure of the Standard Model

In the Standard Model of elementary particles there are three generations of leptons and quarks

$$\begin{pmatrix} \nu_e \\ e \end{pmatrix} \quad \begin{pmatrix} \nu_\mu \\ \mu \end{pmatrix} \quad \begin{pmatrix} \nu_\tau \\ \tau \end{pmatrix}, \quad (2.1)$$

$$\begin{pmatrix} u \\ d \end{pmatrix} \quad \begin{pmatrix} c \\ s \end{pmatrix} \quad \begin{pmatrix} t \\ b \end{pmatrix}, \quad (2.2)$$

and their interactions are described by a gauge field theory with the gauge group  $SU(3)_C \times SU(2)_L \times U(1)_Y$ . The group  $SU(3)$  denotes Quantum Chromodynamics (QCD), which governs the strong interaction among quarks. The transformation property under the electroweak gauge group  $SU(2)_L \times U(1)_Y$  differs for the left and right chiralities of fermions. The right-handed components of the leptons and quarks are singlets under the weak  $SU(2)_L$ , and the weak hypercharge  $Y$  is 0,  $-1$ ,  $2/3$ ,  $-1/3$  for neutrinos, leptons, up-type quarks and down-type quarks, respectively. The left-handed components of leptons transform as doublets under the weak  $SU(2)_L$  while the weak doublets of quarks differ slightly from (2.2) and are given by

$$\begin{pmatrix} u \\ d' \end{pmatrix}_L \quad \begin{pmatrix} c \\ s' \end{pmatrix}_L \quad \begin{pmatrix} t \\ b' \end{pmatrix}_L. \quad (2.3)$$

The weak eigenstates  $(d', s', b')$  are a linear combination of the mass eigenstates  $(d, s, b)$ , being related by a  $3 \times 3$  unitary matrix, referred to as the Cabibbo-Kobayashi-Maskawa (CKM) matrix  $\hat{V}_{\text{CKM}}$  [57, 2], as follows

$$\begin{pmatrix} d' \\ s' \\ b' \end{pmatrix} = \hat{V}_{\text{CKM}} \begin{pmatrix} d \\ s \\ b \end{pmatrix} \equiv \begin{pmatrix} V_{ud} & V_{us} & V_{ub} \\ V_{cd} & V_{cs} & V_{cb} \\ V_{td} & V_{ts} & V_{tb} \end{pmatrix} \begin{pmatrix} d \\ s \\ b \end{pmatrix}. \quad (2.4)$$

The charged current interactions of quarks mediated by the  $W$  boson are described by an interaction Lagrangian

$$\mathcal{L}^{\text{CC}} = -\frac{g_2}{\sqrt{2}} \left( \bar{u} \quad \bar{c} \quad \bar{t} \right)_L \gamma^\mu \begin{pmatrix} d' \\ s' \\ b' \end{pmatrix}_L W_\mu^\dagger + \text{h.c.}$$

$$= -\frac{g_2}{\sqrt{2}} \begin{pmatrix} \bar{u} & \bar{c} & \bar{t} \end{pmatrix}_L \gamma^\mu \hat{V}_{\text{CKM}} \begin{pmatrix} d \\ s \\ b \end{pmatrix}_L W_\mu^\dagger + \text{h.c.}, \quad (2.5)$$

where  $W_\mu$  denotes the  $W$  boson, and  $g_2$  is the gauge coupling corresponding to the gauge group  $SU(2)_L$ . In the low energy effective Hamiltonian it appears as the Fermi constant  $G_F/\sqrt{2} = g_2^2/8M_W^2$ . Due to the misalignment between the up-type and down-type quark fields, the charged current induces transitions among different generations.

In contrast, the neutral current is flavor-conserving, which is ensured by the unitarity of the CKM matrix, and, thus, Flavor Changing Neutral Currents (FCNC) are absent at the tree level in the Standard Model. This is the Glashow-Iliopoulos-Maiani (GIM) mechanism [1]. Even including loop corrections, the FCNC interaction vanishes in the limit of degenerate (up-type) quark masses, due to the unitarity of the CKM matrix.

The CKM matrix is a unitary  $N \times N$  matrix with  $N(=3)$  number of generations, and thus contains  $N^2$  parameters in general. However,  $2N - 1$  phases may be absorbed by rephasing the  $2N$  quark fields (one overall phase is related to the total baryon number conservation and is irrelevant for the quark mixing), and  $(N - 1)^2$  independent parameters remain. Of these,  $\frac{1}{2}(N - 1)N$  are real parameters, which correspond to rotation angles among different generations, while  $\frac{1}{2}(N - 2)(N - 1)$  are imaginary parameters, which are sources of  $CP$ -violation. In the three-generation Standard Model, there are 3 mixing angles and 1  $CP$ -phase.

The standard parametrization of the CKM matrix is the following: [58]

$$V_{\text{CKM}} = \begin{pmatrix} c_{12}c_{13} & s_{12}c_{13} & s_{13}e^{-i\delta} \\ -s_{12}c_{23} - c_{12}s_{23}s_{13}e^{i\delta} & c_{12}c_{23} - s_{12}s_{23}s_{13}e^{i\delta} & s_{23}c_{13} \\ s_{12}s_{23} - c_{12}c_{23}s_{13}e^{i\delta} & -s_{23}c_{12} - s_{12}c_{23}s_{13}e^{i\delta} & c_{23}c_{13} \end{pmatrix}, \quad (2.6)$$

where  $c_{ij} = \cos \theta_{ij}$  and  $s_{ij} = \sin \theta_{ij}$  with  $\theta_{ij}$  ( $ij = 12, 13$  and  $23$ ) the mixing angles, and  $\delta$  is the complex phase. It is known experimentally that the angles are small and exhibit the hierarchy  $1 \gg s_{12} \gg s_{23} \gg s_{13}$ . To make this structure manifest, the Wolfenstein parametrization [59] is often used, in which one sets  $\lambda = |V_{us}| \simeq 0.22$  and

$$V_{\text{CKM}} = \begin{pmatrix} 1 - \lambda^2/2 & \lambda & A\lambda^3(\rho - i\eta) \\ -\lambda & 1 - \lambda^2/2 & A\lambda^2 \\ A\lambda^3(1 - \rho - i\eta) & -A\lambda^2 & 1 \end{pmatrix} + O(\lambda^4), \quad (2.7)$$

with  $A$ ,  $\rho$  and  $\eta$  being real parameters of order unity. In this parametrization the source of  $CP$ -violation is carried by the most off-diagonal elements  $V_{ub}$  and  $V_{td}$ .

Among these four parameters,  $\lambda$  and  $A$  are relatively well known from corresponding semi-leptonic decays:  $|V_{us}| = 0.2196 \pm 0.0026$  from  $K_{l3}$  decays and  $|V_{cb}| = (41.2 \pm 2.0) \times 10^{-3}$  from inclusive and exclusive  $b \rightarrow c l \bar{\nu}_l$  decays [58]. The determination of the other two parameters  $\rho$  and  $\eta$  is conveniently depicted as a contour in the plane of  $(\rho, \eta)$ . It corresponds to the unitarity relation of the CKM matrix applied to the first and third columns

$$V_{ud}V_{ub}^* + V_{cd}V_{cb}^* + V_{td}V_{tb}^* = 0. \quad (2.8)$$

This relation may be presented in the complex plane as in Fig. 2.1 (a), which is called the “unitarity triangle”. Since  $V_{cd}V_{cb}^*$  is real to a good approximation (up to  $O(\lambda^7)$ ), it is convenient to normalize the triangle by  $|V_{cd}V_{cb}^*| = A\lambda^3$  so that the apex has the coordinate  $(\bar{\rho}, \bar{\eta})$  where

$$\bar{\rho} = \rho(1 - \lambda^2/2), \quad \bar{\eta} = \eta(1 - \lambda^2/2), \quad (2.9)$$

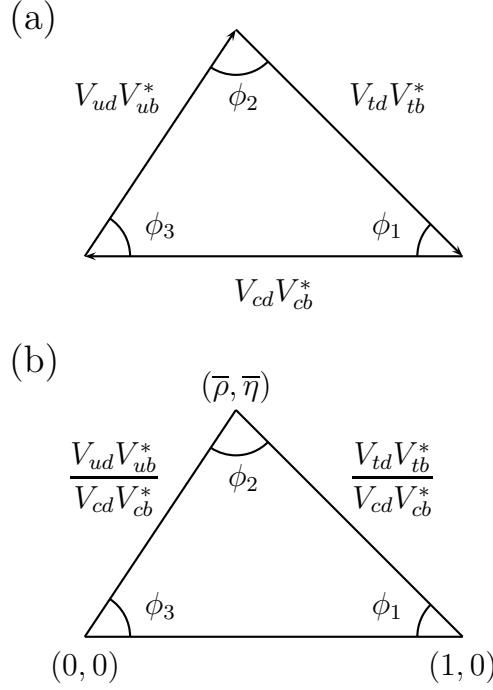


Figure 2.1: Unitarity triangle

(Fig. 2.1 (b)). The three angles of the unitarity triangle represent the complex phase of the combinations

$$\phi_1 = \arg \left[ -\frac{V_{cd}V_{cb}^*}{V_{td}V_{tb}^*} \right], \quad \phi_2 = \arg \left[ -\frac{V_{td}V_{tb}^*}{V_{ud}V_{ub}^*} \right], \quad \phi_3 = \arg \left[ -\frac{V_{ud}V_{ub}^*}{V_{cd}V_{cb}^*} \right]. \quad (2.10)$$

The notation  $\alpha \equiv \phi_2$ ,  $\beta \equiv \phi_1$ ,  $\gamma \equiv \phi_3$  is also used in the literature.

The present constraints on the parameter  $(\bar{\rho}, \bar{\eta})$  are summarized in Fig. 2.2, which is taken from the CKM fitter group (<http://ckmfitter.in2p3.fr/>). Details of the input parameters are discussed, for instance, in [60]. Prospects with SuperKEKB will be discussed in the following sections.

## 2.2 Low Energy Effective Hamiltonians

In  $B$  decays the exchange of a  $W$  boson and virtual loops involving the top quark are effectively point-like interactions, since the relevant length scale of  $B$  meson decays is at least  $O(1/m_b)$  while the  $W$  exchange takes place at a short distance scale  $O(1/M_W)$ . It is theoretically inefficient to calculate the physical amplitudes using the entire  $W$  and top quark propagators, and one may instead introduce a low energy effective Hamiltonian. This framework is based on the Operator Product Expansion (OPE) [61], which allows one to separate the long distance physics from the short distance interactions, occurring at a length scale of  $1/M_W$ , up to the corrections of order  $m_b/M_W$ , which can be safely neglected in many cases.

For instance,  $B^0 - \bar{B}^0$  mixing occurs through the box diagrams shown in Fig. 2.3. The interaction can be described in terms of the  $\Delta B = 2$  effective Hamiltonian

$$\mathcal{H}_{eff}^{\Delta B=2} = \frac{G_F^2}{16\pi^2} (V_{tb}V_{td}^*)^2 M_W^2 S_0(m_t^2/M_W^2) C^{\Delta B=2}(\mu_b) Q^{\Delta B=2}(\mu_b), \quad (2.11)$$



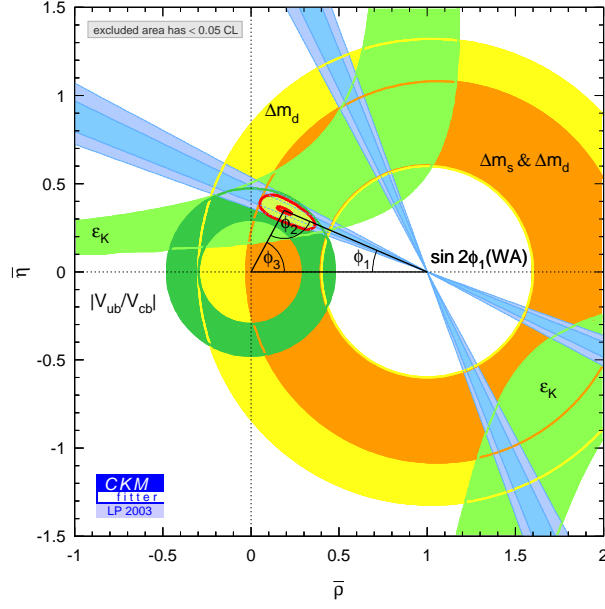


Figure 2.2: A fit of the parameters  $(\bar{\rho}, \bar{\eta})$  using several experimental constraints as of Lepton-Photon 2003. The plot is taken from the CKM fitter page <http://ckmfitter.in2p3.fr/>.

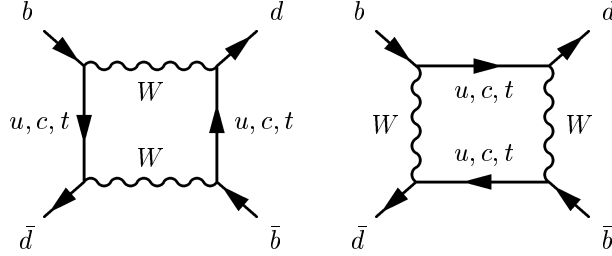


Figure 2.3: Box diagrams to produce the  $\Delta B = 2$  four-quark operator

where the  $\Delta B = 2$  effective four-quark operator is

$$Q^{\Delta B=2} = \bar{d}\gamma_\mu(1 - \gamma_5)b\bar{d}\gamma_\mu(1 - \gamma_5)b. \quad (2.12)$$

The operator is defined at the renormalization scale  $\mu_b$  and the corresponding Wilson coefficient  $C^{\Delta B=2}(\mu_b)$  is calculated using the renormalization group technique as  $C^{\Delta B=2}(\mu_b) = [\alpha_s^{(5)}(\mu_b)]^{-6/23}$  to leading order. The function  $S_0(m_t^2/M_W^2)$  is called the Inami-Lim function [62] and represents the loop effect through the box diagrams.

The  $\Delta B = 1$  transitions are described by the following effective Hamiltonian

$$\mathcal{H}_{eff}^{\Delta B=1} = \frac{4G_F}{\sqrt{2}} V_{CKM} \sum_i C_i(\mu_b) O_i(\mu_b) + \text{h.c.}, \quad (2.13)$$

where  $V_{CKM}$  is the corresponding CKM matrix element. The operators  $O_i(\mu_b)$  defined at the scale  $\mu_b$  are listed below, and the couplings  $C_i(\mu_b)$  are the Wilson coefficients.

The effective operators representing the tree-level  $W$  exchange diagram depicted in Fig. 2.4 are

$$O_1^q = \bar{d}^\alpha \gamma_\mu (1 - \gamma_5) q^\beta \bar{q}^\beta \gamma_\mu (1 - \gamma_5) b^\alpha, \quad q = u, c, \quad (2.14)$$

$$O_2^q = \bar{d}^\alpha \gamma_\mu (1 - \gamma_5) q^\alpha \bar{q}^\beta \gamma_\mu (1 - \gamma_5) b^\beta, \quad q = u, c. \quad (2.15)$$

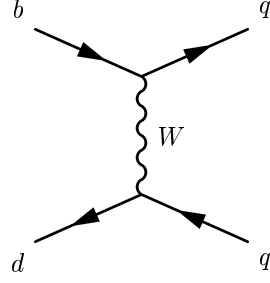


Figure 2.4: Tree-type  $W$  boson exchange diagram.

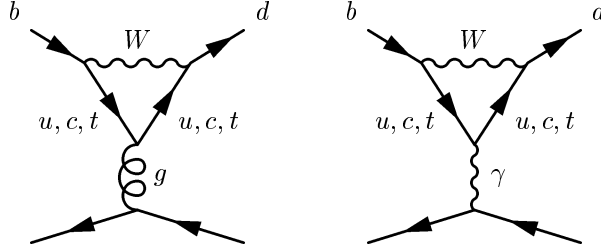


Figure 2.5: Penguin diagrams. The fermion line on the bottom are quarks for the gluon penguin diagram (left), while either quarks or leptons can be involved in the electro-weak penguin (right).

Here the superscripts  $\alpha$  and  $\beta$  specify the color contraction. There is another set of operators obtained by replacing  $d$  by  $s$ .

Many important FCNC decays occur through the so-called penguin diagrams. Some examples are shown in Fig. 2.5.

The gluon penguin diagram (Fig. 2.5 (left)) produces the following operators

$$O_3 = \sum_{q=u,d,s,c} \bar{d}^\alpha \gamma_\mu (1 - \gamma_5) b^\alpha \bar{q}^\beta \gamma_\mu (1 - \gamma_5) q^\beta, \quad (2.16)$$

$$O_4 = \sum_{q=u,d,s,c} \bar{d}^\alpha \gamma_\mu (1 - \gamma_5) b^\beta \bar{q}^\beta \gamma_\mu (1 - \gamma_5) q^\alpha, \quad (2.17)$$

$$O_5 = \sum_{q=u,d,s,c} \bar{d}^\alpha \gamma_\mu (1 - \gamma_5) b^\alpha \bar{q}^\beta \gamma_\mu (1 + \gamma_5) q^\beta, \quad (2.18)$$

$$O_6 = \sum_{q=u,d,s,c} \bar{d}^\alpha \gamma_\mu (1 - \gamma_5) b^\beta \bar{q}^\beta \gamma_\mu (1 + \gamma_5) q^\alpha. \quad (2.19)$$

There are also diagrams in which the gluon or photon is not attached to the fermion line and directly appears in the final state. Such diagrams produce

$$O_{7\gamma} = \frac{e}{8\pi^2} m_b \bar{d} \sigma^{\mu\nu} (1 + \gamma_5) F_{\mu\nu} b, \quad (2.20)$$

$$O_{8g} = \frac{g}{8\pi^2} m_b \bar{d} \sigma^{\mu\nu} (1 + \gamma_5) G_{\mu\nu}^a T^a b, \quad (2.21)$$

where  $F_{\mu\nu}$  and  $G_{\mu\nu}$  are electromagnetic and QCD field strength tensors, respectively. These operators are responsible for the  $b \rightarrow d\gamma$  and  $b \rightarrow dg$  transitions. The operators relevant to the  $b \rightarrow s\gamma$  and  $b \rightarrow sg$  transitions are obtained by replacing  $d$  by  $s$  in (2.20) and (2.21).

The electroweak penguin diagram (Fig. 2.5 (right)) gives a higher order contribution in the electromagnetic coupling constant  $\alpha$  and is thus very small in general. However, since it

may become a source of isospin symmetry breaking, in some cases it could be relevant. The corresponding operators are

$$O_7 = \frac{3}{2} \sum_{q=u,d,s,c} e_q \bar{d}^\alpha \gamma_\mu (1 - \gamma_5) b^\alpha \bar{q}^\beta \gamma_\mu (1 + \gamma_5) q^\beta, \quad (2.22)$$

$$O_8 = \frac{3}{2} \sum_{q=u,d,s,c} e_q \bar{d}^\alpha \gamma_\mu (1 - \gamma_5) b^\beta \bar{q}^\beta \gamma_\mu (1 + \gamma_5) q^\alpha, \quad (2.23)$$

$$O_9 = \frac{3}{2} \sum_{q=u,d,s,c} e_q \bar{d}^\alpha \gamma_\mu (1 - \gamma_5) b^\alpha \bar{q}^\beta \gamma_\mu (1 - \gamma_5) q^\beta, \quad (2.24)$$

$$O_{10} = \frac{3}{2} \sum_{q=u,d,s,c} e_q \bar{d}^\alpha \gamma_\mu (1 - \gamma_5) b^\beta \bar{q}^\beta \gamma_\mu (1 - \gamma_5) q^\alpha. \quad (2.25)$$

$e_q$  is the electromagnetic charge of quarks;  $2/3$  for up-type quarks and  $-1/3$  for down-type quarks. When the fermion line in the bottom of Fig. 2.5 (right) is a lepton ( $e$ ,  $\mu$  or  $\tau$ ), we obtain

$$O_{9V} = \frac{e^2}{16\pi^2} \bar{d} \gamma_\mu (1 - \gamma_5) b \bar{l} \gamma_\mu l, \quad (2.26)$$

$$O_{10A} = \frac{e^2}{16\pi^2} \bar{d} \gamma_\mu (1 - \gamma_5) b \bar{l} \gamma_\mu \gamma_5 l. \quad (2.27)$$

They give rise to the  $b \rightarrow d(s) l^+ l^-$  transitions.

The Wilson coefficients in Eq.(2.13) are calculated using a perturbation theory to next-to-leading order (NLO) [63, 64, 65, 66].

## 2.3 $B - \bar{B}$ Mixing

Neutral  $B$  meson mixing is one of the most important FCNC processes in  $B$  physics. In the Standard Model it involves the CKM matrix element  $V_{td}$  and thus gives a  $CP$ -violating amplitude, which induces a variety of  $CP$ -violating observables through its quantum mechanical interference with other amplitudes.

A  $B^0$  meson produced as an initial state may evolve into its antiparticle  $\bar{B}^0$  through the interaction given by the  $\Delta B = 2$  effective Hamiltonian (2.11). In quantum mechanics the state  $|B^0(t)\rangle$  at time  $t$  is a superposition of two states  $|B^0\rangle$  and  $|\bar{B}^0\rangle$ . The time evolution is described by a Shrödinger equation

$$i \frac{d}{dt} |B(t)\rangle = \left( M - i \frac{\Gamma}{2} \right) |B(t)\rangle, \quad (2.28)$$

where the two-by-two Hermitian matrices  $M$  and  $\Gamma$  denote mass and decay matrices, respectively. The diagonal parts are constrained from  $CPT$  invariance  $M_{11} = M_{22}$  and  $\Gamma_{11} = \Gamma_{22}$ , and the off-diagonal parts  $M_{12}$  ( $M_{21}$ ) and  $\Gamma_{12}/2$  ( $\Gamma_{21}/2$ ) are dispersive and absorptive parts of the  $\Delta B = 2$  transition. The eigenstates of the matrix  $M - i\Gamma/2$  are given by

$$|B_1\rangle = p|B^0\rangle + q|\bar{B}^0\rangle, \quad (2.29)$$

$$|B_2\rangle = p|B^0\rangle - q|\bar{B}^0\rangle, \quad (2.30)$$

and their coefficients  $p$  and  $q$  are obtained by solving

$$\frac{q}{p} = + \sqrt{\frac{M_{12}^* - i\Gamma_{12}^*/2}{M_{12} - i\Gamma_{12}/2}} \quad (2.31)$$

together with the normalization condition  $|p|^2 + |q|^2 = 1$ . The eigenvalues  $M_{1,2} - i\Gamma_{1,2}/2$  are related to observables as follows: the  $B$  meson mass  $M = (M_1 + M_2)/2$ , the  $B$  meson width  $\Gamma = (\Gamma_1 + \Gamma_2)/2$ , the  $B^0 - \bar{B}^0$  mixing frequency  $\Delta M \equiv M_2 - M_1$ , and the width difference  $\Delta\Gamma \equiv \Gamma_1 - \Gamma_2$ .

In the  $B$  meson system there is a relation  $\Delta\Gamma \ll \Delta M$ , which follows from  $\Gamma_{12} \ll M_{12}$ . We may then approximately obtain

$$\Delta M = -2|M_{12}| \left[ 1 + O\left(\left|\frac{\Gamma_{12}}{M_{12}}\right|^2\right) \right], \quad (2.32)$$

$$\Delta\Gamma = 2|\Gamma_{12}| \cos \zeta \left[ 1 + O\left(\left|\frac{\Gamma_{12}}{M_{12}}\right|^2\right) \right], \quad (2.33)$$

and

$$\frac{q}{p} = +\sqrt{\frac{M_{12}^*}{M_{12}}} \left[ 1 - \frac{1}{2} \left| \frac{\Gamma_{12}}{M_{12}} \right| \sin \zeta + O\left(\left|\frac{\Gamma_{12}}{M_{12}}\right|^2\right) \right]. \quad (2.34)$$

The angle  $\zeta$  is the  $CP$  violating phase difference between  $M_{12}$  and  $\Gamma_{12}$

$$\frac{\Gamma_{12}}{M_{12}} = \left| \frac{\Gamma_{12}}{M_{12}} \right| e^{i\zeta}. \quad (2.35)$$

The time evolution of the state  $|B^0\rangle$  and  $|\bar{B}^0\rangle$  produced at time  $t = 0$  is then given by

$$|B^0(t)\rangle = g_+(t)|B^0\rangle + \frac{q}{p}g_-(t)|\bar{B}^0\rangle, \quad (2.36)$$

$$|\bar{B}^0(t)\rangle = g_+(t)|\bar{B}^0\rangle + \frac{p}{q}g_-(t)|B^0\rangle, \quad (2.37)$$

with

$$g_+(t) = e^{-iMt - \Gamma t/2} \left[ \cosh \frac{\Delta\Gamma t}{4} \cos \frac{\Delta M t}{2} - i \sinh \frac{\Delta\Gamma t}{4} \sin \frac{\Delta M t}{2} \right], \quad (2.38)$$

$$g_-(t) = e^{-iMt - \Gamma t/2} \left[ -\sinh \frac{\Delta\Gamma t}{4} \cos \frac{\Delta M t}{2} + i \cosh \frac{\Delta\Gamma t}{4} \sin \frac{\Delta M t}{2} \right]. \quad (2.39)$$

As the initial  $B^0$  (or  $\bar{B}^0$ ) state evolves, it oscillates between  $B^0$  and  $\bar{B}^0$  states with the frequency  $\Delta M$ . The  $CP$ -violating phase arises in the mixing parameter  $q/p$ , which carries the phase of  $M_{12}$  as shown in (2.34).

## 2.4 Time-dependent Asymmetries

One of the key observables at an asymmetric  $B$  factory is the time-dependent asymmetry between  $B^0$  and  $\bar{B}^0$  decays.

Let us consider a decay of the  $B$  meson to a final state  $f$ . The decay rate  $\Gamma(B^0(t) \rightarrow f)$  is time dependent, since the decaying state is a time-dependent superposition of  $|B^0\rangle$  and  $|\bar{B}^0\rangle$ , as discussed in the previous section. We write the decay amplitude of flavor eigenstates as  $A_f = \langle f|B^0\rangle$  and  $\bar{A}_f = \langle f|\bar{B}^0\rangle$ , and define a parameter

$$\lambda_f = \frac{q}{p} \frac{\bar{A}_f}{A_f}. \quad (2.40)$$

If the final state is a  $CP$ -eigenstate  $CP|f\rangle = \xi_f|f\rangle$  with an eigenvalue  $\xi_f = \pm 1$ , then the time dependent asymmetry

$$a_f(t) = \frac{\Gamma(\bar{B}^0(t) \rightarrow f) - \Gamma(B^0(t) \rightarrow f)}{\Gamma(\bar{B}^0(t) \rightarrow f) + \Gamma(B^0(t) \rightarrow f)} \quad (2.41)$$

becomes

$$a_f(t) = \mathcal{A}_f \cos(\Delta Mt) + \mathcal{S}_f \sin(\Delta Mt), \quad (2.42)$$

neglecting the small width difference of the  $B$  meson. Here, the direct and indirect (or mixing-induced)  $CP$  asymmetries are written as

$$\mathcal{A}_f = \frac{|\lambda_f|^2 - 1}{|\lambda_f|^2 + 1}, \quad (2.43)$$

$$\mathcal{S}_f = \frac{2 \operatorname{Im} \lambda_f}{1 + |\lambda_f|^2}. \quad (2.44)$$

Since the absolute value of  $q/p$  is approximately 1, direct  $CP$ -violation  $|\mathcal{A}_f| \neq 0$  requires  $|A_f| \neq |\bar{A}_f|$ , which could happen if  $A_f$  is a sum of (more than one) decay amplitudes having different  $CP$ -phases. Indirect  $CP$ -violation, on the other hand, proves the quantum mechanical interference between the mixing and decay amplitudes.

#### 2.4.1 Measurement of $\sin 2\phi_1$

The mixing-induced asymmetry provides a variety of methods to measure the angles of the Unitarity Triangle (Fig. 2.1). It was first proposed by Bigi, Carter, and Sanda in 1980–1981 [67, 68, 69], and gave strong motivation to construct the present KEK B Factory. The best known example is the case where the final state is  $J/\psi K_S^0$ , whose quark level process is  $\bar{b} \rightarrow \bar{c}c\bar{s}$  followed by the  $K^0 - \bar{K}^0$  mixing. In the case where the decay is dominated by a single amplitude, the ratio of decay amplitudes is given by

$$\frac{\bar{A}_{J/\psi K_S^0}}{A_{J/\psi K_S^0}} = - \left( \frac{V_{cb} V_{cs}^*}{V_{cb}^* V_{cs}} \right) \left( \frac{V_{cs} V_{cd}^*}{V_{cs}^* V_{cd}} \right), \quad (2.45)$$

where one minus sign appears the  $CP$  odd final state  $J/\psi K_S^0$ . Together with the phase in the mixing

$$\frac{q}{p} \simeq \frac{V_{tb}^* V_{td}}{V_{tb} V_{td}^*}, \quad (2.46)$$

the entire ratio  $\lambda_{J/\psi K_S^0}$  becomes

$$\lambda_{J/\psi K_S^0} = - \left( \frac{V_{tb}^* V_{td}}{V_{tb} V_{td}^*} \right) \left( \frac{V_{cb} V_{cs}^*}{V_{cb}^* V_{cs}} \right) \left( \frac{V_{cs} V_{cd}^*}{V_{cs}^* V_{cd}} \right) = -e^{-2i\phi_1}. \quad (2.47)$$

Thus, one can precisely measure the angle  $\phi_1$  from the time-dependent asymmetry

$$a_{J/\psi K_S^0}(t) = \sin(2\phi_1) \sin \Delta Mt. \quad (2.48)$$

There exists an additional decay amplitude through the penguin diagram  $\bar{b} \rightarrow \bar{s}c\bar{c}$ , which involves the CKM factor  $V_{ts} V_{tb}^*$ . Using the unitarity of the CKM matrix  $V_{ts} V_{tb}^* = -V_{cs} V_{cb}^* - V_{us} V_{ub}^*$ , the weak phase of the penguin contribution is the same as that of the tree amplitude  $V_{cs} V_{cb}^*$  up to a doubly Cabibbo-suppressed correction. Therefore, the relation (2.48) holds to an excellent

approximation ( $\sim 1\%$ ), and the mode  $J/\psi K_S^0$  is called the “gold-plated” mode. The precision expected at SuperKEKB is discussed in Section 4.6.

There are other decay modes which develop the same weak phase. Namely, the penguin decays  $\bar{b} \rightarrow \bar{s}s\bar{s}$  are accompanied by the CKM factor  $V_{ts}V_{tb}^*$  just as the penguin contribution to  $\bar{b} \rightarrow \bar{s}c\bar{c}$ . Since there is no direct tree diagram for  $\bar{b} \rightarrow \bar{s}s\bar{s}$ , measurement of the same angle  $\sin 2\phi_1$  through its time dependent asymmetry can be a probe of any new physics phase in the penguin loop process [26]. At the hadron level, the corresponding modes are  $B^0 \rightarrow \phi K_S^0$  and  $B^0 \rightarrow \eta' K_S^0$ . These asymmetries have already been measured as described in Section 1.2, and the expected sensitivity at SuperKEKB is studied in Section 4.2. Possible contaminations from the tree-level process  $\bar{b} \rightarrow \bar{u}u\bar{s}$  with a rescattering of  $u\bar{u}$  to  $s\bar{s}$  may distort the measurement. However, these contributions are expected to be small ( $O(\lambda^2) \sim 5\%$ ) [27], and a model independent bound can be obtained using  $SU(3)$  relations provided that the related modes are observed at higher luminosity  $B$  factories [28].

#### 2.4.2 Measurement of $\phi_2$

If a decay can occur through more than one amplitude with different weak phases, the analysis is more involved. As an example, we consider  $B^0 \rightarrow \pi^+\pi^-$ , whose decay amplitude can be parametrized as

$$A(B^0 \rightarrow \pi^+\pi^-) = T_{\pi\pi} + P_{\pi\pi}. \quad (2.49)$$

The first term represents an amplitude for the tree level  $W$  exchange process  $\bar{b} \rightarrow \bar{u}u\bar{d}$ , which picks up the CKM matrix elements  $V_{ud}V_{ub}^*$ , while the second term is a penguin diagram contribution  $\bar{b} \rightarrow \bar{d}u\bar{u}$  containing the CKM factor  $V_{td}V_{tb}^*$ . If the penguin contribution can be neglected, the ratio  $\lambda_{\pi^+\pi^-}$  in (2.40) reads as

$$\lambda_{\pi^+\pi^-} = \left( \frac{V_{tb}^*V_{td}}{V_{tb}V_{td}^*} \right) \left( \frac{V_{ud}^*V_{ub}}{V_{ud}V_{ub}^*} \right) = e^{2i\phi_2}, \quad (2.50)$$

and the time-dependent asymmetry could be used to determine the angle  $\phi_2$ . However, both amplitudes in (2.49) are the same order in  $\lambda$  ( $\sim \lambda^3$ ), and the penguin contribution is not so suppressed compared to the tree level contribution; the ratio of amplitudes  $|P_{\pi\pi}/T_{\pi\pi}|$  is roughly estimated to be around 0.3 from  $B \rightarrow K\pi$  decays assuming the flavor  $SU(3)$  symmetry.

One solution to the problem is to consider isospin symmetry [70]. The  $B \rightarrow \pi\pi$  decay amplitudes are written as

$$A(B^0 \rightarrow \pi^+\pi^-) = \sqrt{2}(A_2 - A_0), \quad (2.51)$$

$$A(B^0 \rightarrow \pi^0\pi^0) = 2A_2 + A_0, \quad (2.52)$$

$$A(B^+ \rightarrow \pi^+\pi^0) = 3A_2. \quad (2.53)$$

$A_0$  and  $A_2$  are amplitudes for isospin 0 and 2 of two-pion final state, respectively. The tree diagram contributes to both  $A_0$  and  $A_2$ , while the penguin diagram produces only isospin 0. Then, one obtains a relation

$$A(B^0 \rightarrow \pi^+\pi^-) + \sqrt{2}A(B^0 \rightarrow \pi^0\pi^0) = \sqrt{2}A(B^+ \rightarrow \pi^+\pi^0). \quad (2.54)$$

and its  $CP$  conjugate

$$\bar{A}(B^0 \rightarrow \pi^+\pi^-) + \sqrt{2}\bar{A}(\bar{B}^0 \rightarrow \pi^0\pi^0) = \sqrt{2}\bar{A}(B^- \rightarrow \pi^-\pi^0). \quad (2.55)$$

By measuring the branching ratios of the three decay modes and the time dependent asymmetry of  $\pi^+\pi^-$ , one can determine the absolute values  $|A_0|$  and  $|A_2|$  and their relative phase difference  $\arg(A_0A_2^*)$ , through a simple geometric reconstruction. This determines the angle  $\phi_2$  up to a four-fold ambiguity.

Another solution is to consider the isospin relations among  $B \rightarrow \rho\pi$  decays [71]. There are three possible decay chains  $B^0 \rightarrow \{\rho^+\pi^-, \rho^0\pi^0, \rho^-\pi^+\} \rightarrow \pi^+\pi^-\pi^0$ . Together with their  $CP$ -conjugate amplitudes, there exist six different amplitudes, each of which has contributions from both tree and penguin diagrams. By combining the time-dependent asymmetry of this process in the Dalitz plot one may extract the pure tree amplitude, and thus the angle  $\phi_2$ .

If there is non-negligible contribution from the electroweak penguin diagram, the isospin relations are violated, since up and down quarks have different charges [72]. However, such a contribution is suppressed compared to the gluon penguin by a factor  $\alpha_{[\text{weak}]}(m_t^2/m_Z^2)/\alpha_s \ln(m_t^2/m_c^2) \sim 0.1$  [73]. At SuperKEKB, the actual size of the electroweak penguin amplitude can be estimated from the analysis of  $K\pi$  decays [73, 74, 75, 76, 77].

The prospects of measuring the angle  $\phi_2$  at SuperKEKB using these methods are discussed in Section 4.7.

## 2.5 Theoretical Methods

In order to extract fundamental parameters, such as the quark masses and CKM matrix elements, from  $B$  decay experiments, one needs model independent calculations of the decay amplitudes. However, since  $B$  meson decays involve complicated QCD interactions, which are highly non-perturbative in general, the theoretical calculation of physical amplitudes is a non-trivial task.

### 2.5.1 Heavy Quark Symmetry

One useful theoretical method for avoiding hadronic uncertainties is to use symmetries. Using isospin or  $SU(3)$  flavor symmetries, different decay amplitudes can be related to each other. This approach is widely used in  $B$  decay analyses, *e.g.* the isospin analysis of  $\pi\pi$  decays to extract  $\sin 2\phi_2$  discussed in Section 2.4.2.

Another symmetry which is especially important in  $B$  physics is the heavy quark symmetry [78, 79]. In the limit of an infinitely heavy quark mass, the heavy quark behaves as a static color source and the QCD interaction cannot distinguish different flavors, *i.e.* charm or bottom. Consequently the decay amplitudes (or form factors) of  $b$  and  $c$  hadrons are related to each other (heavy quark flavor symmetry). Moreover, since the spin-dependent interaction decouples in the infinitely heavy quark mass limit, some form factors become redundant (heavy quark spin symmetry). The most famous example is the heavy-to-heavy semi-leptonic decay  $\bar{B} \rightarrow D^{(*)}\ell\bar{\nu}_\ell$  form factors. In general there are 6 independent form factors for these exclusive decay modes, but in the heavy quark limit they reduce to one; the Isgur-Wise function, and its normalization in the zero-recoil limit are determined.

A more general formalism has also been developed in the language of effective field theory, *i.e.* Heavy Quark Effective Theory (HQET) [80, 81, 82]. It provides a systematic expansion in terms of  $\Lambda_{\text{QCD}}/m_Q$ .

## 2.5.2 Heavy Quark Expansion

The inclusive decay rate of a  $B$  meson to the final state  $X$  can be written as

$$\Gamma(B \rightarrow X) = \frac{1}{2m_B} \sum_X (2\pi)^4 \delta^4(p_B - p_X) |\langle X | \mathcal{H}_{eff}^{\Delta B=1} | B \rangle|^2, \quad (2.56)$$

where the sum runs over all possible final states and momentum configurations. The effective Hamiltonian  $\mathcal{H}_{eff}^{\Delta B=1}$  is proportional to  $\bar{c}\gamma^\mu P_L b \bar{l}\gamma_\mu P_L \nu_l$  when the  $b \rightarrow c$  semileptonic decay is considered, or to  $\bar{u}\gamma^\mu P_L b \bar{l}\gamma_\mu P_L \nu_l$  if we are interested in using the  $b \rightarrow u$  semileptonic decay process to determine  $|V_{ub}|$ . It could also describe non-leptonic decay by considering a four-quark operator  $\bar{c}\gamma^\mu P_L b \bar{q}\gamma_\mu P_L q'$ . Using the optical theorem, Eq.(2.56) can be rewritten in terms of an absorptive part of a  $B$  meson matrix element

$$\Gamma(B \rightarrow X) = \frac{1}{m_B} \text{Im} \langle B | \mathcal{T} | B \rangle, \quad (2.57)$$

where the operator  $\mathcal{T}$  is

$$\mathcal{T} = i \int d^4x T \left( \mathcal{H}_{eff}^{\Delta B=1}(x) \mathcal{H}_{eff}^{\Delta B=1}(0) \right). \quad (2.58)$$

Since the momentum flowing into the final state quark propagator is large ( $\sim m_b$ ), one can expand the time-ordered product of operators in terms of local operators, using the Operator Product Expansion (OPE) technique [61]. It gives an expansion in terms of the inverse heavy quark mass and is called the Heavy Quark Expansion (HQE) [83, 84, 85, 86, 87].

The lowest dimensional operator is  $\bar{b}b$ , whose matrix element is unity up to  $(\Lambda_{\text{QCD}}/m_b)^2$  corrections. The first non-trivial higher order correction appears at  $1/m_b^2$  with the chromomagnetic operator  $\bar{b}\sigma_{\mu\nu}g_s G^{\mu\nu}b$ . Therefore, at  $O((\Lambda_{\text{QCD}}/m_b)^2)$  the heavy quark expansion can be expressed in terms of two non-perturbative parameters

$$\lambda_1 = \frac{1}{2m_B} \langle B(v) | \bar{h}_v (i\vec{D})^2 h_v | B(v) \rangle, \quad (2.59)$$

$$3\lambda_2 = \frac{g_s}{2m_B} \langle B(v) | \frac{1}{2} \bar{h}_v \sigma_{\mu\nu} G^{\mu\nu} h_v | B(v) \rangle, \quad (2.60)$$

where the operators are defined with the HQET field  $h_v$  and the  $B$  meson state is also defined in the heavy quark limit.  $\lambda_2$  is known from the hyper-fine splitting of the  $B$  meson ( $B$ - $B^*$  splitting) to be  $\lambda_2 \simeq 0.12 \text{ GeV}^2$ , while  $\lambda_1$  has to be calculated using non-perturbative methods, such as QCD sum rules [88, 89] or lattice QCD [90, 91, 92, 93], or to be fitted with experimental data of inclusive  $B$  decays [94, 95, 96, 97, 98].

## 2.5.3 Perturbative Methods

Model independent theoretical calculations of exclusive non-leptonic decay amplitudes are known to be very challenging, as they involve both soft and hard gluon exchanges and clear separation of the perturbative (hard) and non-perturbative (soft) parts is intractable. In the heavy quark limit, however, a formulation to realize such separation of short and long distance physics has recently been developed, ameliorating the perturbative calculation of decay amplitudes.

The intuitive idea is the color transparency argument due to Bjorken [99]. An energetic light meson emitted from  $B$  decay resembles a color dipole, and its soft interaction with the remaining decay products is suppressed by  $\Lambda_{\text{QCD}}/m_b$ . A systematic formulation of such an idea



is provided by QCD factorization [100, 101, 102]. In this formalism, the decay matrix elements of  $B \rightarrow \pi\pi$  can be factorized in the form

$$\begin{aligned} \langle \pi(p') \pi(q) | Q_i | \overline{B}(p) \rangle &= f^{B \rightarrow \pi}(q^2) \int_0^1 du T_i^I(u) \Phi_\pi(u) \\ &+ \int_0^1 d\xi du dv T_i^{II}(\xi, u, v) \Phi_B(\xi) \Phi_\pi(u) \Phi_\pi(v), \end{aligned} \quad (2.61)$$

for a four-quark operator  $Q_i$ . The first term represents a factorization of the amplitude into the  $B \rightarrow \pi$  form factor and an out-going pion wave function  $\Phi_\pi(u)$  convoluted with the hard scattering kernel  $T_i^I(u)$ . Here, the term “factorization” is used for two meanings: one is the factorization of the diagram to  $\langle \pi | V | \overline{B} \rangle \langle \pi | A | 0 \rangle$ , while the other is the separation of hard, collinear and soft interactions. The kernel  $T_i^I(u)$  describes the hard interaction only and, thus, is calculable using perturbation theory. The second term in Eq.(2.61) describes a factorization of the amplitude into three pieces:  $\overline{B} \rightarrow 0$ ,  $0 \rightarrow \pi$ , and  $0 \rightarrow \pi$  convoluted with a hard interaction kernel  $T_i^{II}(\xi, u, v)$ . To make the factorization of collinear and soft degrees of freedom more explicit, an effective theory has also been developed, which is called the Soft Collinear Effective Theory (SCET) [103, 104, 105, 106].

The form factor  $f^{B \rightarrow \pi}(q^2)$  and the light-cone distribution function (or wave function)  $\Phi_B(\xi)$  and  $\Phi_\pi(u)$  contain long-distance dynamics, which has to be treated with non-perturbative methods.

Another method of factorization, Perturbative QCD (PQCD) [107, 108, 109, 110, 111, 112], has also been proposed and is being used for the analysis of various  $B$  decay modes. It relies on the Sudakov suppression of the tail of the wave function, which smears the end-point singularity in the QCD-factorization calculation of the form factor. The form factor  $f^{B \rightarrow \pi}(q^2)$  then becomes factorizable, and the first term in Eq.(2.61) can be rewritten into a formula similar to the second term. The input of the form factor is used to determine the wave functions.

#### 2.5.4 Lattice QCD

Lattice QCD provides a method to calculate non-perturbative hadronic matrix elements from the first principles of QCD [113]. It is a regularization of QCD on a four-dimensional hypercubic lattice, which enables numerical simulation on the computer. Since the calculation is numerically so demanding, one has to introduce several approximations in the calculation and these lead to systematic uncertainties.

For more than a decade, lattice QCD has been applied to the calculation of matrix elements relevant to  $B$  physics. The best-known quantity is the  $B$  meson leptonic decay constant  $f_B$ , for which the systematic uncertainty is now under control at the level of 10–15% accuracy. The important tools to achieve this goal are the following.

- *Effective theories for heavy quarks.* Since the Compton wave-length of the  $b$  quark is shorter than the lattice spacing  $a$ , the discretization error is out of control with the usual lattice fermion action for relativistic particles. Instead, Heavy Quark Effective Theory (HQET) [80] or Non-relativistic QCD (NRQCD) [114, 115, 116] is formulated on the lattice and used to simulate the  $b$  quark. Another related effective theory is the so-called Fermilab action [117, 118], which covers the entire (light to heavy) mass regime with the same lattice action. For the  $B$  meson, the next-to-leading ( $1/m_Q$ ) order calculation provides  $\lesssim 5\%$  accuracy [119].
- *Effective theories to describe discretization errors.* The discretization effect can be expressed in terms of the Lagrangian language, *i.e.* Symanzik effective theory [120, 121].

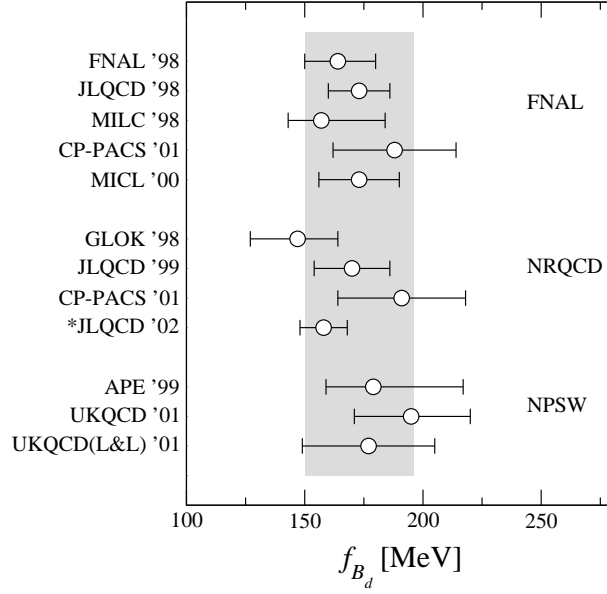


Figure 2.6: Recent quenched lattice calculations of  $f_B$ . The figure is from [126].

It also provides a method to eliminate the error by adding irrelevant operators to the lattice action. The  $O(a)$  error existing in the Wilson fermion action can be removed by adding a dimension-five operator [122]. The cancellation of the  $O(a)$  error can also be done non-perturbatively [123, 124], so that the remaining discretization error is  $O(a^2)$  and not  $O(\alpha_s^n a)$ .

- *Renormalized perturbation theory.* To relate the lattice operators to their continuum counterparts, one has to rely on perturbation theory. For a long time lattice perturbation had bad convergence behavior and the perturbative error was too large if one calculated only the one-loop terms. This problem was cured by Lepage and Mackenzie by taking a renormalized coupling constant as an expansion parameter [125].

A summary of recent lattice calculations of  $f_B$  in the quenched approximation is shown in Fig. 2.6. Results of many groups obtained with different discretizations for heavy quarks agree very well within the error band of  $\sim 13\%$ .

The above results are obtained within the approximation of neglecting the pair creation and annihilation of quarks in the vacuum, which is called the quenched approximation. To include such dynamical quark effects requires much more computer power, and it has only recently become feasible. A recent calculation by the JLQCD collaboration [127] is shown in Fig. 2.7, which represents the light quark mass dependence of  $f_B$  in two-flavor QCD. A major uncertainty in the unquenched simulation comes from the chiral extrapolation, as the present unquenched simulation is limited to relatively heavy sea quark masses ( $m_q \gtrsim m_s/2$ ). Because chiral perturbation theory predicts the chiral logarithm  $m_q \ln m_q$  [128], the chiral extrapolation may bend downwards near the chiral limit as shown by dashed curves in Fig. 2.7. To control this extrapolation one needs simulations with much smaller sea quark masses as adopted in the recent simulations using staggered fermions for sea quarks [129].

Lattice QCD calculations can be applied to several other important quantities:

- $B_B$ . The  $B$  parameter in the  $B^0 - \bar{B}^0$  mixing has been calculated in the unquenched QCD [127], with the result  $f_B \sqrt{\hat{B}_B} = 215(11)(_{-23}^{+0})(15)$  MeV. Here the first error is statistical,

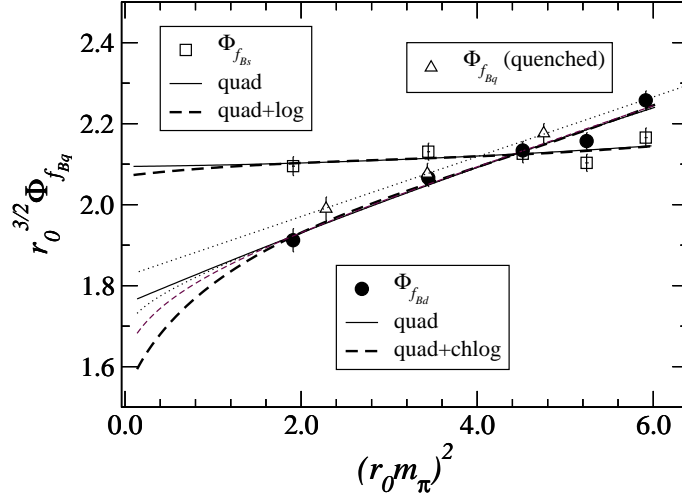


Figure 2.7: Chiral extrapolation of unquenched  $f_B$ . The plot is for  $\Phi_{f_B} \equiv f_B \sqrt{m_B}$  normalized with a Sommer scale  $r_0$ . Figure from [127].

the second is an uncertainty from the chiral extrapolation and the third is from other systematic errors.

- *Heavy-to-heavy semileptonic decay.* The zero recoil form factor of the semileptonic decay  $B \rightarrow D^{(*)} l \nu$  has been calculated rather precisely using a double-ratio technique [130, 131].
- *Heavy-to-light semileptonic decay.* The  $B \rightarrow \pi l \nu$  form factor has been calculated in the quenched QCD to an accuracy of order 20% [132, 133, 134, 135].

These and other recent results have been reviewed at recent conferences [126, 136, 137, 138].

## Chapter 3

# Flavor Structure of the Physics beyond the Standard Model

### 3.1 Motivation for New Physics

The Standard Model of elementary particles has been very successful in explaining a wide variety of existing experimental data. It covers a range of phenomena from low energy (less than a GeV) physics, such as kaon decays, to high energy (a few hundred GeV) processes involving real weak gauge bosons ( $W$  and  $Z$ ) and top quarks. There is, therefore, little doubt that the present Standard Model is a theory to describe the physics below the energy scale of several hundred GeV, which has been explored so far.

However, the Standard Model is not satisfactory as *the* theory of elementary particles beyond the TeV energy scale. First of all, it does not explain the characteristic pattern of the mass spectrum of quarks and leptons. The second generation quarks and leptons are several orders of magnitude heavier than the corresponding first generation particles, and the third generation is even heavier by another order of magnitude. The quark flavor mixing matrix — the CKM matrix — also has a striking hierarchical structure, *i.e.* the diagonal terms are close to unity and  $1 \gg \theta_{12} \gg \theta_{23} \gg \theta_{13}$ , where  $\theta_{ij}$  denotes a mixing angle between the  $i$ -th and  $j$ -th generation. The recent observation of neutrino oscillations implies that there is also a rich flavor structure in the lepton sector. All of these masses and mixings are free parameters in the Standard Model, but ideally they should be explained by higher scale theories.

The particles in the Standard Model acquire masses from the Higgs mechanism. The Higgs potential itself is described by a scalar field theory, which contains a quadratic mass divergence. This means that a Higgs mass of order 100 GeV is realized only after a huge cancellation between the bare Higgs mass squared  $\mu_0^2$  and the quadratically divergent mass renormalization, both of which are quantities of order  $\Lambda^2$  where  $\Lambda$  is the cutoff scale. If  $\Lambda$  is of the order of the Planck scale, then a cancellation of more than 30 orders of magnitude is required. This is often called the hierarchy problem [139, 140, 141]. Therefore it would be highly unnatural if the Standard Model were *the* theory valid at a very high energy scale, such as the Planck scale. Instead, the Standard Model should be considered as an effective theory of some more fundamental theory, which most likely lies in the TeV energy region.

$CP$ -violation is needed in order to produce the observed baryon number (or matter-antimatter) asymmetry in the universe. In the Standard Model, the complex phase of the CKM matrix provides the only source of the  $CP$ -violation<sup>1</sup>, but models of baryogenesis suggest that it is

---

<sup>1</sup>The  $\theta$  parameter in the QCD Lagrangian is another possible source of the  $CP$ -violation, but its value has to

quantitatively insufficient (for a review, see [142]). This is another motivation to consider new physics models.

### 3.2 New physics scenarios

Several scenarios have been proposed for the physics beyond the Standard Model. They introduce new particles, dynamics, symmetries or even extra-dimensions at the TeV energy scale. In the supersymmetry (SUSY) scenarios, one introduces a new symmetry between bosons and fermions, and a number of new particles that form supersymmetric pairs with the existing Standard Model particles. The quadratic divergence of the Higgs mass term then cancels out among superpartners (for reviews, see [143, 144]). Technicolor-type scenarios assume new strong dynamics (like QCD) at the TeV scale and the Higgs field is realized as a composite state of more fundamental particles (for a recent review, see [145]). The large extra space-time dimension models [146, 147] cure the problem by extending the number of spacetime dimensions beyond four (a recent review can be found in [148]). In Little Higgs models the Higgs is a pseudo-Nambu-Goldstone boson, and thus naturally light [149].

Flavor Changing Neutral Current (FCNC) processes, such as  $B^0 - \bar{B}^0$  mixing and the  $b \rightarrow s\gamma$  transition, provide strong constraints on new physics models. If there is no suppression mechanism for FCNC processes, such as the GIM mechanism in the Standard Model, the new physics contribution can easily become too large to be consistent with the experimental data. In fact, if one introduces a FCNC interaction as a higher dimensional operator to represent some new physics interaction, the associated energy scale is typically of order  $10^3$  TeV, which is much higher than the expected scale of the new physics ( $\sim$  TeV). Therefore, one has to introduce some flavor structure in new physics models.

### 3.3 Supersymmetric models

Here, let us consider the supersymmetric (SUSY) model as an example of new physics models at the TeV scale. The SUSY model is attractive not only because it solves the Higgs mass hierarchy problem. It is also consistent with Grand Unification [150, 151], *i.e.* the renormalization group running of the three gauge couplings is modified by the supersymmetric partners, causing them to intersect at the same point at  $\Lambda_{\text{GUT}} \simeq 10^{16}$  GeV.

The general SUSY models have a number of free parameters corresponding to the masses and mixings of the superpartners for each Standard Model particle. Even in the minimal model — the Minimal Supersymmetric Standard Model (MSSM) — the number is more than a hundred. These mass and mixing parameters are, at least partly, governed by the soft supersymmetry breaking mechanism, which is necessary to make the superpartners heavy enough such that they are not detected at existing collider experiments. Therefore, to predict the mass spectrum and flavor mixing of the SUSY particles one has to specify the details of the SUSY breaking mechanism, which should be given at energy scales higher than the TeV scale.

The Minimal Supersymmetric Standard Model (MSSM) is a minimal supersymmetric extension of the Standard Model, containing a superpartner for each particle in the Standard Model and two Higgs doublets. Its matter contents are written in terms of the chiral super-fields as

$$Q_i(3, 2, 1/6), \quad \bar{U}_i(\bar{3}, 1, -2/3), \quad \bar{D}_i(\bar{3}, 1, 1/3) \quad (3.1)$$

---

be unnaturally small  $\theta \leq 10^{-10}$  in order to be consistent with the neutron electron dipole moment experiment. This is another problem — the strong  $CP$  problem.

for the left-handed ( $Q$ ) and right-handed ( $U$  and  $D$ ) quark sector,

$$L_i(1, 2, -1/2), \quad \bar{E}_i(1, 1, 1) \quad (3.2)$$

for the left-handed ( $L$ ) and right-handed ( $E$ ) lepton sector, and

$$H_1(1, 2, -1/2), \quad H_2(1, 2, 1/2) \quad (3.3)$$

for the Higgs fields. The representation (or charge) for the gauge group  $SU(3)_C \times SU(2)_L \times U(1)_Y$  is given in parentheses, and  $i$  ( $= 1, 2$ , or  $3$ ) is a generation index. Under the assumption of  $R$ -parity conservation, which is required to avoid an unacceptably large proton decay rate, the superpotential is written as

$$\mathcal{W}_{\text{MSSM}} = f_D^{ij} \bar{D}_i Q_j H_1 + f_U^{ij} \bar{U}_i Q_j H_2 + f_E^{ij} \bar{E}_i L_j H_1 + \mu H_1 H_2, \quad (3.4)$$

where  $f_U$  and  $f_D$  are the quark Yukawa couplings. The soft supersymmetry breaking terms are

$$\begin{aligned} -\mathcal{L}_{\text{soft}} = & (m_Q^2)_i^j \tilde{q}_i \tilde{q}^{\dagger j} + (m_D^2)_i^j \tilde{d}^{\dagger i} \tilde{d}_j + (m_U^2)_i^j \tilde{u}^{\dagger i} \tilde{u}_j + (m_E^2)_i^j \tilde{e}_i \tilde{e}^{\dagger j} + (m_L^2)_i^j \tilde{l}^{\dagger i} \tilde{l}_j \\ & + \Delta_1^2 h_1^\dagger h_1 + \Delta_2^2 h_2^\dagger h_2 - (B\mu h_1 h_2 + \text{h.c.}) \\ & + A_D^{ij} \tilde{d}_i \tilde{q}_j h_1 + A_U^{ij} \tilde{u}_i \tilde{q}_j h_2 + A_L^{ij} \tilde{u}_i \tilde{q}_j h_2 \\ & + \frac{M_1}{2} \bar{\tilde{B}} \tilde{B} + \frac{M_2}{2} \bar{\tilde{W}} \tilde{W} + \frac{M_3}{2} \bar{\tilde{g}} \tilde{g}. \end{aligned} \quad (3.5)$$

These consist of mass terms for scalar fields ( $\tilde{q}_i$ ,  $\tilde{u}_i$ ,  $\tilde{d}_i$ ,  $\tilde{l}_i$ ,  $\tilde{e}_i$ ,  $h_1$ , and  $h_2$ ), Higgs mixing terms, trilinear scalar couplings, and gaugino ( $\tilde{B}$ ,  $\tilde{W}$ , and  $\tilde{g}$ ) mass terms.

Flavor physics already places strong restrictions on the possible structure of the SUSY breaking sector, since arbitrary terms would induce many flavor violating processes which are easily ruled out by present experimental data. Therefore, in order to comply with the requirement of highly suppressed FCNC interactions, one has to introduce some structure in the soft SUSY breaking terms. Several scenarios have been proposed.

- *Universality.* The SUSY breaking terms have a universal flavor structure at a very high energy scale, such as the Planck scale ( $\sim 10^{18}$  GeV) or the GUT scale ( $\sim 10^{16}$  GeV). It could also be a lower scale ( $\sim 10^{4-6}$  GeV). The universality comes from mediation of the SUSY breaking effect by flavor-blind interactions, such as gravity (for a review of gravity mediation see [143]), the Standard Model gauge interaction (gauge mediation [152, 153, 154] the gaugino mediation [155, 156, 157]), or the super-Weyl anomaly (anomaly mediation [158, 159]). Since the soft SUSY breaking terms are flavor-blind, the squark masses are degenerate at the high energy scale where those terms are generated. The GIM mechanism then works as long as the scalar triple coupling (squark-squark-Higgs), the  $A$  term, is proportional to the Yukawa couplings in the Standard Model. An additional flavor violating effect could appear through the renormalization group running of the squark masses to the low energy scale, which depends on the flavor [160]. For the gauge mediation scenario the effect on FCNC processes is extremely suppressed, since the SUSY breaking scale is low and there is not enough room for the running.
- *Alignment.* Squark and slepton mass matrices could be diagonalized (no flavor changing interaction) in the same basis as quarks and leptons, if one assumes some symmetries involving different generations [161, 162]. Flavor violation is then suppressed and flavor violating processes are induced by incomplete alignment.

- *Decoupling.* The squarks and sleptons of the first and second generations are sufficiently heavy, 10–100 TeV, so that flavor violation in the first and second generations is suppressed [163, 164, 165, 166, 167, 168, 169]. In general such models predict large FCNC effects in the third generation, *i.e.* the  $b$  quark and  $\tau$  lepton decays.

Signals for FCNC processes and  $CP$ -violation largely depend on the structure of the soft SUSY breaking terms.

The Grand Unified Theory (GUT) [150, 151] is one of the motivations for introducing supersymmetry. Besides the unification of couplings, GUTs also relate the Yukawa couplings of the quark and lepton sectors. Since the particle content and symmetry are modified above the GUT scale, they could generate different FCNC effects even if universal soft SUSY breaking is assumed. GUTs also predict some correlation between quark and lepton flavor violation processes. Such studies have been done by several authors [170, 171, 172, 173, 174, 175, 176, 177, 178]

### 3.4 SUSY effect on $b \rightarrow s$ transitions

Here we discuss the possible effects of SUSY particles on  $b \rightarrow s$  transitions. The  $b \rightarrow s$  processes are especially interesting, since the time-dependent  $CP$  asymmetries measured in these processes, in particular  $B \rightarrow \phi K_S^0$  by Belle, deviates from its Standard Model expectation  $\mathcal{S}_{\phi K_S^0} = \mathcal{S}_{J/\psi K_S^0}$  [21]. Since the measurements by BaBar are still consistent with the Standard Model [29], much more data are required to resolve the problem. In the Standard Model the  $B \rightarrow \phi K_S^0$  transition is induced by the  $b \rightarrow s$  penguin diagram, in which there is room for new physics effects to compete with the Standard Model contribution. Supersymmetric GUT models also predict large effects in  $b \rightarrow s$  transitions as a large mixing angle is observed in the neutrino sector between the second and third generations.

We parametrize the effect of soft SUSY breaking terms applying the mass insertion approximation (MIA) [160]. In the MIA, one adopts a basis where the fermion and sfermion mass matrices are rotated in the same way to diagonalize the fermion mass matrix (the super-CKM basis). In this basis, the couplings of fermions and sfermions to neutral gauginos are flavor diagonal, leaving all the sources of flavor violation in the off-diagonal terms of the sfermion mass matrix. These terms are denoted by  $(\Delta_{AB}^q)^{ij}$ , where  $A, B = (L, R)$  and  $q = (u, d)$ . The sfermion propagator can then be expanded as

$$\langle \tilde{q}_A^a \tilde{q}_B^{b*} \rangle = i(k^2 \mathbf{1} - \tilde{m}^2 \mathbf{1} - \Delta_{AB}^q)^{-1}_{ab} \simeq \frac{i\delta_{ab}}{k^2 - \tilde{m}^2} + \frac{i(\Delta_{AB}^q)_{ab}}{(k^2 - \tilde{m}^2)^2} + \dots, \quad (3.6)$$

where  $\mathbf{1}$  is the unit matrix and  $\tilde{m}$  is the averaged squark mass. Here we keep only the first term of the expansion. In this way, the flavor violation in SUSY models can be parameterized in a model independent way by the dimensionless parameters  $(\delta_{AB}^q)_{ij} = (\Delta_{AB}^q)_{ij}/\tilde{m}^2$ , where  $\tilde{m}$  is an average squark mass. Constraints on these parameters from presently available data have been analyzed in [179, 180, 181] (also see [182] for a summary).

Using the MIA, the  $b \rightarrow s\bar{s}s$  transition accompanied by SUSY particles occurs through the diagrams shown in Figure 3.1, and the  $B \rightarrow \phi K_S^0$  data provide a constraint on the mass insertions  $(\delta_{AB}^d)_{23}$  where  $(A, B) = (L, R)$ . In fact, the absolute value of  $(\delta_{AB}^d)_{23}$  is constrained by the branching ratio of  $B \rightarrow X_s \gamma$  as

$$|(\delta_{LL(RR)}^d)_{23}| < 8.2, \quad |(\delta_{LR(RL)}^d)_{23}| < 1.6 \times 10^{-2}, \quad (3.7)$$

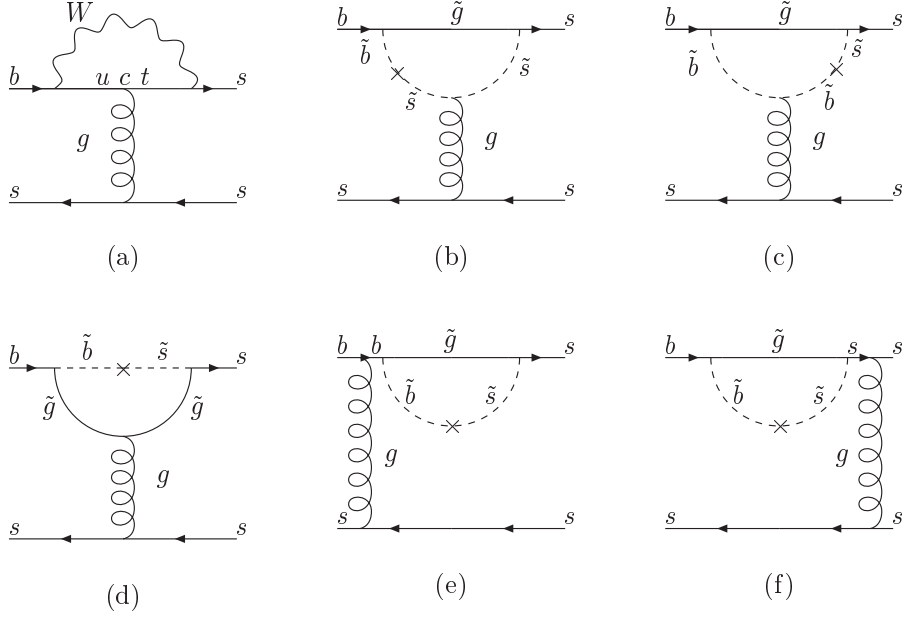


Figure 3.1: The Standard Model contribution (a) and the gluino–down squark contributions (b)–(f) to  $B \rightarrow \phi K_S^0$  decay. The cross represents the mass insertions  $(\delta_{AB}^d)_{23}$ .

for  $m_{\tilde{g}} = 300$  GeV and  $m_{\tilde{q}} = 500$  GeV [181]<sup>2</sup> Thus, an interesting question is whether the observed deviation of  $\mathcal{S}_{\phi K_S^0}$  from  $\mathcal{S}_{J/\psi K_S^0}$  can be obtained while satisfying (3.7).

Here we parameterize the Standard Model and SUSY amplitudes as

$$A^{\text{SM}}(\phi K_S^0) = |A^{\text{SM}}| e^{i\delta_{\text{SM}}}, \quad A^{\text{SUSY}}(\phi K_S^0) = |A^{\text{SUSY}}| e^{i\theta_{\text{SUSY}}} e^{i\delta_{\text{SUSY}}}, \quad (3.8)$$

$$\bar{A}^{\text{SM}}(\phi K_S^0) = |\bar{A}^{\text{SM}}| e^{i\delta_{\text{SM}}}, \quad \bar{A}^{\text{SUSY}}(\phi K_S^0) = |\bar{A}^{\text{SUSY}}| e^{-i\theta_{\text{SUSY}}} e^{i\delta_{\text{SUSY}}}, \quad (3.9)$$

where  $\delta_{\text{SM(SUSY)}}$  is the strong ( $CP$ -conserving) phase and  $\theta_{\text{SUSY}}$  is the weak ( $CP$ -violating) phase. Then, we obtain

$$\mathcal{S}_{\phi K_S^0} = \frac{\sin 2\phi_1 + 2 \left( \frac{|A^{\text{SUSY}}|}{|A^{\text{SM}}|} \right) \cos \delta_{12} \sin(\theta_{\text{SUSY}} + 2\phi_1) + \left( \frac{|A^{\text{SUSY}}|}{|A^{\text{SM}}|} \right)^2 \sin(2\theta_{\text{SUSY}} + 2\phi_1)}{1 + 2 \left( \frac{|A^{\text{SUSY}}|}{|A^{\text{SM}}|} \right) \cos \delta_{12} \cos \theta_{\text{SUSY}} + \left( \frac{|A^{\text{SUSY}}|}{|A^{\text{SM}}|} \right)^2}, \quad (3.10)$$

where  $\delta_{12} \equiv \delta_{\text{SM}} - \delta_{\text{SUSY}}$ . Let us first see how large  $|A^{\text{SUSY}}/A^{\text{SM}}|$  needs to be in order to have  $\mathcal{S}_{\phi K_S^0}$  as small as the experimental central value. Using (3.10), we plot  $\mathcal{S}_{\phi K_S^0}$  in terms of  $\theta_{\text{SUSY}}$  for different values of  $|A^{\text{SUSY}}/A^{\text{SM}}|$  in Figure 3.2, by fixing  $\delta_{12} = 0$  for simplicity and using the central value of the observed  $\sin 2\phi_1$ . We can see that the deviation of  $\mathcal{S}_{\phi K_S^0}$  from  $\mathcal{S}_{J/\psi K_S^0}$  becomes maximal at around  $\theta_{\text{SUSY}} = -\pi/2$  and  $|A^{\text{SUSY}}/A^{\text{SM}}| \gtrsim 0.4$  is required in order to have a negative value of  $\mathcal{S}_{\phi K_S^0}$ .

The effective Hamiltonian for the penguin process can be expressed as

$$\mathcal{H}_{\text{eff}}^{\Delta B=1} = -\frac{G_F}{\sqrt{2}} V_{tb} V_{ts}^* \left[ \sum_{i=3}^6 C_i O_i + C_g O_g + \sum_{i=3}^6 \tilde{C}_i \tilde{O}_i + \tilde{C}_g \tilde{O}_g \right] \quad (3.11)$$

<sup>2</sup>In the following analysis we use  $|(\delta_{LL(RR)}^d)_{23}| < 1$  instead, as the mass insertion approximation does not converge for  $> 1$  and the entire analysis becomes unreliable.



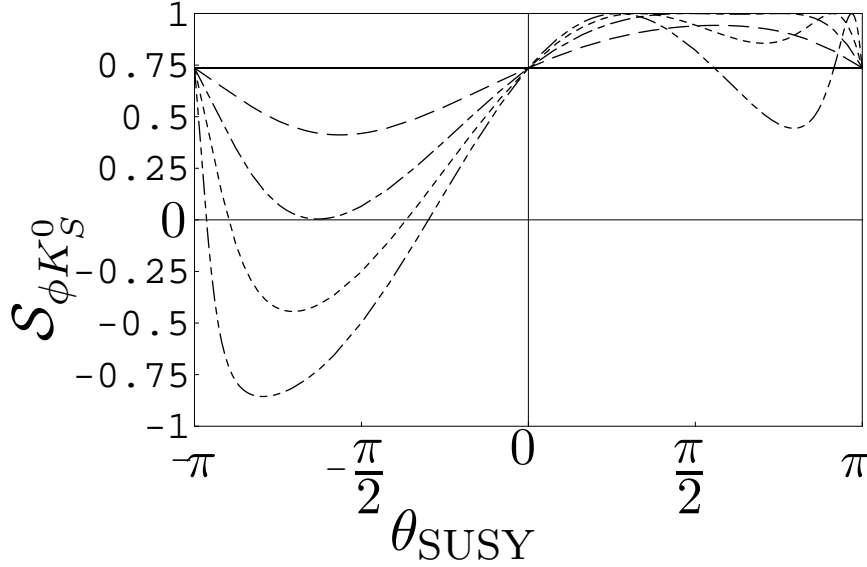


Figure 3.2:  $\mathcal{S}_{\phi K_S^0}$  including SUSY contributions (3.10) as a function of  $\theta_{\text{SUSY}}$  for different values of  $|A^{\text{SUSY}}/A^{\text{SM}}|$ : 0.2 (dashed), 0.4 (dashed-dotted), 0.6 (dotted), 0.8 (dashed-double-dotted). The solid line represents the central value of  $\mathcal{S}_{J/\psi K_S^0}$ . Here we assume that the strong phase difference between SUSY and the Standard Model is negligible  $\delta_{12} \simeq 0$ .

with

$$O_3 = \bar{s}_\alpha \gamma^\mu L b_\alpha \bar{s}_\beta \gamma^\mu L s_\beta, \quad (3.12)$$

$$O_4 = \bar{s}_\alpha \gamma^\mu L b_\beta \bar{s}_\beta \gamma^\mu L s_\alpha, \quad (3.13)$$

$$O_5 = \bar{s}_\alpha \gamma^\mu L b_\alpha \bar{s}_\beta \gamma^\mu L s_\beta, \quad (3.14)$$

$$O_6 = \bar{s}_\alpha \gamma^\mu L b_\beta \bar{s}_\beta \gamma^\mu R s_\alpha, \quad (3.15)$$

$$O_g = \frac{g_s}{8\pi^2} m_b \bar{s}_\alpha \sigma^{\mu\nu} R \frac{\lambda_{\alpha\beta}^A}{2} b_\beta G_{\mu\nu}^A, \quad (3.16)$$

where  $L \equiv (1 - \gamma_5)/2$  and  $R \equiv (1 + \gamma_5)/2$ . The terms with a tilde are obtained from  $C_{i,g}$  and  $O_{i,g}$  by exchanging  $L \leftrightarrow R$ . The Wilson coefficient  $C_{i(g)}$  includes both the Standard Model and SUSY contributions. In the following analysis, we neglect the effect of the operator  $O_\gamma = \frac{e}{8\pi^2} m_b \bar{s}_\alpha \sigma^{\mu\nu} R b_\alpha F_{\mu\nu}$  and the electroweak penguin operators, which give very small contributions. The matrix elements are computed in the naive factorization approximation in the following<sup>3</sup>. The SUSY amplitude  $A^{\text{SUSY}}(\phi K)$  contains gluino and chargino contributions although the latter is negligible. The Wilson coefficients for the gluino contributions that come from box and penguin diagrams are computed in [179]. We note that the dominant SUSY contribution to  $B \rightarrow \phi K_S^0$  comes from the chromo-magnetic operator,  $O_g$  and  $\tilde{O}_g$ .

The numerical result for the ratio of the Standard Model to SUSY amplitude for  $m_{\tilde{g}} \simeq m_{\tilde{q}} = 500$  GeV is as follows [185]

$$\frac{A^{\text{SUSY}}(\phi K_S^0)}{A^{\text{SM}}(\phi K_S^0)} \simeq (0.14 + 0.02i)[(\delta_{LL}^d)_{23} + (\delta_{RR}^d)_{23}] + (65 + 11i)[(\delta_{LR}^d)_{23} + (\delta_{RL}^d)_{23}]. \quad (3.17)$$

<sup>3</sup>The matrix element of  $B \rightarrow \phi K_S^0$  can also be computed using more recent methods: the QCD factorization and the pQCD approach method. Application of these to analyse the SUSY effect on  $\mathcal{S}_{\phi K_S^0}$  can be found in [176, 183] for the former and [184] for the latter.

The tiny imaginary parts in (3.17) are the strong phases coming from the QCD correction terms in the effective Wilson coefficient in [186]. We shall consider SUSY models where one mass insertion is dominant, which is often the case in minimal flavour violation models. Let us start with the models in which  $LL(RR)$  dominates and the remaining mass insertions,  $(\delta_{LR}^d)_{23}$ ,  $(\delta_{RL}^d)_{23}$  and  $(\delta_{RR(LL)}^d)_{23}$  are all negligible. Taking into account the constraints from the  $B \rightarrow X_s \gamma$  branching ratio in (3.7), we obtain a maximum SUSY contribution of  $(|A^{\text{SUSY}}|/|A^{\text{SM}}|)_{LL(RR)} \simeq 0.14$ , which can lead to only a small deviation between  $\mathcal{S}_{\phi K_S^0}$  and  $\mathcal{S}_{J/\psi K_S^0}$  as we learned in Figure 3.2. On the other hand, even if  $LR$  and  $RL$  dominated models are more severely constrained by  $B \rightarrow X_s \gamma$ , the SUSY contribution can reach  $(|A^{\text{SUSY}}|/|A^{\text{SM}}|)_{LR(RL)} \simeq 1.1$ , which gives a negative value of  $\mathcal{S}_{\phi K_S^0}$  for a large range of  $\theta_{\text{SUSY}}$ . Smaller gluino and squark masses,  $m_{\tilde{g}} \simeq m_{\tilde{q}} = 300$  GeV, result in a larger SUSY contribution:

$$\frac{A^{\text{SUSY}}(\phi K_S^0)}{A^{\text{SM}}(\phi K_S^0)} \simeq (0.39 + 0.07i)[(\delta_{LL}^d)_{23} + (\delta_{RR}^d)_{23}] + (110 + 18i)[(\delta_{LR}^d)_{23} + (\delta_{RL}^d)_{23}]. \quad (3.18)$$

In this case, all  $LL$ ,  $RR$ ,  $LR$  and  $RL$  dominated models can lead to a negative value of  $\mathcal{S}_{\phi K_S^0}$ . We see that in order to have a significant difference between  $\mathcal{S}_{\phi K_S^0}$  and  $\mathcal{S}_{J/\psi K_S^0}$ ,  $LL$  and  $RR$  dominated models require small gluino and squark masses. Thus, some  $LL$  and  $RR$  dominated models with large  $m_{\tilde{g}}$  and  $m_{\tilde{q}}$  may be excluded by measurements of  $\mathcal{S}_{\phi K_S^0}$ ; for instance, an observation of  $\mathcal{S}_{\phi K_S^0} < 0$  would exclude  $m_{\tilde{g}} \simeq m_{\tilde{q}} \gtrsim 300$  GeV.

Once more precise experimental data are available and the existence of a new physics contribution in  $\mathcal{S}_{\phi K_S^0}$  is confirmed, it will be necessary to find further evidence to prove that  $\mathcal{S}_{\phi K_S^0}$  indeed includes a SUSY contribution. For this purpose, we are able to benefit from other  $b \rightarrow s$  transitions, which can also be described by the mass insertion  $(\delta_{AB}^d)_{23}$ . In the rest of this section, we shall discuss the process  $B \rightarrow \eta' K_S^0$ .

$CP$ -violation in  $B \rightarrow \eta' K_S^0$  was first reported by the Belle collaboration in summer 2002 [31]. Averaging with the result from the BaBar collaboration reported in spring 2003 [187], we obtain  $S_{\eta' K_S^0} = 0.33 \pm 0.34$ . The  $\eta'$  meson is known to be composed of  $u\bar{u}$ ,  $d\bar{d}$  and  $s\bar{s}$  accompanied by a small amount of other particles such as gluonium and  $c\bar{c}$  etc.<sup>4</sup>. Apart from the exotic particles, the  $B \rightarrow \eta' K_S^0$  process comes from the  $B_d^0 - \bar{B}_d^0$  mixing box diagram and the penguin and tree decay diagrams. While there are two penguin diagrams  $b \rightarrow s\bar{s}s$  and  $b \rightarrow d\bar{d}d$ , there is only one tree diagram, which furthermore is Cabibbo suppressed. As a result, the tree contribution is very small and estimated to be less than 1%. Thus,  $B \rightarrow \eta' K_S^0$  and  $B \rightarrow \phi K_S^0$  are approximately the same apart from the parity of the final states. In the following, we shall investigate whether this parity difference can lead to the experimental observation  $\mathcal{S}_{\phi K_S^0} < 0 < \mathcal{S}_{\eta' K_S^0} < \mathcal{S}_{J/\psi K_S^0}$ .

Let us first see the consequence of this parity difference in the SUSY contributions by comparing the computation of the matrix elements for  $B \rightarrow \phi K_S^0$  and  $B \rightarrow \eta' K_S^0$  in the case of the  $b \rightarrow s\bar{s}s$  transition. In the naive factorization approximation, the amplitudes are written as a product of Wilson coefficients, form factors and decay constants:

$$A(B \rightarrow \phi(\eta') K) \propto C_{\text{Wilson}} F^{B \rightarrow K} f_{\phi(\eta')}. \quad (3.19)$$

The decay constants appear in the calculation by sandwiching the  $V \pm A$  current, corresponding to  $O_i$  and  $\tilde{O}_i$  contributions, respectively, between  $\phi(\eta')$  and the vacuum:

$$\langle 0 | \bar{s} \gamma_\mu (1 \pm \gamma_5) s | \phi \rangle = +m_\phi f_\phi \epsilon_\mu \quad (3.20)$$

$$\langle 0 | \bar{s} \gamma_\mu (1 \pm \gamma_5) s | \eta' \rangle = \pm i f_{\eta'} p_\mu \quad (3.21)$$

---

<sup>4</sup>We do not consider contributions from exotic particles here. However, since an unexpectedly large branching ratio is observed in the  $B \rightarrow \eta' K$  processes, possible large contributions from such particles have been considered. The gluonium contributions to  $B \rightarrow \eta' K_S^0$  including the possibility that SUSY effects also enhance the branching ratio of  $B \rightarrow \eta' K$  is discussed in [188].

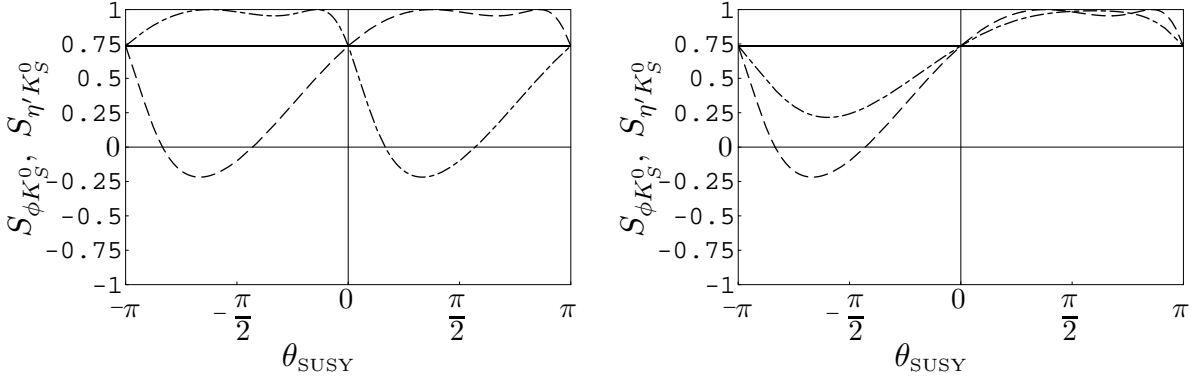


Figure 3.3: Possible solution for the puzzle of  $\mathcal{S}_{\phi K_S^0} < 0 < \mathcal{S}_{\eta' K_S^0} < \mathcal{S}_{J/\psi K_S^0}$ . Dashed and dashed-dotted lines are results for  $\mathcal{S}_{\phi K_S^0}$  and  $\mathcal{S}_{\eta' K_S^0}$ , respectively. Left figure is for the case that  $RR$  and/or  $RL$  are dominant. Right figure is for the case that there are both  $LL$  (and/or  $LR$ ) and  $RR$  (and/or  $RL$ ) contributions and the  $LL$  (and/or  $LR$ ) amplitude is 4 times larger than  $RR$  (and/or  $RL$ ) one whereas the phase of the former is equal to the phase of the latter. For both cases, we fix  $|A^{\text{SUSY}}(\phi K_S^0)/A^{\text{SM}}(\phi K_S^0)| \simeq 0.5$ .

As can be seen from (3.21), the overall sign flips for the  $V + A$  and  $V - A$  currents in the case of  $\eta'$ . Thus, the contributions for  $\mathcal{S}_{\eta' K_S^0}$  coming from  $\tilde{O}_i$  and  $O_i$  have opposite signs. Accordingly, the numerical results are found to be [188]

$$\frac{A^{\text{SUSY}}(\eta' K_S^0)}{A^{\text{SM}}(\eta' K_S^0)} \simeq (0.15 + 0.03i)[(\delta_{LL}^d)_{23} - (\delta_{RR}^d)_{23}] + (69 + 12i)[(\delta_{LR}^d)_{23} - (\delta_{RL}^d)_{23}], \quad (3.22)$$

$$\frac{A^{\text{SUSY}}(\eta' K_S^0)}{A^{\text{SM}}(\eta' K_S^0)} \simeq (0.41 + 0.08i)[(\delta_{LL}^d)_{23} - (\delta_{RR}^d)_{23}] + (115 + 20i)[(\delta_{LR}^d)_{23} - (\delta_{RL}^d)_{23}] \quad (3.23)$$

for  $m_{\tilde{g}} \simeq m_{\tilde{q}} = 500$  GeV and 300 GeV, respectively. As expected, the result is very similar to those for  $B \rightarrow \phi K_S^0$  in (3.17) and (3.18) except for the overall signs of the  $RR$  and  $RL$  mass insertions. Thus, if  $\mathcal{S}_{\phi K_S^0}$  and  $\mathcal{S}_{\eta' K_S^0}$  differ, one would need some contributions from the  $RR$  and/or  $RL$  mass insertion.

Now we shall discuss how we could reproduce the relation  $\mathcal{S}_{\phi K_S^0} < 0 < \mathcal{S}_{\eta' K_S^0} < \mathcal{S}_{J/\psi K_S^0}$  as indicated by experiment. Let us first consider  $RR$  and/or  $RL$  dominated models with  $A^{\text{SUSY}}(\phi K_S^0)/A^{\text{SM}}(\phi K_S^0) \simeq 0.5 e^{i\theta_{\text{SUSY}}}$ . In this case, the overall sign flips for  $\eta' K_S^0$ , so we obtain  $A^{\text{SUSY}}(\eta' K_S^0)/A^{\text{SM}}(\eta' K_S^0) \simeq -0.5 e^{i\theta_{\text{SUSY}}}$ . The results for  $\mathcal{S}_{\phi K_S^0}$  and  $\mathcal{S}_{\eta' K_S^0}$  are shown in Figure 3.3 (left). In this way,  $\mathcal{S}_{\phi K_S^0}$  and  $\mathcal{S}_{\eta' K_S^0}$  may differ and we can obtain  $\mathcal{S}_{\phi K_S^0} < 0 < \mathcal{S}_{\eta' K_S^0}$ . However,  $\mathcal{S}_{\eta' K_S^0}$  is rather large compared to  $\mathcal{S}_{J/\psi K_S^0}$ . To solve this problem, we need to consider models with both sizable  $LL$  (and/or  $LR$ ) and  $RR$  (and/or  $RL$ ) mass insertions. Let us give an example: the amplitude of the  $LL$  (and/or  $LR$ ) mass insertion is 4 times larger than the one for  $RR$  (and/or  $RL$ ) whereas their phases are equal. In this case with the same SUSY contributions to  $\mathcal{S}_{\phi K_S^0}$ ,  $A^{\text{SUSY}}(\phi K_S^0)/A^{\text{SM}}(\phi K_S^0) \simeq 0.5 e^{i\theta_{\text{SUSY}}}$ , we obtain  $A^{\text{SUSY}}(\eta' K_S^0)/A^{\text{SM}}(\eta' K_S^0) \simeq 0.3 e^{i\theta_{\text{SUSY}}}$ . In this way, we are able to reproduce the pattern  $\mathcal{S}_{\phi K_S^0} < 0 < \mathcal{S}_{\eta' K_S^0} < \mathcal{S}_{J/\psi K_S^0}$  (see Figure 3.3 (right)).

### 3.5 Model independent study of $b \rightarrow s\gamma$ and $b \rightarrow s\ell^+\ell^-$ processes

In the previous section we considered the supersymmetric extension of the Standard Model and discussed its possible effects on the  $b \rightarrow s$  transition processes. In contrast, in this section we explain what we can learn from the experimental data in a model independent way. To be specific, we consider the  $b \rightarrow s\gamma$  and  $b \rightarrow s\ell^+\ell^-$  decays [189, 190, 191, 192].

As we discuss below, there are many types of interactions which may contribute to  $b \rightarrow s\gamma$  and  $b \rightarrow s\ell^+\ell^-$ . The new physics effects originate from the energy scale higher than the electro-weak scale, and below that new physics scale, the effects evolve down to the electro-weak scale. Then, at the electro-weak scale, they are matched onto the low energy effective theory, which is valid below the electro-weak scale. The new physics effects can thus be expressed in terms of higher dimensional operators such as four-Fermi interactions and dimension-five interactions. For  $b \rightarrow s\ell^+\ell^-$  and  $b \rightarrow s\gamma$  processes,  $\bar{s}b\ell^+\ell^-$  ( $O_9$  and  $O_{10}$ ),  $\bar{s}\sigma_{\mu\nu}bF^{\mu\nu}$  ( $O_7$ ) and  $\bar{s}\sigma_{\mu\nu}T^{ab}G_{\mu\nu}^a$  ( $O_8$ ) are such operators. (There are several these operators with different chiral structures.) For each operator there is the Wilson coefficient  $C_i^{\text{eff}}$ , in which the new physics effects are encoded. The four-quark operators can contribute to  $b \rightarrow s\ell^+\ell^-$  through the one-loop matrix elements and the operator mixing [192]. We assume that such effects are small compared to the contributions from the tree level matrix elements of  $\bar{s}b\ell^+\ell^-$  operators.

Within the leading logarithmic approximation of QCD corrections, we obtain the following amplitude for  $b \rightarrow s\gamma$ .

$$M(b \rightarrow s\gamma) = \frac{4G_F}{\sqrt{2}} \frac{e}{16\pi^2} V_{tb}V_{ts}^* m_b \left[ C_{7L}^{\text{eff}}(\bar{s}\sigma_{\mu\nu}b_R) + C_{7R}^{\text{eff}}(\bar{s}\sigma_{\mu\nu}b_L) \right] F^{\mu\nu}, \quad (3.24)$$

where  $F_{\mu\nu}$  stands for  $-i(q_\mu\epsilon_\nu^* - q_\nu\epsilon_\mu^*)$ . In the Standard Model  $C_{7R}^{\text{eff}} = \frac{m_s}{m_b}C_{7L}^{\text{eff}}$ . In the left-right symmetric models [193],  $C_{7R}^{\text{eff}}$  can be as large as  $C_{7L}^{\text{eff}}$  [194, 195, 196]. Using the branching ratio of  $B \rightarrow X_s\gamma$ , we can constrain  $|C_{7L}^{\text{eff}}|^2 + |C_{7R}^{\text{eff}}|^2$ .

Since the branching fraction does not tell us about the ratio  $C_{7R}^{\text{eff}}/C_{7L}^{\text{eff}}$ , the observables which are sensitive to the ratio are needed. Three methods using  $B$  meson decays have been proposed. One can extract the ratio from the time dependent CP asymmetry of  $b \rightarrow s\gamma$  [197]. Another measurement which is sensitive to the ratio is the transverse polarization of  $B \rightarrow K^*\gamma$  [198]. This can be measured by using the decay chains  $B \rightarrow K^*\gamma^* \rightarrow K\pi l^+l^-$  [199, 200]. The azimuthal angle distribution is sensitive to the ratio. The distribution at low invariant dilepton mass region must be measured so that the decay amplitude from a  $Z$  exchange and box diagram contribution is suppressed. The other method uses  $B \rightarrow K_{\text{res}}\gamma \rightarrow K\pi\pi\gamma$  and triple momentum correlation  $p_\gamma \cdot (p_K \times p_\pi)$  [201, 202].

We next consider the possible new physics effects on  $b \rightarrow s\ell^+\ell^-$ . In addition to  $C_7^{\text{eff}}$ , there are ten local four Fermi interactions which contribute to  $b \rightarrow s\ell^+\ell^-$ . One can write down the amplitude including all the contributions [190, 191]:

$$\begin{aligned} \mathcal{M}(b \rightarrow s\ell^+\ell^-) = & \frac{G_F\alpha}{\sqrt{2}\pi} V_{ts}^*V_{tb} \\ & \left[ (C_{LL} + C_9^{\text{eff}} - C_{10}) \bar{s}_L\gamma_\mu b_L \bar{\ell}_L\gamma^\mu l_L + (C_{LR} + C_9^{\text{eff}} + C_{10}) \bar{s}_L\gamma_\mu b_L \bar{\ell}_R\gamma^\mu l_R \right. \\ & + C_{RL} \bar{s}_R\gamma_\mu b_R \bar{\ell}_L\gamma^\mu l_L + C_{RR} \bar{s}_R\gamma_\mu b_R \bar{\ell}_R\gamma^\mu l_R \\ & + C_{LRLR} \bar{s}_L b_R \bar{\ell}_L l_R + C_{RLLR} \bar{s}_R b_L \bar{\ell}_L l_R \\ & + C_{LRRR} \bar{s}_L b_R \bar{\ell}_R l_L + C_{RLRL} \bar{s}_R b_L \bar{\ell}_R l_L \\ & + C_T \bar{s}\sigma_{\mu\nu}b \bar{\ell}\sigma^{\mu\nu}l + iC_{TE} \bar{s}\sigma_{\mu\nu}b \bar{\ell}\sigma_{\alpha\beta}l \epsilon^{\mu\nu\alpha\beta} \\ & \left. - 2m_b C_{7R}^{\text{eff}}(\bar{s}i\sigma_{\mu\nu}b_L)(\bar{\ell}\gamma^\mu l)\frac{q^\nu}{q^2} - 2m_b C_{7L}^{\text{eff}}(\bar{s}i\sigma_{\mu\nu}b_R)(\bar{\ell}\gamma^\mu l)\frac{q^\nu}{q^2} \right]. \quad (3.25) \end{aligned}$$

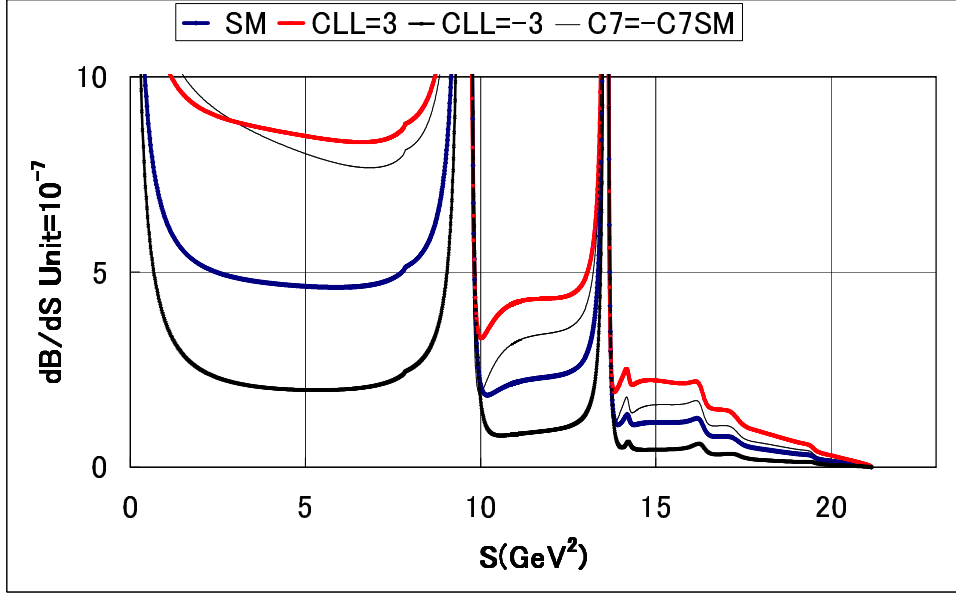


Figure 3.4: Differential branching ratio  $\frac{dB}{dS}$  for  $b \rightarrow s\ell^+\ell^-$ .

The Standard Model predicts to

$$(C_{LL}, C_{LR}, C_{RR}, C_{RL}, C_{RLRL}, C_{LRLR}, C_{LRRL}, C_{RLLR}) = 0, \quad (3.26)$$

$$(C_{7R}^{\text{eff}}, C_{7L}^{\text{eff}}) = \left(\frac{m_s}{m_b}, 1\right) C_{7SM}^{\text{eff}}, \quad (3.27)$$

$$(C_T, C_{TE}) = 0, \quad (3.28)$$

where  $(C_9^{\text{eff}}, C_{10}, C_{7SM}^{\text{eff}})$  are the Standard Model coefficients. The numerical values of the corresponding Wilson coefficients are  $C_9^{NDR} = 4.153$ ,  $C_{10} = -4.546$ ,  $C_{7SM}^{\text{eff}} = -0.311$ .  $C_9^{\text{eff}}$  is close to  $-C_{10}$ . Two-loop calculation has also been completed recently [203, 204]. Beyond the Standard Model, one-loop calculation of these Wilson coefficients is available for the Minimal Supersymmetric Standard Model (see, for example, [205] for a recent paper).

The branching ratio of  $b \rightarrow s\ell^+\ell^-$  is most sensitive to the coefficient  $C_{LL}$ , since the interference of the  $C_{LL}$  and  $C_9^{\text{eff}} - C_{10}$  is large. Depending on the sign of  $C_{LL}$ , the interference with the Standard Model contribution can be constructive or destructive.

In Figures 3.4 and 3.5, we show the differential branching ratio  $\frac{dB}{dS}$  and the forward-backward asymmetry  $\frac{dA}{ds}$ , respectively. We choose three sets of the coefficients and show dilepton mass squared ( $s$ ) distribution. The three cases correspond to: (1)  $C_{LL} = 3$ , (2)  $C_{LL} = -3$ , and (3)  $(C_{7R}^{\text{eff}}, C_{7L}^{\text{eff}}) = -(\frac{m_s}{m_b}, 1) C_{7SM}^{\text{eff}}$ . When  $C_{LL}$  is positive, the branching ratio is larger than the Standard Model value. If  $C_{LL}$  is negative, it decreases. If we change the sign of  $C_7$  compared with the Standard Model, the branching ratio also increases as in the case of  $C_{LL} > 0$ . The case (3) can be clearly distinguished from the Standard Model by studying the forward and backward asymmetry.

As shown in Figure 3.5, in the Standard Model there is a zero crossing point of the forward-backward asymmetry in the low invariant mass squared region. If the sign of  $C_{7L}$  is different from the Standard Model, the zero crossing point may disappear from the forward-backward asymmetry. Such a scenario is suggested in a supergravity model [206]. In another new physics model scenario including the down type SU(2) singlet quark, Z FCNC current may contribute to

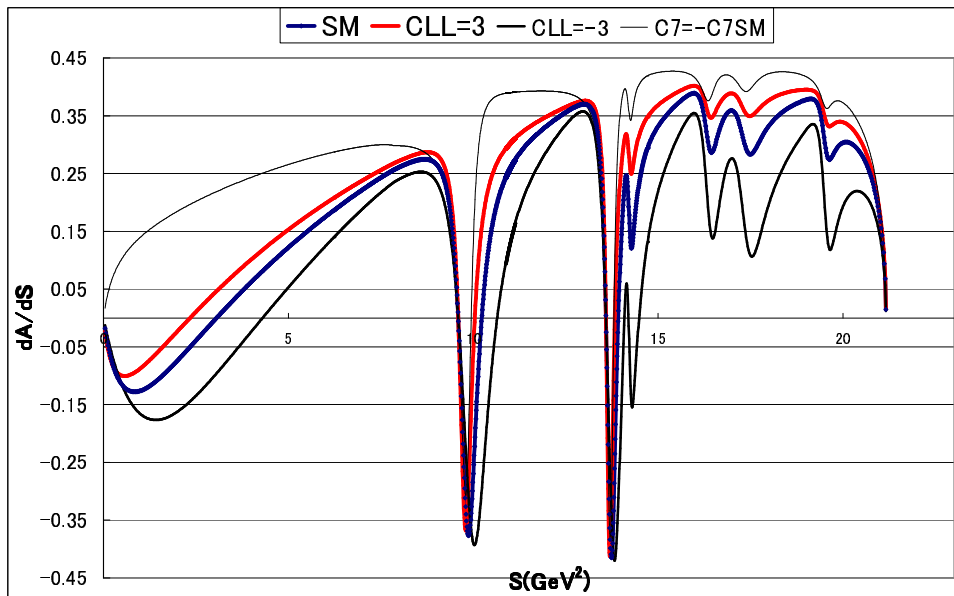


Figure 3.5: Forward-backward asymmetry  $\frac{dA}{ds}$  for  $b \rightarrow sl^+l^-$ .

$b \rightarrow sl^+l^-$  at the tree level. The tree level  $Z$  FCNC contribution may give a large contribution to  $C_{10}$  and can change the sign of the forward-backward asymmetry. Besides the observables mentioned above, the forward-backward CP asymmetry of  $b \rightarrow sl^+l^-$  is useful under the presence of new source of CP violation [207]. To conclude, with various observables and combination of them, we can test the new physics scenarios if they contribute to  $b \rightarrow sl^+l^-$  interactions.

### 3.6 Lepton Flavor Violation

Strictly speaking, the Standard Model already has to be modified by introducing tiny neutrino masses, in order to incorporate the Lepton Flavor Violating (LFV) phenomena observed in the neutrino sector. Neutrino mixing  $\nu_\mu$ - $\nu_\tau$  was first discovered in atmospheric neutrino measurements at Super-Kamiokande [208], and it is being further confirmed by the K2K experiment [209]. The neutrino oscillation was also confirmed in solar neutrinos, which come from  $\nu_e$ - $\nu_\mu$  mixing, by both the Super-Kamiokande [210] and SNO [211, 212] experiments. More recently, the Kamland experiment pinned down the explanation of the solar neutrino problem to the large mixing angle (LMA) solution [213]. Thus, neutrino oscillation experiments are providing high precision measurements in the neutrino sector. It is very interesting that the  $\nu_e$ - $\nu_\mu$  and  $\nu_\mu$ - $\nu_\tau$  mixing angles are found to be almost maximal and the neutrino mass structure is quite different from that of the quark sector.

Now it is known that lepton-flavor symmetries are not exact in Nature. However, the magnitude of LFV processes in the charged lepton sector is not obvious. The tiny neutrino masses do not lead to sizable LFV processes in the charged lepton sector, since the event rates are suppressed by the fourth power of  $(m_\nu/m_W)$ . Thus, searches for LFV in the charged lepton sector will probe physics beyond the Standard Model and the origin of the neutrino masses.

The  $\tau$  lepton is a member of the third generation and is the heaviest charged lepton. It can decay into quarks and leptons in the first and second generations. This may imply that  $\tau$  lepton physics could provide some clues to puzzles in the family structure. In fact, one naively expects

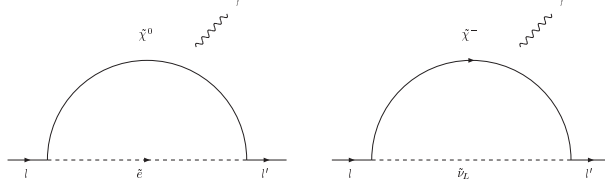


Figure 3.6: Feynman diagrams to generate  $l^- \rightarrow l'^- \gamma$  in the SUSY models with conserved R parity.  $\tilde{e}$ ,  $\tilde{\nu}$ ,  $\tilde{\chi}^0$  and  $\tilde{\chi}^-$  represent charged slepton, sneutrino, chargino, and neutralino, respectively.

the heavier quarks and leptons to be more sensitive to the dynamics responsible for fermion mass generation.

In the following we discuss LFV  $\tau$  lepton decay in SUSY models, especially in the supersymmetric seesaw mechanism and SUSY GUTs, and other models such as extra-dimension models and R-parity violating SUSY models.

### 3.6.1 LFV in the Supersymmetric Models

The LFV in the SUSY extension of the Standard Model comes from the soft SUSY breaking terms, since the supersymmetric interactions have the same flavor structure as in the Standard Model. The soft SUSY breaking terms in the lepton sector are as follows,

$$-\mathcal{L} = (m_E^2)_{ij} \tilde{e}_{Ri}^\dagger \tilde{e}_{Rj} + (m_L^2)_{ij} \tilde{l}_{Li}^\dagger \tilde{l}_{Lj} + \left\{ (A_e)_{ij} H_1 \tilde{e}_{Ri}^\dagger \tilde{l}_{Lj} + h.c. \right\} \quad (3.29)$$

where  $(m_E^2)_{ij}$  and  $(m_L^2)_{ij}$  are mass matrices for the right-handed sleptons  $\tilde{e}_{Rj}$  and the left-handed sleptons  $\tilde{l}_{Lj} (\equiv (\tilde{\nu}_{Lj}, \tilde{e}_{Lj}))$ , respectively.  $(A_e)_{ij}$  is the trilinear scalar coupling matrix.

LFV processes for charged leptons are radiative if R parity is conserved, since the SUSY interactions must be bilinears of the SUSY fields. Thus,  $\tau^- \rightarrow \mu^- (e^-) \gamma$  and  $\mu^- \rightarrow e^- \gamma$  are the most sensitive to the flavor structure of the soft SUSY breaking terms except for some exceptional cases. These processes are generated by diagrams in Figure 3.6. The effective operators relevant to  $l^- \rightarrow l'^- \gamma$  are flavor-violating magnetic moment operators,

$$\mathcal{H} = \sum_{l > l'} \frac{4G_F}{\sqrt{2}} \left[ m_l A_R^{ll'} \tilde{l} \sigma^{\mu\nu} P_R l' + m_l A_L^{ll'} \tilde{l} \sigma^{\mu\nu} P_L l' \right] F_{\mu\nu} + h.c., \quad (3.30)$$

where  $P_{L/R} = (1 \mp \gamma_5)/2$ , and the branching ratios are given as

$$Br(l^- \rightarrow l'^- \gamma) = 384\pi^2 (|A_R^{ll'}|^2 + |A_L^{ll'}|^2) Br(l^- \rightarrow l'^- \nu_l \bar{\nu}_{l'}). \quad (3.31)$$

Here,  $Br(\tau^- \rightarrow \mu^- (e^-) \nu_\tau \bar{\nu}_{\mu(e)}) \simeq 0.17$  and  $Br(\mu^- \rightarrow e^- \nu_\mu \bar{\nu}_e) = 1$ .

The coefficients in Eq. (3.30) are approximately given as

$$A_R^{\tau l'} = \frac{\sqrt{2}e}{4G_F} \frac{\alpha_Y}{4\pi} \frac{\tan \beta}{m_{SUSY}^2} \left[ -\frac{1}{120} \delta_{\tau l'}^R \right], \quad (3.32)$$

$$A_L^{\tau l'} = \frac{\sqrt{2}e}{4G_F} \frac{\alpha_2}{4\pi} \frac{\tan \beta}{m_{SUSY}^2} \left[ \left( \frac{1}{30} + \frac{t_W^2}{24} \right) \delta_{\tau l'}^L \right], \quad (3.33)$$

$$A_R^{\mu e} = \frac{\sqrt{2}e}{4G_F} \frac{\alpha_Y}{4\pi} \frac{\tan \beta}{m_{SUSY}^2} \left[ -\frac{1}{120} \delta_{\mu e}^R + \frac{1}{120} \delta_{\mu\tau}^R \delta_{\tau e}^R - \frac{1}{60} \frac{m_\tau}{m_\mu} \delta_{\mu\tau}^L \delta_{\tau e}^R \right], \quad (3.34)$$

$m_{SUSY}$	$ \delta_{\tau\mu}^L $	$ \delta_{\tau e}^L $	$ \delta_{\mu e}^L $	$ \delta_{\mu\tau}^L\delta_{\tau e}^L $	$ \delta_{\mu\tau}^R\delta_{\tau e}^L $
100 GeV	$2 \times 10^{-2}$	$2 \times 10^{-2}$	$4 \times 10^{-5}$	$1 \times 10^{-4}$ ( $3 \times 10^{-4}$ )	$2 \times 10^{-5}$ ( $7 \times 10^{-3}$ )
300 GeV	$2 \times 10^{-1}$	$2 \times 10^{-1}$	$4 \times 10^{-4}$	$9 \times 10^{-4}$ ( $3 \times 10^{-2}$ )	$2 \times 10^{-4}$ ( $6 \times 10^{-1}$ )
$m_{SUSY}$	$ \delta_{\tau\mu}^R $	$ \delta_{\tau e}^R $	$ \delta_{\mu e}^R $	$ \delta_{\mu\tau}^R\delta_{\tau e}^R $	$ \delta_{\mu\tau}^L\delta_{\tau e}^R $
100 GeV	$3 \times 10^{-1}$	$3 \times 10^{-1}$	$9 \times 10^{-4}$	$9 \times 10^{-4}$ ( $1 \times 10^{-1}$ )	$2 \times 10^{-5}$ ( $7 \times 10^{-3}$ )
300 GeV	3	3	$8 \times 10^{-3}$	$8 \times 10^{-3}$ (9)	$2 \times 10^{-4}$ ( $6 \times 10^{-1}$ )

Table 3.1: Constraints on  $\delta_{ll'}^R$  and  $\delta_{ll'}^L$  from current experimental bounds on  $Br(l^- \rightarrow l'^-\gamma)$ . Here, we use the results of the LFV tau decay search from the Belle experiment. We take  $\tan\beta = 10$  and  $m_{SUSY} = 100$  GeV and 300 GeV. The numbers in parentheses are derived from constraints on  $|\delta_{\tau\mu}^{(L/R)}|$  and  $|\delta_{\tau e}^{(L/R)}|$ .

$$A_L^{\mu e} = \frac{\sqrt{2}e}{4G_F} \frac{\alpha_2}{4\pi} \frac{\tan\beta}{m_{SUSY}^2} \left[ \left( \frac{1}{30} + \frac{t_W^2}{24} \right) \delta_{\mu e}^L - \left( \frac{1}{80} + \frac{7t_W^2}{240} \right) \delta_{\mu\tau}^L \delta_{\tau e}^L - \frac{t_W^2}{60} \frac{m_\tau}{m_\mu} \delta_{\mu\tau}^R \delta_{\tau e}^L \right], \quad (3.35)$$

assuming for simplicity that all SUSY particle masses are equal to  $m_{SUSY}$  and  $\tan\beta \gg 1$ . Here,  $t_W \equiv \tan\theta_W$ , where  $\theta_W$  is the Weinberg angle, and the mass insertion parameters are given as

$$\delta_{ll'}^R = \left( \frac{(m_E^2)_{ll'}}{m_{SUSY}^2} \right), \quad \delta_{ll'}^L = \left( \frac{(m_L^2)_{ll'}}{m_{SUSY}^2} \right). \quad (3.36)$$

When both the 13 and 23 generation components of the slepton mass matrices are non-vanishing,  $\mu^- \rightarrow e^- \gamma$  is generated via a scalar tau lepton exchange. In particular, if both the left-handed and right-handed mixings are sizable, the branching ratio is enhanced by  $(m_\tau/m_\mu)^2$  compared to the case where only left-handed or right-handed mixing angles are non-vanishing. The off-diagonal components in  $(A_e)_{ij}$  are sub-dominant in these processes since the contribution is not proportional to  $\tan\beta$ .

We list constraints on  $\delta_{ll'}^R$  and  $\delta_{ll'}^L$  from current experimental bounds on  $Br(\tau^- \rightarrow \mu^-(e^-)\gamma)$ , which are derived by the Belle experiment, and  $Br(\mu^- \rightarrow e^-\gamma)$  in Table 3.1. In this table, we take  $\tan\beta = 10$  and  $m_{SUSY} = 100$  GeV and 300 GeV. The constraints from  $\mu^- \rightarrow e^-\gamma$  on the slepton mixings are quite stringent. On the other hand, the current bounds on the LFV  $\tau$  lepton decay modes independently give sizable constraints on  $|\delta_{\tau\mu}^L|$  and  $|\delta_{\tau e}^L|$ . Furthermore, while the current constraint on  $|\delta_{\mu\tau}^L\delta_{\tau e}^L|$  from the LFV  $\tau$  lepton decay is weaker than that from the LFV muon decay, improvement of the LFV  $\tau$  lepton decay modes by about an order of magnitude will give a bound on  $|\delta_{\mu\tau}^L\delta_{\tau e}^L|$  competitive with that from the LFV muon decay.

The flavor structure of the soft SUSY breaking terms depends on the origin of the SUSY breaking and the physics beyond the MSSM, as discussed in Section 3.3. Even in the Universal scalar mass scenario, the LFV Yukawa interaction may induce LFV slepton mass terms radiatively. If the heavier leptons have larger LFV Yukawa interactions, the  $\tau$  lepton is the most sensitive to them. In the decoupling scenario, scalar  $\tau$  leptons may be much lighter than other sleptons and have LFV interactions. Thus, the search for LFV  $\tau$  lepton decay is important to



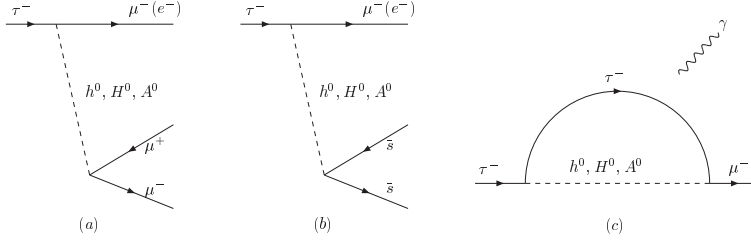


Figure 3.7: Feynman diagrams to generate (a)  $\tau^- \rightarrow \mu^-(e^-)\mu^+\mu^-$ , (b)  $\tau^- \rightarrow \mu^-(e^-)\eta$ , (c)  $\tau^- \rightarrow \mu^-(e^-)\mu^-\gamma$ , induced by anomalous Higgs boson couplings.

probe such new physics. In the next section we present predictions for the LFV  $\tau$  lepton decay in the SUSY seesaw model and SUSY GUTs.

Finally, we discuss other tau LFV processes in SUSY models. In a broader parameter space,  $\tau^- \rightarrow \mu^-(e^-)\gamma$  are the largest tau LFV processes, unless they are suppressed by some accidental cancellation or much heavier SUSY particle masses. The LFV  $\tau$  lepton decay modes to three leptons are dominantly induced by the photon-penguin contributions, and are correlated with  $\tau^- \rightarrow \mu^-(e^-)\gamma$  as follows

$$Br(\tau^- \rightarrow \mu^- e^+ e^-)/Br(\tau^- \rightarrow \mu^- \gamma) \simeq 1/94, \quad (3.37)$$

$$Br(\tau^- \rightarrow \mu^- \mu^+ \mu^-)/Br(\tau^- \rightarrow \mu^- \gamma) \simeq 1/440, \quad (3.38)$$

$$Br(\tau^- \rightarrow e^- e^+ e^-)/Br(\tau^- \rightarrow e^- \gamma) \simeq 1/94, \quad (3.39)$$

$$Br(\tau^- \rightarrow e^- \mu^+ \mu^-)/Br(\tau^- \rightarrow e^- \gamma) \simeq 1/440. \quad (3.40)$$

The LFV  $\tau$  decay modes into pseudoscalar mesons tend to be smaller than those to three leptons since the branching ratios are not proportional to  $\tan^2 \beta$ .

When sleptons are much heavier than the weak scale,  $Br(\tau^- \rightarrow \mu^-(e^-)\gamma)$  is suppressed. In this case, the modes  $\tau^- \rightarrow \mu^-(e^-)\mu^+\mu^-$  and  $\tau^- \rightarrow \mu^-(e^-)\eta$  induced by Higgs boson exchange become relatively important [214]. The LFV anomalous Yukawa coupling for the Higgs bosons is generated by radiative corrections, and it is not suppressed by powers of the slepton masses. While these processes are suppressed by a small Yukawa coupling constant for muons or strange quarks, they may acquire sizable branching ratios when  $\tan \beta$  is large since the branching ratios are proportional to  $\tan^6 \beta$ . When  $\delta_{\tau\mu}^L$  is non-vanishing, the approximate formula for  $Br(\tau^- \rightarrow \mu^- \mu^+ \mu^-)$  is given as [214, 215]

$$\begin{aligned} Br(\tau^- \rightarrow \mu^- \mu^+ \mu^-) &= \frac{m_\mu^2 m_\tau^2 \epsilon_2^2 |\delta_{\tau\mu}^L|^2}{8 \cos^6 \beta} Br(\tau^- \rightarrow \mu^- \nu_\tau \bar{\nu}_\mu) \\ &\times \left[ \left( \frac{\sin(\alpha - \beta) \cos \alpha}{M_{H^0}^2} - \frac{\cos(\alpha - \beta) \sin \alpha}{M_{h^0}^2} \right)^2 + \frac{\sin^2 \beta}{M_{A^0}^4} \right], \\ &\simeq 3.8 \times 10^{-7} \times |\delta_{\tau\mu}^L|^2 \left( \frac{\tan \beta}{60} \right)^6 \left( \frac{M_{A^0}}{100 \text{ GeV}} \right)^{-4}, \end{aligned} \quad (3.41)$$

and  $Br(\tau^- \rightarrow \mu^- \eta)$  is 8.4 times larger than  $Br(\tau^- \rightarrow \mu^- \mu^+ \mu^-)$  [216]. Here,  $\epsilon_2$  is a function of the SUSY particle masses. We take limits of large  $\tan \beta$  and equal SUSY breaking mass parameters in the last step (3.41). Notice that  $\tau^- \rightarrow \mu^- \gamma$  also has a comparable branching ratio to them since the Higgs loop diagram [Figure 3.7(c)] is enhanced by the  $\tau$  lepton Yukawa coupling constant [217]. As a result, the ratio of the branching ratios for these LFV  $\tau$  lepton

decay modes, which are induced by the Higgs boson exchange, is  $Br(\tau^- \rightarrow \mu^- \eta) : Br(\tau^- \rightarrow \mu^- \gamma) : Br(\tau^- \rightarrow \mu^- \mu^+ \mu^-) = 8.4 : 1.5 : 1$ .

### 3.6.2 SUSY Seesaw Mechanism and SUSY GUTs

In general, in seesaw and GUT models, LFV Yukawa interactions are introduced. If the SUSY breaking mediation scale is higher than the GUT [218, 219, 220] or the right-handed neutrino mass scale [221, 222, 223, 224], sizable LFV processes are predicted as mentioned in the previous section.

The most economical way to generate the tiny neutrino masses is the seesaw mechanism. In the seesaw model, a neutrino Yukawa coupling  $Y_\nu$  is introduced, which is lepton-flavor violating. In the supersymmetric extension, the off-diagonal components of the left-handed slepton mass matrix are radiatively induced, and they are approximately given by

$$(\delta m_L^2)_{ij} \simeq -\frac{1}{8\pi^2}(3m_0^2 + A_0^2) \sum_k (Y_\nu^\dagger)_{ki} (Y_\nu)_{kj} \log \frac{M_G}{M_{N_k}}, \quad (3.42)$$

where  $M_{N_i}$  are the  $i$ -th right-handed neutrino masses, and  $M_G$  is the Planck scale. Here we assume the gravity mediation scenario, and the parameters  $m_0$  and  $A_0$  are the universal scalar mass and the universal trilinear scalar coupling. The predicted small neutrino mass matrix is

$$(m_\nu)_{ij} = \sum_k \frac{(Y_\nu)_{ki} (Y_\nu)_{kj} \langle H_2 \rangle^2}{M_{N_k}}. \quad (3.43)$$

(3.42) has a different structure from (3.43). Thus, we may obtain independent information about the seesaw mechanism from the charged LFV searches and the neutrino oscillation experiments.

In Figure 3.8 we show  $Br(\tau^- \rightarrow \mu^- \gamma)$  and  $Br(\tau^- \rightarrow e^- \gamma)$  in the SUSY seesaw mechanism, assuming the gravity mediation scenario for the SUSY breaking. We fix the neutrino Yukawa coupling using the neutrino oscillation data under assumptions for the neutrino Yukawa coupling  $Y_\nu$ , which suppresses  $Br(\mu^- \rightarrow e^- \gamma)$ . The experimental bounds on these  $\tau$  processes have already excluded some of the parameter space. While a natural candidate for the largest LFV  $\tau$  lepton decay mode is  $\tau^- \rightarrow \mu^- \gamma$  from the atmospheric neutrino result, some model-parameters in the seesaw model predict larger  $Br(\tau^- \rightarrow e^- \gamma)$  [225]. This is because (3.42) and (3.43) have different dependences on  $Y_\nu$  and  $M_N$  as mentioned above.

In GUT models, even if the neutrino Yukawa contribution is negligible, LFV processes are predicted. In the  $SU(5)$  SUSY GUT, the right-handed charged leptons are embedded in the **10**-dimensional multiplets with the left-handed quarks and the right-handed up-type quarks. The LFV SUSY breaking terms for the right-handed sleptons are generated by the top-quark Yukawa coupling  $Y_t$  above the GUT scale. The off-diagonal components in the right-handed slepton mass matrix are given as

$$(\delta m_E^2)_{ij} \simeq -\frac{3}{8\pi^2}(3m_0^2 + A_0^2) V_{i3} V_{j3}^* |Y_t|^2 \log \frac{M_G}{M_{\text{GUT}}}, \quad (3.44)$$

where  $V_{ij}$  is the CKM matrix in the SUSY  $SU(5)$  GUT and  $M_{\text{GUT}}$  is the GUT scale.

In the minimal  $SU(5)$  SUSY GUT, in which the neutrino Yukawa coupling is negligible,  $Br(\tau^- \rightarrow \mu^- \gamma)$  is smaller than  $10^{-(9-10)}$ . While the process is enhanced by the top-quark Yukawa coupling, it is suppressed by the CKM matrix element and the  $U(1)_Y$  gauge coupling constant. Furthermore, when the right-handed sleptons have LFV mass terms, an accidental cancellation among the diagrams tends to suppress the branching ratio. However, we notice that

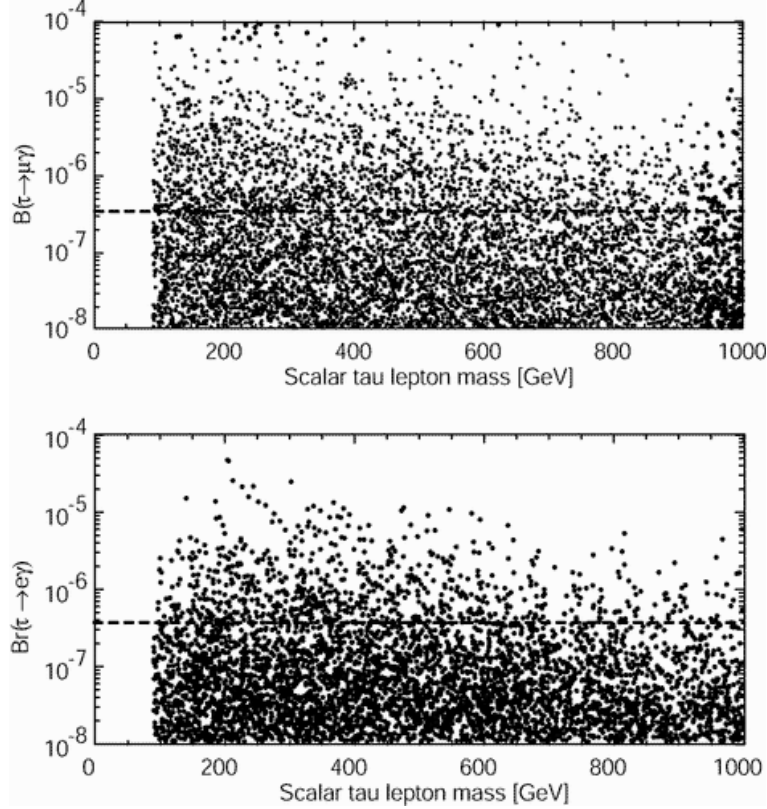


Figure 3.8:  $Br(\tau^- \rightarrow \mu^- \gamma)$  and  $Br(\tau^- \rightarrow e^- \gamma)$  in the SUSY seesaw mechanism, assuming the gravity mediation scenario for the SUSY breaking. Dashed lines show the current experimental bounds from the Belle experiment. Here, we take  $\tan \beta = 30$ , the  $SU(2)_L$  gaugino mass 200 GeV,  $A_0 = 0$ , and positive Higgsino mass. We fix the neutrino Yukawa coupling by using the neutrino oscillation data under assumptions of the neutrino Yukawa coupling.

the CKM matrix elements at the GUT scale may not be the same as ones extrapolated from the low energy data. This is because the quark and lepton mass ratios are not well explained in this model. If  $V_{32}$  is larger, the processes are enhanced [226, 227].

### 3.6.3 Other Theoretical Models

In the previous subsections we discussed LFV  $\tau$  lepton decays in SUSY models assuming that R parity is conserved. In this subsection we review some examples of other models which predict LFV  $\tau$  lepton decays.

In extra-dimension models [146, 147] the “fundamental” scale is expected to be comparable to the weak scale, and the classical seesaw mechanism does not explain the tiny neutrino masses. Instead, singlet neutrinos in the bulk space are introduced [228, 229, 230]. The Yukawa couplings of the left-handed neutrinos with the bulk neutrinos are suppressed by an overlap of the wave functions, and small Dirac neutrino masses are predicted.

In this model the loop diagrams from the Kaluza-Klein states of the bulk neutrinos generate the LFV  $\tau$  lepton and  $\mu$  decay [231, 232]. On the other hand, this model is constrained by short baseline experiments and charged current universality, since the kinetic mixing term for neutrinos is not negligible. In the minimal model, in which the unique source of LFV is the Yukawa coupling of the left-handed neutrinos with the bulk neutrinos,  $Br(\tau^- \rightarrow \mu^- \gamma) \lesssim 10^{-9}$  from the existing constraints, while  $Br(\mu^- \rightarrow e^- \gamma) \lesssim 10^{-(11-13)}$  depending on  $U_{e3}$  [232]. In the non-minimal case, the constraints may be looser.

In R-parity violating SUSY models, there exist lepton flavor and baryon number non-conserving interactions at the tree level. Proton stability gives stringent bounds on such models, as well as other processes, such as the decays of charged leptons and  $B$  and  $D$  mesons, neutral current processes, and FCNC processes. Since the  $\tau$  lepton is the heaviest lepton, various  $\tau$  LFV modes can be induced. These include  $\tau^- \rightarrow \mu^- \mu^+ \mu^-$ ,  $\mu^- e^+ e^-$ ,  $\mu^+ e^- e^-$  and  $\tau^- \rightarrow \mu^- M^0$ ,  $\mu^- V^0$ . Here,  $M^0$  and  $V^0$  are pseudoscalar and vector mesons, respectively. Comprehensive studies of LFV  $\tau$  lepton decay have been performed in [233].

If the masses of the right-handed neutrinos are  $O(1 - 10)$  TeV in the seesaw mechanism, sizable LFV  $\tau$  lepton decay might be possible [234]. It is found in [235] that  $Br(\tau^- \rightarrow \mu^- \gamma)$  and  $Br(\tau^- \rightarrow \mu^- \mu^+ \mu^-)$  are smaller than  $10^{-9}$  and  $10^{-10}$ , respectively. It is also argued that  $Br(\tau^- \rightarrow e^- \gamma)$  and  $Br(\tau^- \rightarrow e^- e^+ e^-)$  can reach  $10^{-8}$  and  $10^{-9}$ , respectively, in various models [235].

## Chapter 4

# Sensitivity at SuperKEKB

### 4.1 Overview

#### 4.1.1 Goals of sensitivity studies

As described in Chapter 1, the primary purpose of SuperKEKB is to perform a comprehensive study of  $B$  decays governed by quark transitions induced by quantum loops, where sizable effects from physics beyond the Standard Model are expected. If the study leads to a conclusion that an observed pattern is inconsistent with the Standard Model expectation, we further proceed to identify underlying flavor structure.

One of major goals of sensitivity studies is to clarify the meaning of the statement above quantitatively. To this end, we estimate statistical, systematic and theoretical errors on key observables at SuperKEKB. The target luminosity of SuperKEKB is  $5 \times 10^{35} \text{ cm}^{-2}\text{s}^{-1}$ , which corresponds to an annual integrated luminosity of  $5 \text{ ab}^{-1}$  assuming 100 days of operation (i.e. the Snowmass year definition). Therefore we estimate expected errors at  $5 \text{ ab}^{-1}$  to describe what will be achieved at an early stage of the SuperKEKB experiment. We also provide errors at  $50 \text{ ab}^{-1}$  as ultimate measurements that can be performed at SuperKEKB. Although this looks rather ambitious, our experience at the Belle experiment tells that an integrated luminosity that is 10 times as large as a target annual luminosity is not a mere dream.

There are a huge number of observables that can be measured at SuperKEKB. It is not the main purpose of our sensitivity studies to cover all of them. Instead, our strategy is to concentrate on observables that are indispensable to reach the primary goal mentioned above. The following points are considered to select such observables:

- A sizable deviation from a prediction of the Standard Model is expected.
- A hadronic uncertainty is negligible or very small.
- A measurement at SuperKEKB is (much) superior to others, in particular to LHCb, whose expected physics performance is regarded as the benchmark of next-generation  $B$  physics programs at hadron colliders.

Selected topics do not necessarily satisfy all of these criteria, but do have clear advantages over others not covered in this chapter.

At SuperKEKB we expect a background level that is about 20 times larger than what we currently observe at Belle. Our investigation leads to a conclusion that under such conditions there is a feasible detector design that guarantees performance equivalent to the present Belle detector. Therefore, throughout our studies, we assume a detector that has the same performance

as the present Belle detector unless otherwise noticed. Any possible gain from an improved detector performance is regarded as a bonus, and our aim is to demonstrate that most of physics goals at SuperKEKB are achieved even without any improvement in the detector performance. One important exception, however, is  $B$  meson vertex reconstruction using the  $K_S^0$ . Here we clearly need to introduce a larger vertex detector to increase vertex reconstruction efficiencies. Therefore we incorporate the proposed detector design in this case.

One of the biggest advantages of the sensitivity studies for Super-KEKB compared with those for hadron collider experiments is that we can fully utilize information obtained by analyzing Belle data. In particular, many of studies described in this chapter rely on Monte Carlo pseudo-experiments (also called “toy Monte Carlo experiments”) in which PDFs are constructed from data. A clear advantage of this approach over genuine Monte Carlo simulations (e.g. GEANT simulation) is that background fractions and detector resolutions are more reliable. For some topics for which pseudo-experiments are not available, however, we also use GEANT simulation and/or FSIM, a parametric Monte Carlo simulator that requires much less CPU power than GEANT.

In the rest of this section we overview two important analysis techniques that are used repeatedly in our studies. One is the procedure to fit a proper-time difference distribution for a time-dependent  $CP$  asymmetry measurement. The other is to reconstruct one  $B$  meson exclusively (or semi-inclusively) so as to study decays of an accompanying  $B$  meson in the cleanest environment. This is called “full reconstruction  $B$  tagging”.

#### 4.1.2 Time-dependent $CP$ asymmetries

In the decay chain  $\Upsilon(4S) \rightarrow B^0 \bar{B}^0 \rightarrow f_{CP} f_{\text{tag}}$ , where one of the  $B$  mesons decays at time  $t_{CP}$  to a final state  $f_{CP}$  and the other decays at time  $t_{\text{tag}}$  to a final state  $f_{\text{tag}}$  that distinguishes between  $B^0$  and  $\bar{B}^0$ , the decay rate has a time dependence given by [67, 68, 69]

$$\mathcal{P}(\Delta t) = \frac{e^{-|\Delta t|/\tau_{B^0}}}{4\tau_{B^0}} \left\{ 1 + q \cdot [\mathcal{S} \sin(\Delta m_d \Delta t) + \mathcal{A} \cos(\Delta m_d \Delta t)] \right\}, \quad (4.1)$$

where  $\tau_{B^0}$  is the  $B^0$  lifetime,  $\Delta m_d$  is the mass difference between the two  $B^0$  mass eigenstates,  $\Delta t = t_{CP} - t_{\text{tag}}$ , and the  $b$ -flavor charge  $q = +1$  ( $-1$ ) when the tagging  $B$  meson is a  $B^0$  ( $\bar{B}^0$ ).  $\mathcal{S}$  and  $\mathcal{A}$  are  $CP$ -violation parameters. For example, to a good approximation, the Standard Model predicts  $\mathcal{S} = -\xi_f \sin 2\phi_1$ , where  $\xi_f = +1$  ( $-1$ ) corresponds to  $CP$ -even ( $-$ odd) final states, and  $\mathcal{A} = 0$  for both  $b \rightarrow c\bar{c}s$  and  $b \rightarrow s\bar{s}s$  transitions.

We determine  $q$  and  $\Delta t$  for each event. Charged leptons, pions, kaons, and  $\Lambda$  baryons that are not associated with a reconstructed  $CP$  eigenstate decay are used to identify the  $b$ -flavor of the accompanying  $B$  meson. The tagging algorithm is described in detail elsewhere [6]. We use two parameters,  $q$  and  $r$ , to represent the tagging information. The first,  $q$ , is already defined above. The parameter  $r$  is an event-by-event Monte Carlo-determined flavor-tagging dilution parameter that ranges from  $r = 0$  for no flavor discrimination to  $r = 1$  for an unambiguous flavor assignment. It is used only to sort data into six intervals of  $r$ , according to estimated flavor purity. We determine directly from data the average wrong-tag probabilities,  $w_l \equiv (w_l^+ + w_l^-)/2$  ( $l = 1, 6$ ), and differences between  $B^0$  and  $\bar{B}^0$  decays,  $\Delta w_l \equiv w_l^+ - w_l^-$ , where  $w_l^{+(-)}$  is the wrong-tag probability for the  $B^0$  ( $\bar{B}^0$ ) decay in each  $r$  interval. The event fractions and wrong-tag fractions are summarized in Table 4.1. The total effective tagging efficiency is determined to be  $\epsilon_{\text{eff}} \equiv \sum_{l=1}^6 \epsilon_l (1 - 2w_l)^2 = 0.287 \pm 0.005$ , where  $\epsilon_l$  is the event fraction for each  $r$  interval. The error includes both statistical and systematic uncertainties.

$l$	$r$ interval	$\epsilon_l$	$w_l$	$\Delta w_l$	$\epsilon_{\text{eff}}^l$
1	0.000 – 0.250	0.398	$0.464 \pm 0.006$	$-0.011 \pm 0.006$	$0.002 \pm 0.001$
2	0.250 – 0.500	0.146	$0.331 \pm 0.008$	$+0.004 \pm 0.010$	$0.017 \pm 0.002$
3	0.500 – 0.625	0.104	$0.231 \pm 0.009$	$-0.011 \pm 0.010$	$0.030 \pm 0.002$
4	0.625 – 0.750	0.122	$0.163 \pm 0.008$	$-0.007 \pm 0.009$	$0.055 \pm 0.003$
5	0.750 – 0.875	0.094	$0.109 \pm 0.007$	$+0.016 \pm 0.009$	$0.057 \pm 0.002$
6	0.875 – 1.000	0.136	$0.020 \pm 0.005$	$+0.003 \pm 0.006$	$0.126 \pm 0.003$

Table 4.1: The event fractions  $\epsilon_l$ , wrong-tag fractions  $w_l$ , wrong-tag fraction differences  $\Delta w_l$ , and average effective tagging efficiencies  $\epsilon_{\text{eff}}^l = \epsilon_l(1 - 2w_l)^2$  for each  $r$  interval. The errors include both statistical and systematic uncertainties. The event fractions are obtained from the  $J/\psi K_S^0$  simulation.

The vertex position for the  $f_{CP}$  decay is reconstructed using leptons from  $J/\psi$  decays or charged hadrons from  $\eta_c$  decays, and that for  $f_{\text{tag}}$  is obtained with well reconstructed tracks that are not assigned to  $f_{CP}$ . Tracks that are consistent with coming from a  $K_S^0 \rightarrow \pi^+\pi^-$  decay are not used. Each vertex position is required to be consistent with the interaction region profile, determined run-by-run, smeared in the  $r$ - $\phi$  plane to account for the  $B$  meson decay length. With these requirements, we are able to determine a vertex even with a single track; the fraction of single-track vertices is about 10% for  $z_{CP}$  and 22% for  $z_{\text{tag}}$ . The proper-time interval resolution function  $R_{\text{sig}}(\Delta t)$  is formed by convolving four components: the detector resolutions for  $z_{CP}$  and  $z_{\text{tag}}$ , the shift in the  $z_{\text{tag}}$  vertex position due to secondary tracks originating from charmed particle decays, and the kinematic approximation that the  $B$  mesons are at rest in the cms [236]. A small component of broad outliers in the  $\Delta z$  distribution, caused by mis-reconstruction, is represented by a Gaussian function. We determine fourteen resolution parameters from the aforementioned fit to the control samples. We find that the average  $\Delta t$  resolution is  $\sim 1.43$  ps (rms). The width of the outlier component is determined to be  $(39 \pm 2)$  ps; the fractions of the outlier components are  $(2.1 \pm 0.6) \times 10^{-4}$  for events with both vertices reconstructed with more than one track, and  $(3.1 \pm 0.1) \times 10^{-2}$  for events with at least one single-track vertex.

We determine  $\mathcal{S}$  and  $\mathcal{A}$  for each mode by performing an unbinned maximum-likelihood fit to the observed  $\Delta t$  distribution. The probability density function (PDF) expected for the signal distribution,  $\mathcal{P}_{\text{sig}}(\Delta t; \mathcal{S}, \mathcal{A}, q, w_l, \Delta w_l)$ , is given by Eq. (4.1) incorporating the effect of incorrect flavor assignment. The distribution is also convolved with the proper-time interval resolution function  $R_{\text{sig}}(\Delta t)$ , which takes into account the finite vertex resolution. We determine the following likelihood value for each event:

$$\begin{aligned}
P_i &= (1 - f_{\text{ol}}) \int_{-\infty}^{\infty} \left[ f_{\text{sig}} \mathcal{P}_{\text{sig}}(\Delta t') R_{\text{sig}}(\Delta t_i - \Delta t') \right. \\
&\quad \left. + (1 - f_{\text{sig}}) \mathcal{P}_{\text{bkg}}(\Delta t') R_{\text{bkg}}(\Delta t_i - \Delta t') \right] d(\Delta t') \\
&\quad + f_{\text{ol}} P_{\text{ol}}(\Delta t_i)
\end{aligned} \tag{4.2}$$

where  $P_{\text{ol}}(\Delta t)$  is a broad Gaussian function that represents an outlier component with a small fraction  $f_{\text{ol}}$ . The signal probability  $f_{\text{sig}}$  depends on the  $r$  region and is calculated on an event-by-event basis as a function of  $\Delta E$  and  $M_{\text{bc}}$ .  $\mathcal{P}_{\text{bkg}}(\Delta t)$  is a PDF for background events, which is modeled as a sum of exponential and prompt components, and is convolved with a sum of two Gaussians  $R_{\text{bkg}}$ . All parameters in  $\mathcal{P}_{\text{bkg}}(\Delta t)$  and  $R_{\text{bkg}}$  are determined by the fit to the  $\Delta t$  distribution of a background-enhanced control sample; i.e. events away from the  $\Delta E$ - $M_{\text{bc}}$  signal

Decay mode	Motivation
$B \rightarrow X_u l \nu$	Precise measurement of $ V_{ub} $
$B \rightarrow \tau \nu$	Measurement of $f_B$
$B \rightarrow K \nu \bar{\nu}, D \tau \nu$	Search for new physics
Inclusive $B$ decays	Detailed study, model independent analysis etc.

Table 4.2: Physics topics that will be studied with the fully-reconstructed  $B$  sample.

region. We fix  $\tau_{B^0}$  and  $\Delta m_d$  at their world-average values. The only free parameters in the final fit are  $\mathcal{S}$  and  $\mathcal{A}$ , which are determined by maximizing the likelihood function  $L = \prod_i P_i(\Delta t_i; \mathcal{S}, \mathcal{A})$  where the product is over all events.

### 4.1.3 $B$ tagging with full reconstruction

At SuperKEKB,  $B\bar{B}$  meson pairs will be produced from  $\Upsilon(4S)$  decays. To study  $B$  meson decays that include neutrinos, photons,  $\pi^0$  mesons in the final states, it is useful to tag one of the  $B$  mesons through the full reconstruction. This method has the following attractive features:

- The momentum vector and flavor of the other  $B$  meson can be identified, *i.e.* single  $B$  meson beams can practically be obtained offline.
- Continuum and combinatoric  $B\bar{B}$  backgrounds can be significantly reduced.

If we take advantage of these features, it will be possible to measure the  $B$  decays listed in Table 4.2. Some of these decays have more than one neutrino in the final states. Therefore, it is very difficult to perform such studies even in the clean environment of  $e^+e^-$  collider unless the full reconstruction  $B$  tagging is applied.

Because of the modest full reconstruction efficiency [ $\mathcal{O}(0.1\%)$ ], this method has not been extensively applied at the current  $B$  factory experiments. However, a very large  $B$  meson sample at SuperKEKB will make it possible to extract useful results.

### Hadronic $B$ Tagging

Most  $B$  meson decays are hadronic decays. However, the branching fraction of each mode is less than  $\mathcal{O}(1\%)$ . Therefore, we need to collect as many modes as possible to achieve a high efficiency. In Fig. 4.1, the beam-constrained mass distribution for the main decay modes,  $B \rightarrow D^{(*)}(\pi, \rho, a_1)^-$ , are shown. The yields including other decay modes are also shown in Table 4.3. With a 152 million  $B\bar{B}$  sample, we already have a sample of more than  $10^5$  fully-reconstructed  $B$  meson tags. The tagging efficiency is 0.20% (0.09%) for charged (neutral)  $B$  mesons with a purity of 78% (83%) [237].

The tagging efficiency can be improved largely by loosening selection criteria. In this case, however, the purity becomes lower. Therefore the best selection criteria should be searched for in each analysis. In the case of hadronic  $B$  tagging mentioned above, we achieve a tagging efficiency of 0.33% (0.20%) for charged (neutral)  $B$  mesons with a purity of 58% (52%).

If a  $B$  meson is reconstructed semi-inclusively, we can further improve the efficiency. At BaBar, the  $B \rightarrow D^{(*)}(n_1\pi^\pm n_2 K^\pm n_3 K_S n_4 \pi^0)^-$  process is reconstructed, where  $n_1 + n_2 \leq 5$ ,  $n_3 \leq 2$  and  $n_4 \leq 2$ . As a result, the higher efficiency, 0.5 (0.3) % for charged (neutral)  $B$  mesons, is obtained. However, due to combinatoric backgrounds, the purity is only around



	decay mode	yield	eff. (%)	purity(%)
Charged B	$B^- \rightarrow D^{(*)0}(\pi, \rho, a_1)^-$	132723	0.17	79
	$B^- \rightarrow D^{(*)0} D_s^{(*)-}$	8700	0.01	60
	$B^- \rightarrow J/\psi K^-$	9373	0.01	96
	total	150796	0.20	78
Neutral B	$B^0 \rightarrow D^{(*)+}(\pi, \rho, a_1)^-$	56898	0.07	85
	$B^0 \rightarrow D^{(*)+} D_s^{(*)-}$	4390	0.006	60
	$B^0 \rightarrow (J/\psi, \psi(2s), \chi_{c1}) K_S, J/\psi K^{*0}$	7275	0.01	94
	total	68563	0.09	83

Table 4.3: Full reconstructed  $B$  events for hadronic modes with 152 million  $B\bar{B}$  sample.

25 %. These samples are used for the  $|V_{ub}|$  measurement using  $B \rightarrow X_u l \nu$  decays, where the background can be reduced by requiring a lepton in the recoil side [238, 239].

### Semileptonic $B$ tagging

If we use semileptonic  $B$  decays to tag one  $B$  meson, we cannot use information about the  $B$  momentum vector due to the missing neutrino. However, we still have relatively clean tagged samples. Semileptonic  $B$  decays are dominated by  $B \rightarrow D l \nu$  and  $D^* l \nu$ , with a total branching fraction of around 15%. At Belle, these samples were used for a  $|V_{ub}|$  measurement with inclusive  $B \rightarrow X_u l \nu$  decays. If we require a semileptonic decay on the recoil side, we can apply a kinematical constraint, and the  $B$  momentum vector can be determined with a two-fold ambiguity. The background contribution is significantly suppressed in this case. This method yields a  $B \rightarrow D^* l \nu$  efficiency of 0.3 (0.2)% for charged (neutral)  $B$  decays [240].

It is also notable that we include other  $B \rightarrow D X l \nu$  decays as  $B$  tags in the  $D l \nu$  mode, because the signal in the missing mass spectrum is too broad for separation. The missing mass distribution for  $B^- \rightarrow D^0 l \nu$  is shown in Fig. 4.2. The full reconstruction tagging efficiency is estimated to be 1.7% including the contribution from the  $B^- \rightarrow D^{(*)0} l \nu$  decays of around 15% [237]. Other background is mostly combinatoric. Although the tagging quality is not good in this case, it is still useful for the study of rare  $B$  decays with low track multiplicities in the final states. In BaBar, this method was used to search for the  $B \rightarrow K \nu \bar{\nu}$  and  $\tau \nu$  decays [241, 242] to provide improved upper limits.

### Conclusions

In summary, the tagging efficiency will be around 0.2% (0.1%) for the clean hadronic tagging for charged (neutral)  $B$  mesons, and around 1% for the semileptonic  $B$  tagging that has a lower purity. The efficiency for the hadronic tagging can be around 0.3% (0.2%) if we loosen the selection criteria, with a tolerable decrease in the purity of the tagging.

With a  $1 \text{ ab}^{-1}$  of data, there will be at least 2 million clean tags and around 10 million semileptonic tags. With these samples, the physics topics listed in Table 4.2 will be studied.

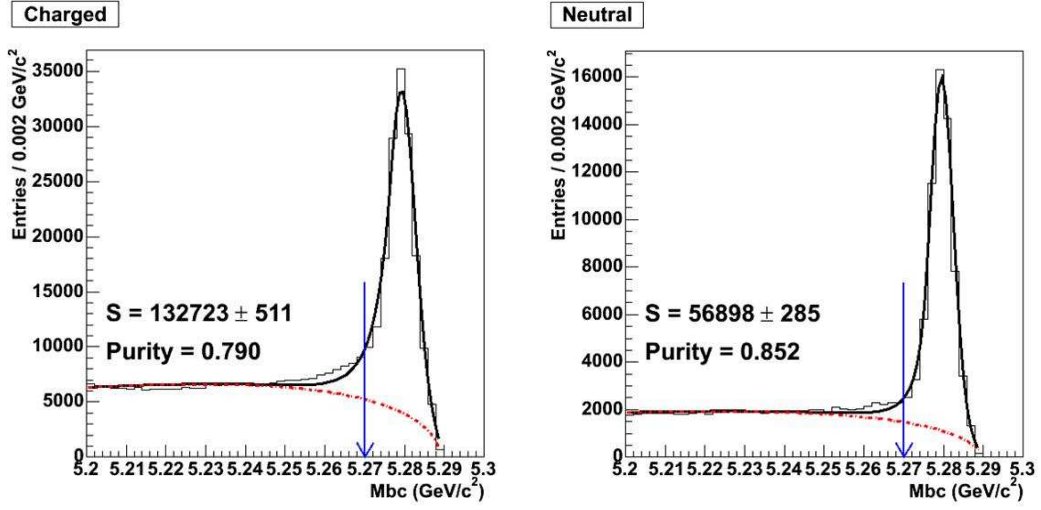


Figure 4.1: Beam-constrained mass distribution for  $B \rightarrow D^{(*)}(\pi, \rho, a_1)^-$  with the 152 million  $B\bar{B}$  sample recorded by Belle.

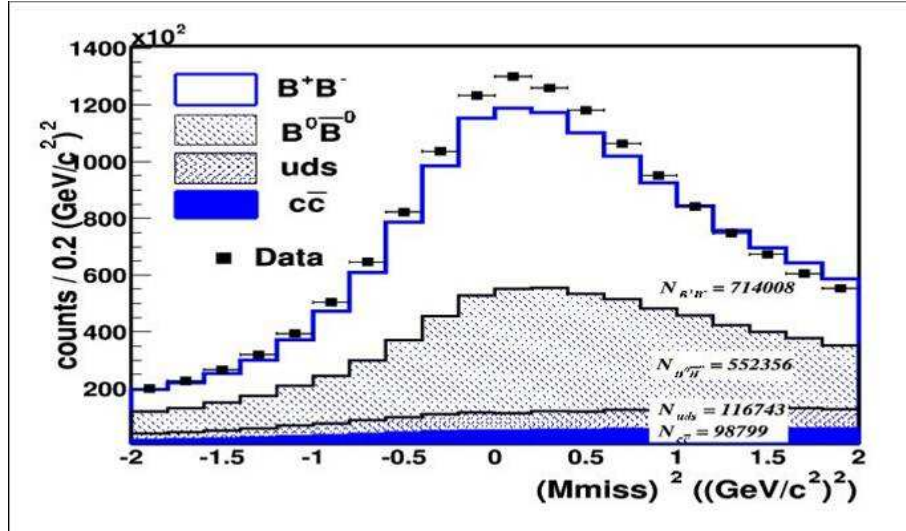


Figure 4.2: Missing mass squared distribution for  $B^- \rightarrow D^0 l \nu$  with a sample of  $85 \times 10^6$   $B\bar{B}$  pairs.

## 4.2 New $CP$ -violating phase in $b \rightarrow s\bar{q}q$

### 4.2.1 Introduction

Despite the great success of the KM mechanism, additional  $CP$ -violating phases are inevitable in most theories involving new physics (NP) beyond the SM [243]. Some of them allow large deviations from the SM predictions for  $B$  meson decays. Examples include supersymmetric grand-unified theories with the see-saw mechanism that can accommodate large neutrino mixing [170, 244, 175]. Therefore it is of fundamental importance to measure  $CP$  asymmetries that are sensitive to the difference between the SM and NP. Additional sources of  $CP$  violation are also highly desirable to understand the origin of the matter-antimatter asymmetry of the universe; detailed studies have found no way that  $CP$  violation in the SM alone could explain baryogenesis [245]. Many methods to search for a new source of  $CP$  violation in  $B$  meson decays have been proposed up to now. One of the most promising ways is to compare the mixing-induced  $CP$  asymmetries in the  $B \rightarrow \phi K_S^0$  decay [25], which is dominated by the  $b \rightarrow s\bar{s}s$  transition that is known to be sensitive to possible NP effects, with those in the  $B^0 \rightarrow J/\psi K_S^0$  decay [68, 69]. Ignoring a strong phase difference between the amplitude of NP ( $A_{\text{NP}}$ ) and SM ( $A_{\text{SM}}$ )<sup>1</sup>, we obtain

$$\mathcal{S}_{\phi K_S^0} = \frac{\sin 2\phi_1 + 2\rho \sin(2\phi_1 + \Theta_{\text{NP}}) + \rho^2 \sin(2\phi_1 + 2\Theta_{\text{NP}})}{1 + \rho^2 + 2\rho \cos \Theta_{\text{NP}}}, \quad (4.3)$$

where  $\rho \equiv A_{\text{NP}}/A_{\text{SM}}$  is an amplitude ratio of NP to the SM. Since  $\mathcal{S}_{J/\psi K_S^0} \simeq \sin 2\phi_1$  is expected in many extensions of the SM, the difference  $\Delta\mathcal{S}_{\phi K_S^0} \equiv (-\xi_f)\mathcal{S}_{\phi K_S^0} - \mathcal{S}_{J/\psi K_S^0}$  is a gold-plated observable to search for a new  $CP$ -violating phase.

Recent measurements by Belle [21] and BaBar [29] collaborations yield values smaller than the SM expectation; a difference by 2.6 standard deviations is obtained when two results are combined. The other charmless decays  $B^0 \rightarrow \eta' K_S^0$  and  $B^0 \rightarrow K^+ K^- K_S^0$ , which are mediated by  $b \rightarrow s\bar{s}s$ ,  $s\bar{u}u$  and  $s\bar{d}d$  transitions, also provide additional information [21, 29]. The present world average (as of August 2003) with  $B^0 \rightarrow \phi K_S^0$ ,  $\eta' K_S^0$  and  $K^+ K^- K_S^0$  combined is different from the average with  $B^0 \rightarrow J/\psi K_S^0$  and related modes by 3.1 standard deviations [246] as shown in Figure 4.3. Possible theoretical implications of these measurements are already discussed in Section 3.4.

In this section we describe the expected sensitivities for  $\mathcal{S}(\phi K_S^0)$ ,  $\mathcal{S}(\eta' K_S^0)$  and  $\mathcal{S}(K^+ K^- K_S^0)$  based on the measurements performed with the present Belle detector. It will be crucial to measure as many observables as possible and to check correlations among them. Therefore we also describe several other new methods to access a new  $CP$ -violating phase in the  $b \rightarrow s$  transition.

### 4.2.2 $B^0 \rightarrow \phi K_S^0$ , $\eta' K_S^0$ and $K^+ K^- K_S^0$

As mentioned in the previous section, the  $B^0 \rightarrow \phi K_S^0$  decay is one of the most promising decays in which to search for a new  $CP$ -violating phase in  $b \rightarrow s\bar{s}s$  transitions. The other charmless decays  $B^0 \rightarrow \eta' K_S^0$  and  $B^0 \rightarrow K^+ K^- K_S^0$  provide additional information. As most of the experimental procedure for these three modes is common, we discuss them here together. Note that the theoretical uncertainties for  $\Delta\mathcal{S}$  within the SM depend on the decay mode. We discuss this issue in Section 4.2.5. Note also that the three-body decay  $B^0 \rightarrow K^+ K^- K_S^0$  is in general a mixture of  $CP$ -even and  $CP$ -odd eigenstates. The Belle collaboration finds that the  $K^+ K^- K_S^0$  state is primarily  $\xi_f = +1$ ; a measurement of the  $\xi_f = +1$  fraction with a  $140 \text{ fb}^{-1}$  data set

<sup>1</sup>The formula with the strong phase is given in Section 3.4 [Eq. (3.10)].

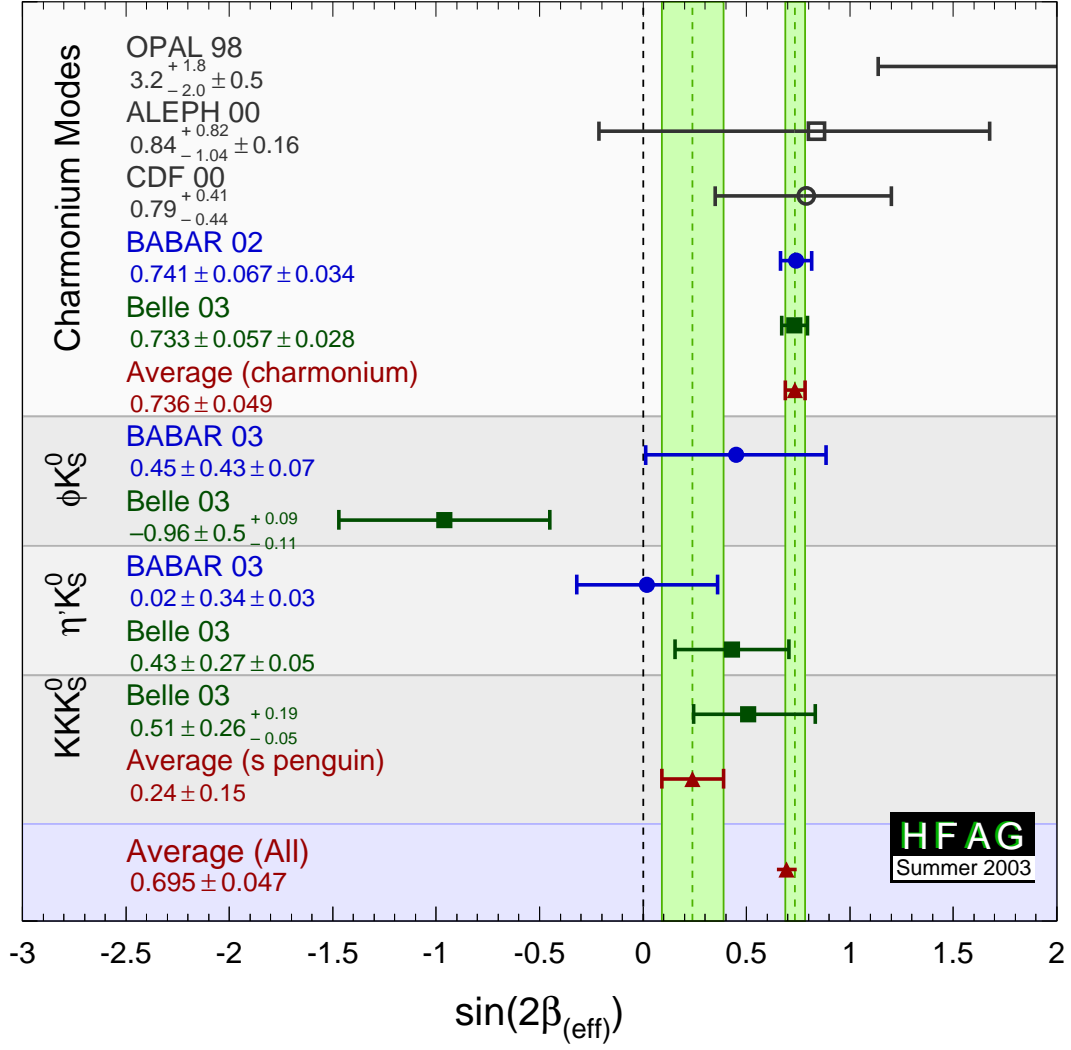


Figure 4.3:  $\mathcal{S}$  terms measured with decay modes governed by  $b \rightarrow c\bar{c}s$  or  $b \rightarrow s\bar{s}s$  transitions.

yields  $1.03 \pm 0.15(\text{stat}) \pm 0.05(\text{syst})$  [21]. The uncertainty in the  $CP$ -asymmetry parameters, which arises from the  $\xi_f = -1$  component, is included in the systematic error.

We estimate the expected sensitivities at SuperKEKB by extrapolating the present experimental results. Therefore we first explain Belle's analysis with a data sample of  $140 \text{ fb}^{-1}$  [21].

We reconstruct  $B^0$  decays to  $\phi K_S^0$  and  $\eta' K_S^0$  final states for  $\xi_f = -1$ , and  $B^0 \rightarrow K^+ K^- K_S^0$  decays that are a mixture of  $\xi_f = +1$  and  $-1$ .  $K^+ K^-$  pairs that are consistent with  $\phi \rightarrow K^+ K^-$  decay are excluded from the  $B^0 \rightarrow K^+ K^- K_S^0$  sample. We find that the  $K^+ K^- K_S^0$  state is primarily  $\xi_f = +1$ ; a measurement of the  $\xi_f = +1$  fraction with a  $140 \text{ fb}^{-1}$  data set yields  $1.03 \pm 0.15(\text{stat}) \pm 0.05(\text{syst})$ . In the following determination of  $\mathcal{S}$  and  $\mathcal{A}$ , we fix  $\xi_f = +1$  for this mode. The intermediate meson states are reconstructed from the following decay chains:  $\eta' \rightarrow \rho^0(\rightarrow \pi^+ \pi^-) \gamma$  or  $\eta' \rightarrow \pi^+ \pi^- \eta(\rightarrow \gamma \gamma)$ ,  $K_S^0 \rightarrow \pi^+ \pi^-$ , and  $\phi \rightarrow K^+ K^-$ .

Pairs of oppositely charged tracks are used to reconstruct  $K_S^0 \rightarrow \pi^+ \pi^-$  decays. The  $\pi^+ \pi^-$  vertex is required to be displaced from the IP by a minimum transverse distance of 0.22 cm for high momentum ( $> 1.5 \text{ GeV}/c$ ) candidates and 0.08 cm for those with momentum less than  $1.5 \text{ GeV}/c$ . The direction of the pion pair momentum must agree with the direction defined by the IP and the vertex displacement within 0.03 rad for high-momentum candidates, and within 0.1 rad for the remaining candidates.

Candidate  $\phi \rightarrow K^+ K^-$  decays are found by selecting pairs of oppositely charged tracks that are not pion-like ( $P(K/\pi) > 0.1$ ), where a kaon likelihood ratio,  $P(K/\pi) = \mathcal{L}_K/(\mathcal{L}_K + \mathcal{L}_\pi)$ , has values between 0 (likely to be a pion) and 1 (likely to be a kaon). The likelihood  $\mathcal{L}_{K(\pi)}$  is derived from  $dE/dx$ , ACC and TOF measurements. The vertex of the candidate charged tracks is required to be consistent with the interaction point (IP) to suppress poorly measured tracks. In addition, candidates are required to have a  $K^+ K^-$  invariant mass that is less than  $10 \text{ MeV}/c^2$  from the nominal  $\phi$  meson mass.

Since the  $\phi$  meson selection is effective in reducing background events, we impose only minimal kaon-identification requirements. We use more stringent kaon-identification requirements to select non-resonant  $K^+ K^-$  candidates for the  $B^0 \rightarrow K^+ K^- K_S^0$  decay. We reject  $K^+ K^-$  pairs that are consistent with  $D^0 \rightarrow K^+ K^-$ ,  $\chi_{c0} \rightarrow K^+ K^-$ , or  $J/\psi \rightarrow K^+ K^-$  decay.  $D^+ \rightarrow K_S^0 K^+$  candidates are also removed.

To reconstruct  $\eta'$  candidates, we first require that all of the tracks have associated SVD hits and radial impact parameters  $|dr| < 0.1 \text{ cm}$  projected on the  $r$ - $\phi$  plane. Particle identification information from the ACC, TOF and CDC  $dE/dx$  measurements are used to form a likelihood ratio in order to distinguish pions from kaons with at least  $2.5\sigma$  separation for laboratory momenta up to  $3.5 \text{ GeV}/c$ . Candidate photons from  $\eta_{\gamma\gamma}$  ( $\eta'_{\rho\gamma}$ ) decays are required to be isolated and have  $E_\gamma > 50$  (100) MeV from the ECL measurement. The invariant mass of  $\eta_{\gamma\gamma}$  candidates is required to be between  $500 \text{ MeV}/c^2$  and  $570 \text{ MeV}/c^2$ . A kinematic fit with an  $\eta$  mass constraint is performed using the fitted vertex of the  $\pi^+ \pi^-$  tracks from the  $\eta'$  as the decay point. For  $\eta'_{\rho\gamma}$  decays, the candidate  $\rho^0$  mesons are reconstructed from pairs of vertex-constrained  $\pi^+ \pi^-$  tracks with an invariant mass between 550 and  $920 \text{ MeV}/c^2$ . The  $\eta'$  candidates are required to have a reconstructed mass from 940 to  $970 \text{ MeV}/c^2$  for the  $\eta'_{\eta\pi\pi}$  mode and 935 to  $975 \text{ MeV}/c^2$  for  $\eta'_{\rho\gamma}$  mode. Charged  $K^\pm$  candidates are selected for the decay  $B^\pm \rightarrow \eta' K^\pm$  based on the particle identification information.

We also reconstruct events where only one of the charged pions has associated SVD hits. In this case, the requirement on the impact parameter is relaxed for the track without SVD hits, while a higher threshold is imposed on the likelihood ratio.

For reconstructed  $B \rightarrow f_{CP}$  candidates, we identify  $B$  meson decays using the energy difference  $\Delta E \equiv E_B^{\text{cms}} - E_{\text{beam}}^{\text{cms}}$  and the beam-energy constrained mass  $M_{\text{bc}} \equiv \sqrt{(E_{\text{beam}}^{\text{cms}})^2 - (p_B^{\text{cms}})^2}$ , where  $E_{\text{beam}}^{\text{cms}}$  is the beam energy in the cms, and  $E_B^{\text{cms}}$  and  $p_B^{\text{cms}}$  are the cms energy and mo-

Mode	$\xi_f$	$N_{\text{sig}}$	Purity	Statistical error	
				$\mathcal{S}$	$\mathcal{A}$
$\phi K_S^0$	-1	2400	0.64	0.074	0.051
$K^+ K^- K_S^0$	+1(100%)	7100	0.55	0.040	0.028
$\eta' K_S^0$	-1	8700	0.58	0.042	0.028

Table 4.4: Expected numbers of  $B^0 \rightarrow f_{CP}$  signal events,  $N_{\text{sig}}$ , and estimated signal purities in the  $\Delta E$ - $M_{\text{bc}}$  signal region for each  $f_{CP}$  mode at  $5 \text{ ab}^{-1}$ .

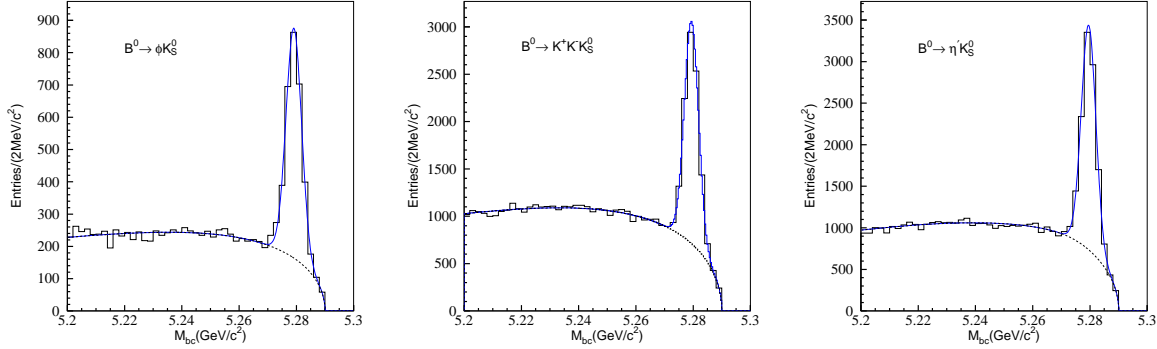


Figure 4.4: Beam-constrained mass ( $M_{\text{bc}}$ ) distributions for (left)  $B^0 \rightarrow \phi K_S^0$ , (middle)  $B^0 \rightarrow K^+ K^- K_S^0$ , and (right)  $B^0 \rightarrow \eta' K_S^0$  decays within the  $\Delta E$  signal region expected at  $5 \text{ ab}^{-1}$ . Solid curves show results of fits to signal plus background distributions, and dashed curves show the background contributions.

momentum of the reconstructed  $B$  candidate, respectively. The  $B$  meson signal region is defined as  $|\Delta E| < 0.06 \text{ GeV}$  for  $B^0 \rightarrow \phi K_S^0$ ,  $|\Delta E| < 0.04 \text{ GeV}$  for  $B^0 \rightarrow K^+ K^- K_S^0$ ,  $|\Delta E| < 0.06 \text{ GeV}$  for  $B^0 \rightarrow \eta'(\rightarrow \rho\gamma) K_S^0$ , or  $-0.10 \text{ GeV} < \Delta E < 0.08 \text{ GeV}$  for  $B^0 \rightarrow \eta'(\rightarrow \pi^+ \pi^- \eta) K_S^0$ , and  $5.27 \text{ GeV}/c^2 < M_{\text{bc}} < 5.29 \text{ GeV}/c^2$  for all decays. In order to suppress background from the  $e^+ e^- \rightarrow u\bar{u}, d\bar{d}, s\bar{s}, \text{ or } c\bar{c}$  continuum, we form signal and background likelihood functions,  $\mathcal{L}_S$  and  $\mathcal{L}_{\text{BG}}$ , from a set of variables that characterize the event topology, and impose thresholds on the likelihood ratio  $\mathcal{L}_S/(\mathcal{L}_S + \mathcal{L}_{\text{BG}})$ . The threshold value depends both on the decay mode and on the flavor-tagging quality.

The vertex reconstruction, flavor tagging and the unbinned maximum likelihood fit to the  $\Delta t$  distributions are the same as those described for the  $\sin 2\phi_1$  measurement (Section 4.6) with  $B^0 \rightarrow J/\psi K_S^0$  decays. By using the identical procedure for both cases, we can reduce the systematic uncertainties in the differences  $\Delta \mathcal{S}_{\phi K_S^0} \equiv \mathcal{S}_{\phi K_S^0} - \mathcal{S}_{J/\psi K_S^0}$  etc.

After flavor tagging and vertex reconstruction, we expect the signal yields and the purities listed in Table 4.4.

Figure 4.4 shows the  $M_{\text{bc}}$  distributions for the reconstructed  $B$  candidates that have  $\Delta E$  values within the signal region.

Unbinned maximum likelihood fits yield expected statistical errors on  $\mathcal{S}$  and  $\mathcal{A}$  shown also in Table 4.4. It is seen that errors are rather small even for these rare  $B$  decays. Hence systematic uncertainties become crucial.

Major sources of the systematic uncertainties on  $\mathcal{S}$  and  $\mathcal{A}$  are common to those for  $B^0 \rightarrow$

Mode	5 ab <sup>-1</sup>		50 ab <sup>-1</sup>	
	$\Delta\mathcal{S}$	$\Delta\mathcal{A}$	$\Delta\mathcal{S}$	$\Delta\mathcal{A}$
$\phi K_S^0$	0.079	0.055	0.031	0.024
$K^+K^-K_S^0$	0.056	0.036	0.026	0.020
$\eta' K_S^0$	0.049	0.035	0.024	0.019

Table 4.5: Expected total errors on  $\Delta\mathcal{S}$  and  $\Delta\mathcal{A}$  at 5 ab<sup>-1</sup> and 50 ab<sup>-1</sup>.

$J/\psi K_S^0$ , which will be described in Section 4.6. For the  $K^+K^-K_S^0$  mode, the  $CP$ -even fraction is expected to be determined more precisely as the integrated luminosity increases. Therefore we assume that the systematic uncertainty due to the uncertainty in the  $CP$ -even fraction is *reducible*; *e.g.* it is proportional to  $1/\sqrt{\mathcal{L}_{\text{tot}}}$ . An additional systematic error for  $B^0 \rightarrow \phi K_S^0$  arises from the  $B^0 \rightarrow f_0 K_S^0$  and  $K^+K^-K_S^0$  backgrounds. These background fractions are estimated at 140 fb<sup>-1</sup> from the  $K^+K^-$  invariant mass distribution to be  $1.6^{+1.9}_{-1.5}\%$  and  $7.2 \pm 1.7\%$ , respectively. We assume that the errors on these fractions will be reduced as the integrated luminosity increases. We also assume that the  $CP$ -violating parameters for these decays are also determined experimentally with errors that will also decrease as the integrated luminosity increases. Therefore, the systematic errors on  $\mathcal{S}$  and  $\mathcal{A}$  due to these backgrounds are also assumed to be *reducible*.

Some of the systematic errors cancel when we calculate  $\Delta\mathcal{A}$  or  $\Delta\mathcal{S}$ . For example, the effect of the tag-side interference cancels in  $\Delta\mathcal{A}_{\phi K_S^0}$  and  $\Delta\mathcal{S}_{\phi K_S^0}$  since it causes a bias in the same direction for  $\mathcal{S}_{\phi K_S^0}$  and  $\mathcal{S}_{J/\psi K_S^0}$  measurements. On the other hand, a special care on the systematic bias from the tag-side interference needs to be taken for  $\Delta\mathcal{A}_{K^+K^-K_S^0}$ . In this case, the effect does not cancel because the bias has the opposite sign to each other. We use information from  $B^0 \rightarrow J/\psi K_L^0$  decays to reduce this uncertainty on  $\Delta\mathcal{A}_{K^+K^-K_S^0}$ .

Figure 4.5 shows the resulting total errors on  $\Delta\mathcal{S}$  and  $\Delta\mathcal{A}$  as a function of integrated luminosity. Table 4.5 also shows the corresponding values at 5 ab<sup>-1</sup> and 50 ab<sup>-1</sup>.

Based on the above estimates, we perform Feldman-Cousins analyses to obtain 5 $\sigma$  discovery regions at 5 ab<sup>-1</sup> and at 50 ab<sup>-1</sup> in the 2-dimensional plane of  $\mathcal{A}$  and  $\mathcal{S}$ . Results are shown in Figure 4.6. At SuperKEKB, even a small deviation of  $\Delta\mathcal{S} \sim 0.1$  can be established with a 5 $\sigma$  significance as far as the statistical and systematic errors are concerned. Therefore it is important to understand levels of theoretical uncertainties within the SM very well. This issue will be discussed in Section 4.2.5.

### 4.2.3 $B^0 \rightarrow K_S^0 K_S^0 K_S^0$ and $\pi^0 K_S^0$

In this section we discuss the feasibility of time-dependent  $CP$  asymmetry measurements using only a  $K_S^0$  and a constraint from the interaction point to determine the  $B$  decay vertices. In particular, we consider  $B^0 \rightarrow K_S^0 K_S^0 K_S^0$  and  $\pi^0 K_S^0$  decays as the most promising modes in this class of decays to study a new  $CP$ -violating phase in  $b \rightarrow s$  transitions (another important mode  $B^0 \rightarrow K^{*0}(\rightarrow K_S^0 \pi^0)\gamma$  is discussed in Sec. 4.3.5). Recently, the BaBar collaboration has succeeded in measuring the  $B$  decay vertex in  $B^0 \rightarrow K_S^0 \pi^0$  [247]. The possibility of obtaining  $B$  vertex information from  $K_S^0$  mesons makes time-dependent analyses of these decays feasible.

Recently it was pointed out [248] that in decays of the type  $B^0 \rightarrow P^0 Q^0 X^0$ , where  $P^0$ ,  $Q^0$  and  $X^0$  represent any  $CP$  eigenstate spin-0 neutral particles, the final state is a  $CP$  eigenstate. First we give a brief proof of this statement. In what follows,  $L$  denotes the angular momentum of the  $P^0 Q^0$  system, and  $L'$  denotes the angular momentum of  $X^0$  relative to the  $P^0 Q^0$  system.

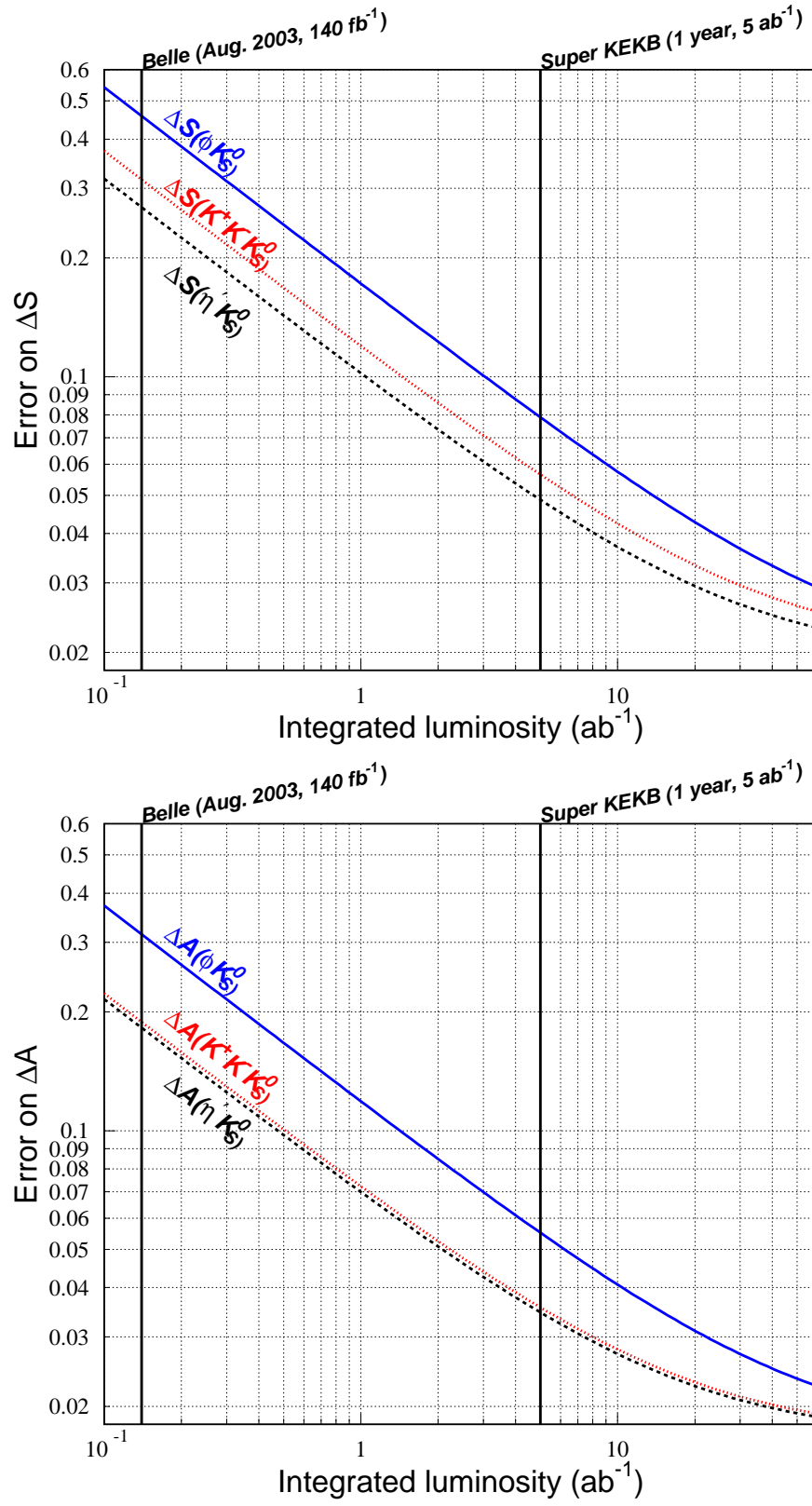


Figure 4.5: Expected total errors on  $\Delta S$  (top) and  $\Delta A$  (bottom) as a function of integrated luminosity.



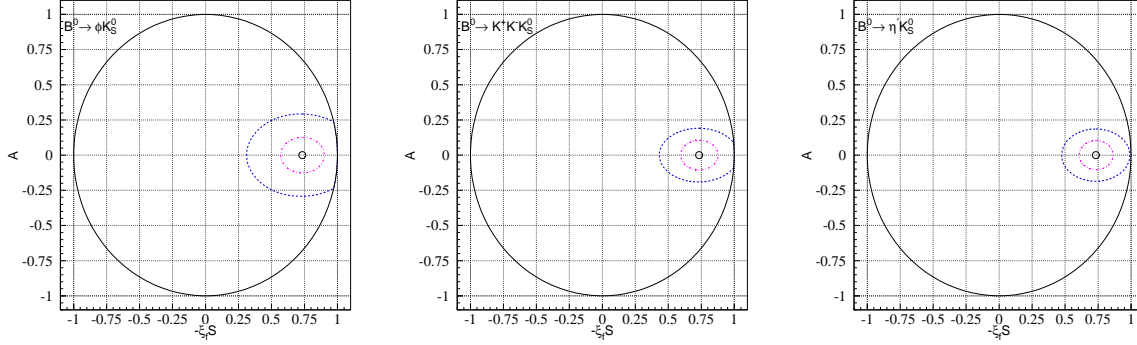


Figure 4.6:  $5\sigma$  confidence regions for  $\mathcal{A}$  and  $\mathcal{S}$  in (left)  $B^0 \rightarrow \phi K_S^0$ , (middle)  $B^0 \rightarrow K^+ K^- K_S^0$  and (right)  $B^0 \rightarrow \eta' K_S^0$  decays at  $5 \text{ ab}^{-1}$  and  $50 \text{ ab}^{-1}$ . Input values are  $\mathcal{S} = 0.73$  and  $\mathcal{A} = 0$ .

By conservation of angular momentum in the decay  $B^0 \rightarrow P^0 Q^0 X^0$ , we obtain

$$\mathbf{J}_{B^0} = \mathbf{L} + \mathbf{L}' + \mathbf{S}_{P^0} + \mathbf{S}_{Q^0} + \mathbf{S}_{X^0} \quad (4.4)$$

$$\mathbf{0} = \mathbf{L} + \mathbf{L}', \quad (4.5)$$

since the neutral  $B$  meson is a spin-0 particle, as are  $P^0$ ,  $Q^0$  and  $X^0$ . In the above equations,  $\mathbf{J}$ ,  $\mathbf{L}$  and  $\mathbf{S}$  represent the total, orbital and intrinsic angular momentum, respectively (and elsewhere  $J$ ,  $L$  and  $S$  represent their magnitudes). Therefore, the angular momentum between the  $P^0 Q^0$  system and  $X^0$  ( $L'$ ) must be equal to  $L$ , and we can write down the  $CP$  of the  $P^0 P^0 X^0$  system:

$$CP(P^0 Q^0 X^0) = CP(P^0) \times CP(Q^0) \times CP(X^0) \times (-1)^L \times (-1)^{L'} \quad (4.6)$$

$$= CP(P^0) \times CP(Q^0) \times CP(X^0). \quad (4.7)$$

Thus there are many three-body  $B$  decays that can be used in time-dependent  $CP$  asymmetry measurements *without any angular analysis*. In particular, the decay  $B^0 \rightarrow K_S^0 K_S^0 K_S^0$  is promising. In terms of phenomenology, it has an advantage over  $B^0 \rightarrow K^+ K^- K_S^0$ , since the latter includes a contribution from the  $b \rightarrow u$  tree diagram, which has a different weak phase. Although this contribution (“tree pollution”) is expected to be small as will be discussed in Section 4.2.5, it might be an issue at SuperKEKB. In the case of  $B^0 \rightarrow K_S^0 K_S^0 K_S^0$ , however, there is no  $u$  quark in the final state. The  $b \rightarrow s\bar{u}u$  tree diagram followed by rescattering into  $s\bar{d}d$  or  $s\bar{s}s$  is OZI-suppressed. Therefore these are almost pure penguin decays. There can be contributions from both  $b \rightarrow s\bar{s}s$  with additional  $d\bar{d}$  production, and  $b \rightarrow s\bar{d}d$  with additional  $s\bar{s}$  production, but these diagrams have the same weak phase. Any new physics contribution expected in the  $B^0 \rightarrow \phi K_S^0$  decay can also affect  $B^0 \rightarrow K_S^0 K_S^0 K_S^0$ , and in the absence of new physics it should exhibit the same  $CP$  violating effects as  $J/\psi K_S^0$ .

Turning to experimental considerations, we note that this mode has been observed at Belle [30]. From  $78 \text{ fb}^{-1}$  of data recorded on the  $\Upsilon(4S)$  resonance,  $12.2_{-3.8}^{+4.5}$  signal events are found. From Figure 4.7 (left), we can count the number of candidates in the region  $-0.1 \text{ GeV} < \Delta E < 0.1 \text{ GeV}$ , to estimate the signal purity. There are 21 candidates in this region giving a purity of  $\sim 0.6$ , which is approximately the same purity as  $\eta' K_S^0$ . The efficiency to reconstruct a  $K_S^0$  vertex reflects the probability for the  $K_S^0$  to decay inside the vertex detector, and so depends on the  $K_S^0$  momentum and on the size of the vertex detector. In a three body

$B^0 \rightarrow K_S^0 K_S^0 K_S^0$  decay, at least one  $K_S^0$  must have fairly low momentum in the  $B^0$  rest frame. Therefore, we expect a high vertex efficiency for  $B^0 \rightarrow K_S^0 K_S^0 K_S^0$ , if the vertex efficiency for  $B^0 \rightarrow K_S^0 \pi^0$  (where the  $K_S^0$  has high momentum) is moderate. In the time-dependent analysis of  $B^0 \rightarrow K_S^0 \pi^0$  by the BaBar collaboration, a vertex efficiency of 65% is obtained [247]. Since the size of SuperKEKB vertex detector is comparable to the BaBar SVT, we expect that vertex efficiencies for  $B^0 \rightarrow K_S^0 K_S^0 K_S^0$  of close to 100% may be obtained. Using these assumptions, we estimate the statistical error on  $\mathcal{S}_{K_S^0 K_S^0 K_S^0}$  to be

$$\begin{aligned}\delta\mathcal{S}_{K_S^0 K_S^0 K_S^0} &= 0.14 \text{ (at } 5 \text{ ab}^{-1}\text{)} \\ \delta\mathcal{S}_{K_S^0 K_S^0 K_S^0} &= 0.04 \text{ (at } 50 \text{ ab}^{-1}\text{)}.\end{aligned}\tag{4.8}$$

The authors of [249] claim that  $K_S \pi^0$  is one of the gold-plated modes to study a new  $CP$ -violating phase in the  $b \rightarrow s$  transition. As mentioned before, the BaBar group recently showed a preliminary result on the time-dependent  $CP$  asymmetries in this decay, demonstrating the feasibility of measuring the  $B$  meson decay point using only a  $K_S^0$  and the interaction point constraint.

Belle's result based on  $78 \text{ fb}^{-1}$  of data is shown in Figure 4.7 (right). The signal yield is  $72.6 \pm 14.0$ . Since this estimation includes the tail region in the  $\Delta E$  distribution where rare  $B$  decay backgrounds are not negligible, a more stringent selection is necessary for the time-dependent  $CP$  asymmetry measurements. Using  $|\Delta E| < 0.1 \text{ GeV}$  and assuming a vertex reconstruction efficiency of 50%, the signal yield with reconstructed vertices at  $5 \text{ ab}^{-1}$  is  $\sim 1900$  for a purity of 0.46. Based on these numbers, we obtain

$$\begin{aligned}\delta\mathcal{S}_{\pi^0 K_S^0} &= 0.10 \text{ (at } 5 \text{ ab}^{-1}\text{)} \\ \delta\mathcal{S}_{\pi^0 K_S^0} &= 0.03 \text{ (at } 50 \text{ ab}^{-1}\text{)}.\end{aligned}\tag{4.9}$$

#### 4.2.4 $B^\pm \rightarrow \phi\phi X_s^\pm$

In this section we discuss a new method to study direct  $CP$  violation that arises from a new  $CP$ -violating phase in  $B^\pm \rightarrow \phi\phi X_s^\pm$  decays [251]. Here  $X_s^\pm$  represents a final state with a specific strange flavor such as  $K^\pm$  or  $K^{*\pm}$ . These non-resonant direct decay amplitudes are dominated by the  $b \rightarrow s\bar{s}s\bar{s}$  transition. A contribution from the  $b \rightarrow u\bar{u}s$  transition followed by rescattering into  $s\bar{s}s$  is expected to be below 1% because of CKM suppression and the OZI rule [251]. In these decays, when the invariant mass of the  $\phi\phi$  system is within the  $\eta_c$  resonance region, they interfere with the  $B^\pm \rightarrow \eta_c(\rightarrow \phi\phi)X_s^\pm$  decay that is dominated by the  $b \rightarrow c\bar{c}s$  transition. The decay width of  $\eta_c$  is sufficiently large [58, 252] to provide a sizable interference. Within the SM, this interference does not cause sizable direct  $CP$  violation because there is no weak phase difference between the  $b \rightarrow s\bar{s}s\bar{s}$  and the  $b \rightarrow c\bar{c}s$  transitions. On the other hand, a NP contribution with a new  $CP$ -violating phase can create a large weak phase difference. Thus large  $CP$  asymmetries can appear only from NP amplitudes, and an observation of direct  $CP$  violation in these decays is an unambiguous manifestation of physics beyond the SM.

Although the same argument so far is applicable to the  $B^\pm \rightarrow \phi X_s^\pm$  decays, there is no guaranteed strong phase difference that is calculable reliably for these decays. In contrast, the Breit-Wigner resonance provides the maximal strong phase difference in the case of  $B^\pm \rightarrow (\phi\phi)_{m \sim m_{\eta_c}} X_s^\pm$  decays. Since present experimental knowledge of the decay rate for  $b \rightarrow s\bar{s}s$  is still limited, a large  $CP$  asymmetry up to 0.4 is allowed.

The Belle Collaboration recently announced evidence for  $B \rightarrow \phi\phi K$  decays [253]. The signal purity is close to 100% when the  $\phi\phi$  invariant mass is within the  $\eta_c$  mass region. Belle [252]

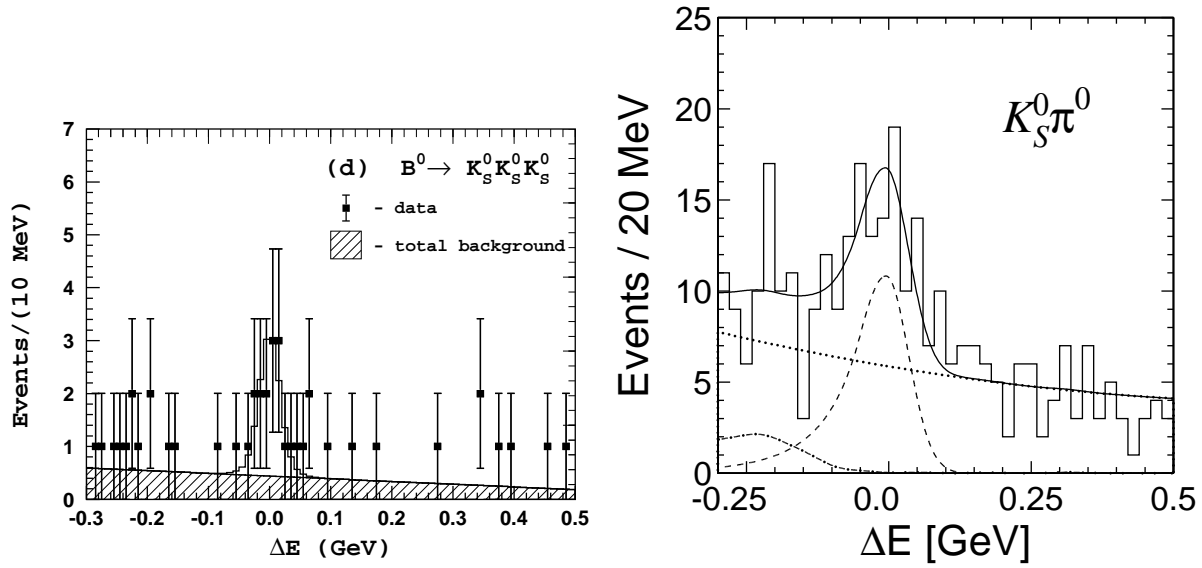


Figure 4.7: (left) Observation of  $B^0 \rightarrow K_S^0 K_S^0 K_S^0$  [30]. From  $78 \text{ fb}^{-1}$  of data recorded on the  $\Upsilon(4S)$  resonance, a signal yield of  $12.2^{+4.5}_{-3.8}$  is obtained, leading to a branching fraction of  $\mathcal{B}(B^0 \rightarrow K_S^0 K_S^0 K_S^0) = (4.2^{+1.6}_{-1.3} \pm 0.8) \times 10^{-6}$ . (right) Observation of  $B^0 \rightarrow K_S^0 \pi^0$  [250]. From  $78 \text{ fb}^{-1}$  of data recorded on the  $\Upsilon(4S)$  resonance, a signal yield of  $72.6 \pm 14.0$  is obtained, leading to a branching fraction of  $\mathcal{B}(B^0 \rightarrow K_S^0 K_S^0 K_S^0) = (11.7 \pm 2.3^{+1.2}_{-1.3}) \times 10^{-6}$ .

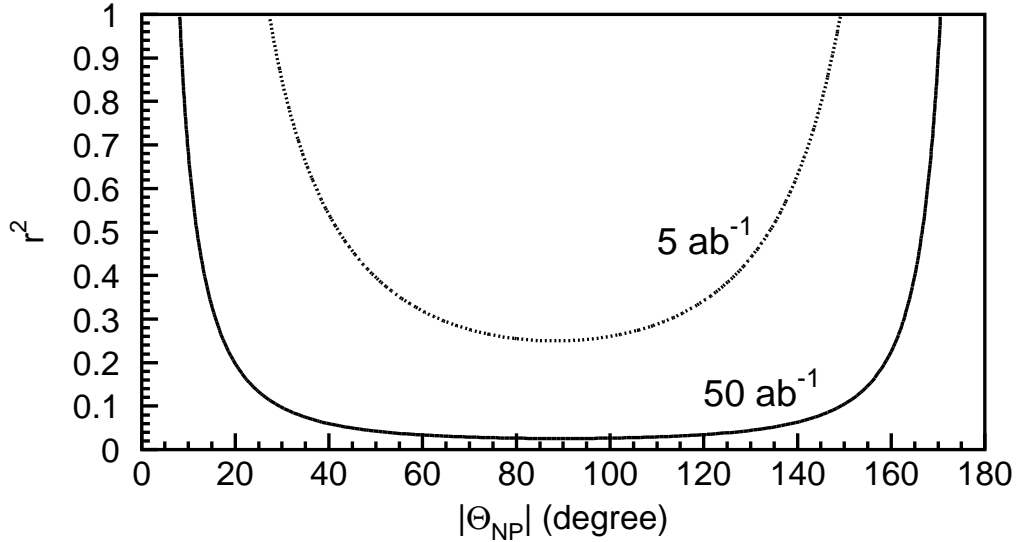


Figure 4.8: Expected sensitivities on direct  $CP$  violation in the  $B^\pm \rightarrow \phi\phi K^\pm$  decay at  $5 \text{ ab}^{-1}$  (dotted line) and at  $50 \text{ ab}^{-1}$  (solid line). In the regions above the curves, direct  $CP$  violation can be measured with a  $5\sigma$  significance or larger.

has also reported the first observation of the  $B^0 \rightarrow \eta_c K^{*0}$  decay. This implies that other modes such as  $B^+ \rightarrow \eta_c K^{*+}$  will also be seen with a similar branching fraction, so that we will be able to study semi-inclusive  $B^\pm \rightarrow \eta_c X_s^\pm$  transitions experimentally. The semi-inclusive branching fraction of  $B^\pm \rightarrow \eta_c X_s^\pm$  is not yet measured, but is expected to be comparable to the branching fraction of the semi-inclusive decay  $B^\pm \rightarrow J/\psi X_s^\pm$  [254, 255, 256].

We have performed Monte Carlo simulation for the  $B^\pm \rightarrow \phi\phi K^\pm$  decay and estimated statistical errors on the  $CP$  asymmetry parameter. The procedure and the fit parameters are the same as those described in [251]. The reconstruction efficiency and the  $\phi\phi$  mass resolution are estimated using a GEANT-based detector simulator for the present Belle detector [257]. We perform an unbinned maximum-likelihood fit to the differential decay rate distribution. Figure 4.8 shows the  $5\sigma$  search regions at  $5 \text{ ab}^{-1}$  (dotted line) and at  $50 \text{ ab}^{-1}$  (solid line), where  $r^2$  is the ratio between the NP amplitude and the SM amplitude, and  $\Theta_{NP}$  is the  $CP$ -violating phase from NP. Direct  $CP$  violation can be observed in a large parameter space with significance above  $5\sigma$ .

Figure 4.9 shows the expected significance of the new phase  $\Theta_{NP}$  at  $5 \text{ ab}^{-1}$  for  $B^\pm \rightarrow \phi\phi K^\pm$  decay ( $r^2 = 0.5$ ) and for time-dependent  $CP$  violation in the  $B^0 \rightarrow \phi K_S^0$  decay ( $|A_{NP}/A_{SM}|^2 = 0.5$ ).

The significance for  $\Delta\mathcal{S}_{\phi K_S^0}$  depends on the sign of  $\Theta_{NP}$ , which is not the case for the  $B^\pm \rightarrow \phi\phi K^\pm$  decay. The sign dependence arises from an asymmetric range for  $\Delta\mathcal{S}_{\phi K_S^0}$ ; to a good approximation, we have  $-1 - \sin 2\phi_1 \leq \Delta\mathcal{S} \leq 1 - \sin 2\phi_1$  where  $\sin 2\phi_1 = +0.736 \pm 0.049$  [246]. Therefore the  $B^\pm \rightarrow \phi\phi K^\pm$  decay plays a unique role in searching for a new  $CP$ -violating phase.

Experimental sensitivities can be improved by adding more final states. The technique to reconstruct  $X_s$ , which has been successfully adopted for the measurements of semi-inclusive

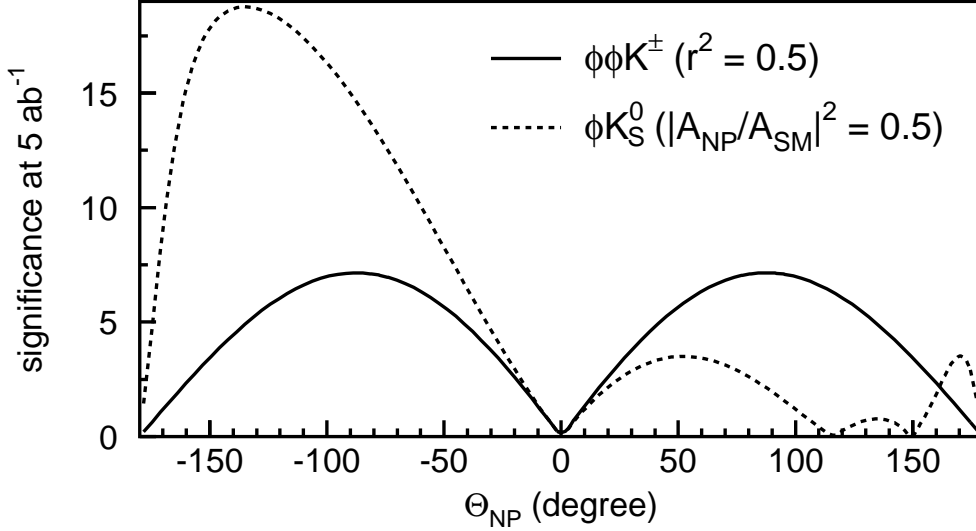


Figure 4.9: Expected statistical significance of deviations from the SM for direct  $CP$  violation in the  $B^\pm \rightarrow \phi\phi K^\pm$  decay with  $r^2 = 0.5$  (solid line) and for time-dependent  $CP$  violation in the  $B^0 \rightarrow \phi K_S^0$  decay with  $|A_{\text{NP}}/A_{\text{SM}}|^2 = 0.5$  (dashed line). For each case, significance is calculated at  $5 \text{ ab}^{-1}$ .

$B \rightarrow X_s \ell \ell$  transitions [20], can be used for this purpose. Flavor-specific neutral  $B$  meson decays, such as  $B^0 \rightarrow \phi\phi K^{*0} (\rightarrow K^+ \pi^-)$ , and other charmonia such as the  $\chi_{c0} \rightarrow \phi\phi$  decay can also be included.

#### 4.2.5 Discussion

As is discussed in the previous sections, statistical errors in new phase measurements can be at a few percent level at SuperKEKB. Figure 4.10 shows an example of a fit to events in a MC pseudo-experiment for the  $B^0 \rightarrow \phi K_S^0$  and  $J/\psi K_S^0$  decays at  $5 \text{ ab}^{-1}$ , where the input value of  $\mathcal{S}(\phi K_S^0) = +0.24$  is chosen to be the world average value of the  $\mathcal{S}$  term for  $B^0 \rightarrow \phi K_S^0$ ,  $\eta' K_S^0$  and  $K^+ K^- K_S^0$ .

This level of large deviation can easily be observed only with a single decay channel  $B^0 \rightarrow \phi K_S^0$  at SuperKEKB. Combining all the available modes described in the previous sections allows us to measure a deviation of  $\sim 0.1$ . At this level, even the SM may be able to create non-zero values of  $\Delta\mathcal{S}$ . Therefore it is important to evaluate  $\Delta\mathcal{S}$  within the SM.

Grossman, Isidori and Worah [27] analyzed the possible pollution in the  $B^0 \rightarrow \phi K_S^0$  decay, which comes from the  $b \rightarrow u\bar{u}s$  transition that contains  $V_{ub}$ . They estimate that the pollution is at most  $O(\lambda^2) \sim 5\%$ . In addition, they claim that the upper limit of the pollution will be obtained experimentally from the ratios of branching fractions  $\mathcal{B}(B^+ \rightarrow \phi\pi^+)/\mathcal{B}(B^0 \rightarrow \phi K_S)$  and  $\mathcal{B}(B^+ \rightarrow K^* K^+)/\mathcal{B}(B^0 \rightarrow \phi K_S)$ . This is due to the fact that enhancement of  $b \rightarrow u\bar{u}s$  should also be detected in these modes. Therefore they conclude that new physics is guaranteed if  $|\Delta\mathcal{S}(\phi K_S^0)| > 0.05$  is established.

For the  $B^0 \rightarrow \eta' K_S^0$  decay, London and Soni [26] discussed the tree ( $b \rightarrow u\bar{u}s$ ) pollution by

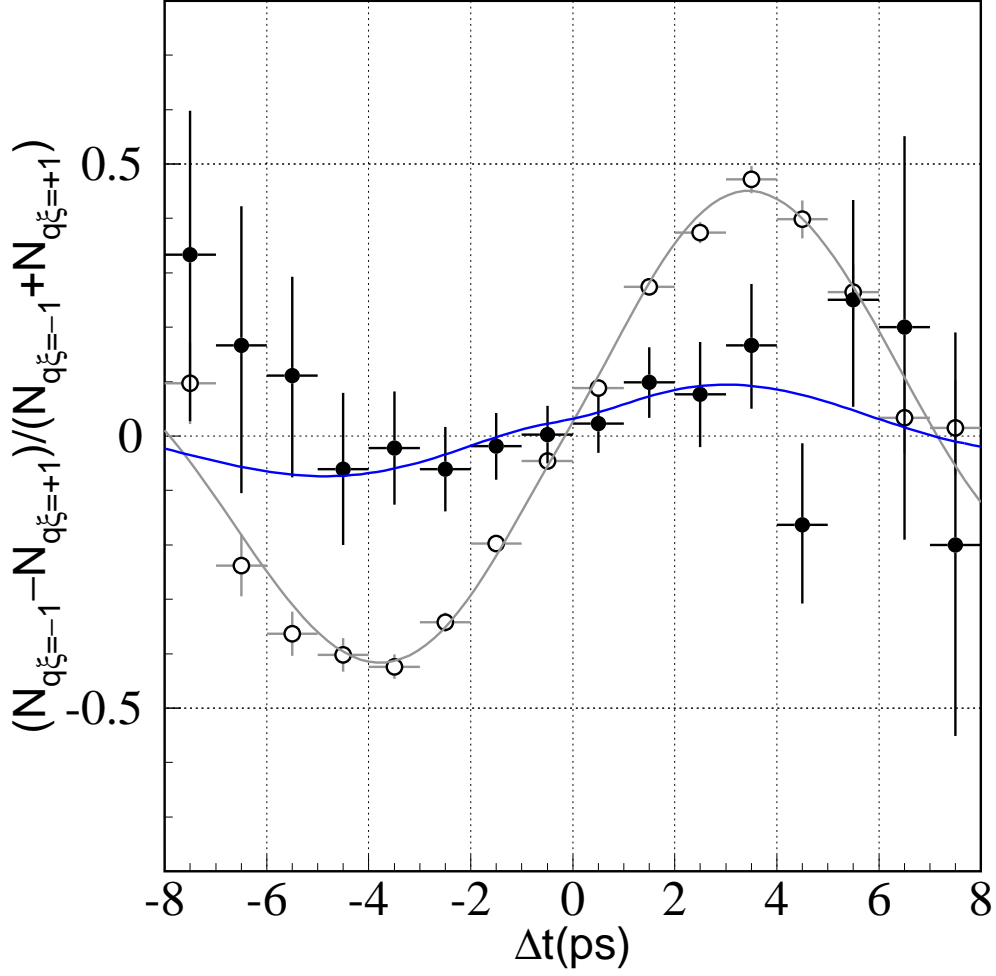


Figure 4.10: Raw asymmetries for  $B^0 \rightarrow \phi K_S^0$  and  $B^0 \rightarrow J/\psi K_S^0$  at  $5 \text{ ab}^{-1}$ . Input values are  $\mathcal{S}_{\phi K_S^0} = +0.24$  and  $\mathcal{A}_{\phi K_S^0} = +0.07$ , which are the HFAG average for the  $b \rightarrow s$  transition as of LP03 [246].

evaluating  $T(\eta'K_S)/P(\eta'K_S) = T(\eta'K_S)/T(\pi^+\pi^-) \times T(\pi^+\pi^-)/P(\eta'K_S)$ , and concluded that manifestation of new physics is established if  $|\Delta\mathcal{S}(\eta'K_S^0)| > 0.1$  is observed.

The above studies aim at providing estimates of the possible deviation within the SM based on some models of QCD. A different approach has recently been proposed by Y. Grossman, Z. Ligeti, Y. Nir and H. Quinn [28]. They do not rely on specific QCD models but instead use SU(3) relations to estimate or bound the contributions to these amplitudes proportional to  $V_{ub}^*V_{us}$ , which induce a non-zero  $\mathcal{S}$  value within the SM. At present, the power of the method is limited by the uncertainties on branching fractions of charmless two-body decays. As a result, they conclude that  $\Delta\mathcal{S}(\phi K_S^0) < 0.25$ ,  $\Delta\mathcal{S}(K^+K^-K_S^0) \sim 0.13$  and  $\Delta\mathcal{S}(\eta'K_S^0) < 0.36$ . As data improve, these bounds could become significantly stronger. Taking these theoretical considerations into account, we conclude that SuperKEKB can provide precision measurements of  $\Delta\mathcal{S}$  up to the limit of hadronic uncertainties, which will be a few percent level.

## 4.3 $b \rightarrow s\gamma$ and $b \rightarrow s\ell^+\ell^-$

### 4.3.1 Introduction

In this section, we discuss the radiative and electroweak processes  $b \rightarrow s(d)\gamma$  and  $b \rightarrow s(d)\ell^+\ell^-$ . The corresponding exclusive decays are  $B \rightarrow K^*(\rho)\gamma$  and  $B \rightarrow K^{(*)}\ell^+\ell^-$ . Due to the GIM mechanism, the radiative process  $b \rightarrow s\gamma$  starts at one-loop order, but still has a large branching fraction because of the non-decoupling effect of the top quark loop and the large CKM factor  $V_{tb}V_{ts}^*$ . The other processes,  $b \rightarrow s\ell^+\ell^-$  and  $b \rightarrow d\gamma$ , are suppressed with respect to  $b \rightarrow s\gamma$  by two orders of magnitude mainly due to additional  $\alpha_{\text{em}}$  and  $|V_{td}/V_{ts}|^2$  factors, respectively;  $b \rightarrow d\ell^+\ell^-$  is suppressed by four orders of magnitude due to both of them. These decay processes are sensitive to new physics effects that are predicted in extensions to the Standard Model. Moreover, new physics effects from flavor changing neutral interactions contribute to  $b \rightarrow s(d)\gamma$  and to  $b \rightarrow s(d)\ell^+\ell^-$  in a different way. Typically in the former case new physics effects always appear at a one-loop or higher orders, while in the latter process they may arise at the tree-level, *i.e.*, violating the GIM mechanism. Therefore, even if no new physics effect is found in  $b \rightarrow s\gamma$ , there could be a significant effect in  $b \rightarrow s(d)\ell^+\ell^-$ .

The  $b \rightarrow s\gamma$  process was first observed by CLEO a decade ago and has been extensively studied since then. The  $b \rightarrow s\ell^+\ell^-$  process has recently been measured first by Belle and later by BaBar. The measured branching fractions are consistent with Standard Model predictions. No  $b \rightarrow d\gamma$  process has been measured yet, but it is expected to be observed sooner or later. With a much larger data sample expected at SuperKEKB, it will become possible to measure various distributions and asymmetries accurately enough to observe possible deviations from the Standard Model, in addition to significant improvements in branching fraction measurements. Various properties of  $b \rightarrow d$  transitions can also be measured. These measurements will be essential in order to understand the parity, chirality and Lorentz structures that may differ from the Standard Model, before, and especially after, the discovery of new physics beyond the Standard Model, elsewhere if not in these decays.

The major targets of SuperKEKB for these decays are as follows.

1. Precision test of the Standard Model with improved accuracy,
2. search for a deviation from the Standard Model in various distributions, *e.g.* in the forward-backward asymmetry of  $B \rightarrow K^*\ell^+\ell^-$ ,
3. search for a lepton flavor dependence of  $b \rightarrow s\ell^+\ell^-$ ,
4. measurement of mixing induced  $CP$  violation in  $b \rightarrow s\gamma$ ,
5. search for direct  $CP$  violation in  $B \rightarrow K^*\gamma$ , and
6. study of flavor changing transitions in the  $b \rightarrow d$  sector, *i.e.*  $B \rightarrow \rho\gamma$ , and hopefully an exclusive  $b \rightarrow d\ell^+\ell^-$  processes such as  $B \rightarrow \pi\ell^+\ell^-$ .

Both exclusive and inclusive modes are useful to test the strong interaction in weak decays. In the past decade, perturbative QCD corrections to the radiative and electroweak  $B$  decays were computed beyond the leading order which leads to the predictions with higher accuracy [258]. The theoretical errors from this part are reduced to a few percent level coming from the renormalization point dependence and a charm quark mass uncertainty. To include non-perturbative effects for inclusive decays, we may apply the heavy quark expansion. The photon energy spectrum  $d\Gamma/dE_\gamma$  in  $b \rightarrow s\gamma$  is sensitive to the non-perturbative effects, *e.g.* Fermi-motion effects that are encoded in the shape function of the  $B$  meson. Such non-perturbative



effects can be determined by measuring the moments of the photon energy spectrum. Because the structure function is process independent, we can apply the one determined in  $b \rightarrow s\gamma$  to other inclusive modes such as  $B \rightarrow X_s \ell^+ \ell^-$  [259]. As for the exclusive processes, there remain large uncertainties from the form factors of the hadronic matrix elements; these form factors have usually been calculated using QCD sum rules, for which no clear idea on how to reduce their errors is available. The situation might improve by using a new approach with lattice QCD. It is usually thought that a large fraction of uncertainty is canceled by measuring a ratio or an asymmetry of two decay rates. Experimental information is essential to check the various theoretical models, to evaluate the size of the errors especially for cases where the uncertainties are expected to cancel.

Predictions for exclusive rare  $B$  decays by factorization, perturbative QCD (PQCD), light-front QCD, lattice QCD and other models can be compared with the experimental data. This certainly improves understanding of the weak decays of  $B$  mesons. Interestingly, a complete understanding of the long-distance effects in  $B \rightarrow X_s \ell^+ \ell^-$  is not yet available. This effect comes from the decay chains  $B \rightarrow J/\psi(\psi') X_s \rightarrow \ell^+ \ell^- X_s$  [260]. By measuring the dilepton mass squared distribution near the charmonium resonances, we may study the long-distance effects experimentally.

In order to search for or constrain so many predictions from extensions of the Standard Model described above, a model independent study is a useful approach. New physics effects may appear as a modification to the short-distance couplings, which can be expressed as modifications to the Wilson coefficients. The  $b \rightarrow s\gamma$  transition is sensitive to the coefficient  $C_7$  for the  $bs\gamma$ -coupling and to a lesser extent to  $C_8$  for the  $bsg$ -coupling through higher order corrections; the  $b \rightarrow s \ell^+ \ell^-$  transition is sensitive to  $C_9$  and  $C_{10}$  for the vector and axial-vector  $bs \ell^+ \ell^-$ -coupling in addition.

One can further generalize this approach [190, 192]. New physics effects that may affect  $b \rightarrow s\gamma$  can be parametrized by four types of interactions, which include two types of  $b \rightarrow sg$  interactions and two types of  $b \rightarrow s\gamma$  transitions. In addition to these, there are four Fermi-interactions with the form of the bilinear products of  $\bar{b}s$  and  $\ell^+ \ell^-$ . They can be parametrized by 12 types of interactions in  $B \rightarrow X_s \ell^+ \ell^-$  [190]. With the data at SuperKEKB, we can improve the situation and may pinpoint the new physics effect in a model independent way, which covers a wider class of models than the present analysis.

Among the various interesting aspects of these decay channels, we select the following observables that will be tested with SuperKEKB: the  $B \rightarrow X_s \gamma$  inclusive branching fraction, the forward-backward asymmetry of  $B \rightarrow K^* \ell^+ \ell^-$ , the ratio of  $B \rightarrow K \mu^+ \mu^-$  to  $B \rightarrow K e^+ e^-$ , the mixing induced CP asymmetry in  $B \rightarrow K^* \gamma$ , and the direct CP asymmetry in  $B \rightarrow X_s \gamma$ .

### 4.3.2 $B \rightarrow X_s \gamma$ branching fraction

The excellent agreement between the measured  $B \rightarrow X_s \gamma$  branching fraction and the theoretical prediction, within about 10% accuracy both for the measurement and theory, has constrained various new physics scenarios; for example, the charged Higgs constructively interferes with the SM amplitude, and its mass must be above 3.5 TeV if no other new physics contribution cancels the enhancement. Neither the measurement nor theory errors can be reduced substantially due to systematic uncertainties. Therefore one can not expect to measure a significant deviation in the near future. Nevertheless, improved measurements of  $B \rightarrow X_s \gamma$  are extremely important to fix the magnitude of the Wilson coefficient  $C_7$  and the photon energy spectrum for other measurements.

The theoretical uncertainty, which is now determined by the accuracy of the next-to-leading-

order corrections, is expected to be reduced down to 5% when all next-to-next-to-leading-order corrections are included. The work is on-going, and is expected to be completed within a few years.

There have been two techniques to measure  $B \rightarrow X_s \gamma$ : a fully inclusive method just to tag the photon in which the background subtraction is the main issue, and a method of summing up exclusive modes, in which the extrapolation to the un-measured modes is the key issue. The former method has several options; to eliminate backgrounds we can either require a lepton-tag or a full-reconstruction tag for the other side  $B$ , if it is not statistically limited. The latter method gives more stringent constraints, but is seriously affected by the hadronization model uncertainty that makes it unsuitable for a precision measurement.

The measurements are currently limited by a systematic error that arises from a minimum photon energy requirement typically at 2.0 GeV. One can in principle reduce the systematic error to 5% by reducing the minimum photon energy requirement close to 1.5 GeV. This is not a straightforward task, however, since the background increases rapidly in the lower photon energy range while the signal decreases, as shown in Figure 4.11. Typically, twice as much data is required to decrease the minimum photon energy by 0.1 GeV while keeping the same statistical error. Therefore,  $B \rightarrow X_s \gamma$  is a suitable measurement at SuperKEKB; scaling from the currently available results, about  $5 \text{ ab}^{-1}$  on-resonance plus  $0.5 \text{ ab}^{-1}$  off-resonance data will be needed to decrease the photon energy requirement down to 1.5 GeV and to reduce the statistical error to be a half at the same time, so that the total error becomes around 5%. The dominant background is from continuum, which can be reliably subtracted using the off-resonance sample. The second largest background is from  $B \rightarrow \pi^0 X$  (and  $\eta X$ ), which can be also subtracted using a photon energy spectrum inferred from a measured  $\pi^0$  momentum distribution. The problematic part will be the background from neutral hadrons ( $K_L^0$ , neutrons and anti-neutrons), for which control samples of  $e^+e^- \rightarrow \phi\gamma$ ,  $\phi \rightarrow K_S^0 K_L^0$  and inclusive  $\Lambda$  ( $\bar{\Lambda}$ ) events have to be studied.

### 4.3.3 $B \rightarrow K^* \ell^+ \ell^-$ forward-backward asymmetry

The forward-backward asymmetry in  $B \rightarrow K^* \ell^+ \ell^-$ , defined as

$$\bar{A}_{\text{FB}}(q^2) = \frac{N(q^2; \theta_{B\ell^+} > \theta_{B\ell^-}) - N(q^2; \theta_{B\ell^+} < \theta_{B\ell^-})}{N(q^2; \theta_{B\ell^+} > \theta_{B\ell^-}) + N(q^2; \theta_{B\ell^+} < \theta_{B\ell^-})}, \quad (4.10)$$

is an ideal quantity to disentangle the Wilson coefficients  $C_9$  and  $C_{10}$  together with the sign of  $C_7$ .

As discussed in Section 3.5, in a SUSY scenario the sign of the  $b \rightarrow s\gamma$  amplitude ( $C_7$ ) can be opposite to the Standard Model prediction, while the transition rate may be the same as in the Standard Model. This case can be discriminated by measuring the forward-backward asymmetry of  $B \rightarrow X_s \ell^+ \ell^-$  or  $B \rightarrow K^* \ell^+ \ell^-$ . Within the Standard Model, there is a zero crossing point of the forward-backward asymmetry in the low dilepton invariant mass region, while the crossing point may disappear in some SUSY scenarios. Another important new physics effect can be searched for by using the  $B \rightarrow K^* \ell^+ \ell^-$  forward-backward asymmetry. In a model with  $SU(2)$  singlet down-type quarks, tree-level  $Z$  flavor-changing-neutral-currents are induced. In this case, the larger effect is expected on the axial-vector coupling ( $C_{10}$ ) to the dilepton than on the vector coupling ( $C_9$ ). Because the forward-backward asymmetry is proportional to the axial-vector coupling, the sign of the asymmetry can be opposite to the Standard Model. The same new physics effect is also effective for  $B^0 \rightarrow \phi K_S^0$  where anomalous mixing-induced  $CP$  violation can occur. A correlation is expected between  $b \rightarrow s\ell^+ \ell^-$  and  $b \rightarrow s\bar{s}s$ .

The forward-backward asymmetry is roughly proportional to  $C_{10}(2C_7 + C_9\hat{s})$ . In the SM,  $C_7$  is about  $-0.3$  and  $C_9$  is about  $4$ , so this function crosses zero around  $\hat{s} \sim 0.15$ , or  $q^2 \sim$

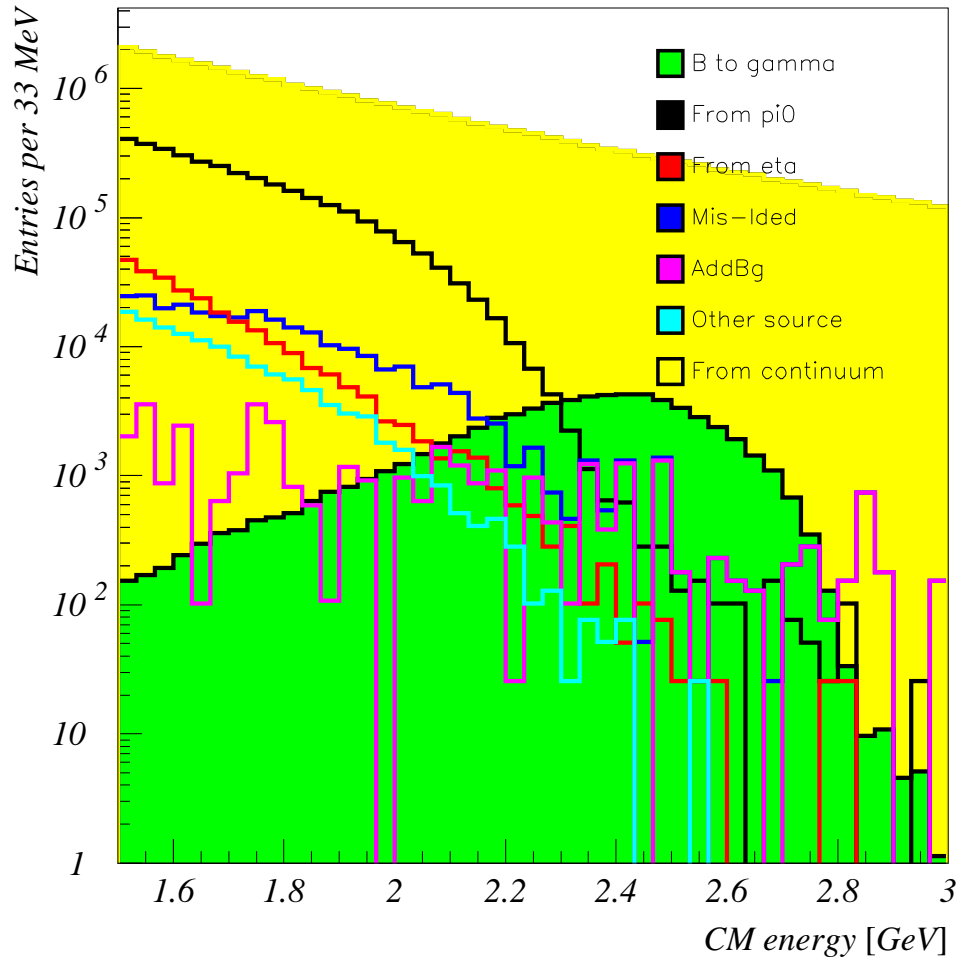


Figure 4.11: Photon energy spectrum (MC) for  $140 \text{ fb}^{-1}$ .

$(3.5 \text{ GeV}/c^2)^2$ . Figure 4.12 shows the expected  $\overline{A}_{\text{FB}}$  at 5 and 50  $\text{ab}^{-1}$ . It can be seen that this crossing pattern of the forward-backward asymmetry will be already visible at 5  $\text{ab}^{-1}$ , and will be clearly observed at 50  $\text{ab}^{-1}$ . The fitted curves in Fig. 4.12 have empirical functional forms that are proportional to  $C_{10}(2C_7 + C_9\hat{s})$ . From these fits, it is possible to disentangle  $C_{10}$  and  $C_9$ , if the size of  $C_7$  is fixed using  $b \rightarrow s\gamma$ . From a fit to the 50  $\text{ab}^{-1}$  sample, we obtain  $\delta C_9 = 0.43$  and  $\delta C_{10} = 0.59$ , or roughly 10% and 14% errors, respectively. The uncertainty due to  $C_7$  is small. We note that a more realistic fitting function that includes all next-to-next-to-leading order corrections and form factors is needed. The result will be improved by combining it with a  $B \rightarrow X_s \ell^+ \ell^-$  branching fraction measurement and  $q^2$  fit results, which will only be possible at  $e^+e^-$   $B$ -factories.

#### 4.3.4 $B \rightarrow K\mu^+\mu^-$ versus $B \rightarrow Ke^+e^-$

Branching fractions for the exclusive decays  $B \rightarrow K^{(*)}\ell^+\ell^-$  have already been measured to be consistent with SM predictions. The measurement error is already smaller than that for the theory. Theory predictions suffer from large model dependent and irreducible uncertainties in the form-factors of at least  $\pm 30\%$ , and the currently available predictions vary by a factor of two or more. However, one can still utilize the measurements in such a way that the theory uncertainties cancel.

In new physics models with a different Higgs sector from that of the Standard Model, scalar and pseudo-scalar types of interactions may arise in  $b \rightarrow s\ell^+\ell^-$ . Depending on the lepton flavor  $\ell = e$  and  $\ell = \mu$ , the new physics effects can differ. By measuring  $R_{K^{(*)}} = \mathcal{B}(B \rightarrow K^{(*)}\mu^+\mu^-)/\mathcal{B}(B \rightarrow K^{(*)}e^+e^-)$ , such new physics effects can be searched for. A particular example can be found in a minimal supergravity model [192, 261].

In the SM, the branching fractions for  $B \rightarrow Ke^+e^-$  and  $B \rightarrow K\mu^+\mu^-$  are predicted to be equal except for a tiny phase space difference due to the lepton masses. For  $B \rightarrow K^*\ell^+\ell^-$  modes, the branching fraction for  $B \rightarrow K^*e^+e^-$  is larger than  $B \rightarrow K^*\mu^+\mu^-$  for small dilepton masses, due to a larger interference contribution from  $B \rightarrow K^*\gamma$  in  $B \rightarrow K^*e^+e^-$ . However, this situation may be modified in the models mentioned above, in which a neutral SUSY Higgs contribution can significantly enhance only the  $B \rightarrow K^{(*)}\mu^+\mu^-$  channel if  $\tan\beta$  is large. Therefore, the ratio  $R_K = \mathcal{B}(B \rightarrow K\mu^+\mu^-)/\mathcal{B}(B \rightarrow Ke^+e^-)$  is an observable that is sensitive to new physics if it is larger than unity.

From current Belle results on the branching fractions, we obtain  $R_K = 1.0 \pm 0.4$  or  $R_K < 1.7$  (90% CL). The error on  $R_K$  is currently dominated by the statistical error, and the error will simply scale with the luminosity even at 50  $\text{ab}^{-1}$ . The expected error is

$$\begin{aligned} \delta R_K &= 0.07 \quad (\text{at } 5 \text{ ab}^{-1}), \\ \delta R_K &= 0.02 \quad (\text{at } 50 \text{ ab}^{-1}). \end{aligned} \tag{4.11}$$

The systematic error in the ratio is dominated by the error on the lepton identification efficiency, which will still be much smaller than the statistical error even at 50  $\text{ab}^{-1}$ .

Since the  $b \rightarrow s\ell^+\ell^-$  transition diagram is equivalent to  $B_s \rightarrow \mu^+\mu^-$ , there already exists a bound from the CDF's limit, which corresponds to  $R_K < 1.6$ . However, this limit is model dependent unless  $B_s \rightarrow e^+e^-$  is observed, which is very unlikely.

#### 4.3.5 Mixing induced CP asymmetry in $B \rightarrow K^*\gamma$

Mixing-induced  $CP$  asymmetry in  $b \rightarrow s\gamma$  is an excellent window to study a new phase that may also be observed in the hadronic transition  $b \rightarrow s\bar{s}s$ . The  $CP$  asymmetry parameter  $\mathcal{S}_{K^*\gamma}$  is

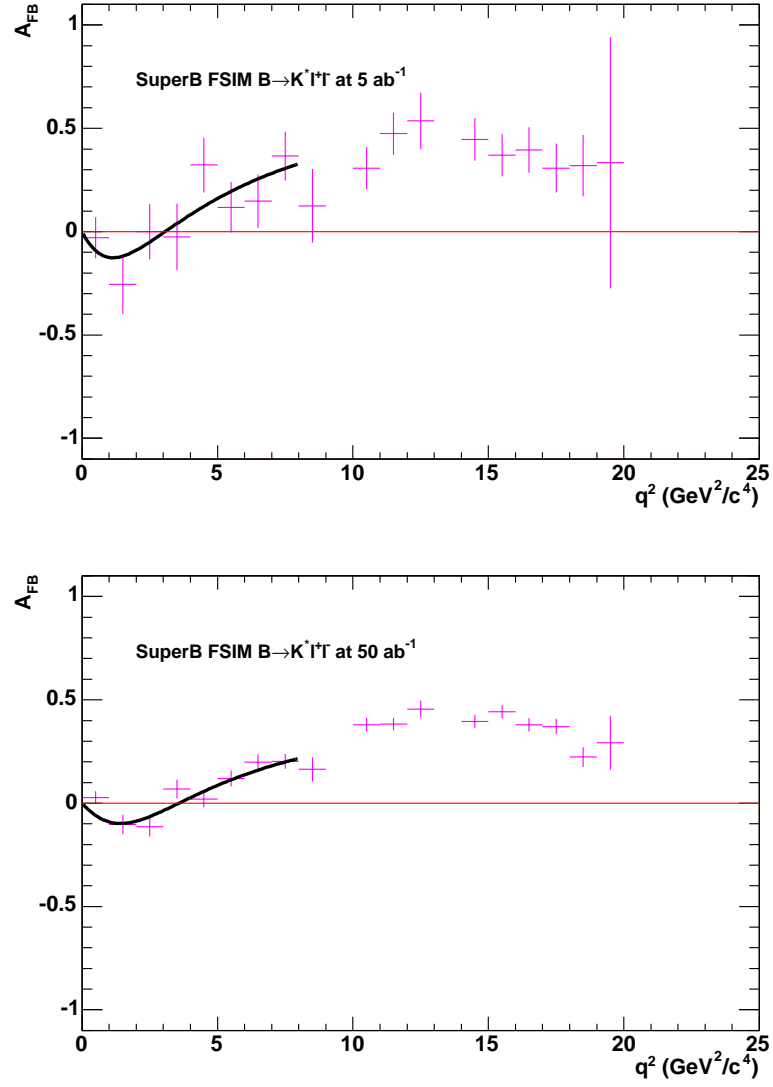


Figure 4.12: Forward-backward asymmetry in  $B \rightarrow K^* \ell^+ \ell^-$  at 5 ab<sup>-1</sup> (top) and 50 ab<sup>-1</sup> (bottom).

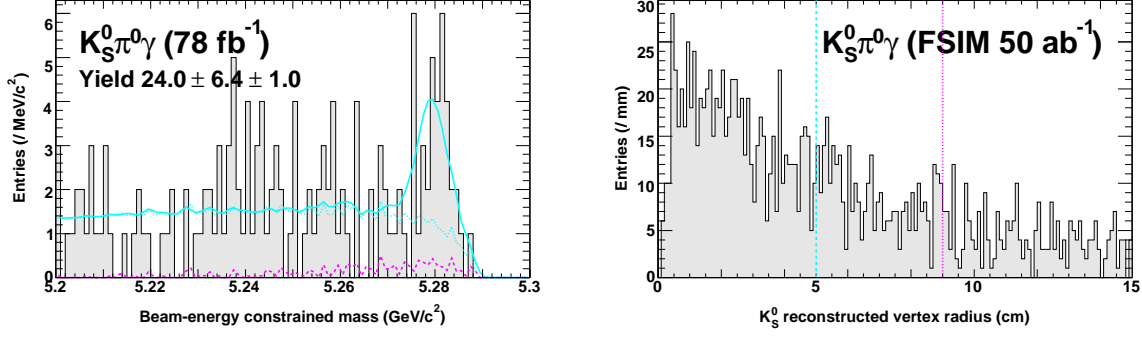


Figure 4.13:  $B^0 \rightarrow K^{*0} \gamma$ ,  $K^{*0} \rightarrow K_S^0 \pi^0$  signal with 78 fb<sup>-1</sup> (left) and the radial  $K_S^0$  decay vertex distribution (right).

expected to be  $\mathcal{O}(m_s/m_b)$  in the SM within an error of a few percent, and any deviation would be a sign of new physics.

For example, the existence of the neutrino mass suggests that the left-right symmetry is restored at a higher energy, while parity is spontaneously broken at a low energy. In left-right symmetric models, the helicity of the photon from  $b \rightarrow s \gamma$  can be a mixed state of two possible photon helicities, while the left-handed photon is dominant in the Standard Model. This case can be tested by using the mixing induced  $CP$  asymmetry in  $b \rightarrow s \gamma$ . It can also be checked by measuring the azimuthal angle distribution of  $B \rightarrow K^* \ell^+ \ell^-$  [200].

In order to measure the mixing-induced  $CP$  asymmetry, a suitable  $CP$  final state is needed. The final state  $B^0 \rightarrow K^{*0} \gamma$ ,  $K^{*0} \rightarrow K_S^0 \pi^0$  is such a  $CP$  eigenstate, and the technique for the  $\sin 2\phi_1$  measurement is applicable. This mode was previously considered to be technically challenging due to the detached  $K_S^0$  decay vertex; however, it is now found to be feasible from recent studies of  $B \rightarrow K_S^0 \pi^0$ , if one requires hits for the  $K_S^0 \rightarrow \pi^+ \pi^-$  tracks in the silicon vertex detector.

Although the branching fraction for  $B^0 \rightarrow K^{*0} \gamma$  is sizable ( $\sim 4 \times 10^{-5}$ ), the number of events in the  $K_S^0 \pi^0 \gamma$  final state is rather limited due to its small sub-decay branching fraction and a low efficiency. However, the signal is clearly observed already at 78 fb<sup>-1</sup> as shown in Fig. 4.13-a.

The efficiency for the current data is about 1%. Assuming that the efficiency is unchanged for SuperKEKB, one expects about  $2 \times 10^3$  ( $2 \times 10^4$ ) events at 5 (50) ab<sup>-1</sup>. The useful events with at least two hits in the present Silicon Vertex Detector (SVD) must have the decay vertex within about 5 cm in radius, which corresponds to a half of the total, as shown in Fig. 4.13-b. This will increase to about 70% for a radius of 9 cm. Using the result of  $B \rightarrow \eta' K_S^0$ , which has a similar signal-to-noise ratio, and assuming that a worse  $\Delta t$  resolution in  $K_S^0 \pi^0 \gamma$  than in  $\eta' K_S^0$  would be compensated by the expected better SVD performance for SuperKEKB, the anticipated statistical error of the  $S$  term is

$$\begin{aligned} \delta S_{K^{*0} \gamma} &= 0.14 \text{ (at } 5 \text{ ab}^{-1}\text{)}, \\ \delta S_{K^{*0} \gamma} &= 0.04 \text{ (at } 50 \text{ ab}^{-1}\text{)}. \end{aligned} \quad (4.12)$$

There are other exclusive decay channels for the mixing-induced  $CP$  asymmetry study in which no difficulty exists in the vertex reconstruction. One possible channel is  $B^0 \rightarrow K_S^0 \phi \gamma$  for which a  $3\sigma$  signal is already observed ( $5\sigma$  signal is observed for the corresponding charged decay  $B^+ \rightarrow K^+ \phi \gamma$ ). Since  $K_S^0 \phi \gamma$  is not a  $CP$  eigenstate, one has to perform an angular analysis. From the past experience with  $B \rightarrow J/\psi K^{*0}$ , we obtain an error of 0.63 with 89 events. At 5 (50) ab<sup>-1</sup>, we expect 150 (1500)  $K_S^0 \phi \gamma$  events that will lead to an error of 0.5 (0.15) in the

$S$  term, and it therefore becomes interesting with  $50 \text{ ab}^{-1}$  or more. The other possibility is to use higher resonances, namely  $B \rightarrow K_1(1270)^0 \gamma$ ,  $K_1(1270) \rightarrow K_S^0 \rho^0$ . However, this is now considered to be difficult, because these modes have not been observed yet and one has to disentangle them from  $K_1(1270) \rightarrow K^{*+} \pi^-$  that has the same  $K_S^0 \pi^+ \pi^-$  final state.

#### 4.3.6 $B \rightarrow X_s \gamma$ direct $CP$ asymmetry

The direct  $CP$  asymmetry for  $B \rightarrow X_s \gamma$  is one of the quantities with theoretical uncertainties smaller than experimental errors. The predicted SM  $CP$  asymmetry is  $A_{CP} = 0.0042^{+0.0017}_{-0.0012}$  [262], while its magnitude could be above 10% in many extensions of the SM. Therefore, a large space remains to be explored.

The sensitivity at SuperKEKB can be obtained by extrapolating the latest Belle results,  $A_{CP}(B \rightarrow X_s \gamma) = -0.004 \pm 0.051(\text{stat}) \pm 0.038(\text{syst})$ . This measurement was performed by summing up exclusive modes,  $X_s \rightarrow Kn(\pi)$  ( $n = 1$  to 4) and  $X_s \rightarrow KK^+K^-(\pi)$ , where  $K$  is a  $K^\pm$  or  $K_S^0$  and most one  $\pi^0$  is allowed. This method has an advantage of suppressing the  $B \rightarrow X_d \gamma$  contribution to a negligible level. Another method that uses the inclusive photon and tags the charge by an additional lepton, cannot distinguish the  $B \rightarrow X_d \gamma$  contribution; however it is another interesting subject because of the partial sensitivity to the  $B \rightarrow X_d \gamma$  channel.

The SM prediction for the combined asymmetry  $A_{CP}^{s\gamma+d\gamma}$  is essentially zero, in contrast to  $A_{CP}$  for  $b \rightarrow s\gamma$  alone. This is because  $b \rightarrow s\gamma$  and  $b \rightarrow d\gamma$  contribute to  $A_{CP}^{s\gamma+d\gamma}$  with an opposite sign and practically with an equal magnitude, which is a consequence of the unitarity of the CKM matrix, the small mass difference  $m_s - m_d$  and the real Wilson coefficient  $c_7$  [42]. In models beyond the SM,  $A_{CP}^{s\gamma+d\gamma}$  can be non-zero, and is usually dominated by the  $b \rightarrow s\gamma$  component. In addition, the contributions to  $A_{CP}^{s\gamma+d\gamma}$  from  $b \rightarrow s\gamma$  and  $b \rightarrow d\gamma$  can have the same or opposite sign [263, 264, 262].

Although the systematic error is not much smaller than the statistical error, most of the systematic errors are limited by the statistics of the control samples and hence can be reduced with a larger statistics. Note that systematic errors in the tracking efficiency and particle identification cancel in the asymmetry. The breakdown of the errors at  $140 \text{ fb}^{-1}$  are, from the signal shape ( $\sim 0.008$ ) partly due to the uncertainty in the  $M(X_s)$  spectrum and partly due to the multiplicity distribution, from the possible  $A_{CP}$  in the charmless  $B$  decay background (0.02), and from a charge asymmetry in the background suppression requirements (0.029). The  $M(X_s)$  shape and charmless contributions will be known better with more data, and other errors just scale with the statistics. The irreducible model error of the first error is about 0.003, giving the expected errors of

$$\begin{aligned} \delta A_{CP}(\text{at } 5 \text{ ab}^{-1}) &= \pm 0.009 (\text{stat}) \pm 0.006 (\text{syst}), \\ \delta A_{CP}(\text{at } 50 \text{ ab}^{-1}) &= \pm 0.003 (\text{stat}) \pm 0.002 (\text{syst}) \pm 0.003 (\text{model}). \end{aligned} \quad (4.13)$$

Therefore, at  $50 \text{ ab}^{-1}$ , the measurement is more or less limited by the systematic error. While it is still insufficient to measure the predicted SM asymmetry beyond a  $1\sigma$  significance at  $50 \text{ ab}^{-1}$ , this precision is sufficient to observe a  $CP$  asymmetry of  $\sim 0.03$  with a  $5\sigma$  significance.

#### 4.3.7 $b \rightarrow d\gamma$ and $b \rightarrow d\ell^+\ell^-$

Finding new physics effects in a  $b \rightarrow d$  transition may be easier than in a  $b \rightarrow s$  transition because the Standard Model amplitude is suppressed in the  $b \rightarrow d$  transition. Therefore, measurements of the decay rates of  $B \rightarrow \rho\gamma$  will be a good test of the Standard Model. By combining  $|V_{td}V_{tb}^*|$  measured in the  $B_d^0\text{--}\overline{B}_d^0$  mixing, we can search for new physics effects in the  $b \rightarrow d\gamma$

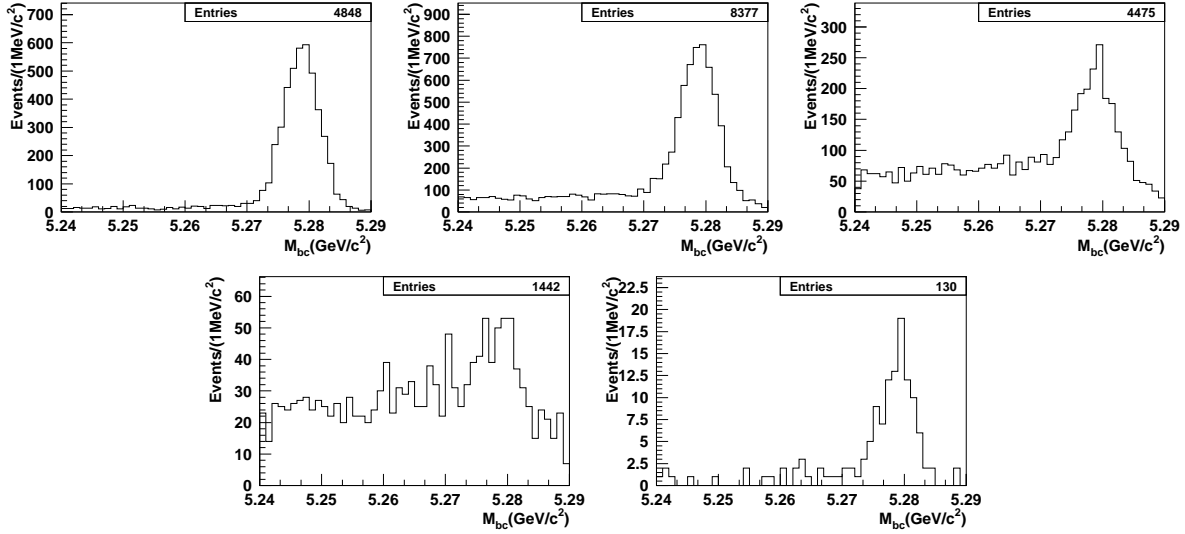


Figure 4.14: Breakdown of the expected  $B \rightarrow X_s \gamma$  exclusive modes:  $K\pi\gamma$  other than  $B \rightarrow K^* \gamma$ ,  $K\pi\pi\gamma$ ,  $K\pi\pi\pi\gamma$ , and  $KK^+K^-\gamma$  from left-top to right-bottom.

mode	$5 \text{ ab}^{-1}$	$50 \text{ ab}^{-1}$
$\mathcal{B}(B \rightarrow X_s \gamma)$	5%	5%
$A_{CP}(B \rightarrow X_s \gamma)$	$0.009 \pm 0.006$	$0.003 \pm 0.002 \pm 0.003$
Mixing induced $S_{K^* \gamma}$	0.14	0.04
$R_K(B \rightarrow K \ell^+ \ell^-)$	0.07	0.02
$\overline{A}_{\text{FB}}(B \rightarrow K \ell^+ \ell^-)$		
$C_9$ from $\overline{A}_{\text{FB}}(B \rightarrow K^* \ell^+ \ell^-)$	32%	10%
$C_{10}$ from $\overline{A}_{\text{FB}}(B \rightarrow K^* \ell^+ \ell^-)$	44%	14%

Table 4.6: Summary of the expected errors for  $b \rightarrow s(d)\gamma$  and  $b \rightarrow s\ell^+\ell^-$  at SuperKEKB.

transition [265]. In the SM,  $b \rightarrow s\gamma$  and  $b \rightarrow d\gamma$  are both mediated by a common Wilson coefficient,  $c_7$ . This is also true in any model with a minimal flavor-violating framework *i.e.* where flavor changing interactions are determined by the CKM angles. However, in models with tree-level FCNCs,  $C_7$  for  $b \rightarrow d\gamma$  can differ from  $C_7$  for  $b \rightarrow s\gamma$ . Examples include SUSY models with gluino mediated FCNCs [266] and models with a non-unitary CKM matrix [264]. Since the Standard Model prediction for the  $B \rightarrow \rho\gamma$  branching fraction suffers from a large model-dependent uncertainty, ideally it is necessary to measure the inclusive rate for  $B \rightarrow X_d \gamma$ .

Although it has yet to be measured, the  $b \rightarrow d\gamma$  process will provide various interesting new physics probes.

### 4.3.8 Summary

We have discussed various decay channels of  $b \rightarrow s(d)\gamma$  and  $b \rightarrow s\ell^+\ell^-$  that are good probes of new physics effects. The sensitivity results are summarized in Table 4.6.



Decay	SM Prediction	BELLE (60 fb <sup>-1</sup> )	BABAR (81 fb <sup>-1</sup> )
$B^\pm \rightarrow e^\pm \nu$	$9.2 \times 10^{-12}$	$\leq 5.4 \times 10^{-6}$	
$B^\pm \rightarrow \mu^\pm \nu$	$3.9 \times 10^{-7}$	$\leq 6.8 \times 10^{-6}$	$\leq 6.6 \times 10^{-6}$
$B^\pm \rightarrow \tau^\pm \nu$	$8.7 \times 10^{-5}$		$\leq 4.1 \times 10^{-4}$

Table 4.7: SM predictions and current experimental limits from BELLE/BABAR.

## 4.4 More than one neutrino I: $B \rightarrow K^{(*)} \nu \bar{\nu}$ and $B \rightarrow \tau \nu$

### 4.4.1 Introduction

In the Standard Model the rare FCNC decay  $b \rightarrow s \nu \bar{\nu}$  proceeds at the one-loop level through penguin and box diagrams. Additional new physics heavy particles may therefore contribute to this decay mode, leading to significant enhancements of the branching fraction. Since the final state leptons do not have electric charge, this mode is not affected by long distance effects from vector resonances ( $\rho$ ,  $J/\psi$ ,  $\psi'$  etc.) and its theoretical predictions are cleaner than those for  $b \rightarrow s l^+ l^-$ . The inclusive branching fraction is estimated to be  $4 \times 10^{-5}$  [267, 268] for the sum of three neutrino flavors, whereas the exclusive branching fractions are predicted to be  $Br(B^- \rightarrow K^- \nu \bar{\nu}) \approx 4 \times 10^{-6}$  [269].

However, the experimental measurement of  $b \rightarrow s \nu \bar{\nu}$  is quite challenging due to two missing neutrinos. The best inclusive limit to date is from ALEPH  $Br(b \rightarrow s \nu \bar{\nu}) < 6.4 \times 10^{-4}$  [270], and a limit of  $< 2.4 \times 10^{-4}$  at 90% confidence level on the exclusive branching fraction of  $B \rightarrow K \nu \bar{\nu}$  was set by CLEO [271]. BABAR has recently reported a preliminary upper limit  $Br(B \rightarrow K \nu \bar{\nu}) < 7.0 \times 10^{-5}$  [272]. At SuperKEKB, measurements of these decay branching fractions will become possible, as millions of fully reconstructed  $B$  samples will be accumulated.

The purely leptonic decays  $B^\pm \rightarrow l^\pm \nu$  in the SM proceed via annihilation to a  $W^\pm$  and are proportional to the square of the  $B$  meson decay constant ( $f_B$ ). In models beyond the SM there can be additional tree-level contributions such as a  $H^\pm$  ( $s$ -channel) [273], [274] or sfermions ( $s, t$ -channels) in  $R$  parity violating SUSY models [275]. The SM predictions and the current experimental upper limits are shown in Table 4.7, where we take  $f_B = 200$  MeV. Observation of such decays would provide the first direct measurement of  $f_B$  or even evidence for new physics. In particular, the sensitivity of the  $\tau^\pm \nu$  and  $\mu^\pm \nu$  channels to any  $H^\pm$  contribution is complementary and competitive with that of the exclusive semi-leptonic decay  $B \rightarrow \bar{D} \tau^\pm \nu$  that is described in Sec. 4.5. The tree-level partial width (including only  $W^\pm$  and  $H^\pm$  contributions) is as follows [273]:

$$\Gamma(B^\pm \rightarrow \ell^\pm \nu) = \frac{G_F^2 m_B m_\ell^2 f_B^2}{8\pi} |V_{ub}|^2 \left(1 - \frac{m_\ell^2}{m_B^2}\right)^2 \times r_H \quad (4.14)$$

where  $r_H$  is independent of the lepton flavour and is given by

$$r_H = \left(1 - \frac{\tan^2 \beta}{1 + \tilde{\epsilon}_0 \tan \beta} \frac{m_B^2}{m_{H^\pm}^2}\right)^2 \quad (4.15)$$

The overall factor of  $m_\ell^2$  arises from helicity suppression for  $W^\pm$  and Yukawa suppression for  $H^\pm$ . The parameter  $\tilde{\epsilon}_0$  encodes the effects of large SUSY corrections to the  $b$  quark Yukawa coupling, and is typically constrained  $|\tilde{\epsilon}_0| \leq 0.01$ . In Fig. 4.15 we plot  $r_H$  as a function of  $\tan \beta / m_{H^\pm}$  for several values of  $\tilde{\epsilon}_0 (m_{H^\pm} / 100 \text{ GeV})$ . The current experimental limits from Table

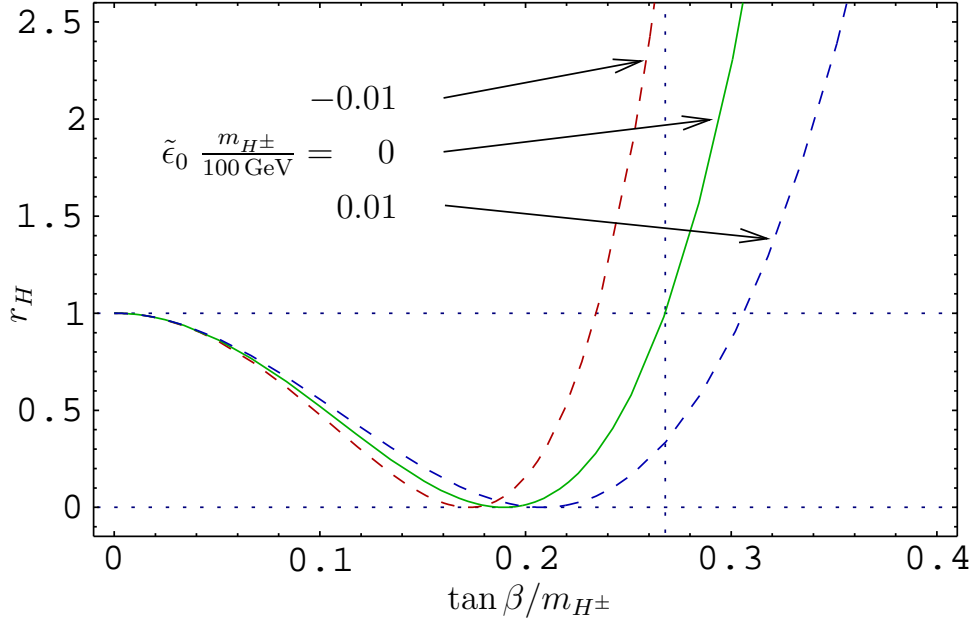


Figure 4.15:  $r_H$  as a function of  $\tan \beta / m_{H^\pm}$ . We show curves for  $\tilde{\epsilon}_0 \frac{m_{H^\pm}}{100 \text{ GeV}} = 0, \pm 0.01$ .

4.7 constrain  $r_H < 4.7$  and  $r_H < 17.4$  from the  $\tau^\pm \nu$  and  $\mu^\pm \nu$  channels, respectively. Sensitivity to the SM rate ( $r_H = 1$ ) is expected in both channels with data samples of a few  $ab^{-1}$ , so that Super-KEKB might actually be able to measure  $r_H$ . One can see that  $r_H = 1$  is obtained for  $\tan \beta / m_{H^\pm} = 0.27 \pm 0.03 \text{ GeV}^{-1}$ , while complete cancellation can occur around  $\tan \beta / m_{H^\pm} = 0.2 \text{ GeV}^{-1}$ . Importantly, any signal of a  $H^\pm$  in the decay  $B \rightarrow \bar{D} \tau^\pm \nu$  (which is sensitive to  $\tan \beta / m_{H^\pm} > 0.14$  with  $5 ab^{-1}$ ) would also manifest itself in both  $B^\pm \rightarrow \tau^\pm \nu$  and  $B^\pm \rightarrow \mu^\pm \nu$ .

An additional observable in which  $f_B$  cancels out is the ratio  $R_{\tau\mu}$  defined by:

$$R_{\tau\mu} = \frac{BR(B^\pm \rightarrow \tau^\pm \nu)}{BR(B^\pm \rightarrow \mu^\pm \nu)} \quad (4.16)$$

Assuming only  $W^\pm$  and  $H^\pm$  contributions,  $r_H$  would also cancel out, and thus  $R_{\tau\mu} \sim m_\tau^2 / m_\mu^2$ . However, sizeable deviations of  $R_{\tau\mu}$  from this value are possible in  $R$  parity violating SUSY models, since  $r_H$  is in general no longer independent of the lepton flavour. In addition, in such models the decay  $B^\pm \rightarrow e^\pm \nu$  may be enhanced to experimental observability.

#### 4.4.2 Estimation of signal and background

To estimate the sensitivity for these decays, we start with the decay mode,  $B^- \rightarrow K^- \nu \bar{\nu}$ , taking a conservative full reconstruction efficiency of 0.2% for  $B^+$  using high quality hadronic tags, with an integrated luminosity of  $50 ab^{-1}$ . Although the physics is different, the  $B$  decay to  $\tau \nu$  has the same topology when one prong  $\tau$  decay modes are used to observe the signal. Thus, in the following the  $B \rightarrow \tau \nu$  decay will be analyzed as well.

The signature of a  $B^- \rightarrow K^- \nu \bar{\nu}$  decay is a single kaon and nothing else recoiling against the reconstructed  $B$  meson. In order to estimate backgrounds for this decay, we first identify other  $B$  decay modes that have only one charged particle in the final state, using the QQ generator. We find that examples of such decays are: semi-leptonic  $B$  decays,  $B \rightarrow D^{(*)} \ell \nu$  in which the

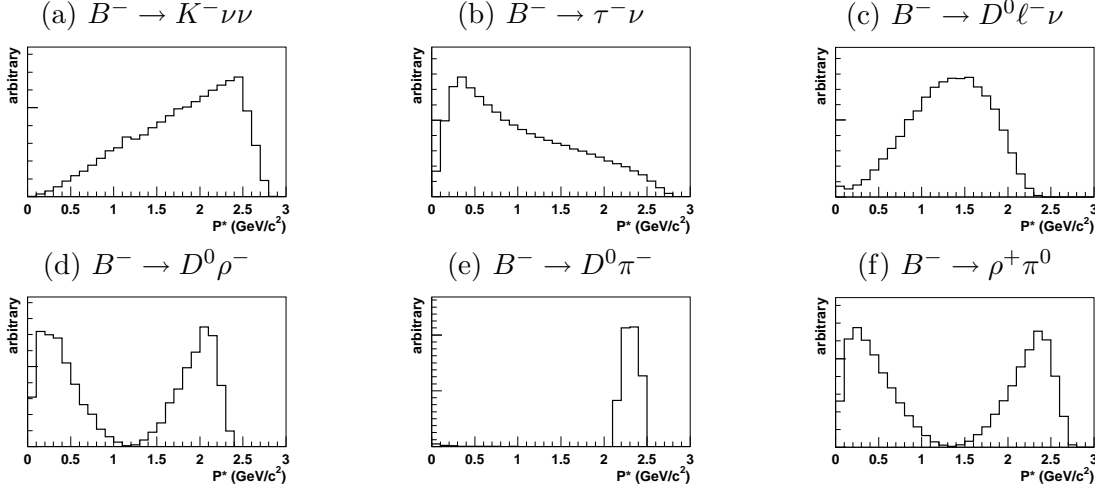


Figure 4.16: Momentum distributions of the only charged particle for various  $B$  decays.

$D$  decays to  $K_L\pi^0$ ,  $B \rightarrow D\rho$ ,  $D\pi$  with  $D \rightarrow K_L\pi^0$ ; charmless  $B$  decays such as  $B^+ \rightarrow \rho^+\pi^0$ . Figure 4.16 shows the momentum distributions of the charged particle in these decays as well as in the signal modes. A three body phase space decay for  $B \rightarrow K\nu\bar{\nu}$  is assumed.

We then estimate the amount of signal and background assuming  $50 \text{ ab}^{-1}$  using a full simulation program based on GEANT3 for the Belle experiment. We assume that the full reconstruction is perfect and its efficiency is 0.2%. Figure 4.17 shows the total energy deposited in the electro-magnetic calorimeter by the signal side “B” meson decay, unmatched hadronic interactions and beam related backgrounds. We select events in which only one charged track is observed with a momentum cut;  $|\vec{p}^*| > 0.7 \text{ GeV}/c$ . Particle identification cuts are not applied on the charged particle. These criteria are rather similar to the recent analyses. It is obvious that we need tighter selection criteria to observe signals.

We optimize the momentum selection to  $2.0 \text{ GeV}/c < |\vec{p}^*| < 2.7 \text{ GeV}/c$  using Fig. 4.16. We also apply tight KID requirements. Figure 4.18 shows the total energy distribution after applying these selection criteria. If we define the signal region to be  $E < 0.5 \text{ GeV}$ , the number of  $B \rightarrow K\nu\bar{\nu}$  events is estimated to be  $43.0 \pm 1.1$ , while the contribution from the background is  $29.3 \pm 3.4$  events. This corresponds to a significance of  $5.1\sigma$ . Table 4.8 summarizes the background contribution for each decay mode. Large contributions from semi-leptonic decays are reduced by applying a tight kaon identification selection.

#### 4.4.3 Discussion

Further improvements for this analysis are expected. The efficiency for the full reconstruction tagging technique can be improved. Optimisation of the tag side efficiency and background can be studied separately for the discovery of the decay and setting upper limit. Likelihood methods can be used for the tag side as well as information on the signal single charged track and energy deposits in the calorimeter. Better solid angle coverage will improve both the tagging efficiency and the signal reconstruction efficiency. Much better kaon identification and rejection of other species will reduce the backgrounds. More effective rejection of the events that contain  $K_L$ ’s can be studied. On the other hand, the environment may become much harsher as luminosity increases and beam related backgrounds will certainly increase if the detector performance remains the same. As a result we may suffer from a smaller tagging efficiency and more energy

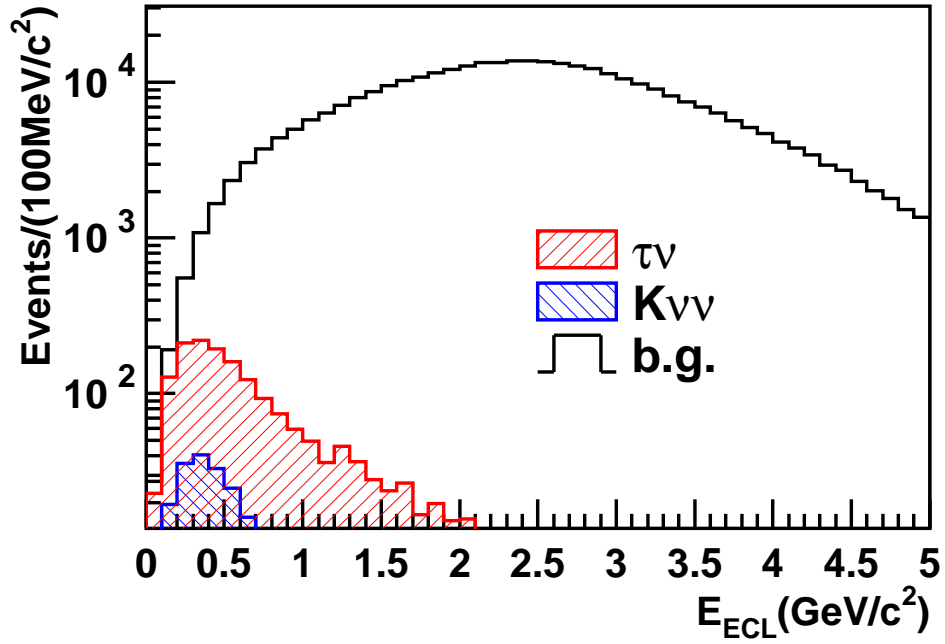


Figure 4.17: ECL energy distribution for  $B \rightarrow K\nu\bar{\nu}$ ,  $B \rightarrow \tau\nu$  and background MC (log scale). The only requirement applied to the charged particle is  $|\vec{p}^*| > 0.7 \text{ GeV}/c$ .

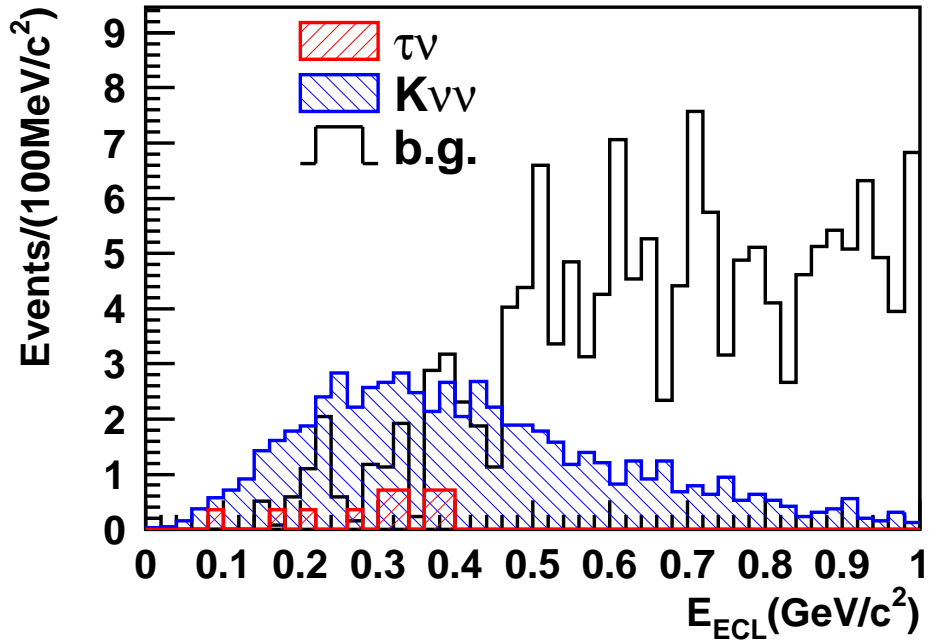


Figure 4.18: ECL energy distribution for  $B \rightarrow K\nu\bar{\nu}$ ,  $B \rightarrow \tau\nu$  and background MC, with  $2.0 \text{ GeV}/c < |\vec{p}^*| < 2.7 \text{ GeV}/c$  and a tight KID requirement applied to the charged particle.

Table 4.8: Backgrounds in the  $B \rightarrow K\nu\bar{\nu}$ 

Mode	$E < 1.0$ GeV	$E < 1.0$ GeV with KID	$E < 0.5$ GeV with KID
$B^- \rightarrow D^{*0}\mu^-\bar{\nu}$	$265.7 \pm 11.7$	$8.2 \pm 2.1$	$2.1 \pm 1.0$
$B^- \rightarrow D^0\pi^-$	$199.0 \pm 10.1$	$7.7 \pm 2.0$	$3.1 \pm 1.3$
$B^- \rightarrow D^{*0}e^-\bar{\nu}$	$181.1 \pm 9.6$	$8.7 \pm 2.1$	$2.1 \pm 1.0$
$B^- \rightarrow D^0\mu^-\bar{\nu}$	$131.3 \pm 8.2$	$25.1 \pm 3.6$	$5.1 \pm 1.6$
$B^- \rightarrow D^{*0}\pi^-$	$110.3 \pm 7.5$	$3.6 \pm 1.4$	$0.0 \pm 0.0$
$B^- \rightarrow D^0\rho^-$	$95.9 \pm 7.0$	$6.2 \pm 1.8$	$1.0 \pm 0.7$
$B^- \rightarrow D^0e^-\bar{\nu}$	$85.7 \pm 6.6$	$19.5 \pm 3.2$	$4.1 \pm 1.5$
$B^- \rightarrow D^{*0}\rho^-$	$43.6 \pm 4.7$	$3.6 \pm 1.4$	$0.5 \pm 0.5$
$B^- \rightarrow D^0K^-$	$13.3 \pm 2.6$	$8.7 \pm 2.1$	$2.1 \pm 1.0$
$B^- \rightarrow D^{*0}K^-$	$5.6 \pm 1.7$	$4.6 \pm 1.5$	$0.5 \pm 0.5$
Other $b \rightarrow c$ decays	$29.8 \pm 3.9$	$3.1 \pm 1.3$	$1.0 \pm 0.7$
$b \rightarrow c$ decays total	$1161.4 \pm 24.4$	$99.0 \pm 7.1$	$21.5 \pm 3.3$
$B^- \rightarrow K^{*-}\pi^-\pi^+$	$28.0 \pm 1.5$	$0.8 \pm 0.2$	$0.2 \pm 0.1$
$B^- \rightarrow \pi^-\bar{K}^0$	$22.8 \pm 1.3$	$0.5 \pm 0.2$	$0.0 \pm 0.0$
$B^- \rightarrow \rho^+\pi^0$	$21.1 \pm 1.3$	$0.4 \pm 0.2$	$0.0 \pm 0.0$
$B^- \rightarrow K^-f'_2(1525)$	$19.1 \pm 1.2$	$12.5 \pm 1.0$	$1.1 \pm 0.3$
$B^- \rightarrow K^-\pi^0$	$18.5 \pm 1.2$	$12.7 \pm 1.0$	$3.3 \pm 0.5$
$B^- \rightarrow K^{*-}\rho^0$	$13.6 \pm 1.0$	$0.2 \pm 0.1$	$0.1 \pm 0.1$
$B^- \rightarrow K^{*-}f_2(1270)$	$10.9 \pm 0.9$	$0.4 \pm 0.2$	$0.0 \pm 0.0$
$B^- \rightarrow K^{*-}f'_2(1525)$	$10.7 \pm 0.9$	$8.2 \pm 0.8$	$1.3 \pm 0.3$
$B^- \rightarrow \pi^-\pi^0$	$9.3 \pm 0.8$	$0.4 \pm 0.2$	$0.2 \pm 0.1$
$B^- \rightarrow K^{*-}\gamma$	$7.9 \pm 0.8$	$0.0 \pm 0.0$	$0.0 \pm 0.0$
$B^- \rightarrow \rho^+K^0$	$7.1 \pm 0.7$	$0.1 \pm 0.1$	$0.0 \pm 0.0$
$B^- \rightarrow \pi^-K^{*0}$	$6.0 \pm 0.7$	$0.1 \pm 0.1$	$0.0 \pm 0.0$
$B^- \rightarrow K^-\eta'$	$4.5 \pm 0.6$	$3.2 \pm 0.5$	$0.2 \pm 0.1$
$B^- \rightarrow K^-f_0(1370)$	$4.0 \pm 0.6$	$2.2 \pm 0.4$	$0.2 \pm 0.1$
$B^- \rightarrow K^-\eta$	$3.9 \pm 0.5$	$2.7 \pm 0.5$	$0.5 \pm 0.2$
$B^- \rightarrow K^-f_2(1270)$	$3.5 \pm 0.5$	$2.4 \pm 0.4$	$0.2 \pm 0.1$
$B^- \rightarrow \bar{K}_0^*(1430)^0\pi^-$	$2.8 \pm 0.5$	$0.2 \pm 0.1$	$0.1 \pm 0.1$
$B^- \rightarrow \rho^-\eta$	$2.8 \pm 0.5$	$0.0 \pm 0.0$	$0.0 \pm 0.0$
$B^- \rightarrow K^-K^0$	$2.5 \pm 0.4$	$1.7 \pm 0.4$	$0.4 \pm 0.2$
Other rare $B$ decays	$16.7 \pm 1.1$	$3.2 \pm 0.5$	$0.2 \pm 0.1$
Rare $B$ decays total	$215.6 \pm 4.1$	$51.6 \pm 2.0$	$7.8 \pm 0.8$
Total	$1377.0 \pm 24.7$	$150.6 \pm 7.3$	$29.3 \pm 3.4$

deposits in the calorimeter. So far we are not able to estimate such effects quantitatively, but will continue to study this important decay mode.

## 4.5 More than one neutrino II: $B \rightarrow \bar{D}\tau^+\nu_\tau$

The decay  $B \rightarrow \bar{D}\tau^+\nu_\tau$  is sensitive to the exchange of charged Higgs boson as introduced in the Minimal Supersymmetric Standard Model (MSSM), since the amplitude is roughly proportional to  $m_\tau m_b \tan \beta$ . The branching fraction of  $B \rightarrow \bar{D}\tau^+\nu_\tau$  is expected to be large ( $\sim 8 \times 10^{-3}$ ) in the SM, but much more data are required to measure this process because of the presence of two or more neutrinos in the decay final state. This mode consequently requires the tagging of the other side  $B$ , for which a reconstruction efficiency is estimated to be 0.2%, which has been discussed in Section 4.1.3. Therefore, the study of the MSSM Higgs through this decay mode is only possible with the statistical power of SuperKEKB.

### 4.5.1 Introduction

In the MSSM, the coupling of the charged Higgs bosons,  $H^\pm$ , to quarks and leptons is given by

$$\begin{aligned} \mathcal{L}_H = & (2\sqrt{2}G_F)^{1/2} \left[ \tan \beta (\bar{u}_L V_{KM} M_d d_R + \bar{\nu}_L M_\ell \ell_R) + \frac{1}{\tan \beta} \bar{u}_R V_{CKM} M_u d_L \right] H^\pm \\ & + h.c., \end{aligned} \quad (4.17)$$

where  $M_u$  and  $M_d$  are the quark mass matrices,  $M_\ell$  is the lepton ( $\ell = e, \mu$ , or  $\tau$ ) mass matrix,  $V_{CKM}$  is the Cabibbo-Kobayashi-Maskawa matrix, and  $\tan \beta = v_2/v_1$  is the ratio of the vacuum expectation values of the Higgs fields. Therefore, the decay amplitude of  $B \rightarrow \bar{D}\tau^+\nu_\tau$  that is mediated by  $\bar{b} \rightarrow c\tau^+\nu$  has a term proportional to  $M_b M_\tau \tan^2 \beta$  [276, 277]. The large  $\tau$  mass is an advantage of this decay in measuring the charged Higgs mass compared to other semi-leptonic decays.

Figure 4.19 (top) shows the ratio  $B$ :

$$B = \frac{\Gamma(B \rightarrow \bar{D}\tau^+\nu_\tau)}{\Gamma(B \rightarrow \bar{D}\mu^+\nu_\mu)_{\text{SM}}} \quad (4.18)$$

as a function of the charged Higgs mass with several  $\tan \beta$  values. The width of each band represents uncertainty in the  $B \rightarrow D$  semi-leptonic form factor. The form factor is modeled as a function of the momentum transfer  $q^2$  using a slope parameter  $\rho_1^2$  [278], and the uncertainty is from the error of  $\rho_1^2$ . The Belle collaboration has measured  $\rho_1^2$  as  $\rho_1^2 = 1.33 \pm 0.22$  [279]. Figure 4.19 (bottom) shows the  $\delta B/B|_{\text{exp}}$  distribution as a function of  $\delta \rho_1^2/\rho_1^2|_{\text{exp}}$ . In the figure we show several curves with varying  $R \equiv M_W \tan \beta/M_H^\pm$ .

### 4.5.2 $B \rightarrow \bar{D}\tau^+\nu_\tau$ Reconstruction

Final states for the  $B \rightarrow \bar{D}\tau^+\nu_\tau$  decay include two  $\tau$ -neutrinos after taking into account the sub-decay of the  $\tau$ ; one additional neutrino exists when  $\tau$  decays into a leptonic mode. Because of the presence of two or more invisible particles, the decay of  $B \rightarrow \bar{D}\tau^+\nu_\tau$  has few kinematic constraints. To reduce the number of combinations of the reconstructed  $D$  and  $\tau$ , we first remove particles originating from the other  $B$  ( $B_{\text{ful}}$ ), which does not decay into  $B \rightarrow \bar{D}\tau^+\nu_\tau$  ( $B_{\text{sig}}$ ). We then reconstruct  $D$  and  $\tau$  candidates using the remaining particles. Finally, we apply kinematic selection requirements on the reconstructed  $D$  and  $\tau$  combination to reduce background.

In the following paragraphs we describe the reconstruction of  $B \rightarrow \bar{D}\tau^+\nu_\tau$ . A detailed description of the full reconstruction of  $B_{\text{ful}}$  mesons is given in subsection 4.1.2.

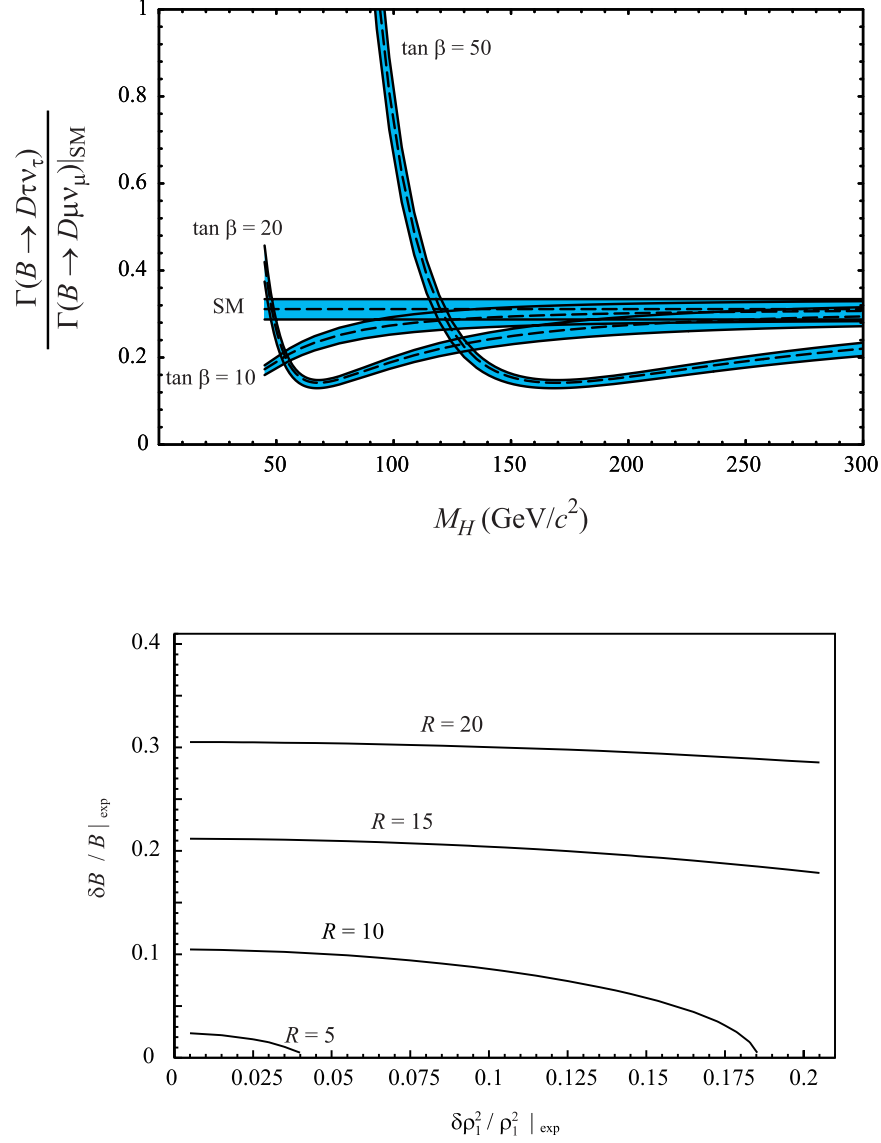


Figure 4.19: The top figure shows the ratio of  $\Gamma(B \rightarrow \bar{D}\tau^+\nu_\tau)$  to  $\Gamma(B \rightarrow \bar{D}\mu^+\nu_\mu)$ . The flat band is the prediction of the Standard Model; also shown is the charged Higgs contribution, which is a function of the charged Higgs mass with several  $\tan\beta$  values. The width of each band is due to uncertainty in the form factor. The bottom figure shows the  $\delta B/B|_{\text{exp}}$  distribution as a function of  $\delta\rho_1^2/\rho_1^2|_{\text{exp}}$  with varying  $R \equiv M_W \tan\beta/M_H^\pm$ .



**Light Meson Reconstructions** The  $K_S^0$  mesons are reconstructed from a pair of oppositely charged  $\pi$  tracks. The invariant mass of the  $\pi$  pair should be within  $|M_{\pi\pi} - M_{K_S^0}| < 15 \text{ GeV}/c^2$ . The position of closest approach of the  $\pi$  tracks should be displaced from the interaction point in the plane perpendicular to the beam axis.

Neutral pions are reconstructed from a pair of two photons. The  $\pi^0$  invariant mass is required to be within  $|M_{\gamma\gamma} - M_{\pi^0}| < 16 \text{ MeV}/c^2$ . We require the photon energy deposit in the calorimeter to be greater than 50 MeV.

**Charmed Meson Reconstructions** We reconstruct  $D$  mesons from  $\bar{D}^0 \rightarrow K^+\pi^-(\pi^0)$ ,  $K^+\pi^+\pi^-\pi^-(\pi^0)$ ,  $K_S^0\pi^+\pi^-(\pi^0)$ , and  $K_S^0\pi^0$ , where  $(\pi^0)$  indicates zero or one neutral pion. Charge conjugate modes are implicitly included throughout this section. These channels cover 35% of the total  $\bar{D}^0$  decay width. The charged  $D$  meson is reconstructed from  $D^+ \rightarrow K^-\pi^+\pi^+(\pi^0)$  and  $K_S^0\pi^+$ , covering 16% of the total  $D^+$  decay width.

We construct kaon ( $\mathcal{L}(K)$ ) and pion ( $\mathcal{L}(\pi)$ ) likelihoods to identify the particle species of each charged particle by combining the  $dE/dx$  in the drift chamber, the hit in the time of flight counter and the ring imaging Cherenkov counter. The charged particle is identified as a kaon if  $\mathcal{L}(K)/[\mathcal{L}(\pi) + \mathcal{L}(K)]$  exceeds 0.4; otherwise it is a pion.

The reconstructed  $D^0$  or  $D^+$  should have an invariant mass within  $|M_{K\pi\pi} - M_D| < 30 \text{ MeV}/c^2$ .

If more than one  $D$  meson is reconstructed, the  $D$  meson that has the closest invariant mass to the world average value is taken [58].

**$B$  Meson Reconstructions** The  $B \rightarrow \bar{D}\tau^+\nu_\tau$  decay is reconstructed from  $B^0 \rightarrow D^-\tau^+\nu_\tau$  and  $B^+ \rightarrow \bar{D}^0\tau^+\nu_\tau$ , where the  $\tau^+$  is identified in one of four following sub-decays:  $\tau^+ \rightarrow \pi^+\nu_\tau$ ,  $\rho^+(\pi^+\pi^0)\nu_\tau$ ,  $e^+\nu_\tau\bar{\nu}_e$ , and  $\mu^+\nu_\tau\bar{\nu}_\mu$ .

The  $B \rightarrow \bar{D}\tau^+\nu_\tau$  candidate is reconstructed by adding one charged particle, which is assumed to originate from the  $\tau^+$  decay, to the reconstructed  $D$  meson. Positively identified protons are rejected.

If the additional charged particle is consistent with the electron or muon hypothesis, the  $\tau^+$  decay is treated as a leptonic mode ( $\tau^+ \rightarrow \ell^+\nu_\tau\bar{\nu}_\ell$ ); otherwise the  $\tau^+$  decay is considered as a hadronic mode ( $\tau^+ \rightarrow \pi^+\nu_\tau$ ).

In the case of  $\tau^+ \rightarrow \pi^+\nu_\tau$  decay, one neutral pion (if it exists) that is associated to neither  $B_{\text{ful}}$  nor  $D$  decay is added to the  $\pi^+\nu_\tau$  final state to reconstruct  $\tau^+ \rightarrow \rho^+(\pi^+\pi^0)\nu_\tau$  mode. In this case, the  $\pi^+\pi^0$  invariant mass should be within  $|M_{\pi^+\pi^0} - M_{\rho^+}| < 300 \text{ MeV}/c^2$ .

To reject  $B \rightarrow \bar{D}^*\tau\nu_\tau$  events, we reconstruct  $D^*$ 's by adding a  $\pi^0$  to the reconstructed  $D$ . When  $|(M_{K\pi\pi\pi^0} - M_{K\pi\pi}) - \Delta M_{D^*-D}| < 10 \text{ MeV}/c^2$ , we discard the event.

If any charged particle and/or  $K_L^0$  candidate remains after the reconstructions of  $B_{\text{ful}}$  and  $B_{\text{sig}}$ , the event is rejected.

### 4.5.3 Kinematic Event Selection

We use three kinematic parameters to select  $B \rightarrow \bar{D}\tau^+\nu_\tau$  signal events from the reconstructed candidates.

The first is the residual cluster energy in the calorimeter ( $E_{\text{res}}$ ). We require  $E_{\text{res}} < 100 \text{ MeV}$ .

The second is the missing-mass squared defined by

$$|MM|^2 \equiv |p_{B_{\text{sig}}} - p_D - p_{X^+}|^2, \quad (4.19)$$

---

<sup>2</sup>Throughout this section, the symbol  $\ell$  indicates leptons except  $\tau$  unless otherwise specified.

where  $p_{X^+}$  is the charged particle momentum originating from the  $\tau^+$  decay. The momentum  $p_{B_{\text{sig}}}$  is given by  $p_{B_{\text{sig}}} = p_{\Upsilon(4S)} - p_{B_{\text{ful}}}$ .

The last is the cosine of the angle between the momenta of the two  $\tau$ -neutrinos ( $\cos\theta$ ) in the frame where  $\vec{p}_{B_{\text{sig}}} = \vec{p}_D$ . This parameter can only be defined for the  $\tau^+ \rightarrow h^+ \bar{\nu}_\tau$  sub-decay. Energy-momentum conservation for the  $B_{\text{sig}} \rightarrow D\tau^+(h^+ \bar{\nu}_\tau)\nu_\tau$  decay is expressed by

$$p_{B_{\text{sig}}} = p_D + p_{h^+} + p_{\bar{\nu}_\tau} + p_{\nu_\tau}. \quad (4.20)$$

The  $\tau^+$  and neutrino masses are given by

$$(p_{h^+} + p_{\bar{\nu}_\tau})^2 = m_\tau^2, \quad (4.21)$$

$$p_{\bar{\nu}_\tau}^2 = p_{\nu_\tau}^2 = 0. \quad (4.22)$$

We then boost the system to the frame where

$$\vec{p}_{B_{\text{sig}}} = \vec{p}_D. \quad (4.23)$$

Using Eq. (4.20)-(4.23), we have

$$(E_{B_{\text{sig}}} - E_D)^2 - 2E_{\nu_\tau}(E_{B_{\text{sig}}} - E_D) = m_\tau^2. \quad (4.24)$$

Then, the energies of the two neutrinos can be expressed in terms of measurable parameters as

$$E_{\nu_\tau} = \frac{(E_{B_{\text{sig}}} - E_D)^2 - m_\tau^2}{2(E_{B_{\text{sig}}} - E_D)}, \quad E_{\bar{\nu}_\tau} = E_{B_{\text{sig}}} - E_D - E_{h^+} - E_{\nu_\tau}. \quad (4.25)$$

Finally, we can measure  $\cos\theta$  using the following equation:

$$\begin{aligned} (\vec{p}_{B_{\text{sig}}} - \vec{p}_D - \vec{p}_{h^+})^2 &= (\vec{p}_{\bar{\nu}_\tau} + \vec{p}_{\nu_\tau})^2 \\ &= 2\vec{p}_{\bar{\nu}_\tau} \cdot \vec{p}_{\nu_\tau} \\ &= 2E_{\bar{\nu}_\tau}E_{\nu_\tau}\cos\theta. \end{aligned} \quad (4.26)$$

The  $\cos\theta$  of the signal events is limited from  $-1$  to  $+1$ , while that of the background events is unrestricted.

The background contamination is studied by using generic  $B$  decay MC samples. We generate samples of  $3.2 \times 10^6$  MC events with the fast simulator for generic charged and neutral  $B$  decays. In this case,  $8 \times 10^{-3}$  is taken as the branching fraction of  $B \rightarrow \bar{D}\tau^+\nu_\tau$  decay for both charged and neutral  $B$ . To increase statistics, the  $B_{\text{ful}}$  is pseudo-reconstructed using generator information, i.e.: the  $B_{\text{ful}}$  is fully reconstructed with perfect efficiency and purity.

Figure 4.20 shows the distribution of the reconstructed  $B^+ \rightarrow \bar{D}^0\tau^+(h^+\bar{\nu}_\tau)\nu_\tau$  candidates in the  $|MM|^2$ - $\cos\theta$  plane. The left column figures show the signal events only and the right ones show the background distribution (gray points) with the signal distributions (black points) superimposed. We determine the optimal signal region to be  $|MM|^2 > 0.1$  ( $\text{GeV}/c^2$ )<sup>2</sup> and  $-1.0 < \cos\theta < 0.8$ , irrespectively of the  $\tau^+ \rightarrow \pi^+\bar{\nu}_\tau$  or  $\tau^+ \rightarrow \rho^+\bar{\nu}_\tau$  by maximizing  $S/\sqrt{S+B}$  (FOM), where  $S$  and  $B$  are the numbers of reconstructed signal and background events, respectively.

Figure 4.21 shows the  $|MM|^2$  distribution of the reconstructed candidates of  $B^+ \rightarrow \bar{D}^0\tau^+(\ell^+\bar{\nu}_\tau\nu_\ell)\nu_\tau$ . For that decay irrespectively of the lepton flavor from the  $\tau$  decay, we determine the selection criteria  $|MM|^2 > 1.2$  ( $\text{GeV}/c^2$ )<sup>2</sup> by maximizing the FOM.

We find that  $|MM|^2$  and  $\cos\theta$  for the neutral  $B$  decay have similar distributions in both signal and background as the charged  $B$  decay. Therefore, the selection criteria determined by charged  $B$  decays are also applied to neutral  $B$  decays.

Table 4.9 summarizes the reconstruction efficiency. The numbers of reconstructed signal and the background events in the generic  $B$  decay MC samples are also shown.

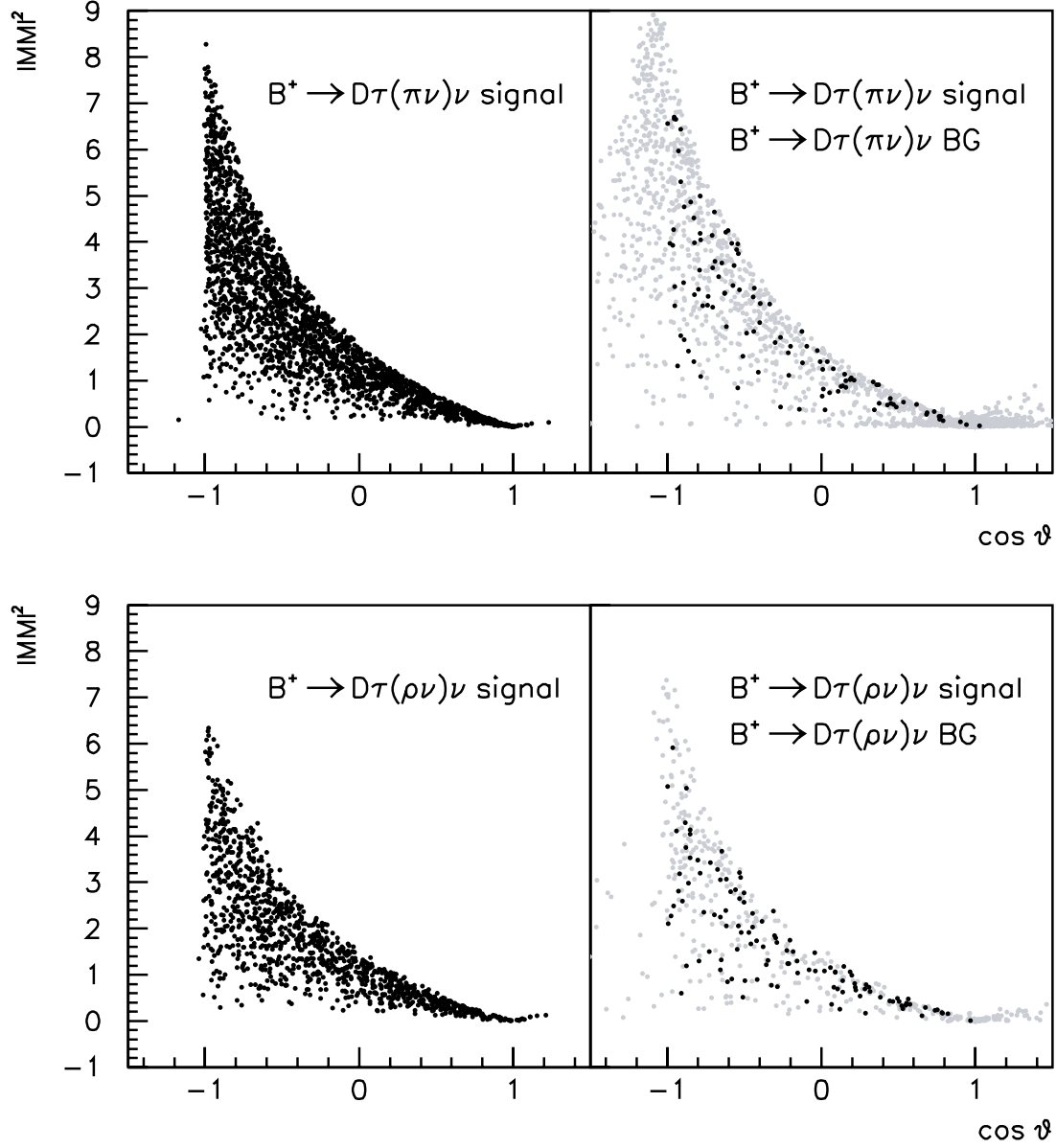


Figure 4.20: A scatter plot of the reconstructed  $B^+ \rightarrow \bar{D}^0 \tau^+ (h^+ \bar{\nu}_\tau) \nu_\tau$  candidates in the  $|MM|^2$ - $\cos \theta$  plane. The upper two figures are obtained in the  $\tau^+ \rightarrow \pi^+ \bar{\nu}_\tau$  decay, and the lower two figures are obtained in the  $\tau^+ \rightarrow \rho^+ (\pi^+ \pi^0) \bar{\nu}_\tau$  decay. The left figures show the distributions obtained from signal MC. In the right figures, the background distributions are shown by gray points and the signal distributions are shown by black points.

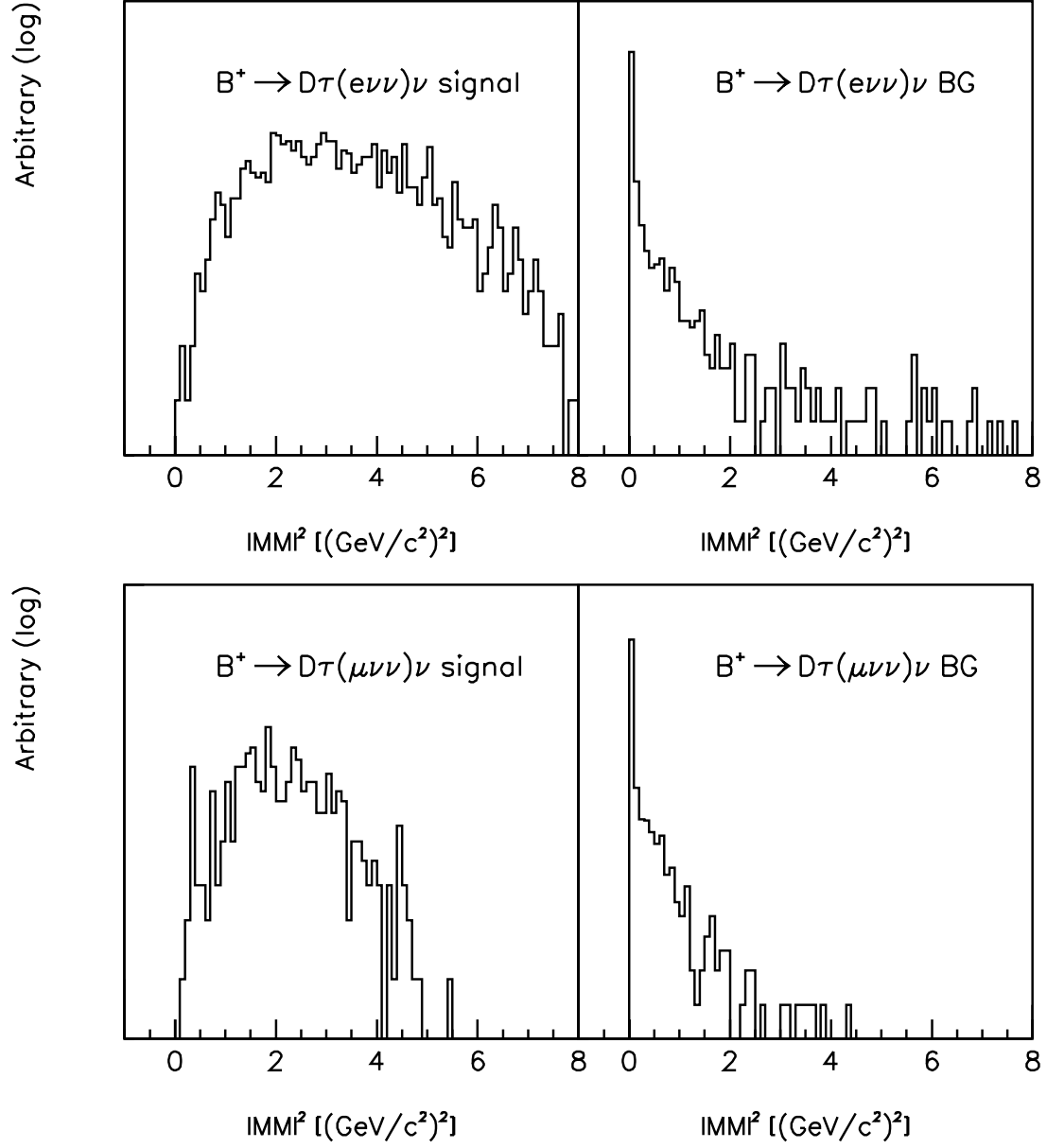


Figure 4.21: The  $|MM|^2$  distribution for reconstructed  $B^+ \rightarrow \bar{D}^0\tau^+(e^+\bar{\nu}_\tau\nu_e)\nu_\tau$  candidates (upper) and  $B^+ \rightarrow \bar{D}^0\tau^+(\mu^+\bar{\nu}_\tau\nu_\mu)\nu_\tau$  candidates (lower). The left figures show the distributions obtained from signal MC, and the right figures show the background.

Decay mode	efficiency (%)	$Br$	$N_{\text{sig}}$	$N_{\text{bkg}}$
$D^0\tau^+(\ell^+\bar{\nu}_\tau\nu_\ell)\nu_\tau$	$4.9 \pm 0.3$	$13.5 \times 10^{-4}$	213	293
$D^0\tau^+(h^+\bar{\nu}_\tau)\nu_\tau$	$10.9 \pm 0.5$	$13.6 \times 10^{-4}$	476	2085
$D^-\tau^+(\ell^+\bar{\nu}_\tau\nu_\ell)\nu_\tau$	$0.7 \pm 0.2$	$6.2 \times 10^{-4}$	15	22
$D^-\tau^+(h^+\bar{\nu}_\tau)\nu_\tau$	$3.3 \pm 0.4$	$6.4 \times 10^{-4}$	68	194

Table 4.9: Summary of the reconstruction efficiencies. The numbers of reconstructed signal ( $N_{\text{sig}}$ ) and the background events ( $N_{\text{bkg}}$ ) in generic  $B$  decay MC samples are also shown, where  $Br(B \rightarrow \bar{D}\tau^+\nu_\tau) = 8 \times 10^{-3}$  is assumed.

#### 4.5.4 Background Components

The dominant background source in the  $B^+ \rightarrow \bar{D}^0\tau^+(h^+\bar{\nu}_\tau)\nu_\tau$  signal region is the decay  $B^+ \rightarrow D^{*-}\ell^+\nu_\ell\pi^+$ , due mainly to a missing  $\ell^+$  and a slow pion from the  $D^{*-}$ . The next largest background modes are  $B^+ \rightarrow \bar{D}^{*0}\ell^+\nu_\ell$  with a missing  $\gamma$  or  $\pi^0$  from the  $\bar{D}^{*0}$  and misidentification of  $\ell^+$  as  $\pi^+$ , and the  $B^+ \rightarrow \bar{D}^{*0}\tau^+\nu_\tau$  with a missing slow pion. In this study the  $B^+ \rightarrow \bar{D}^0\tau^+(\ell^+\bar{\nu}_\tau\nu_\ell)\nu_\tau$  decay is considered as a background for the  $B^+ \rightarrow D^-\tau^+(h^+\bar{\nu}_\tau)\nu_\tau$  analysis; they contribute to the signal region due mostly to misidentification of the  $\ell^+$  from the  $\tau^+$  decay as  $\pi^+$ . The sum of the background modes listed above are  $\sim 45\%$  of the total background. The contribution from  $D_s$  inclusive decays is  $\sim 8\%$  of the total.

The largest contribution to the  $B^+ \rightarrow \bar{D}^-\tau^+(\ell^+\bar{\nu}_\tau\nu_\ell)\nu_\tau$  signal region comes from  $B^+ \rightarrow \bar{D}^{*-}\ell^+\nu_\ell\pi^+$  where both pions from  $B^+$  and  $\bar{D}^{*-}$  are missed. The next largest background components are  $B^+ \rightarrow \bar{D}^{*0}\ell^+\nu_\ell$  and  $B^+ \rightarrow \bar{D}^{*0}\tau^+\nu_\tau$  when the  $\gamma$  or  $\pi^0$  from the  $\bar{D}^{*0}$  are missed.

The dominant background mode in the  $B^0 \rightarrow D^-\tau^+(h^+\bar{\nu}_\tau)\nu_\tau$  signal region is  $B^0 \rightarrow D^-\tau^+\nu_\tau$  with a mis-reconstructed  $\tau^+$ ; the next largest is  $B^0 \rightarrow D^{*-}\mu^+\nu_\mu$ , although it is only  $\sim 20\%$  of the total. No other background modes make significant contributions in the signal region.

For the  $B^0 \rightarrow D^-\tau^+(\ell^+\bar{\nu}_\tau\nu_\ell)\nu_\tau$  mode, because of the small MC statistics, we cannot yet evaluate the background.

#### 4.5.5 Statistical Significance

As described in subsection 4.1.2, the full reconstruction efficiencies for charged (neutral)  $B$  mesons are estimated to be around 0.2% (0.1%) for a purity of about 80%.

Table 4.10 lists the expected signal yields and backgrounds at integrated luminosities of 5 and 50  $\text{ab}^{-1}$ . The values include a correction for the purity of  $B_{\text{ful}}$  reconstruction. We assume  $Br(B \rightarrow \bar{D}\tau^+\nu_\tau) = 8 \times 10^{-3}$  in the table. The values listed are obtained by scaling the results in Table 4.9 according to the integrated luminosity. The expected uncertainties in the measured branching fraction ( $\delta(Br)/Br$ ) are also shown.

The branching fraction for  $B^+ \rightarrow \bar{D}^0\tau^+\nu_\tau$  is expected to be determined with  $12\sigma$  statistical significance at an integrated luminosity of 5  $\text{ab}^{-1}$ . The branching fractions of the neutral  $B$  modes can also be measured at 50  $\text{ab}^{-1}$  with  $11\sigma$  significance.

#### 4.5.6 Systematic Uncertainty

Major sources of systematic uncertainty in the branching fraction measurement in  $B \rightarrow \bar{D}\tau^+\nu_\tau$  decay are expected to be  $B_{\text{ful}}$  reconstruction efficiency and purity, particle identification efficiency and purity, and the slow pion detection efficiency.

Decay mode	5 ab <sup>-1</sup>			50 ab <sup>-1</sup>		
	$N_{\text{sig}}$	$N_{\text{bkg}}$	$\delta(Br)/Br$	$N_{\text{sig}}$	$N_{\text{bkg}}$	$\delta(Br)/Br$
$\bar{D}^0 \tau^+ (\ell^+ \bar{\nu}_\tau \nu_\ell) \nu_\tau$	$280 \pm 20$	$550 \pm 20$	7.9%	$2800 \pm 50$	$5500 \pm 70$	2.5%
$\bar{D}^0 \tau^+ (h^+ \bar{\nu}_\tau) \nu_\tau$	$620 \pm 20$	$3600 \pm 60$		$6200 \pm 80$	$36000 \pm 200$	
$D^- \tau^+ (\ell^+ \bar{\nu}_\tau \nu_\ell) \nu_\tau$	$10 \pm 3$	$21 \pm 5$	28.5%	$98 \pm 10$	$210 \pm 10$	9.0%
$D^- \tau^+ (h^+ \bar{\nu}_\tau) \nu_\tau$	$45 \pm 7$	$170 \pm 10$		$450 \pm 20$	$1700 \pm 40$	

Table 4.10: The expected signal yields and backgrounds at integrated luminosities of 5 and 50 ab<sup>-1</sup>, assuming  $Br(B \rightarrow \bar{D} \tau^+ \nu_\tau) = 8 \times 10^{-3}$ . The expected uncertainties in the measured branching fraction ( $\delta(Br)/Br$ ) are also shown.

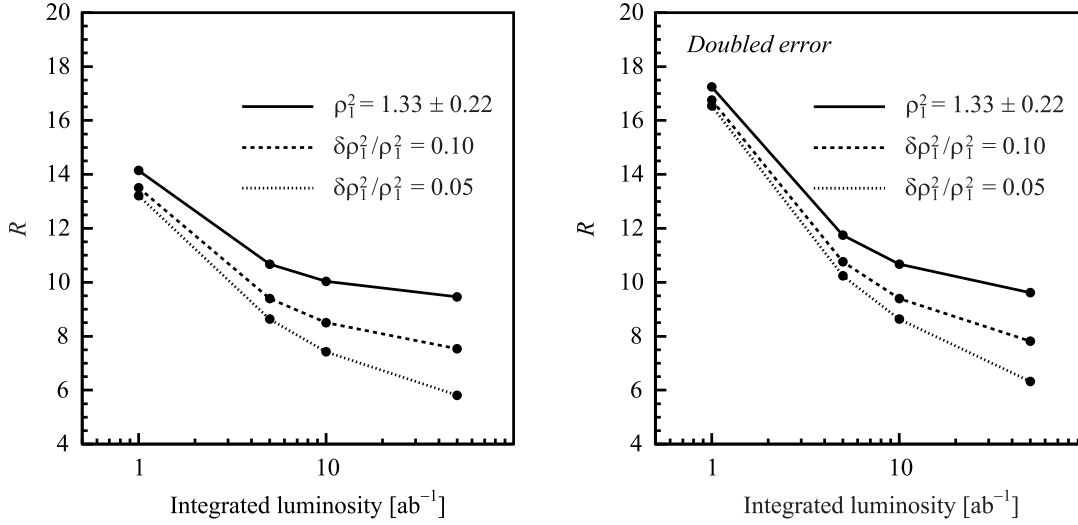


Figure 4.22: The left figure shows the maximum  $R$  constrained by the  $B^+ \rightarrow \bar{D}^0 \tau^+ \nu_\tau$  branching fraction measurement as a function of the integrated luminosity for several values of  $\delta \rho_1^2 / \rho_1^2|_{\text{exp}}$ . The right figure shows the same plot for the case with double the uncertainty in the measured branching fraction

#### 4.5.7 Constraints on the Charged Higgs Mass

Figure 4.22 (left) shows the maximum  $R$  value constrained by the branching fraction measurement of  $B^+ \rightarrow \bar{D}^0 \tau^+ \nu_\tau$  as a function of the integrated luminosity for several  $\delta \rho_1^2 / \rho_1^2|_{\text{exp}}$ . The right figure shows the case assuming a doubled uncertainty of the measured branching fraction. The systematic uncertainty in the branching fraction measurement is not considered. We ignore the uncertainty in  $\delta B/B|_{\text{exp}}$  that comes from the uncertainty in the  $B^+ \rightarrow \bar{D}^0 \mu^+ \nu_\mu$  branching fraction because it can be determined much precisely than that of  $\bar{D}^0 \tau^+ \nu_\tau$ . We expect

$$M_H > \frac{M_W \tan \beta}{11}$$

at an integrated luminosity of 5 ab<sup>-1</sup>, assuming that the current  $\rho_1^2$  precision is unchanged.

#### 4.5.8 Summary

The  $B \rightarrow \bar{D}\tau^+\nu_\tau$  decay is a sensitive mode to probe the charged Higgs in the MSSM. Using this decay mode we expect that the charged Higgs mass will be constrained by  $M_H > M_W \tan \beta/11$  at an integrated luminosity of  $5 \text{ ab}^{-1}$ .

Source	Irreducible	Error of $\sin 2\phi_1$
Wrong tag		0.007
Physics parameters		0.002
Vertexing	✓	0.012
Background fraction		0.006
Background $ \Delta t $ shape		0.001
Resolution function		0.005
Resolution parameterization	✓	0.006
Tag-side interference	✓	0.001
Possible fit bias		0.008
Total		0.019

Table 4.11: Systematic errors for  $\sin 2\phi_1$  measured with the  $J/\psi K_S$  mode at  $140 \text{ fb}^{-1}$ .

## 4.6 $\sin 2\phi_1$

Very precise measurements of  $\sin 2\phi_1$ , or  $\mathcal{S}_{J/\psi K_S^0}$ , will remain important at SuperKEKB. There are two major reasons. One is to search for a new  $CP$ -violating phase from the SM in  $CP$  violation in  $b \rightarrow s$  transitions by testing a SM prediction  $\mathcal{S}_{\phi K_S^0} = \mathcal{S}_{J/\psi K_S^0}$ . The other is to check the consistency of the Unitarity Triangle. As explained in Section 2.4.1,  $\sin 2\phi_1$  is determined using the  $B^0 \rightarrow J/\psi K_S^0$  mode with very small hadronic uncertainties. It is also insensitive to effects beyond the SM. Thus it serves as a reliable reference point for the SM.

The present world average value for  $\sin 2\phi_1$  is obtained with the modes  $B^0 \rightarrow J/\psi K_L^0$ ,  $J/\psi K^{*0}$ ,  $\psi(2S)K_S^0$ ,  $\chi_{c1}K_S^0$  and  $\eta_c K_S^0$  in addition to the  $B^0 \rightarrow J/\psi K_S^0$  decay. This is to reduce statistical uncertainties. With an integrated luminosity of  $5 \text{ ab}^{-1}$ , however, the systematic uncertainties will be dominant. Therefore, in this study we use only the gold-plated mode  $B^0 \rightarrow J/\psi(\rightarrow \ell^+\ell^-)K_S^0(\pi^+\pi^-)$  to minimize systematic uncertainties. We perform MC pseudo-experiments assuming that the performance of the detector at SuperKEKB is identical to that of the present Belle detector. The analysis procedure for the measurements of time-dependent  $CP$  asymmetries at Belle is described in Section 4.1.2. In addition to the standard 2-parameter fit, we also test a 1-parameter fit with  $\sin 2\phi_1$  as the free parameter assuming  $\mathcal{A}_{J/\psi K_S^0} = 0$ . Because of the additional assumption, the error on  $\sin 2\phi_1$  is slightly smaller than that for  $\mathcal{S}_{J/\psi K_S^0}$ . In the following, we treat these two cases separately. An example of a fit to a  $\Delta t$  distribution for  $B^0 \rightarrow J/\psi K_S^0$  candidates in a MC pseudo-experiment at  $5 \text{ ab}^{-1}$  is shown in Fig. 4.23.

Sources of systematic errors include uncertainties in the flavor tagging, in the vertex reconstruction, in the background fractions and  $\Delta t$  distributions, in the resolution function, in  $\Delta m_d$  and  $\tau_{B^0}$ , a possible bias in the fit, and the effect of interference [280] in the  $f_{\text{tag}}$  final state. Some of these uncertainties are evaluated from control samples, which have large but finite statistics. As the integrated luminosity increases, this part of the systematic error will decrease. In order to estimate the expected systematic error at  $5 \text{ ab}^{-1}$ , we therefore need to separate such *reducible* systematic errors from the other part, which is *irreducible*. In this study, we conservatively assume that uncertainties that do not arise from statistics of control samples are irreducible, and use estimates obtained for the  $140 \text{ fb}^{-1}$  data for any integrated luminosity. Further studies on these “*irreducible*” errors will probably find a way to reduce them. Table 4.11 and 4.12 summarize the sources of systematic errors for  $\sin 2\phi_1$  (1-parameter fit) and  $\mathcal{S}$  and  $\mathcal{A}$  (2-parameter fit), respectively. All the values are evaluated at  $140 \text{ fb}^{-1}$ .

The total irreducible systematic error for  $\mathcal{S}$  is estimated to be 0.014 (0.013) for  $\mathcal{S}_{J/\psi K_S^0}$



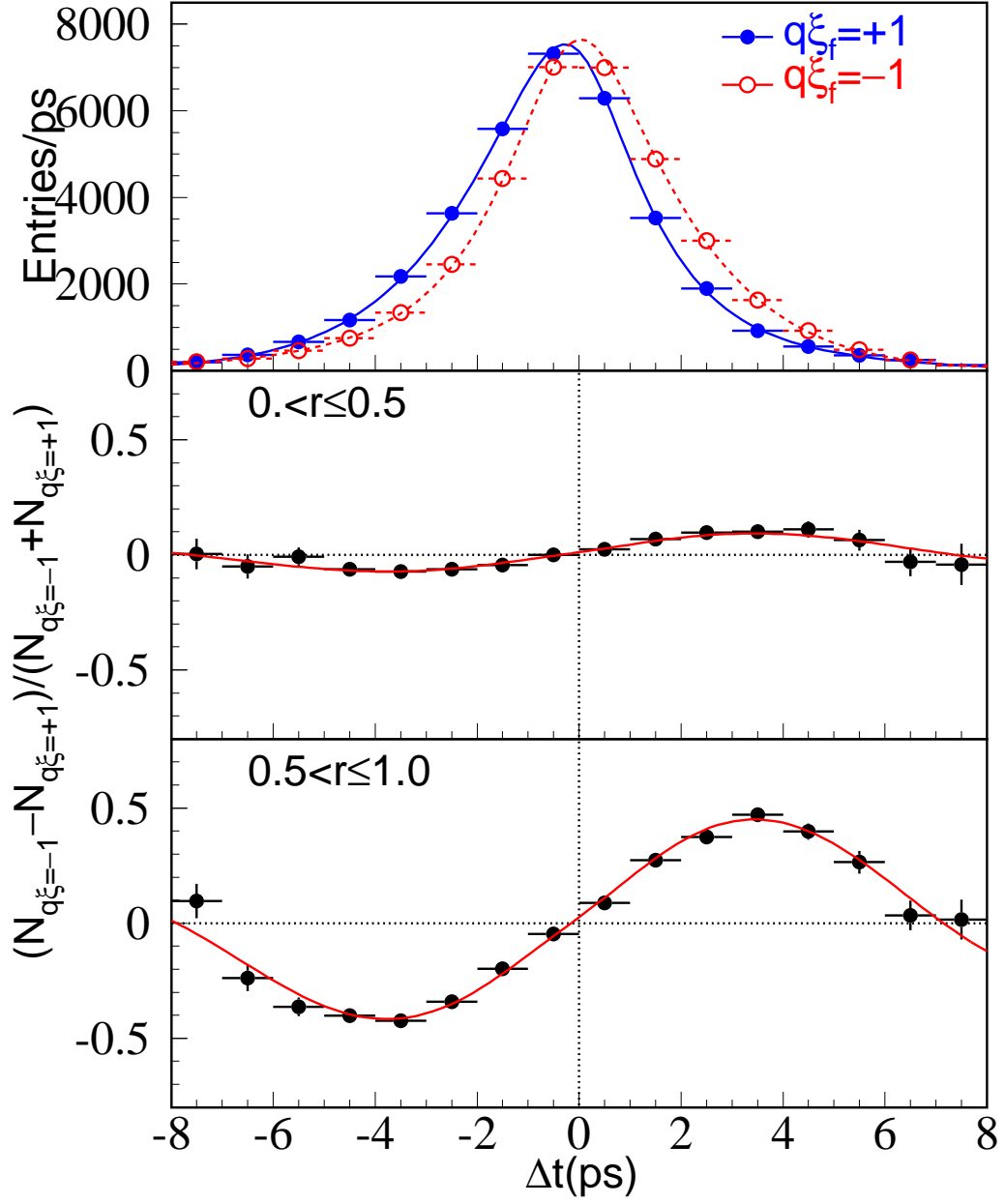


Figure 4.23: An example of a fit to a MC pseudo-experiment at  $5 \text{ ab}^{-1}$ .

Source	Irreducible	Error of $\mathcal{S}$	Error of $\mathcal{A}$
Wrong tag		0.007	0.008
Physics parameters		0.002	0.001
Vertexing	✓	0.012	0.026
Background fraction		0.006	0.012
Background $ \Delta t $ shape		0.001	0.000
Resolution function		0.005	0.007
Resolution parameterization	✓	0.006	0.002
Tag-side interference	✓	0.001	0.027
Possible fit bias		0.008	0.006
Total		0.019	0.041

Table 4.12: Systematic errors on  $\mathcal{A}$  and  $\mathcal{S}$  measured with the  $J/\psi K_S$  mode at  $140 \text{ fb}^{-1}$ .

		Statistical	Systematic		Total
			reducible	irreducible	
$\sin 2\phi_1$	( $140 \text{ fb}^{-1}$ )	0.080	0.014		0.082
	( $5 \text{ ab}^{-1}$ )	0.013	0.002	0.013	0.019
	( $50 \text{ ab}^{-1}$ )	0.004	0.001		0.014
$\mathcal{S}_{J/\psi K_S^0}$	( $140 \text{ fb}^{-1}$ )	0.080	0.014		0.082
	( $5 \text{ ab}^{-1}$ )	0.013	0.002	0.014	0.019
	( $50 \text{ ab}^{-1}$ )	0.004	0.001		0.015
$\mathcal{A}_{J/\psi K_S^0}$	( $140 \text{ fb}^{-1}$ )	0.056	0.017		0.070
	( $5 \text{ ab}^{-1}$ )	0.009	0.003	0.038	0.039
	( $50 \text{ ab}^{-1}$ )	0.003	0.001		0.038

Table 4.13: Expected errors at  $140 \text{ fb}^{-1}$ ,  $5 \text{ ab}^{-1}$  and  $50 \text{ ab}^{-1}$ .

( $\sin 2\phi_1$ ). The dominant sources of the irreducible systematic error are the effect of detector misalignment (0.008) and uncertainties in the resolution function determination (0.007). The systematic error for  $\mathcal{A}$  is dominated by the tag-side interference. As mentioned above, there will be a possibility to reduce these “*irreducible*” errors from dedicated studies. Table 4.13 lists the expected errors at  $140 \text{ fb}^{-1}$ ,  $5 \text{ ab}^{-1}$  and  $50 \text{ ab}^{-1}$ .

The total error for  $\mathcal{S}_{J/\psi K_S^0}$ ,  $\sigma_{\text{tot}}(\mathcal{S}_{J/\psi K_S^0})$ , is obtained from

$$\sigma_{\text{tot}}(\mathcal{S}_{J/\psi K_S^0}) = \sqrt{0.080^2 \times 0.14/\mathcal{L}_{\text{int}} + 0.014^2 \times 0.14/\mathcal{L}_{\text{int}} + 0.014^2}, \quad (4.27)$$

where  $\mathcal{L}_{\text{int}}$  is the integrated luminosity in the unit of  $\text{ab}^{-1}$ . We obtain  $\sigma_{\text{tot}}(\mathcal{S}_{J/\psi K_S^0}) = 0.019$  at  $\mathcal{L}_{\text{int}} = 5 \text{ ab}^{-1}$ , which is much smaller than the statistical uncertainties for  $\mathcal{S}_{\phi K_S^0}$  and  $\mathcal{S}_{\eta' K_S^0}$ .

	central value WA from [246]	error at 140 fb <sup>-1</sup>	error at 500 fb <sup>-1</sup>	error at 5 ab <sup>-1</sup>	error at 50 ab <sup>-1</sup>
$BR(\pi^+\pi^-)$	$4.55 \pm 0.44$	0.50	0.25	0.082	0.026
$BR(\pi^+\pi^0)$	$5.27 \pm 0.79$	0.88	0.47	0.15	0.47
$BR(\pi^0\pi^0)$	$1.90 \pm 0.47$	0.65	0.34	0.11	0.034
$\mathcal{S}_{\pi\pi}$	$-0.58 \pm 0.20$	0.23	0.12	0.039	0.012
$\mathcal{A}_{\pi\pi}$	$+0.38 \pm 0.16$	0.19	0.10	0.031	0.010
$\mathcal{A}_{\pi^0\pi^0}$	0.0	1.00	0.53	0.17	0.053

Table 4.14: Estimated errors for the  $\pi\pi$  branching ratios and asymmetries.

## 4.7 $\phi_2$

The CKM angle  $\phi_2$  can be measured using multi-pion final states coming from the quark-level decay  $b \rightarrow u\bar{u}d$ . As discussed in Section 2.4 the determination through the time-dependent asymmetry of  $B^0 \rightarrow \pi^+\pi^-$  suffers from large penguin contributions. Here we consider two methods to eliminate an effect of the penguin amplitude: an isospin analysis of  $B \rightarrow \pi\pi$  [70], and Dalitz analysis of  $B \rightarrow \rho\pi$  [71].

### 4.7.1 Status of the $B^0 \rightarrow \pi^+\pi^-$ analysis

Time-dependent  $CP$  asymmetries defined in (2.41) for  $B^0 \rightarrow \pi^+\pi^-$  decays have been measured by the Belle [13, 281] and BaBar [282] collaborations. Based on  $152 \times 10^6$  [13] and  $88 \times 10^6$  [282]  $B\bar{B}$  pairs, they obtain

$$\mathcal{A}_{\pi\pi} = +0.58 \pm 0.15 \pm 0.07, \quad \mathcal{S}_{\pi\pi} = -1.00 \pm 0.21 \pm 0.07 \quad [281], \quad (4.28)$$

$$\mathcal{A}_{\pi\pi} = +0.30 \pm 0.25 \pm 0.04, \quad \mathcal{S}_{\pi\pi} = -0.02 \pm 0.34 \pm 0.05 \quad [282]. \quad (4.29)$$

The first and the second errors are statistical and systematic errors, respectively. BaBar also showed a preliminary result at Lepton Photon 2003 based on 123 million  $B\bar{B}$  pairs; they obtain  $\mathcal{A}_{\pi\pi} = +0.19 \pm 0.19 \pm 0.05$  and  $\mathcal{S}_{\pi\pi} = -0.40 \pm 0.22 \pm 0.03$ . The world average values using the latest results are  $\mathcal{A}_{\pi\pi} = +0.46 \pm 0.13$  and  $\mathcal{S}_{\pi\pi} = -0.74 \pm 0.16$  [246].

From the latest Belle result [281], the case that  $CP$  symmetry is conserved,  $\mathcal{A}_{\pi\pi} = \mathcal{S}_{\pi\pi} = 0$ , is ruled out at a level of 5.2 standard deviations. Thus this is the first observation of  $CP$ -violating asymmetries in  $B^0 \rightarrow \pi^+\pi^-$  decays. A 95.5% CL region of  $\mathcal{A}_{\pi\pi}$  and  $\mathcal{S}_{\pi\pi}$  gives  $90^\circ \leq \phi_2 \leq 146^\circ$  with a modest assumption of  $|P_{\pi\pi}/T_{\pi\pi}| < 0.45$ . From the theoretical side, QCD factorization gives  $-6 \pm 12\%$  for the direct  $CP$  asymmetry  $\mathcal{A}_{\pi\pi}$  [102], while perturbative QCD (pQCD) suggests a larger direct asymmetry in the range (16–30%) [283].

### 4.7.2 Isospin analysis for $B \rightarrow \pi\pi$

Here we describe the expected sensitivity for the determination of  $\phi_2$  at SuperKEKB using the  $\pi\pi$  isospin analysis.

Estimated errors for the branching ratios and asymmetries at the target luminosities are shown in Table 4.14. We assume the current world average [246] for the central values, and also assume that the direct  $CP$  violation is absent for the  $B^0 \rightarrow \pi^0\pi^0$  decay *i.e.*,  $\mathcal{A}_{\pi^0\pi^0} = 0.0$ . In the following analysis we use the CKMfitter program [284].

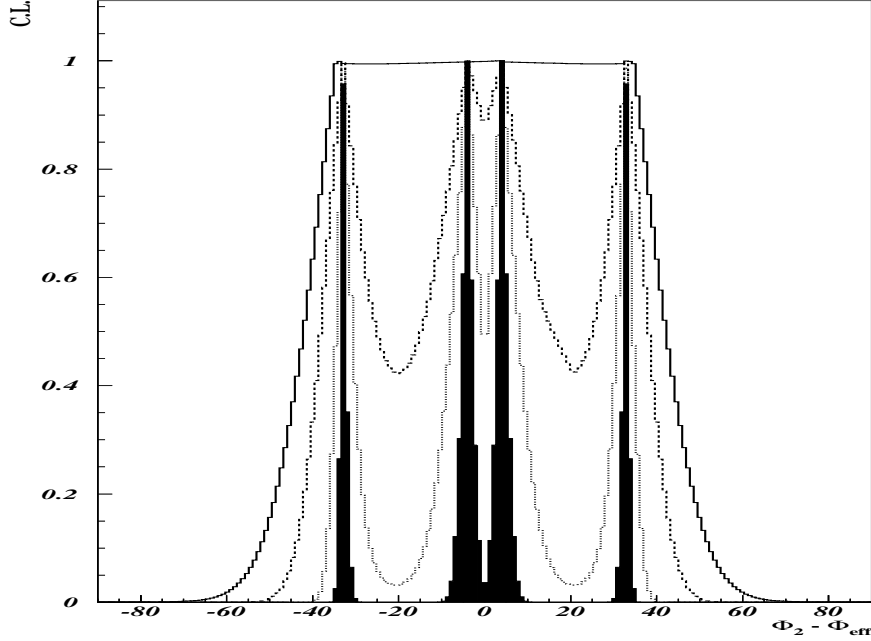


Figure 4.24: CL versus  $\phi_2 - \phi_{2\text{eff}}$  (deg) for the inputs given in Table 4.14 at 140 fb $^{-1}$  (solid curve), 500 fb $^{-1}$  (dashed curve), 5 ab $^{-1}$  (dotted curve), and 50 ab $^{-1}$  (shaded area).

From the  $\pi^+\pi^-$  time-dependent asymmetry we may extract the parameters  $\mathcal{S}_{\pi\pi}$  and  $\mathcal{A}_{\pi\pi}$ . The phase of the parameter  $\lambda_{\pi\pi} = (q/p)(\bar{A}_{\pi\pi}/A_{\pi\pi})$  is extracted as

$$\sin 2\phi_{2\text{eff}} = \frac{\mathcal{S}_{\pi\pi}}{\sqrt{1 - \mathcal{A}_{\pi\pi}^2}}, \quad (4.30)$$

which is equal to  $\sin 2\phi_2$  if the decay is dominated by the tree amplitude. In the presence of a penguin contribution, we have to subtract the penguin amplitude using isospin relations (2.54) and (2.55).

The results for  $\phi_2 - \phi_{2\text{eff}}$  and  $\phi_2$  are plotted in Figures 4.24 and 4.25, respectively. In those figures the confidence level is plotted at target luminosities up to 50 ab $^{-1}$ . The absence of direct  $CP$  violation for the  $B^0 \rightarrow \pi^0\pi^0$  decay leads to the symmetric solutions shown in the figures.

When flavor tagging for  $B^0 \rightarrow \pi^0\pi^0$  is missing as in the 140 fb $^{-1}$  case, only the outer borders of the curves can be obtained. By knowing the flavor of  $B^0 \rightarrow \pi^0\pi^0$  the inner structure shows up, and  $\phi_2 - \phi_{2\text{eff}}$  is determined up to a four-fold ambiguity and  $\phi_2$  is determined up to an eight-fold ambiguity in the range  $(0^\circ, 180^\circ)$ .

Although we have assumed  $\mathcal{A}_{\pi^0\pi^0} = 0$  in the estimation above, theoretical predictions for  $\mathcal{A}_{\pi^0\pi^0}$  allow large values [285]. Figure 4.26 shows CL as a function of  $\phi_2$  at 50 ab $^{-1}$  for several values of  $\mathcal{A}_{\pi^0\pi^0}$ . The best  $\phi_2$  resolution ( $0.8^\circ \sim 1.4^\circ$ ) is expected at  $\mathcal{A}_{\pi^0\pi^0} = -0.13$ , for which the angle between  $A^{+0}$  and  $A^{+-}$  is the same as the angle between  $\bar{A}^{+0}$  and  $\bar{A}^{+-}$ . At  $\mathcal{A}_{\pi^0\pi^0} = -0.86$  and  $+0.35$ , on the other hand, one isospin triangle is squashed, and the expected  $\phi_2$  resolution is about  $2.6^\circ$  except for the region where two solutions overlap.

Since the decay  $B^+ \rightarrow \pi^+\pi^0$  has no strong penguin contribution, the occurrence of the direct  $CP$  violation in this decay mode would imply an electroweak penguin contribution. The effect

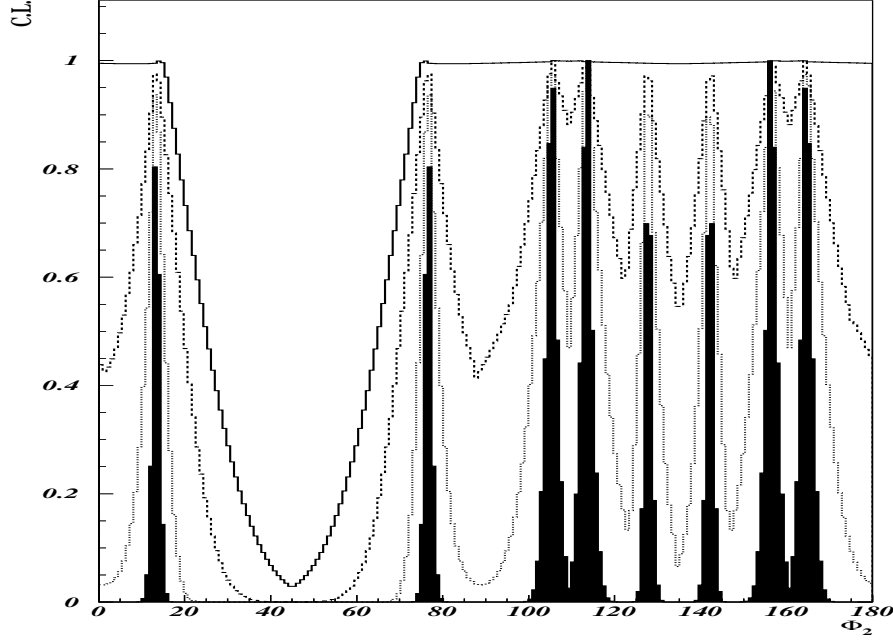


Figure 4.25: CL versus  $\phi_2$  (deg) for the inputs given in Table 4.14 at  $140 \text{ fb}^{-1}$  (solid curve),  $500 \text{ fb}^{-1}$  (dashed curve),  $5 \text{ ab}^{-1}$  (dotted curve), and  $50 \text{ ab}^{-1}$  (shaded area).

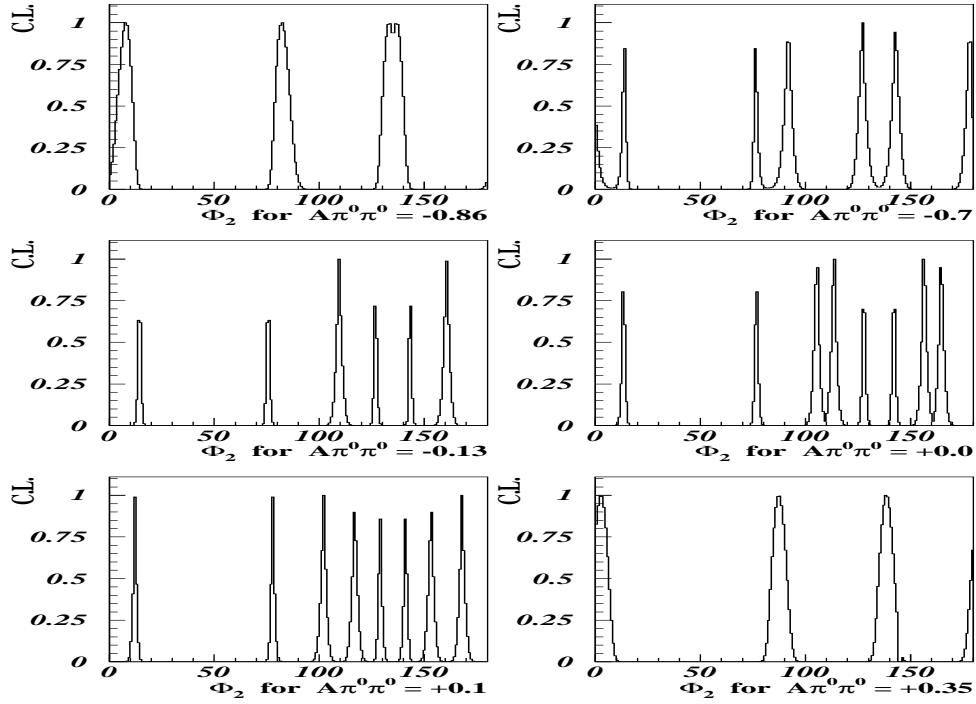


Figure 4.26: CL versus  $\phi_2$  (deg) at  $50 \text{ ab}^{-1}$  for  $\mathcal{A}_{\pi^0\pi^0} = -0.86$  (top left),  $-0.7$  (top right),  $-0.13$  (middle left),  $0.0$  (middle right),  $+0.1$  (bottom left), and  $+0.35$  (bottom right).

amplitudes	$ A^{+0}  (\times 10^{-4})$	$ A^{+-}  (\times 10^{-4})$	$ A^{00}  (\times 10^{-4})$
with EWP	1.68	2.30	0.82
w/o EWP	1.69	2.31	0.87
difference	0.5%	0.5%	6.5%
amplitudes	$ \bar{A}^{+0}  (\times 10^{-4})$	$ \bar{A}^{+-}  (\times 10^{-4})$	$ \bar{A}^{00}  (\times 10^{-4})$
with EWP	1.68	2.90	0.96
w/o EWP	1.69	2.90	1.01
difference	0.5%	0.0%	5.5%

Table 4.15: A perturbative QCD calculation of the  $B \rightarrow \pi\pi$  amplitudes with and without electroweak penguin contributions.

of the electroweak penguin to  $\pi\pi$  amplitudes is estimated in Table 4.15 using the perturbative QCD calculation with and without the electroweak penguin (EWP) amplitude. This calculation suggests that the effect on  $\pi^+\pi^-$  and  $\pi^\pm\pi^0$  is negligible, while the effect on  $\pi^0\pi^0$  is at a level of several percent.

#### 4.7.3 Status of the $B^0 \rightarrow \rho\pi$ analysis

In principle, the CKM angle  $\phi_2$  can be measured even in the presence of penguin contributions, using a full Dalitz plot analysis. However, there are difficulties from combinatorics and from the low efficiency in a three-body topology with a  $\pi^0$  as well as large backgrounds from mis-reconstructed signal events and other decays. In order to extract  $\phi_2$  cleanly, data with large statistics are thus required.

Unlike the  $B^0 \rightarrow \pi^+\pi^-$  decay,  $B^0 \rightarrow \rho^\pm\pi^\mp$  is not a  $CP$  eigenstate. In  $B^0 \rightarrow \rho^\pm\pi^\mp$  decay, four different flavor decays ( $B^0(\bar{B}^0) \rightarrow \rho^\pm\pi^\mp$ ) must be considered. Following a quasi-two-body approach, the current analysis by the BaBar collaboration [286] is restricted to the two regions of the  $\pi^\pm\pi^0 h^\pm$  Dalitz plot ( $h = \pi$  or  $K$ ) that are dominated by  $\rho^\pm h^\mp$ . The decay rate is given by

$$f_q^{\rho^\pm h^\mp}(\Delta t) = (1 \pm A_{CP}^{\rho h}) \frac{e^{-|\Delta t|/\tau_{B^0}}}{4\tau_{B^0}} \times [1 + q \cdot \{(S_{\rho h} \pm \Delta S_{\rho h}) \sin(\Delta m_d \Delta t) - (C_{\rho h} \pm \Delta C_{\rho h}) \cos(\Delta m_d \Delta t)\}], \quad (4.31)$$

where  $\Delta t = t_{\rho h} - t_{\text{tag}}$  is the time interval between the decay of  $B_{\rho h}^0$  and that of the other  $B^0$  meson. One finds a relation

$$S_{\rho\pi} \pm \Delta S_{\rho\pi} = \sqrt{1 - (C_{\rho\pi} \pm \Delta C_{\rho\pi})^2} \sin(2\phi_{2\text{eff}}^\pm \pm \delta), \quad (4.32)$$

where  $2\phi_{2\text{eff}}^\pm = \arg[(q/p)(\bar{A}_{\rho\pi}^\pm/A_{\rho\pi}^\mp)]$  and  $\delta = \arg[A_{\rho\pi}^-/A_{\rho\pi}^+]$ .  $\arg[q/p]$  is the  $B^0 - \bar{B}^0$  mixing phase, and  $A_{\rho\pi}^+(A_{\rho\pi}^-)$  and  $\bar{A}_{\rho\pi}^-(\bar{A}_{\rho\pi}^+)$  are the transition amplitudes for the processes  $B^0(\bar{B}^0) \rightarrow \rho^+\pi^-$  and  $B^0(\bar{B}^0) \rightarrow \rho^-\pi^+$ , respectively. The angles  $\phi_{2\text{eff}}^\pm$  are equal to  $\phi_2$  if contributions from penguin amplitudes are absent.

With a data sample of  $89 \times 10^6$   $B\bar{B}$  pairs the BaBar Collaboration obtained [286]

$$A_{CP}^{\rho\pi} = -0.18 \pm 0.08 \pm 0.03, \quad (4.33)$$

$$C_{\rho\pi} = +0.36 \pm 0.18 \pm 0.04, \quad S_{\rho\pi} = +0.19 \pm 0.24 \pm 0.03, \quad (4.34)$$

$$\Delta C_{\rho\pi} = +0.28 \pm 0.19 \pm 0.04, \quad \Delta S_{\rho\pi} = +0.15 \pm 0.25 \pm 0.03. \quad (4.35)$$

#### 4.7.4 Dalitz plot analysis of $B^0 \rightarrow \rho\pi$

A measurement of  $\phi_2$  using isospin relations among  $B \rightarrow \pi\pi$  decays has a four-fold ambiguity as we mentioned in Section 2.4. This ambiguity can be avoided with a full Dalitz plot analysis of the  $B^0 \rightarrow \rho\pi \rightarrow \pi^+\pi^-\pi^0$  decay [71].

Using the notation of [287], the decay amplitudes of  $B \rightarrow \rho\pi$  are expressed as

$$\sqrt{2}A(B^+ \rightarrow \rho^+\pi^0)(\equiv S_1) = T^{+0} + 2P_1, \quad (4.36)$$

$$\sqrt{2}A(B^+ \rightarrow \rho^0\pi^+)(\equiv S_2) = T^{0+} - 2P_1, \quad (4.37)$$

$$A(B^0 \rightarrow \rho^+\pi^-)(\equiv S_3) = T^{+-} + P_1 + P_0, \quad (4.38)$$

$$A(B^0 \rightarrow \rho^-\pi^+)(\equiv S_4) = T^{-+} - P_1 + P_0, \quad (4.39)$$

$$A(B^0 \rightarrow \rho^0\pi^0)(\equiv S_5) = T^{+0} + T^{0+} - T^{+-} - T^{-+} - 2P_0. \quad (4.40)$$

Here  $T^{ij}$  ( $i, j = +, -, \text{ or } 0$ ) are the tree amplitudes, and  $P_0$  and  $P_1$  are the penguin amplitudes for  $I = 0$  and 1 final states, respectively. Similarly, for the  $CP$ -conjugate channels, we define the amplitudes  $\bar{S}$ ,  $\bar{T}^{ij}$ , and  $\bar{P}_i$  which differ from the original amplitudes only in the sign of the weak phase of each term. From isospin constraints, the following relation is held:

$$S_1 + S_2 = S_3 + S_4 + S_5, \quad (4.41)$$

$$\bar{S}_1 + \bar{S}_2 = \bar{S}_3 + \bar{S}_4 + \bar{S}_5. \quad (4.42)$$

In the full Dalitz plot analysis for the  $\pi^+\pi^-\pi^0$  final states, we do not specify which intermediate state the  $\pi^+\pi^-\pi^0$  final state comes from. Thus, we can see the quantum interference. The amplitude of the  $B^0 \rightarrow \pi^+\pi^-\pi^0$  decay is expressed as

$$A(f) = f^+S_3 + f^-S_4 + f^0S_5/2, \quad (4.43)$$

while the amplitude of the  $CP$ -conjugate channel is given by

$$\bar{A}(f) = f^- \bar{S}_3 + f^+ \bar{S}_4 + f^0 \bar{S}_5/2. \quad (4.44)$$

$f^i$  is the Breit-Wigner kinematical distribution function for  $\rho^{\pm,0}$

$$f(m, \theta) = \frac{\cos \theta \Gamma_\rho/2}{m_\rho - m - i\Gamma_\rho/2}, \quad (4.45)$$

where  $m_\rho$  and  $\Gamma_\rho$  are the mass and width of  $\rho$  meson, respectively. The decay rate is given as a function of  $\Delta t$ , the invariant mass  $m_i$  and helicity angle  $\theta_i$  of  $\rho$  by

$$\begin{aligned} \mathcal{P}_{sig}(\Delta t, m_+, m_-, m_0, \theta_+, \theta_-, \theta_0) &= \frac{e^{-|\Delta t|/\tau_{B^0}}}{4\tau_{B^0}} \left[ (|\bar{A}|^2 + |A|^2) \right. \\ &\quad \left. + q \left( (|\bar{A}|^2 - |A|^2) \cos(\Delta m \Delta t) + 2\text{Im}\left(\frac{\bar{A}}{A}\right) \sin(\Delta m \Delta t) \right) \right] \end{aligned} \quad (4.46)$$

where  $q = 1$  for  $B_{tag} = B^0$  and  $q = -1$  for  $B_{tag} = \bar{B}^0$ . To clarify fit parameters, we denote  $T^{ij}$  and  $P_0$  as follows:

$$T = T^{+0} + T^{0+} = |T|e^{i\phi_3}e^{i\delta_T}, \quad (4.47)$$

$$\bar{T} = \bar{T}^{+0} + \bar{T}^{0+} = |T|e^{-i\phi_3}e^{i\delta_T}, \quad (4.48)$$

$$T^{+-} = |T^{+-}|e^{i\phi_3}e^{i\delta_{+-}}, \quad \bar{T}^{+-} = |T^{+-}|e^{-i\phi_3}e^{i\delta_{+-}}, \quad (4.49)$$

$$T^{-+} = |T^{-+}|e^{i\phi_3}e^{i\delta_{-+}}, \quad \bar{T}^{-+} = |T^{-+}|e^{-i\phi_3}e^{i\delta_{-+}}, \quad (4.50)$$

$$P_0 = |P_0|e^{-i\phi_1}e^{i\delta_0}, \quad \bar{P}^0 = |P_0|e^{i\phi_1}e^{i\delta_0}, \quad (4.51)$$

$$P_1 = |P_1|e^{-i\phi_1}e^{i\delta_1}, \quad \bar{P}^1 = |P_1|e^{i\phi_1}e^{i\delta_1}. \quad (4.52)$$

$\phi_2$	1.57 (90 deg)		
$ T $	1.59	$\delta_T$	-0.65
$ T^{+-} $	1	$\delta_{T_{+-}}$	0
$ T^{-+} $	0.78	$\delta_{T_{-+}}$	-2.91
$ P_0 $	0.19	$\delta_{P_0}$	-0.61
$ P_1 $	0.19	$\delta_{P_1}$	1.04

Table 4.16: Input parameters for a full Dalitz plot analysis of  $B^0 \rightarrow \pi^+\pi^-\pi^0$  decay.

We have 9 fit parameters

$$\phi_2, |T|, \delta_T, |T^{+-}|, \delta_{+-}, |P_0|, \delta_0, |P_1|, \delta_1 \quad (4.53)$$

and set  $|T^{+-}| = 1$  and  $\delta_{+-} = 0$ .

We use ensembles of the Monte Carlo (MC) pseudo-experiments for this study. Each pseudo-experiment consists of events generated with the nominal probability density functions (PDFs). At present, we consider only continuum events as a source of backgrounds. Assuming  $BR(B^0 \rightarrow \rho\pi) = 25 \times 10^{-6}$  and the detection efficiency of 15%, we generate 10080 candidate events equivalent to a  $300\text{fb}^{-1}$  data sample. There are about 1240 signal event in this sample. We parametrize the continuum background as

$$\mathcal{P}_{q\bar{q}} = \frac{1}{2} \mathcal{M}(m_+, m_-, m_0, \theta_+, \theta_-, \theta_0) \left\{ f_\tau \frac{e^{-|\Delta t|/\tau_{\text{bkg}}}}{2\tau_{\text{bkg}}} + (1 - f_\tau) \delta(\Delta t) \right\}, \quad (4.54)$$

where  $f_\tau$  is the fraction of the background with an effective lifetime  $\tau_{\text{bkg}}$ , and  $\mathcal{M}$  is a PDF in the Dalitz plane for the continuum background. We define a likelihood value for each event as a function of the 9 parameters:

$$P_i(\Delta t_i, m_+, m_-, m_0, \theta_+, \theta_-, \theta_0) = (1 - f_{ol}) \int_{-\infty}^{+\infty} d\Delta t' \{ f_{sig} \mathcal{P}_{sig}(\Delta t', q, w_l) + f_{q\bar{q}} \mathcal{P}_{q\bar{q}}(\Delta t') \cdot R_{q\bar{q}}(\Delta t_i - \Delta t') \} + f_{ol} \mathcal{P}_{ol}(\Delta t_i), \quad (4.55)$$

where  $f_{sig}$  and  $f_{q\bar{q}}$  are the probability functions for signal events and the continuum background, respectively. They are determined on an event-by-event basis. The signal fraction is estimated using the data taken by the Belle detector by the summer of 2002. For signal events, we use the same values of resolution parameters as those used for the  $\sin 2\phi_1$  analysis. We estimate the parameters for the continuum background using sideband data.

The input values of the fit parameters used here are listed in Table 4.16 [288]. The result is shown in Figure 4.27. We obtain an error for  $\phi_2$  of  $\delta\phi_2 = 11.4^\circ$  at  $300\text{fb}^{-1}$  and  $\delta\phi_2 = 3.5^\circ$  at  $3\text{ab}^{-1}$ . From these results, the error of  $\phi_2$  is expected to be  $2.9^\circ$  at  $5\text{ab}^{-1}$  and  $0.9^\circ$  at  $50\text{ab}^{-1}$ .



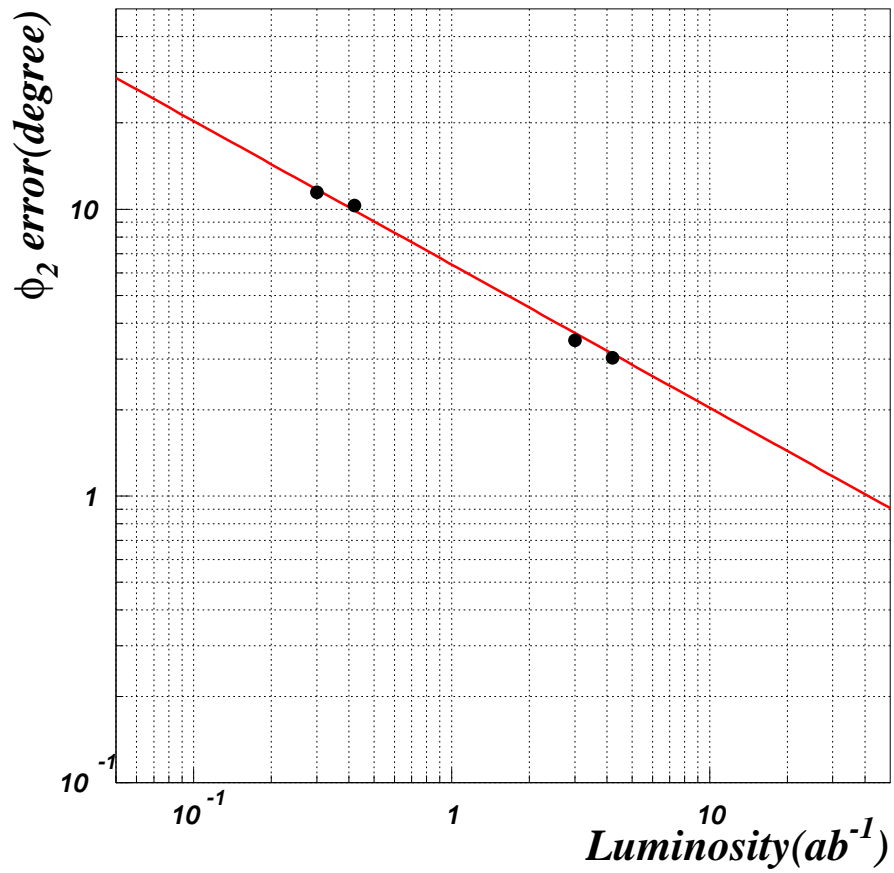


Figure 4.27:  $\phi_2$  error as a function of luminosity. Dots are the results from the MC pseudo-experiments and the line is a linear fit to these dots.

## 4.8 $\phi_3$

### 4.8.1 Introduction

The angle  $\phi_3$  is defined as

$$\phi_3 \equiv -\arg \left[ \frac{V_{ud}V_{ub}^*}{V_{cd}V_{cb}^*} \right], \quad (4.56)$$

which is independent of the quark phase convention. In the standard phase convention, all elements of the CKM matrix except for  $V_{ub}$  and  $V_{td}$  are nearly real, and in particular both  $V_{ud}$  and  $-V_{cd}V_{cb}^*$  are (nearly) real and positive, and we have

$$\phi_3 \equiv \arg V_{ub}^*. \quad (\text{standard phase convention}) \quad (4.57)$$

There are several decay channels that can be used to extract information on  $\phi_3$ , and each has distinct merits and drawbacks. Here, we will investigate the following channels:

**$D^{(*)-}\pi^+$  modes** The flavor-tagged time-dependent measurement of  $D^{(*)-}\pi^+$  and its charge-conjugate mode. This mode measures  $\sin(2\phi_1 + \phi_3)$  and is affected by a strong phase. There is, however, no penguin contribution. One could fully reconstruct the  $D^-\pi^+$  and  $D^{*-}\pi^+$  final states, or one could use a partial-reconstruction technique where  $\bar{D}^0$  of the decay  $D^{*-} \rightarrow \bar{D}^0\pi^+$  is not explicitly detected. The latter has more statistics but with more background. In both cases, the value of  $r$ , the ratio of Cabibbo-favored amplitude to the Cabibbo-suppressed amplitude, needs to be input externally.

**$B^+ \rightarrow DK^{(*)+}$  (ADS method)**  $B^+ \rightarrow DK^{(*)+}$ ,  $D \rightarrow PP$ , where  $D$  is  $D^0$  or  $\bar{D}^0$ , and their charge-conjugate modes. Even though there are strong phases involved,  $\phi_3$  can be extracted in a theoretically-clean manner if one uses more than one kind of  $D$  decays. The required statistics, however, is quite large. The value of the relevant amplitude ratio  $r$  can be obtained by the fit. If it is known, one can improve the statistical power significantly.

**$B^\pm \rightarrow DK^\pm$  (Dalitz analysis)**  $B^\pm \rightarrow DK^\pm$ ,  $D \rightarrow PPP$ , where  $D$  is  $D^0$  or  $\bar{D}^0$ , and their charge-conjugate modes. This mode takes advantage of the interferences that occur in the Dalitz plot of the  $D \rightarrow PPP$  decay to extract  $\phi_3$  as well as the strong phase. The value of the amplitude ratio  $r$  is also obtained in the fit. This analysis has a good statistical power; it requires, however, a detailed understanding of the structure of the Dalitz plot.

More on the theoretical frameworks for each mode as well as the sensitivities are covered in later subsections.

### 4.8.2 $D^{(*)-}\pi^+$ modes

For the final state  $D^{(*)-}\pi^+$ , the amplitudes of diagrams shown in Figure 4.8.2 interfere. The two diagrams contributing to the amplitude  $a$  (or  $\bar{b}$ ) have the same CKM factors, and information on  $\phi_3$  is contained in

$$\rho \equiv \frac{q\bar{b}}{pa} = -r \exp(\delta - \phi_w), \quad \phi_w \equiv 2\phi_1 - \phi_3, \quad (4.58)$$

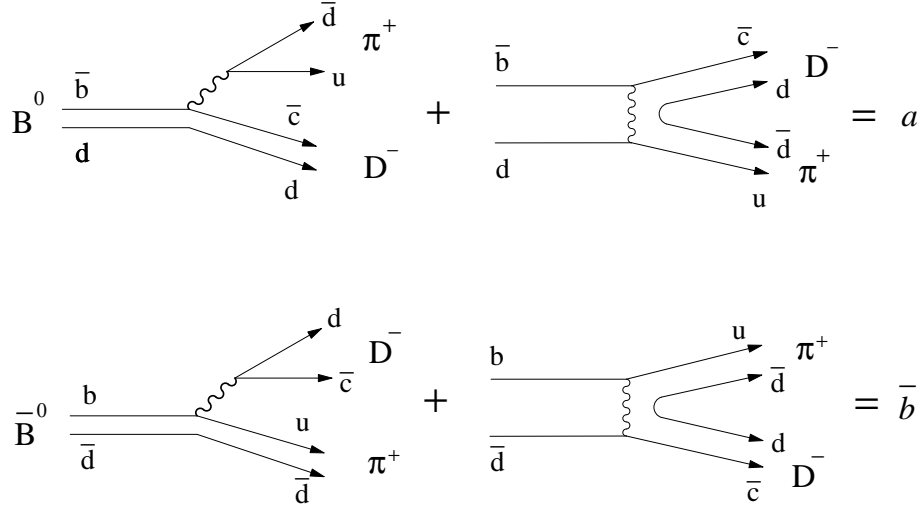


Figure 4.28: Diagrams for  $B^0, \bar{B}^0 \rightarrow D^- \pi^+$ .

where  $B_H = pB^0 - q\bar{B}^0$ ,  $r \equiv |\rho|$  and  $\delta$  is the relative strong phase between  $\bar{b}$  and  $a$ . The time-dependent distributions are then given by

$$\begin{aligned}
 \Gamma_{\ell^-, D^- \pi^+}(\Delta t) &= N e^{-\gamma|\Delta t|} [(1+r^2) + (1-r^2) \cos \delta m \Delta t - 2r \sin(\phi_w - \delta) \sin \delta m \Delta t] \\
 \Gamma_{\ell^+, D^+ \pi^-}(\Delta t) &= N e^{-\gamma|\Delta t|} [(1+r^2) + (1-r^2) \cos \delta m \Delta t + 2r \sin(\phi_w + \delta) \sin \delta m \Delta t] \\
 \Gamma_{\ell^-, D^+ \pi^-}(\Delta t) &= N e^{-\gamma|\Delta t|} [(1+r^2) - (1-r^2) \cos \delta m \Delta t - 2r \sin(\phi_w + \delta) \sin \delta m \Delta t] \\
 \Gamma_{\ell^+, D^- \pi^+}(\Delta t) &= N e^{-\gamma|\Delta t|} [(1+r^2) - (1-r^2) \cos \delta m \Delta t + 2r \sin(\phi_w - \delta) \sin \delta m \Delta t]
 \end{aligned} \tag{4.59}$$

where  $\Gamma_{\ell^-, D^- \pi^+}(\Delta t)$  is the distribution of  $\Delta t \equiv t_{D\pi} - t_{\text{tag}}$  when the tag-side is  $\bar{B}^0$ , etc., and  $D\pi$  can also be  $D^*\pi$  in which case  $r$  and  $\delta$  will be replaced by  $r^*$  and  $\delta^*$ , respectively. The two relevant observables are  $r \sin(\phi_w + \delta)$  and  $r \sin(\phi_w - \delta)$ . The value of  $r$  cannot be obtained by the fit itself, while the expected value of  $r^{(*)}$  is roughly 0.02. One way to obtain  $r^*$  experimentally is to use the  $SU(3)$ -related modes  $B^0 \rightarrow D_s^{(*)-} \pi^+$ . However, there will be uncertainty associated with the validity of  $SU(3)$  and the size of the exchange diagram which is missing for  $D_s^{(*)-} \pi^+$ .

The distributions are plotted in Figure 4.29 where the value of  $r$  is artificially enhanced to 0.1 in order to show the  $CP$  violating effects clearly. The top two of (4.59) can be called unmixed modes and the bottom two mixed modes. As may be noticeable in the figure, most of information on  $CP$  violation is in the mixed modes where  $CP$  violation appears as the height asymmetry of  $\Delta t > 0$  vs  $\Delta t < 0$  and the shift of the minimum from  $\Delta t = 0$ . Note that  $r \sin(\phi_w + \delta)$  can be obtained from the third distribution alone and  $r \sin(\phi_w - \delta)$  from the fourth alone. The final state  $D^{*-} \pi^+$  can be detected by full reconstruction using the standard technique, it or can also

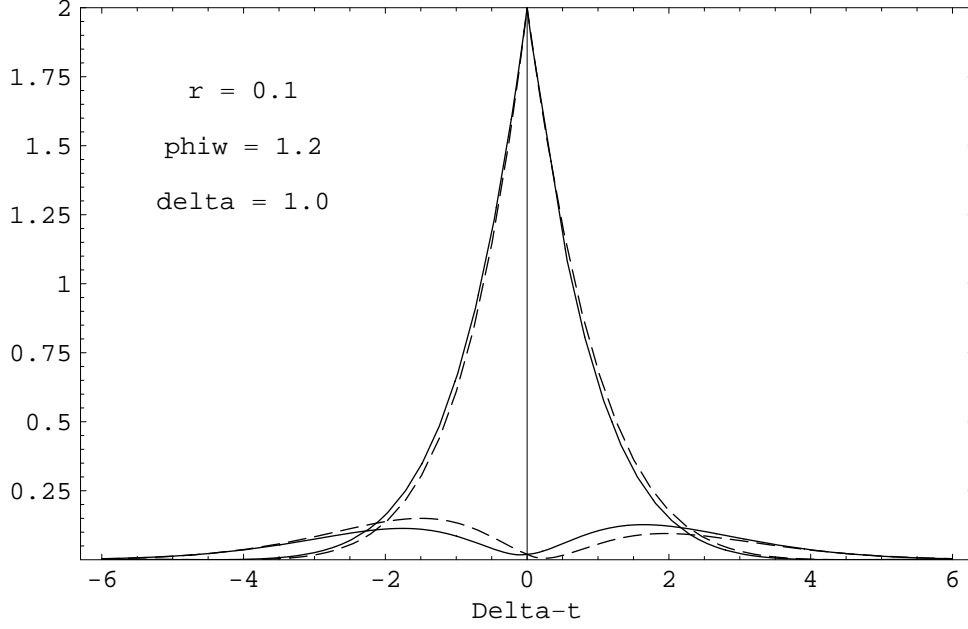


Figure 4.29: The  $\Delta t$  distributions of the flavor-tagged  $D\pi$  modes for  $r = 0.1$ ,  $\phi_w = 1.2$  radian, and  $\delta = 1.0$  radian. The solid lines are for  $D^-\pi^+$  final state and dashed lines are for  $D^+\pi^-$  final states. The mixing parameter  $x$  is taken to be 0.71.

be reconstructed by a partial reconstruction method where the  $\bar{D}^0$  meson in  $D^{*-} \rightarrow \bar{D}^0\pi^-$  is not explicitly reconstructed. Note that the  $D^{(*)-}\pi^+$  methods work even when there are sizable exchange diagrams while the value of  $r^{(*)}$  needs to be supplied externally.

The distributions of  $\Delta t$  for  $\bar{B}^0$ -tagged  $D^{*+}\pi^-$  and  $D^{*-}\pi^+$  are shown in Figure 4.30 for events with good tagging quality. The analysis was performed on  $140fb^{-1}$  of data [289]. The full-reconstruction analysis gave the following preliminary results:

$$\begin{aligned}
2r^* \sin(\phi_w + \delta^*) &= 0.109 \pm 0.057 \pm 0.019 \\
2r^* \sin(\phi_w - \delta^*) &= 0.011 \pm 0.057 \pm 0.019 \\
2r \sin(\phi_w + \delta) &= 0.087 \pm 0.054 \pm 0.018 \\
2r \sin(\phi_w - \delta) &= 0.037 \pm 0.052 \pm 0.018.
\end{aligned} \tag{4.60}$$

For  $5 \text{ ab}^{-1}$  and  $50 \text{ ab}^{-1}$  of data, the statistical errors will be

$$\delta 2r^* \sin(\phi_w + \delta^*) \sim \delta 2r \sin(\phi_w + \delta) \sim \begin{cases} 0.009 & (5 \text{ ab}^{-1}) \\ 0.003 & (50 \text{ ab}^{-1}) \end{cases}. \tag{4.61}$$

We note that the value of  $r^{(*)}$  is approximately 0.02; thus, the above errors correspond to the errors on  $\sin(\phi_w \pm \delta^{(*)})$  of 0.23 and 0.07, respectively. If the value of  $r^{(*)}$  is known,  $\phi_w = 2\phi_1 + \phi_3$  (and  $\delta^{(*)}$ ) can be extracted from  $\sin(\phi_w \pm \delta^{(*)})$ . At this time, determining the value of  $r^{(*)}$  to 23% seems reasonably possible while 7% seems quite challenging. On the other hand, our knowledge on  $r^{(*)}$  will improve significantly by the time  $50 \text{ ab}^{-1}$  of data is taken. It is possible that the systematic error on  $\phi_3$  due to  $r^{(*)}$  is not overwhelming even with  $50 \text{ ab}^{-1}$  of data.

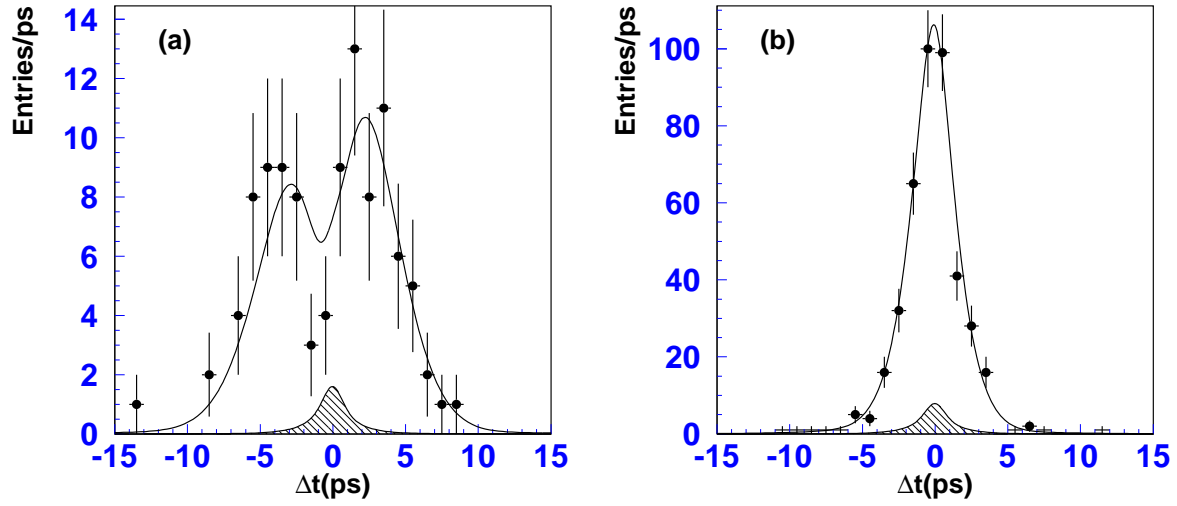


Figure 4.30: The distributions of  $\Delta t$  for  $\bar{B}^0$ -tagged  $D^{*+}\pi^-$  (a) and  $D^{*+}\pi^-$  (b). For fully-reconstructed events with good-quality tags. ( $140fb^{-1}$ )

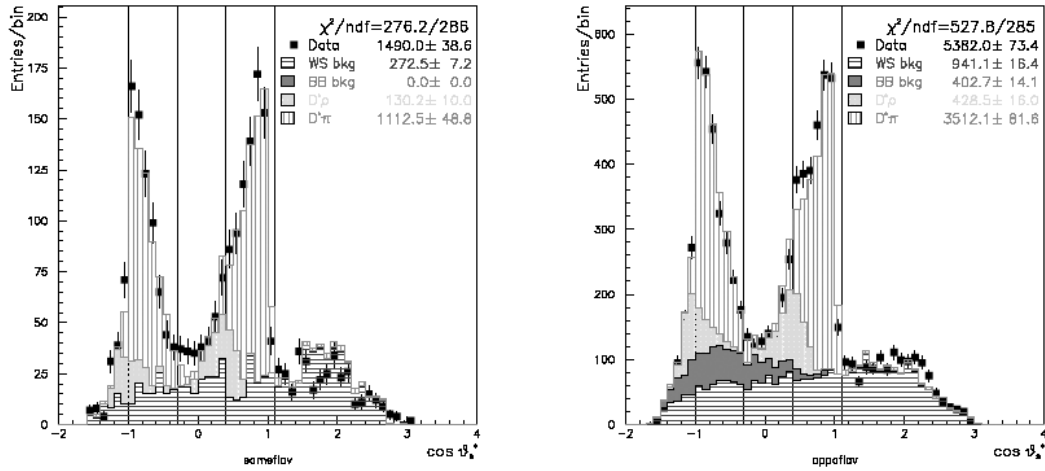


Figure 4.31: The partial reconstruction of  $D^*\pi$ . The distributions of  $\cos \theta^*$  for two lepton tagged samples, same-flavor and opposite-flavor tags. Based on  $78 \text{ fb}^{-1}$  of data.

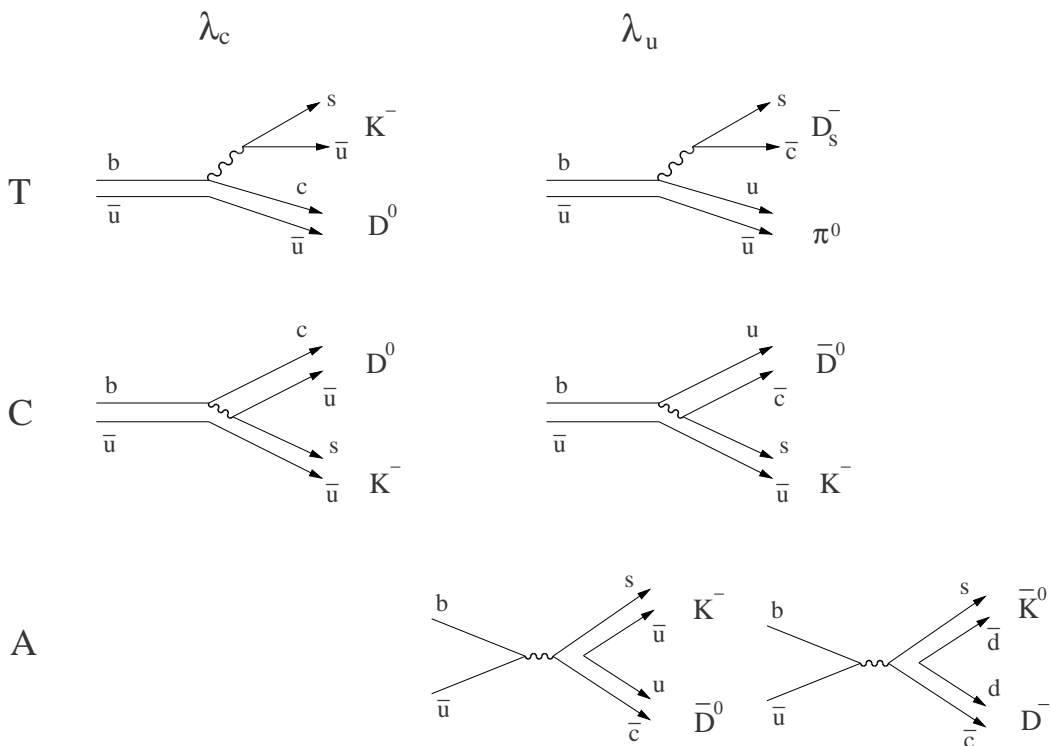


Figure 4.32: Diagrams contributing to  $B^\pm \rightarrow DK^\pm$  and related modes.

The statistical situation with the partially-reconstructed  $D^{*+}\pi^-$  is substantially better. The helicity of  $D^{*+}$  in the  $B$  rest frame is 0 due to conservation of angular momentum. Thus, the decay angle  $\theta^*$  of the decay  $D^{*+} \rightarrow D^0\pi^+$  should have the  $\cos^2\theta^*$  shape. One can reconstruct  $\cos\theta^*$  without explicitly detecting  $D^0$ , and the distributions based on  $78\text{ fb}^{-1}$  of data are shown in Figure 4.31 separately for the two lepton-tagged datasets. There are  $1110 \pm 50$  signal events in the same-flavor sample and  $3510 \pm 80$  signal events in the opposite-flavor sample. As a result of a  $\Delta t$  fit, the error on  $2r^*\sin(\phi_w \pm \delta^*)$  was found to be 0.029. The statistical errors extrapolated to  $5\text{ ab}^{-1}$  and  $50\text{ ab}^{-1}$  of data are

$$\delta 2r^* \sin(\phi_w + \delta^*) \sim \begin{cases} 0.005 & (5 \text{ ab}^{-1}) \\ 0.0015 & (50 \text{ ab}^{-1}) \end{cases} \quad (\text{partial rec.}). \quad (4.62)$$

The background is about 30% and comes mainly from  $B$  decays such as  $D^*\rho$  and  $D^{**}\pi$ . The accuracy of these background estimations is likely to improve with statistics. The uncertainty of  $r^*$ , however, may become a limiting systematic.

### 4.8.3 $B^\pm \rightarrow DK^{*\pm}$ (ADS method)

In  $B^\pm \rightarrow DK^\pm$ , the number of  $c$  or  $\bar{c}$  quark in the final state is one, and as a result the penguin processes  $b \rightarrow s/d$  cannot contribute. When the neutral  $D$  meson is detected in a final state that can come from  $D^0$  and  $\bar{D}^0$ , the two processes  $B^- \rightarrow D^0 K^-$  and  $B^- \rightarrow \bar{D}^0 K^-$  interfere. Diagrams contributing to  $B^\pm \rightarrow DK^\pm$  and related modes are shown in Figure 4.32. They are categorized in terms of the CKM factors involved ( $\lambda_c = V_{cb}V_{us}^*$  and  $\lambda_u = V_{ub}V_{cs}^*$ ) and type

of processes (T: color-favored tree, C: color-suppressed tree, A: annihilation).  $B^- \rightarrow D^0 K^-$  receives contributions from T and C both with the CKM factor  $\lambda_c$ , while  $B^- \rightarrow \bar{D}^0 K^-$  can proceed by C and A both with the CKM factor  $\lambda_u$ . Thus,

$$\arg \frac{Amp(B^- \rightarrow \bar{D}^0 K^-)}{Amp(B^- \rightarrow D^0 K^-)} = \delta_B - \phi_3, \quad \arg \frac{Amp(B^+ \rightarrow D^0 K^-)}{Amp(B^+ \rightarrow \bar{D}^0 K^-)} = \delta_B + \phi_3, \quad (4.63)$$

where  $\delta_B$  is the strong phase. We have noted

$$\arg \frac{\lambda_u}{\lambda_c} = \arg \frac{V_{ub} V_{cs}^*}{V_{cb} V_{us}^*} = -\phi_3, \quad (\text{standard phase convention}) \quad (4.64)$$

and that when charge conjugate decay is taken, the weak phase changes sign while the strong phase does not. On the other hand, the absolute size of  $Amp(B^- \rightarrow \bar{D}^0 K^-)$  or  $Amp(B^- \rightarrow D^0 K^-)$  is the same for charge conjugate decays:

$$|Amp(B^- \rightarrow \bar{D}^0 K^-)| = |Amp(B^+ \rightarrow D^0 K^+)| \equiv B, \quad (4.65)$$

$$|Amp(B^- \rightarrow D^0 K^-)| = |Amp(B^+ \rightarrow \bar{D}^0 K^+)| \equiv A. \quad (4.66)$$

If  $D^0$  and  $\bar{D}^0$  are detected in a  $CP$  eigenstate such as  $K^- K^+$  (which is  $CP+$ ; i.e.  $D_1 = (D^0 + \bar{D}^0)/\sqrt{2}$ ), the decay rates of  $B^\pm$  are, up to an overall constants of  $1/2$ ,

$$\Gamma(B^- \rightarrow D_1 K^-) = |A + B e^{i(\delta_B - \phi_3)}|^2 = A^2 + B^2 + 2AB \cos(\delta_B - \phi_3), \quad (4.67)$$

$$\Gamma(B^+ \rightarrow D_1 K^+) = |A + B e^{i(\delta_B + \phi_3)}|^2 = A^2 + B^2 + 2AB \cos(\delta_B + \phi_3). \quad (4.68)$$

Then, there can be a decay rate asymmetry [290, 291] between  $B^- \rightarrow D_1 K^-$  and  $B^+ \rightarrow D_1 K^+$ :

$$A_1 \equiv \frac{\Gamma_{D_1 K^-} - \Gamma_{D_1 K^+}}{\Gamma_{D_1 K^-} + \Gamma_{D_1 K^+}} = \frac{-2r \sin \delta_B \sin \phi_3}{1 + r^2 + 2r \cos \delta_B \cos \phi_3}, \quad (4.69)$$

with

$$r \equiv \frac{B}{A}. \quad (4.70)$$

The value of this  $r$  is expected to be around 0.1 to 0.2. For a  $CP-$  final states (such as  $K_S \pi^0$ ; i.e.  $D_2 = (D^0 - \bar{D}^0)/\sqrt{2}$ ), the asymmetry becomes

$$A_2 \equiv \frac{\Gamma_{D_2 K^-} - \Gamma_{D_2 K^+}}{\Gamma_{D_2 K^-} + \Gamma_{D_2 K^+}} = \frac{2r \sin \delta_B \sin \phi_3}{1 + r^2 + 2r \cos \delta_B \cos \phi_3}. \quad (4.71)$$

Thus, once the value of  $r$  is given, the measurements of  $A_1$  and  $A_2$  can give  $\delta_B$  and  $\phi_3$  (2 equations and 2 unknowns). In practice, however, it is difficult to measure the value of  $r$  because of the doubly-Cabibbo-suppressed decays of  $D^0$  [292, 293]. It was pointed out, however, that by taking more than one final states to which both  $D^0$  and  $\bar{D}^0$  can decay, one can solve for  $r$  and  $\delta_B$  (the ADS method [292, 293]).

The authors of [292, 293] used  $B^- \rightarrow DK^{*-}$  and assumed the  $D$  decay modes listed in Table 4.17. The strong phase  $\delta_i$  includes that for the  $B$  decay as well as that for the  $D$  decay. The table also shows the number of events expected for  $10^8 B^\pm$  or roughly  $0.1 \text{ ab}^{-1}$ , where the detection efficiencies for each  $DK^{*-}$  are taken to be the same as the branching fraction of  $D \rightarrow i$  where  $i$  is the  $D$  decay mode shown. Namely, the detection efficiency of  $K^{*-}$  and those of the  $D$  decay final states shown are assumed to be unity. Under these assumptions, the estimated

mode	#event	scale factor	strong phase $\delta_i$
$K^+\pi^-$	83	1	$10^\circ$
$K_s\pi^0$	791	0.34	$20^\circ$
$K^+\rho^-$	224	0.5	$30^\circ$
$K^+a_1^-$	791	0.22	$49^\circ$
$K_s\rho^0$	362	0.30	$200^\circ$
$K^{*+}\pi^-$	65	0.33	$50^\circ$

Table 4.17: The  $D$  decay modes used for the sensitivity study of  $B^- \rightarrow DK^{*-}$  mode and the strong phases assumed. The number of events are for  $10^8 B^\pm$  when the  $DK^{*+}$  detection efficiency is assumed to be  $Br(D \rightarrow i)$ . The scale factors are relative to the  $K^+\pi^-$  mode for realistic detection efficiencies described in the text.

sensitivity on  $\phi_3$  is  $9^\circ$ . The scale factor includes 2/3 per track, 1/2 per  $\pi^0$ , and relevant branching fractions where  $K^{*+}$  is assumed to be detected as  $K^-\pi^0$  and  $K_S\pi^-$ . The value of  $\phi_3$  is taken to be  $60^\circ$  and  $r$  to be 0.1. Figure 4.33 shows the  $\Delta E$  distribution for  $B^- \rightarrow DK^-$ ,  $D \rightarrow K^+\pi^-$  using  $78 \text{ fb}^{-1}$  of data. The detection efficiency was estimated by MC to be 0.27. With the measured background and the expected signal yield, S/N is estimated to be 1/7. Combining all the above, the required integrated luminosity for  $\delta\phi_3$  of  $9^\circ$  becomes  $31 \text{ ab}^{-1}$ , or equivalently

$$\delta\phi_3 = \begin{cases} 22^\circ & (5 \text{ ab}^{-1}) \\ 7^\circ & (50 \text{ ab}^{-1}) \end{cases} \quad (DK^*). \quad (4.72)$$

If the value of  $r$  is larger than 0.1, the sensitivities will be better. This analysis is theoretically clean and will probably be limited by statistics even for  $50 \text{ ab}^{-1}$  of data. Approximately the same sensitivity is expected from  $DK^-$  mode and the combined sensitivities will be  $1/\sqrt{2}$  times those shown above; namely,

$$\delta\phi_3 = \begin{cases} 16^\circ & (5 \text{ ab}^{-1}) \\ 5^\circ & (50 \text{ ab}^{-1}) \end{cases} \quad (DK^* + DK). \quad (4.73)$$

If the value of  $r$  is known, then one can use  $CP$  eigenstates of  $D$  decays such as  $K^+K^-$  ( $CP+$ ) and  $K_s\pi^0$  ( $CP-$ ) to extract  $\phi_3$  as well as the strong phase  $\delta_B$ . This method is statistically more powerful than the ADS method described above; the value of  $r$ , however, is not known well at this time and seems to be more difficult than the value of  $r$  for the  $D^{(*)}\pi$  modes. It should be noted, however, that the value of  $r$  measured in the Dalitz analysis of the following section may be used for this analysis.

#### 4.8.4 $B^\pm \rightarrow DK^\pm$ (Dalitz analysis)

Use of the Dalitz plots in  $B^\pm \rightarrow DK^\pm$  has been suggested in [292, 293] and recently by [294]. In this analysis, the  $D$  meson is detected in the final state  $K_S\pi^+\pi^-$ . If the amplitude of  $D^0$  decaying to a point in the Dalitz plot,  $m^2(K_S\pi^+) = m_+^2$  and  $m^2(K_S\pi^-) = m_-^2$ , is given by  $f(m_+^2, m_-^2)$ , then that of  $\bar{D}^0$  decaying to the same final state can be written as  $f(m_-^2, m_+^2)$  where the two arguments are simply exchanged. This is due to the approximate  $CP$  conservation of the  $D$  decay. Explicitly,

$$\begin{aligned} \text{Amp}(D^0)(m_{K_S\pi^+} = m_+, m_{K_S\pi^-} = m_-) &\equiv f(m_+^2, m_-^2) \\ \text{Amp}(\bar{D}^0)(m_{K_S\pi^+} = m_+, m_{K_S\pi^-} = m_-) &\equiv f(m_-^2, m_+^2) \end{aligned} \quad (4.74)$$



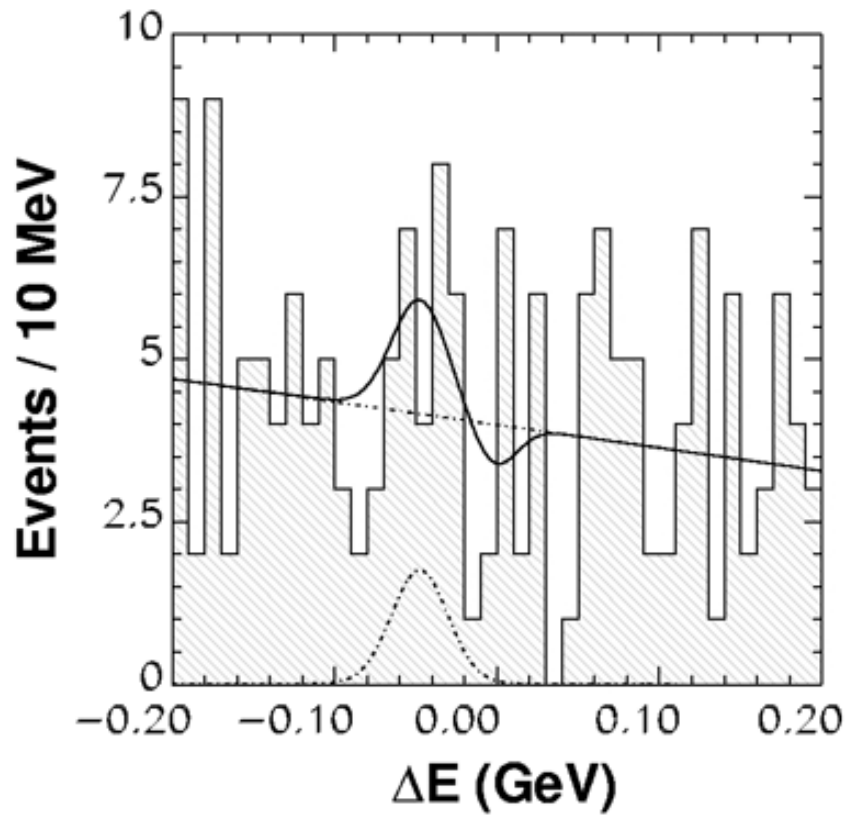


Figure 4.33: Search for  $B^- \rightarrow DK^-$ ,  $D \rightarrow K^+\pi^-$ . The data is  $78 \text{ fb}^{-1}$ .

The total decay amplitude for  $B^- \rightarrow DK^-$ ,  $D \rightarrow K_S \pi^+ \pi^-$  is then

$$\begin{aligned} M_- &= \text{Amp}(D^0 \rightarrow_{K_S \pi^+ \pi^-} K^-) + \text{Amp}(\bar{D}^0 \rightarrow_{K_S \pi^+ \pi^-} K^-) \\ &= A[f(m_+^2, m_-^2) + r e^{i(\delta_B - \phi_3)} f(m_-^2, m_+^2)], \end{aligned} \quad (4.75)$$

where  $A, r, \delta_B$  are defined in the previous section. The total decay amplitude for  $B^+ \rightarrow DK^+$ ,  $D \rightarrow K_S \pi^+ \pi^-$ , where  $m^2(K_S \pi^+) = m_+^2$  and  $m^2(K_S \pi^-) = m_-^2$ , is similarly

$$\begin{aligned} M_+ &= \text{Amp}(\bar{D}^0 \rightarrow_{K_S \pi^+ \pi^-} K^+) + \text{Amp}(D^0 \rightarrow_{K_S \pi^+ \pi^-} K^+) \\ &= A[f(m_-^2, m_+^2) + r e^{i(\delta_B + \phi_3)} f(m_+^2, m_-^2)], \end{aligned} \quad (4.76)$$

where the sign of  $\phi_3$  has flipped while the strong phase  $\delta_B$  remains the same.

The Dalitz plot for  $D^0 \rightarrow K_S \pi^+ \pi^-$  based on the CLEO measurement [295] is shown in Figure 4.34. As can be seen from the Dalitz plot, the distribution is highly asymmetric under the exchange of  $m_{K_S \pi^+}$  and  $m_{K_S \pi^-}$  which indicates that the interference in the Dalitz plot has a good sensitivity on the phase between the two terms of (4.75) and (4.76). The phase angles  $\delta_B - \phi_3$  and  $\delta_B + \phi_3$  are obtained from the separate fits of  $B^-$  and  $B^+$  decays and  $\phi_3$  can be extracted therefrom.

Figure 4.35 shows the  $\Delta E$  and  $M_B$  distributions for  $B^\pm \rightarrow DK^\pm$ ,  $D \rightarrow K_S \pi^+ \pi^-$ , based on  $140 \text{ fb}^{-1}$  of data, and the Dalitz plots of the  $D$  decays are shown in Figure 4.36 separately for  $B^+$  and  $B^-$  [16]. The results of an unbinned maximum likelihood fit for the parameters  $r(=a)$ ,  $\delta_B(=\delta)$ , and  $\phi_3$  are shown in Figure 4.37. For  $\phi_3$  and  $\delta_B$ , the fit yields

$$\begin{aligned} \phi_3 &= 95_{-20}^{+25} \pm 13 \pm 10 (^\circ) \\ \delta_B &= 162_{-25}^{+20} \pm 12 \pm 24 (^\circ) \end{aligned} \quad (4.77)$$

where the first errors are statistical, the second are experimental systematic errors, such as from background shapes and efficiency shapes, and the third errors are additional systematic errors due to the  $D$  decay model dependence. With  $5 \text{ ab}^{-1}$  and  $50 \text{ ab}^{-1}$  of data, the statistical errors will be

$$\delta\phi_3 = \begin{cases} 4^\circ & (5 \text{ ab}^{-1}) \\ 1.2^\circ & (50 \text{ ab}^{-1}) \end{cases} . \quad (4.78)$$

With more statistics, the Dalitz distribution of  $D^0 \rightarrow K_S \pi^+ \pi^-$  will be measured more accurately using  $D^{*+} \rightarrow D^0 \pi^+$ . Even though it is not clear at present if the uncertainty due to the  $D$  decay modeling can be reduced to a level of one degree, it is quite possible that the measurement is not overwhelmed by systematics at  $5 \text{ ab}^{-1}$ . Furthermore, the value of  $r$  measured in this mode can be used in the  $B^\pm \rightarrow DK^\pm$  modes.

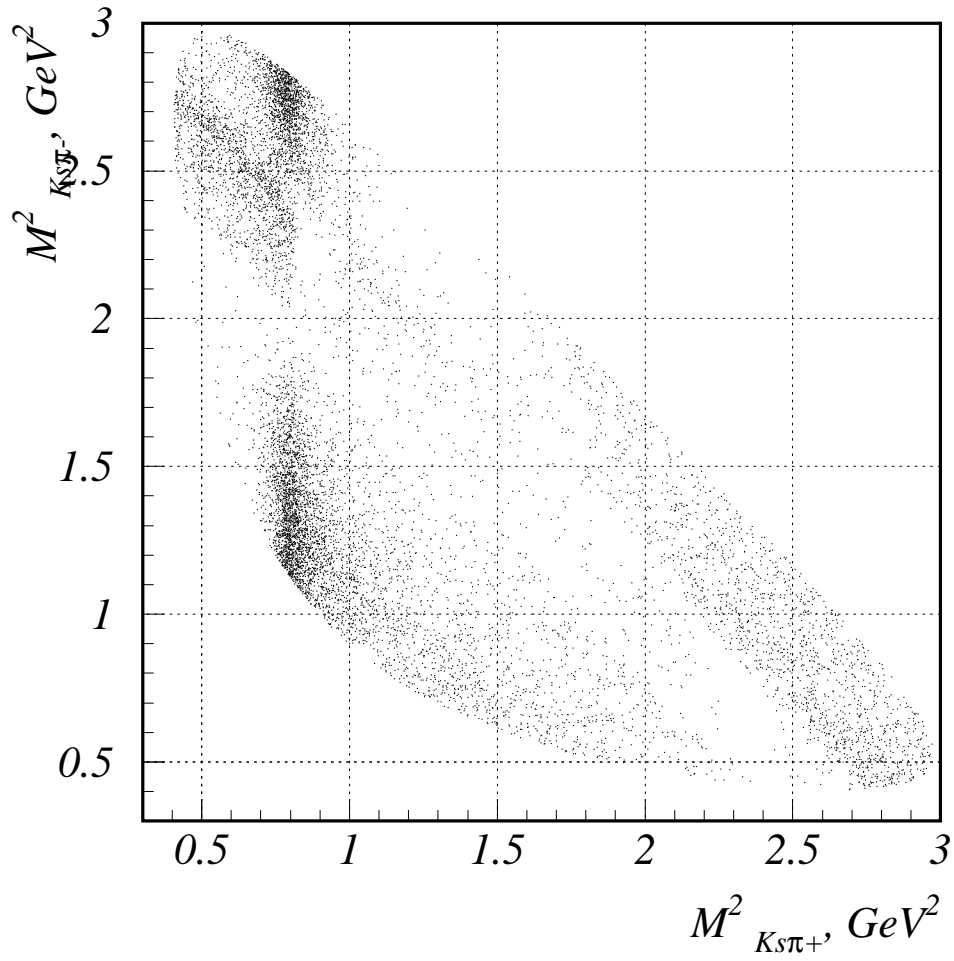


Figure 4.34: The Dalitz plot for  $D^0 \rightarrow K_S \pi^+ \pi^-$  based on the CLEO measurement.

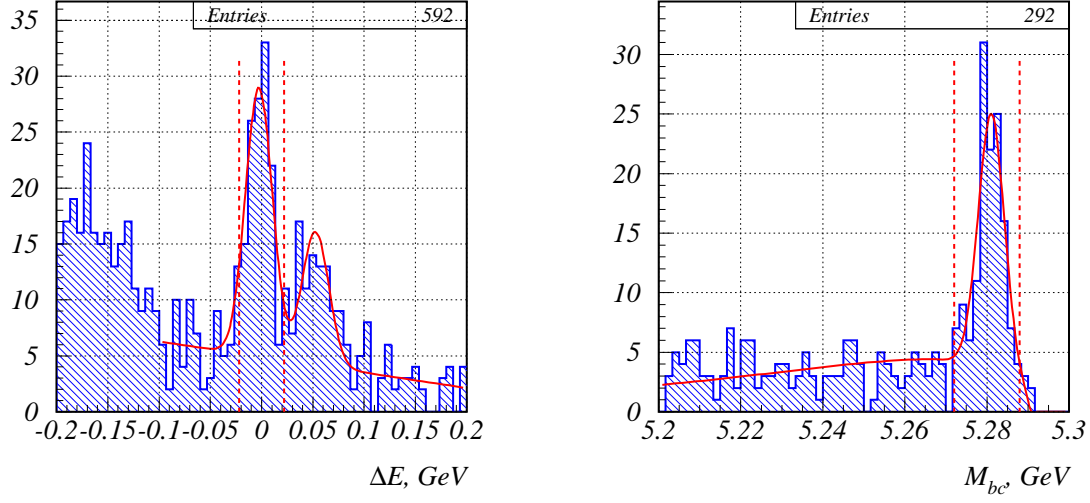


Figure 4.35: The  $\Delta E$  and  $M_B$  distributions for  $B^\pm \rightarrow DK^\pm$ ,  $D \rightarrow K_S \pi^+ \pi^-$ , based on  $140 \text{ fb}^{-1}$  of data.

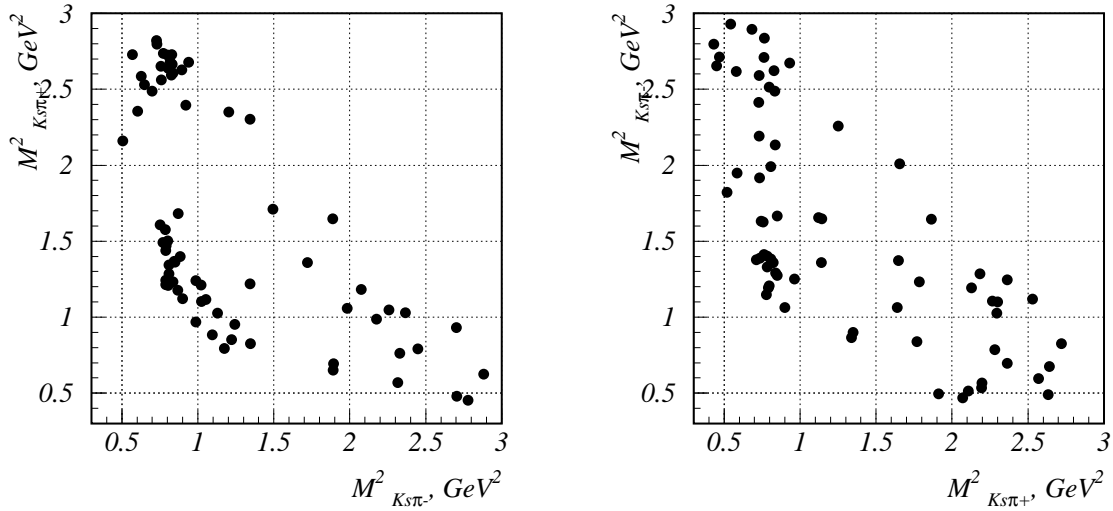


Figure 4.36: The Dalitz distributions for  $B^+ \rightarrow DK^+$  (left) and  $B^- \rightarrow DK^-$  (right), where  $D \rightarrow K_S \pi^+ \pi^-$  based on  $140 \text{ fb}^{-1}$  of data.

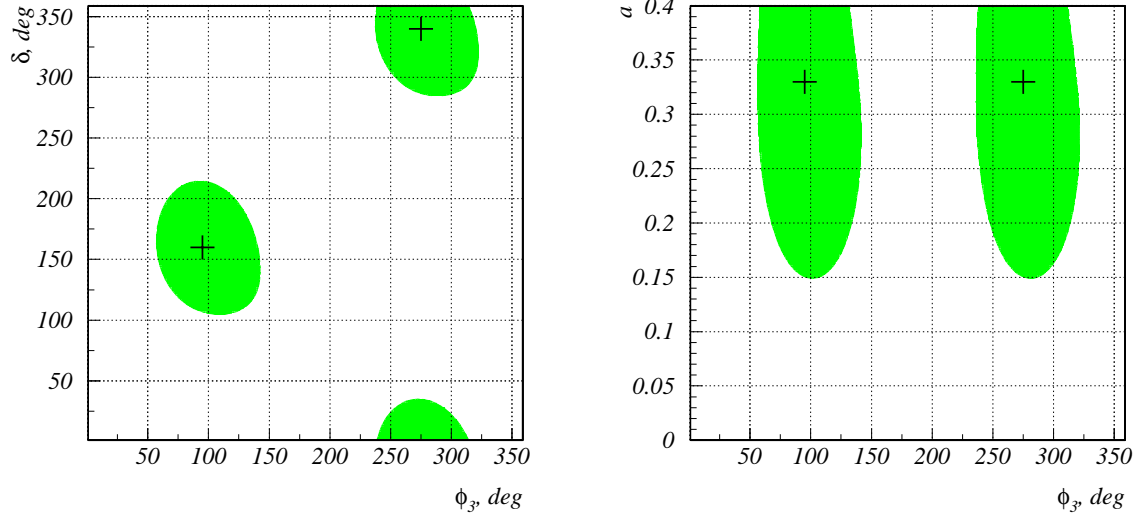


Figure 4.37: The results of the fit for  $r(=a)$ ,  $\delta_B(=\delta)$ , and  $\phi_3$ .

## 4.9 $|V_{ub}|$

### 4.9.1 Introduction

Precise determination of the magnitude of the Cabibbo-Kobayashi-Maskawa matrix element  $V_{ub}$  is of fundamental importance in over-constraining the unitarity triangle, and thereby finding effects of physics beyond the Standard Model. Such a serious examination would require precision of a few percent. A high luminosity SuperKEKB/Belle experiment will provide such a unique opportunity.

In principle,  $|V_{ub}|$  can be determined using data for semileptonic  $B \rightarrow X_u \ell \nu$  decays, where  $X_u$  denotes a hadronic system containing a  $u$ -quark. Both inclusive and exclusive measurements are useful. However, the present error in  $|V_{ub}|$  determination is about  $\pm 20\%$  [58], and limited by both experimental and theoretical systematic errors. The high luminosity at the SuperKEKB will enable us to perform high statistics measurements of  $B \rightarrow X_u \ell \nu$  decays with “ $B$  tagging”. This will lead to rate measurements with significantly reduced experimental systematic errors and also to  $|V_{ub}|$  extraction much less biased by theoretical ambiguities. These features are unique at a high luminosity  $e^+e^-$   $B$ -factory, and cannot be achieved at  $e^+e^-$  machines with the luminosity available so far nor at present or future hadron machines.

In this section, we discuss strategy and prospects for determination of  $|V_{ub}|$  at the SuperKEKB/Belle experiment using both inclusive and exclusive semileptonic  $B \rightarrow X_u \ell \nu$  decays.

### 4.9.2 Theoretical formalisms for the semileptonic $B$ decays

#### Inclusive decays

The amplitude for  $B \rightarrow X_u \ell \nu$  inclusive decay can be computed in perturbative QCD using the Operator Product Expansion (OPE). Since the  $b$  quark inside the  $B$  meson has momentum  $(m_b v + k)^\mu$ , where  $k$  is the residual momentum of  $O(\Lambda_{QCD})$ , the OPE is carried out by expanding the quark propagator as

$$\frac{1}{(m_b v + k - q)^2} = \frac{1}{(m_b v - q)^2} \left[ 1 - \frac{(m_b v - q) \cdot k}{(m_b v - q)^2} - \frac{k^2}{(m_b v - q)^2} + \dots \right]. \quad (4.79)$$

Denoting the invariant mass and the energy of the hadron state  $X_u$  as  $m_X$  and  $E_X$ , the first term is of order  $E_X \Lambda_{QCD}/m_X^2$  while the second term is of order  $\Lambda_{QCD}^2/m_X^2$ .

The phase space can be divided into the following three regions (see Figure 4.38): (i) a generic region where  $\Lambda_{QCD}/m_X$ ,  $(E_X \Lambda_{QCD})/m_X^2 \ll 1$ . In this region, the differential decay rate can be successfully expanded by the OPE; (ii) a shape function region (or collinear region) where  $\Lambda_{QCD}/m_X \ll 1$  and  $(E_X \Lambda_{QCD})/m_X^2 \sim 1$ . In this region, a class of  $\Lambda_{QCD} E/m_X^2$  terms must be resummed, which can be described by the shape function of the  $B$  meson [296, 297, 298] and its higher twist corrections; (iii) a resonance region where  $\Lambda_{QCD}/m_X \sim 1$ . In this region, the differential decay rate is dominated by a few exclusive states so that neither the OPE nor the twist expansion work.

Since the  $B \rightarrow X_u \ell \nu$  decay suffers from  $B \rightarrow X_c \ell \nu$  decay background one has to introduce the cut of the following kinds:

- lepton energy cut :  $E_l > (m_B^2 - m_D^2)/(2m_B)$ .
- hadron invariant mass cut :  $m_X^2 < m_D^2$ .
- lepton mass cut :  $q^2 < (m_B - m_D)^2$ .

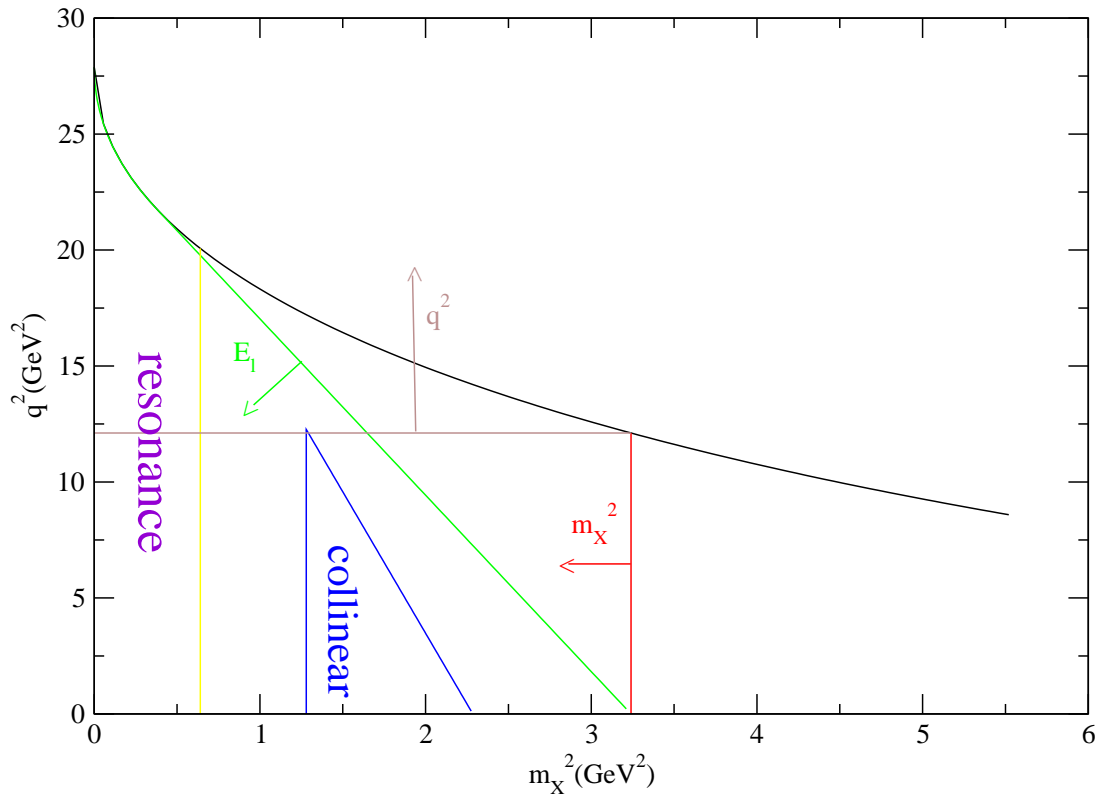


Figure 4.38: Phase space for  $B \rightarrow X_u l \nu$  decay.

- combined  $(q^2, m_X^2)$  cut.

For the  $E_l$  cut, only 10% of the rate is available, which is dominated by the shape function region. In this region, the lepton energy spectrum at the leading order is given by

$$\frac{d\Gamma}{dE_l} = \frac{G_F^2 |V_{ub}|^2 m_b^4}{96\pi^3} \int d\omega \theta(m_b - 2E_l - \omega) f(\omega), \quad (4.80)$$

where  $f(\omega)$  is the shape function define by

$$f(\omega) = \frac{1}{2m_B} \langle B | \bar{h} \delta(in \cdot D + \omega) | B \rangle. \quad (4.81)$$

Since this function is a universal quantity of the  $B$  meson, it can be measured experimentally through other processes. For example, the photon spectrum of  $B \rightarrow X_s \gamma$  decay is given by [299]

$$\frac{d\Gamma}{dE_\gamma} = \frac{G_F^2 |V_{tb} V_{ts}^*|^2 \alpha_{QED} m_b^5}{32\pi^4} f(\omega). \quad (4.82)$$

Therefore, the extraction of  $|V_{ub}|$  can be done without the theoretical uncertainty of the shape function, if one considers a ratio of weighted integrals over the endpoint regions of  $B \rightarrow X_u \nu$  decays and the photon spectrum in  $B \rightarrow X_s \gamma$  decays as [300, 301]

$$\left| \frac{V_{ub}}{V_{tb} V_{ts}^*} \right|^2 = \frac{3\alpha_{QED}}{\pi} K_{pert}(E_0) \frac{\Gamma_u(E_0)}{\Gamma_s(E_0)} + \mathcal{O}(\Lambda/M_B), \quad (4.83)$$

where

$$\Gamma_u(E_0) = \int_{E_0}^{M_B/2} dE_l \frac{d\Gamma(B \rightarrow X_u \nu)}{dE_l}, \quad (4.84)$$

$$\Gamma_s(E_0) = \frac{2}{M_B} \int_{E_0}^{M_B/2} dE_\gamma (E_\gamma - E_0) \frac{d\Gamma(B \rightarrow X_s \gamma)}{dE_\gamma}. \quad (4.85)$$

The coefficient  $K_{pert}(E_0)$  is a factor from short-distance effect which can be calculated in perturbative QCD. There are two major sources of uncertainties. The first is the unknown higher twist corrections to the shape function  $1/m_b$  [302, 303, 304, 305]. Based on model calculations this higher twist correction is expected to be of order 15% for  $E_l^{cut} = 2.3$  GeV. The second is the weak annihilation contribution of  $O(1/m_b^2)$ , which is estimated as 10% for  $E_l^{cut} = 2.3$  GeV [306, 307]. These two uncertainties can be reduced below 10% by lowering the lepton energy cut by combining with other cuts.

For the  $m_X^2$  cut [308, 309, 310, 311, 312], 80% of the kinematic range is available but still the results are sensitive to the shape function. This cut also suffers from the singularity due to the bremsstrahlung diagram when the partonic invariant mass  $s = (m_b - v)^2$  is zero.

For the pure  $q^2$  cut, 20% of the rate is available and the decay rate is not sensitive to the shape function [313]. However, the kinematic range is sensitive to the resonance region and the convergence of the OPE as well as the convergence in the perturbative expansion in  $\alpha_s$  are slower. The largest error comes from the weak annihilation contribution of  $O(1/m_b^3)$ . The rate with  $q^2$  is also sensitive to the uncertainty of  $m_b$  [314] as can be seen from the  $m_b$  dependence of the partial decay rate parametrized as  $\Gamma(q^2 > q_{cut}^2) \propto m_b^{\Delta(q_{cut}^2)}$ , where  $\Delta(q_{cut}^2) \sim 10 + \frac{q_{cut}^2 - (m_B - m_D)^2}{1 \text{ GeV}^2}$ .

To summarize, possible sources of errors are (1) perturbative error from unknown two-loop corrections, (2) shape function contributions and bremsstrahlung, (3) uncertainties in  $m_b$ , and



Cuts on $(q^2, m_X^2)$	$G(q_{\text{cut}}^2, m_{\text{cut}})$	$\Delta_{\text{struct}}G$	$\Delta_{\text{pert}}G$	$\frac{\Delta_{m_b}G}{\pm 80/30 \text{ MeV}}$	$\Delta_{1/m^3}G$	$\Delta G$
Combined cuts						
6 GeV <sup>2</sup> , 1.86 GeV	0.38	-4%	4%	13%/5%	6%	15%/9%
8 GeV <sup>2</sup> , 1.7 GeV	0.27	-6%	6%	15%/6%	8%	18%/12%
11 GeV <sup>2</sup> , 1.5 GeV	0.15	-7%	13%	18%/7%	16%	27%/22%
Pure $q^2$ cuts						
$(m_B - m_D)^2, m_D$	0.14	--	15%	19%/7%	18%	30%/24%
$(m_B - m_{D^*})^2, m_{D^*}$	0.17	--	13%	17%/7%	14%	26%/20%

Table 4.18:  $G(q_{\text{cut}}^2, m_{\text{cut}})$  and its errors for different choices of  $(q_{\text{cut}}^2, m_{\text{cut}})$ .  $\Delta_{\text{struct}}G$  gives the fractional effect of the structure function  $f(k_+)$  in the simple model which is not included in the error estimate. The total error is obtained by adding each error in quadrature. The two values correspond to  $\Delta m_b^{1S} = \pm 80 \text{ MeV}$  and  $\pm 30 \text{ MeV}$ . Table is from [315].

(4)  $O(1/m_b^3)$  power corrections. The optimized method would be obtained by combining the  $q^2$  and  $m_X^2$  cuts [315]. The kinematical constraints  $m_X < m_D$  and  $q_{\text{cut}}^2 > m_B m_b - (m_X^{\text{cut}})^2$  reduce the charm background. If we raise  $q_{\text{cut}}^2$  the errors (3) and (4) gets larger while if we lower  $q_{\text{cut}}^2$  the errors (2) gets larger and (1) is small in the intermediate  $q^2$  region. Thus it is important to find the best cut that minimizes the sum of these errors.

In Table 4.18, we give results of [315] for the errors of the partial decay rate normalized by the total tree level parton decay rate defined as

$$\frac{G_F^2 |V_{ub}|^2 m_b^5}{192\pi^3} G(q_{\text{cut}}^2, m_{\text{cut}}) \equiv \int_{\hat{q}_{\text{cut}}^2}^1 d\hat{q}^2 \int_0^{\hat{s}_0} d\hat{s} \frac{d\Gamma}{d\hat{q}^2 d\hat{s}}. \quad (4.86)$$

In order to achieve the  $|V_{ub}|$  determination with a few percent accuracy,  $q_{\text{cut}}^2 = 6 \text{ GeV}^2$  (and  $m_{X_{\text{cut}}}^2 = m_D^2$ ) is the optimal choice. The dominant error in this case is the uncertainty in  $m_b$ . It is therefore important to determine the bottom quark mass to 30 MeV/ $c^2$  accuracy.

## Exclusive decays

The exclusive semileptonic decay  $B \rightarrow \pi l \nu$  determines the CKM matrix element  $|V_{ub}|$  through the following formula,

$$\frac{d\Gamma}{dq^2} = \frac{G_F^2}{24\pi^3} |(v \cdot k_\pi)^2 - m_\pi^2|^{3/2} |V_{ub}|^2 |f^+(q^2)|^2, \quad (4.87)$$

where the form factor  $f^+$  is defined as

$$\langle \pi(k) | \bar{q} \gamma^\mu b | B(p) \rangle = f^+(q^2) \left[ (p+k)^\mu - \frac{m_B^2 - m_\pi^2}{q^2} q^\mu \right] + f^0(q^2) \frac{m_B^2 - m_\pi^2}{q^2} q^\mu, \quad (4.88)$$

with  $p$  and  $k$  the  $B$  and  $\pi$  meson momenta.  $q = p - k$  is the momentum transfer and  $q^2 = m_B^2 + m_\pi^2 - 2m_B v \cdot k$ , where  $v$  is the velocity of the  $B$  meson. Since the most promising approach in which systematic improvement based on the first principle calculations is possible is lattice QCD, we focus on the lattice computation of the form factors.

Lattice calculation suffers from three major limitations. One is the discretization error from the large energy of the initial and final hadrons. In order to avoid such error, spatial momenta

method	stat.	disc.	1/M extrap.	pert.
NRQCD (JLQCD)	10%	16%	–	4%
extrap. (APE)	10%	5%	15%	–
NRQCD (future)	< 5%	4-10%	–	4%
extrap.+ HQET (future)	< 5%	5%	5%	–

Table 4.19: Typical errors of the form factor  $f^+(q^2)$  for  $q^2 > 16 \text{ GeV}^2$  at present and future prospects. “stat.”, “disc.”, “1/M extrap”, and “pert.” stand for statistical, discretizations, 1/M extrapolation, and perturbative errors.

must be much smaller than the cutoff, *i.e.*  $|\vec{p}_B|, |\vec{k}_\pi| < 1 \text{ GeV}$ . This means that the form factors can be computed reliably only in the range of  $v \cdot k \equiv E_\pi < 1 \text{ GeV}$  or equivalently  $q^2 > 18 \text{ GeV}^2$ . Another limitation is the fact that due to the limited computer power the light quark mass range for practical simulations is  $m_s/3 \leq m_q \leq m_s$  or  $m_\pi = 0.4 \sim 0.8 \text{ GeV}$ . In order to obtain physical results chiral extrapolation in the light quark masses is necessary. The last limitation is the large discretization error from the  $b$ -quark mass. In the present simulations, the lattice cutoff is limited to  $a^{-1} = 2 - 3 \text{ GeV}$ , so that the  $b$ -quark mass in lattice unit is larger than unity. This makes the discretization error of  $O(am_b)$  completely out of control. In order to avoid this error, one either carries out simulations around a charm quark mass region and extrapolate the result in the inverse heavy quark mass  $1/m_Q$  (extrapolation method), or use heavy quark effective theories, such as NRQCD action or Fermilab action (HQET). In both cases, extrapolation or interpolation of the form factors in  $1/m_Q$  may be performed using the HQET-motivated form factors  $f_1(v \cdot k)$  and  $f_2(v \cdot k)$  [316]

$$\langle \pi(k) | \bar{q} \gamma^\mu b | B(p) \rangle = 2 \left[ f_1(v \cdot k) v^\mu + f_2(v \cdot k) \frac{k^\mu}{v \cdot k} \right]. \quad (4.89)$$

With this choice the heavy quark scaling law is explicit, and the form factors are simply expanded in terms of  $1/m_Q$ .

So far all lattice calculations of the form factors have been performed only in the quenched approximation, in which the sea quark effects are neglected. The systematic error due to quenching is hard to estimate but typical errors in many quantities such as light hadron masses and decay constants are expected to be at 10-15% level.

Recently five lattice collaborations have carried out quenched QCD calculations of  $B \rightarrow \pi l \nu$  form factors using extrapolation methods [132, 133], the Fermilab action [134], and the NRQCD action [135, 317] for the heavy quark. Figure 4.39 shows the results from different lattice groups.  $f^+(q^2)$  agrees within systematic errors, while  $f^0(q^2)$  shows deviations among different methods. The reason for the discrepancies in  $f^0(q^2)$  can be attributed to the systematic error in the chiral extrapolation and heavy quark mass extrapolation (interpolation) error. The error of the form factors in the present calculations is around 20%. In addition to the quenching error and the chiral extrapolation error, the major errors are the statistical error, the discretization error and the  $1/M$  extrapolation error.

Table 4.19 shows the errors by the JLQCD collaboration (NRQCD) and the APE collaboration (the extrapolation method). We also list expected errors in unquenched lattice calculations with  $a^{-1} = 2^3 \text{ GeV}$  in the near future. The present NRQCD method (JLQCD) has a large discretization error since  $a^{-1} = 1.6 \text{ GeV}$  is used. It would be possible to carry out simulations with  $a^{-1} = 2 - 3 \text{ GeV}$ , so that the error of  $O((ak)^2)$  are reduced to 4-10%. The discretization error in the extrapolation method appears in the lattice results for the charm quark region

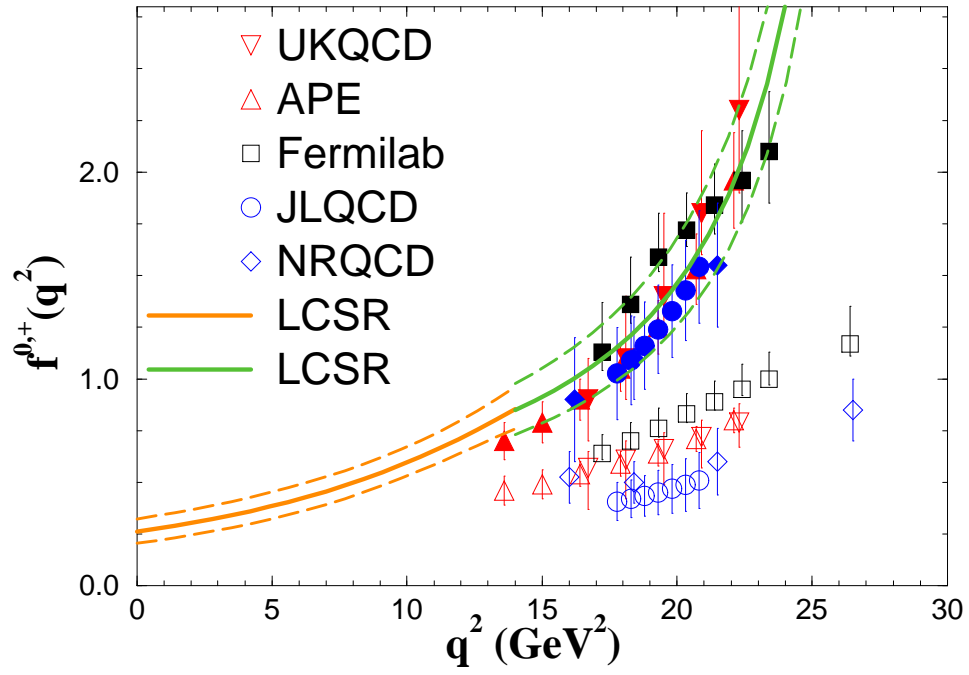


Figure 4.39:  $B \rightarrow \pi l \nu$  form factors by different lattice groups. Filled symbols represent  $f^+(q^2)$  and open symbols are  $f^0(q^2)$ .

themselves, which is propagated through the final result by extrapolation in  $1/M$ . Since the present quenched calculation is carried out with  $a^{-1} = 2.7$  GeV, they will remain to be of the same order.

There are several proposals to improve the form factor determination. The quenching error can be resolved only by performing the unquenched calculations. Recently, the JLQCD collaboration has accumulated  $n_f = 2$  unquenched lattice configurations with  $O(a)$ -improved Wilson fermions [318], and  $n_f = 2 + 1$  unquenched configurations with improved staggered fermions have been produced by the MILC collaboration [129]. These unquenched QCD data should be applied to form factor calculations.

Using the heavy quark symmetry is another way of improvement. Since the CLEO-c experiment can measure form factors for  $D \rightarrow \pi l \nu$  to a few percent accuracy, their results will be a good approximation for the  $B \rightarrow \pi l \nu$  form factors. Then the task for lattice QCD is to provide the  $1/m_Q$  dependence of the form factors. The  $B$  to  $D$  ratio  $\frac{d\Gamma(B \rightarrow \pi l \nu)/d(v \cdot k_\pi)}{d\Gamma(D \rightarrow \pi l \nu)/d(v \cdot k_\pi)}$  with the same recoil energy  $v \cdot k_\pi$  would be a nice quantity to measure on the lattice, since a large part of the statistical error, the perturbative error and the chiral extrapolation errors are expected to cancel in this ratio.

In the large recoil momentum region the light-cone QCD sum rule (LCSR) may be used to calculate the form factors [319, 320, 321, 322]. In Figure 4.39 the latest result [322] is also shown on top of the lattice calculations. The curve below  $q^2 = 14$  GeV<sup>2</sup> is the LCSR result. At  $q^2 = 14$  GeV<sup>2</sup>, it is connected to a pole dominance model  $f^+(q^2) = c/(1 - q^2/m_{B^*}^2)$ , which is expected to be a good approximation when  $q^2$  is close to  $m_{B^*}^2$ .

Model independent bounds for the whole  $q^2$  range can be obtained with dispersion relation, perturbative QCD, and lattice QCD data [323]. Reducing the lattice errors or having other inputs would significantly improve the results. More elaborate studies along this line would be important.

Recently, the UKQCD collaboration [324] and the SPQcdR collaboration [325] performed studies of  $B \rightarrow \rho l \nu$  form factors. Both collaborations use  $O(a)$ -improved Wilson action for the heavy quark and extrapolate the numerical results of  $m_Q \sim m_c$  toward the physical  $b$  quark mass. UKQCD obtained the partially integrated decay rate in the region  $12.7 \text{ GeV}^2 < q^2 < 18.2 \text{ GeV}^2$  as  $\Gamma = (4.9_{-10}^{+12} \pm 0) \times 10^{12} \text{ s}^{-1} |V_{ub}|^2$ .

### 4.9.3 Measurement of inclusive $b \rightarrow u$ semileptonic decays

Measurement of the inclusive rate for  $B \rightarrow X_u \ell \nu$  decays is the most straightforward approach to determine  $|V_{ub}|$ . OPE provides a firm theoretical basis to convert the measured rate to  $|V_{ub}|$ . However, this is true only when the total rate can be measured with a small enough error. Experimentally, however, we have to introduce cuts on kinematical variables, such as  $E_\ell$ ,  $m_X$  and  $q^2$ , to reduce the huge  $B \rightarrow X_c \ell \nu$  background, and only a limited phase space is available in a practical measurement. This complicates the situation, and the cut has to be chosen carefully to minimize the theoretical uncertainties. As discussed in the above section, one of the best strategies is to apply a combined cut on  $(q^2, m_X)$ .

In  $\Upsilon(4S)$  experiments, a correct measurement of  $(q^2, m_X)$  is possible when the accompanying  $B$  decays are fully reconstructed. This technique, referred to as “full reconstruction tagging”, allows us to isolate tracks from the signal  $B$  decays for correct reconstruction of  $m_X$ , and also to determine the momentum vector of the signal-side  $B$  meson. The latter helps to improve reconstruction of the missing neutrino, leading to correct reconstruction of  $q^2$  and better discrimination of  $B \rightarrow X_c \ell \nu$  background leaking into the signal phase space. Full reconstruction

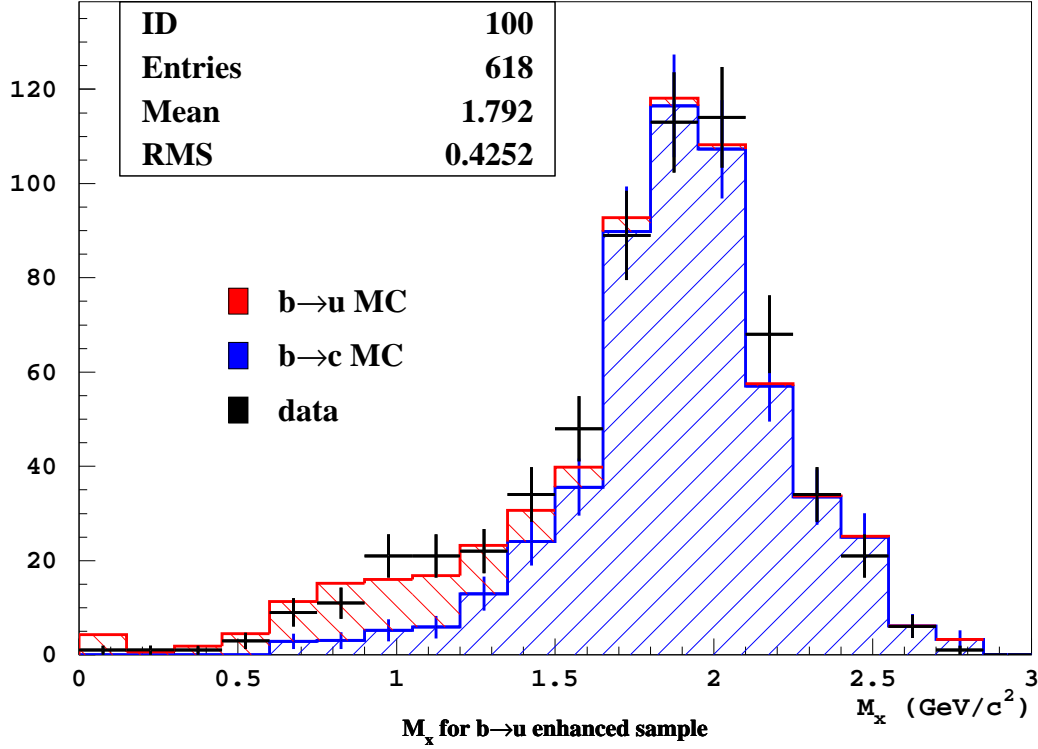


Figure 4.40: Distribution of reconstructed  $m_X$  with a full reconstruction analysis using 141 fb<sup>-1</sup> of data.

tagging also allows us to determine the flavor and charge of the signal-side  $B$ . It helps to identify the signal lepton using the correlation between the  $B$  flavor and lepton charge, and also to measure the decay rate separately for neutral and charged  $B$  mesons. However, this ultimate measurement requires a large accumulation of  $B\bar{B}$  data because of the relatively small efficiency in the full reconstruction of the accompanying  $B$ 's (a few times 0.1%). Therefore, the high luminosity of the SuperKEKB provides a unique opportunity to perform this measurement with high statistics.

Such analysis with the full reconstruction tagging is being performed with the present Belle data, although with limited statistics. Figure 4.40 shows the distribution of reconstructed  $m_X$  for the  $q^2$  region above 6 GeV<sup>2</sup>, based on 140 fb<sup>-1</sup> of data accumulated by Summer 2003. In this data sample, the number of fully reconstructed events is about  $1.4 \times 10^5$  ( $9.1 \times 10^4$  of  $B^+$  and  $4.7 \times 10^4$  of  $B^0$  events), and it corresponds to the full reconstruction efficiency ( $\epsilon_{frecon}$ ) of 0.1%. In the low  $m_X$  region, one can see a clear enhancement of the  $B \rightarrow X_u \ell \nu$  signal over the expected  $B \rightarrow X_c \ell \nu$  background. In the region  $m_X < 1.5$  GeV/c<sup>2</sup>, for example, the observed signal ( $S$ ) is 68 with a predicted background ( $B$ ) of 56, resulting in a signal-to-background ratio ( $S/B$ ) of 1.2. Table 4.20 summarizes the efficiency to detect the  $B \rightarrow X_u \ell \nu$  signal once the accompanying  $B$  is fully reconstructed ( $\epsilon_{b \rightarrow u}$ ), and the signal-to-background ratio ( $S/B$ ). Here, values are shown for three  $m_X$  cuts,  $m_X < 1.5, 1.7$  and  $1.86$  GeV/c<sup>2</sup>, with the  $q^2$  cut fixed at 6 GeV<sup>2</sup>. We note that a similar analysis by the BaBar collaboration has better  $S/B$  by a factor of 2 [238].

Quantity	$m_{Xcut}$		
	1.5 GeV/ $c^2$	1.7 GeV/ $c^2$	1.86 GeV/ $c^2$
$\epsilon_{b \rightarrow u}$	0.14	0.17	0.17
$S/B$	1.21	0.61	0.32

Table 4.20: Efficiencies to detect the  $B \rightarrow X_u \ell \nu$  signal for the fully reconstructed events ( $\epsilon_{b \rightarrow u}$ ) and the signal-to-background ratio ( $S/B$ ) for three different cut values.

Based on extrapolation of the present Belle results and realistic assumptions for the improvement in  $\epsilon_{frec}$  and  $S/B$ , we have estimated the  $|V_{ub}|$  precision at a SuperKEKB/Belle experiment. We consider here the statistical, experimental systematic and theoretical errors, and estimate them as follows.

**Statistical error:** The statistical error ( $\Delta_{stat}$ ) is simply scaled with the integrated luminosity ( $L$ ),

$$\Delta_{stat} = \frac{1}{2} \times \sqrt{\frac{1 + (S/B \times f_{S/B})^{-1}}{n_0 \times f_{frec} \times \epsilon_{b \rightarrow u} \times L}} \quad , \quad (4.90)$$

where  $n_0$  is the rate of  $B \rightarrow X_u \ell \nu$  decays after full reconstruction, estimated as  $68/(0.14 \times 141) = 3.2/\text{fb}^{-1}$ . The factor  $f_{frec}$  accounts for the improvement in  $\epsilon_{frec}$ , that is  $2.2 \times 10^5/1.4 \times 10^5 = 1.6$  (see Table 4.3). The factor  $f_{S/B}$  accounts for a possible improvement in  $S/B$  from the results in Table 4.20, and is assumed to be  $f_{S/B} = 2$  based on the above mentioned BaBar result.

**Experimental systematic error:** The major source of experimental systematic error ( $\Delta_{syst}$ ) will be associated with the background subtraction, and largely depend on the signal-to-background ratio. For instance, the  $(q^2, m_X)$  measurement by Belle using an advanced neutrino reconstruction technique [326] has  $S/B = 0.18$  and the total experimental systematic error (in  $Br(B \rightarrow X_u \ell \nu)$ ) of 18.1%, dominated by the  $B\bar{B}$  background subtraction error of 16.8%. Relying on this result and assuming a naive scaling of the background subtraction error with  $(S/B)^{-1}$ ,  $\Delta_{syst}$  is estimated as,

$$\Delta_{syst} = \frac{1}{2} \times [0.168 \times \frac{0.18}{S/B \times f_{S/B}} \oplus 0.03] \quad . \quad (4.91)$$

Here, we add in quadrature a 3% error associated with the signal detection efficiency. The estimation then gives  $\Delta_{syst} = 2.8\%$  in  $|V_{ub}|$ .

**Theoretical error:** As discussed in Section 4.9.2, the theoretical error ( $\Delta_{theo}$ ) is minimum at a choice of  $(q_{cut}^2, m_{Xcut}) = (6\text{GeV}^2, 1.86\text{GeV}/c^2)$ . The dominant error in this case is the uncertainty in the  $b$ -quark mass. Based on a combined fit to recent experimental data of  $B$  semileptonic decays, Bauer, Ligeti, Luke and Manohar have deduced  $m_b^{1S} = 4.74 \pm 0.10 \text{ GeV}$ , where the error is dominated by experimental uncertainties [327]. If the experimental uncertainties are eliminated in the future, the present 100 MeV error shrinks to 30 MeV. Then  $\Delta_{theo} = 1/2 \times 9 = 4.5\%$  in  $|V_{ub}|$ , according to Table 4.18.

Adding the above three error sources in quadrature, Figure 4.41 demonstrates the expected improvement of  $|V_{ub}|$  error as a function of the integrated luminosity  $L$ , with the optimal choice of  $(q_{cut}^2, m_{Xcut}) = (6\text{GeV}^2, 1.86\text{GeV}/c^2)$ . In conclusion, with a precise determination of the  $b$ -quark mass, a  $|V_{ub}|$  error of less than 5% is achievable at  $L = 5 \text{ ab}^{-1}$ .

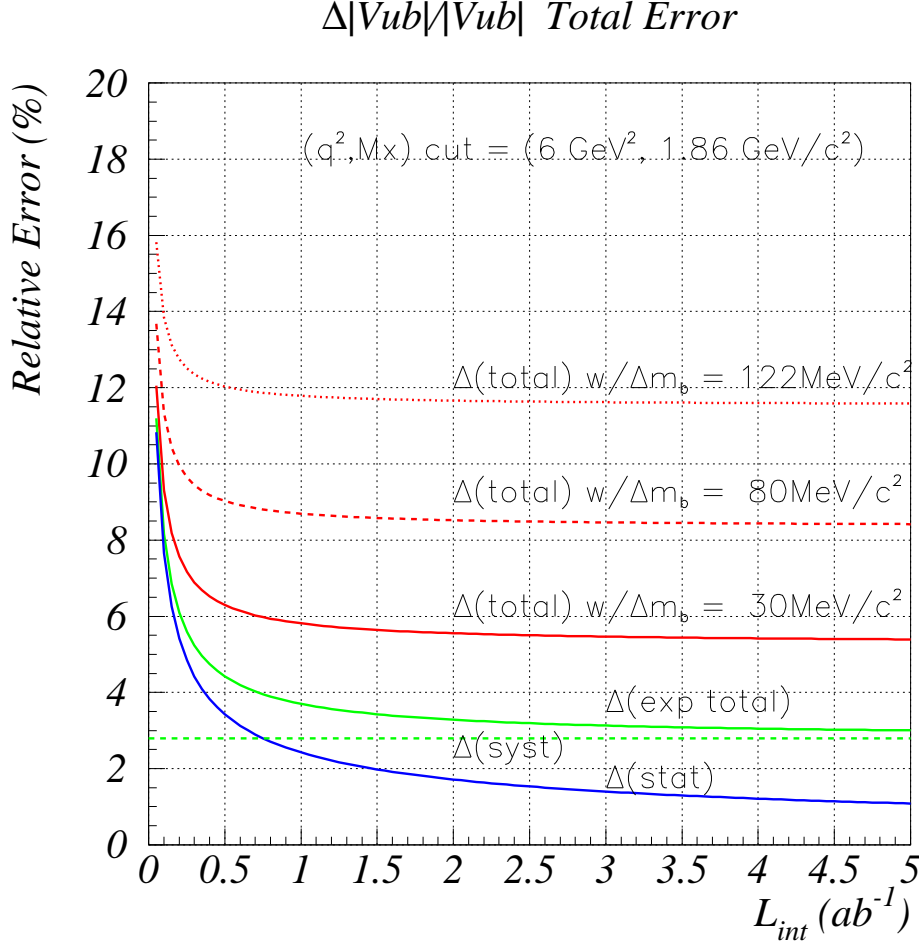


Figure 4.41: Expected improvement of  $|V_{ub}|$  error as a function of  $L$ .

#### 4.9.4 Measurement of exclusive $b \rightarrow u$ semileptonic decays

The measurement of the inclusive  $B \rightarrow X_u \ell \nu$  decay is insensitive to theoretical ambiguities, but experimentally challenging because of the large background from  $B \rightarrow X_c \ell \nu$  decays. Complementary to this, the measurement of exclusive decays, such as  $B \rightarrow \pi \ell \nu$  and  $B \rightarrow \rho \ell \nu$ , provides experimentally cleaner information, but is subject to large theoretical uncertainties in the form factors. On the experimental side, it is essential to provide precise data for the differential rates  $d\Gamma/dq^2$  of each exclusive channel. This is because  $d\Gamma/dq^2$  varies depending on theory models, and such data helps to test the model. Precise data in the high  $q^2$  region is especially important, since lattice-QCD calculations, the most promising tool for reliable model-independent determination of  $|V_{ub}|$ , are possible only in the region  $q^2 > 18 \text{ GeV}^2$ , as discussed in Section 4.9.2. While there have been several exclusive measurements in the literature [328, 329, 330, 331, 332, 333], these data lack information on the  $q^2$  distribution or, even if they include such information, suffer from poor statistics and from relatively large systematic errors. A high luminosity SuperKEKB/Belle

experiment will enable us to measure the  $q^2$  distributions with high statistics and less systematic uncertainties. Combined with improvements in lattice QCD with unquenched calculations in future, this will lead to useful determinations of  $|V_{ub}|$ .

One of key experimental issues in measuring the exclusive  $B \rightarrow \pi\ell^+\nu/\rho\ell^+\nu$  decays is the reconstruction of the undetected neutrino in the final state. Information on missing energy and momentum of the event have been used to infer information about the missing neutrino (“neutrino reconstruction”). This method, originally developed by CLEO, has been applied in existing measurements and exploits the known kinematics of the  $e^+e^- \rightarrow \Upsilon(4S)$  reaction and near  $4\pi$  coverage (“hermeticity”) of the detector. In reality, however, hermeticity of a detector is never complete. This lack of hermeticity allows background from both  $B\bar{B}$  and cross-feed (*e.g.*,  $\pi\ell\nu \leftrightarrow \rho\ell\nu$ ) to contribute, where the latter is serious especially in the high  $q^2$  region. For instance, the recent CLEO measurement [331] provides  $Br(B \rightarrow \pi\ell\nu)$  with a statistical error of 13.5(36.0)% and an experimental systematic error of 8.6(18.3)% for the whole  $q^2$  ( $q^2(> 16\text{GeV}^2)$ ) region. The experimental systematic errors are mainly associated with the neutrino reconstruction; 6.8% in the whole  $q^2$  region and 17.2% in the  $q^2 > 16\text{GeV}^2$  region. The CLEO result has been obtained with event sample of only  $\sim 10 \text{ fb}^{-1}$ , and we can quickly improve the statistical error to a few %. However, the systematic error arising mainly from the neutrino reconstruction will soon limit the experimental uncertainties.

As in the case of the inclusive measurement, which is discussed in the previous section, analyses with full reconstruction tagging improve the situation substantially, and make best use of the high luminosity at SuperKEKB/Belle. Figure 4.42 compares the missing mass resolution for (a) full reconstruction tagging (for  $B \rightarrow D^0\ell^+\nu$  with  $78 \text{ fb}^{-1}$ ), and (b) classical  $\nu$  reconstruction (for  $B \rightarrow \omega\ell^+\nu$  with  $78 \text{ fb}^{-1}$ ) in the present Belle analyses. An improvement in the FWHM by almost a factor of 50 is seen for the full reconstruction analysis. We can also consider semileptonic tagging, where one tags more abundant  $B \rightarrow D^{(*)}\ell^+\nu$  decays in the accompanying  $B$  decays. This technique provides about 4 times more statistics by sacrificing purity and  $q^2$  resolution. Belle has presented a preliminary inclusive analysis result using this method [334]. An exclusive analysis using this method is also in progress.

Figure 4.43 shows the expected improvement of the experimental error in  $|V_{ub}|$  as a function of the integrated luminosity  $L$ , for the whole  $q^2$  and the high  $q^2$  regions. Here, the errors are estimated by extrapolating the present Belle analysis using semileptonic tagging, and are compared with the classical neutrino reconstruction. One can see that the classical neutrino reconstruction will soon hit the systematic limit. At a few times  $100 \text{ fb}^{-1}$ , the tagging analysis will provide more precise results. The experimental precisions in  $|V_{ub}|$  expected at 5 and  $50 \text{ ab}^{-1}$  are 2.3% and 1.9%, respectively, for the whole  $q^2$  region, and 2.9% and 2.1%, respectively, for the  $q^2 > 16\text{GeV}^2$  region.



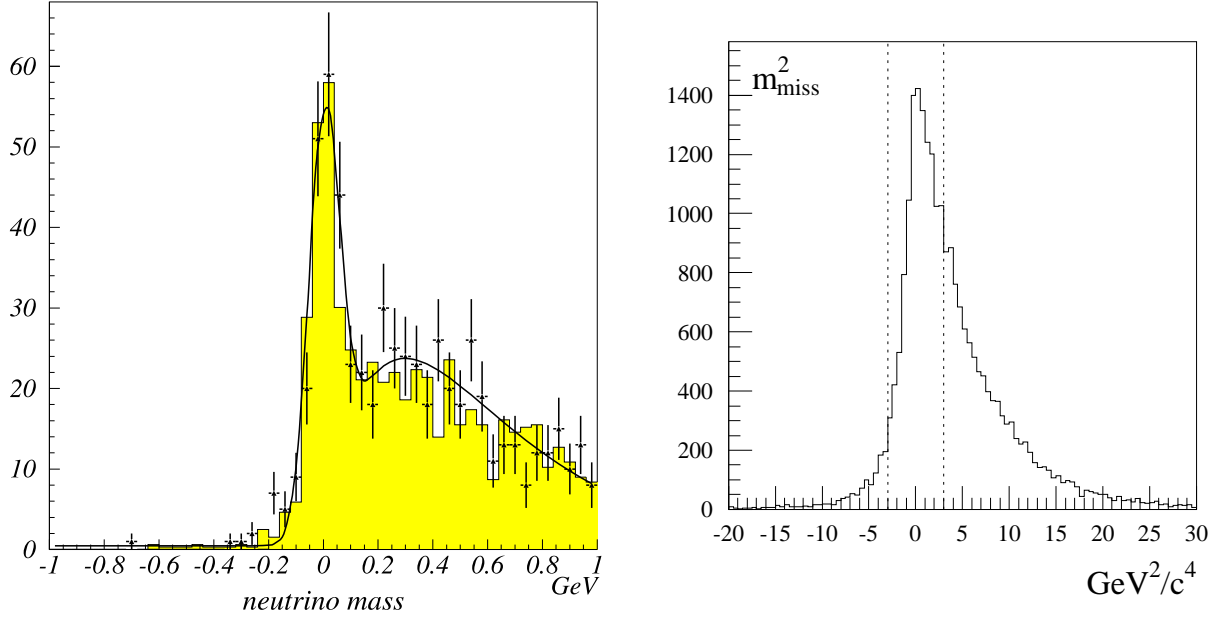


Figure 4.42: Missing mass resolution in (left) a full reconstruction analysis and (right) a classical neutrino reconstruction analysis.

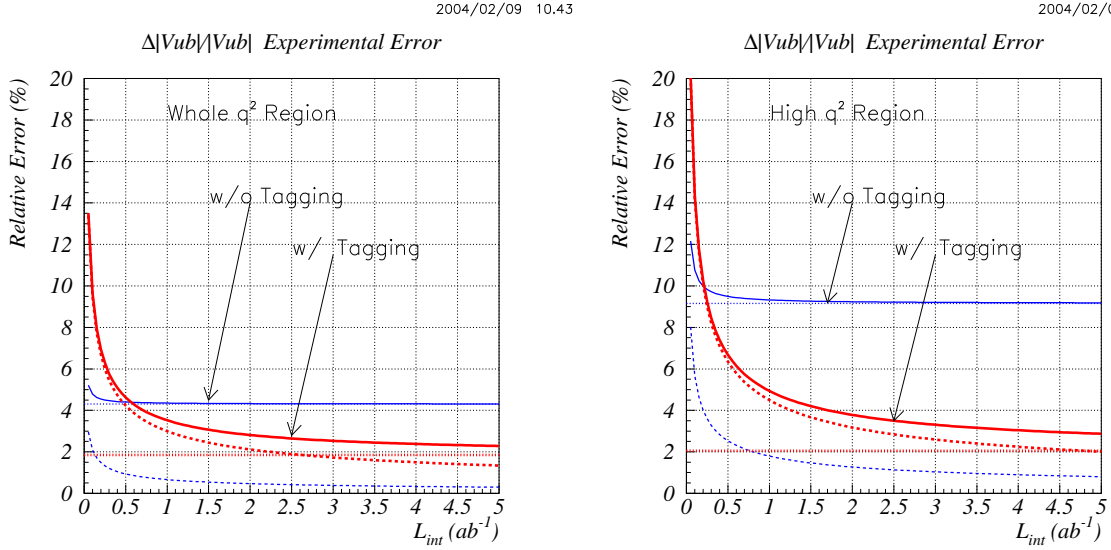


Figure 4.43: Expected improvement of the experimental error in  $|V_{ub}|$  as a function of the integrated luminosity  $L$ , (left) for the whole  $q^2$  and (right) the high  $q^2$  regions.

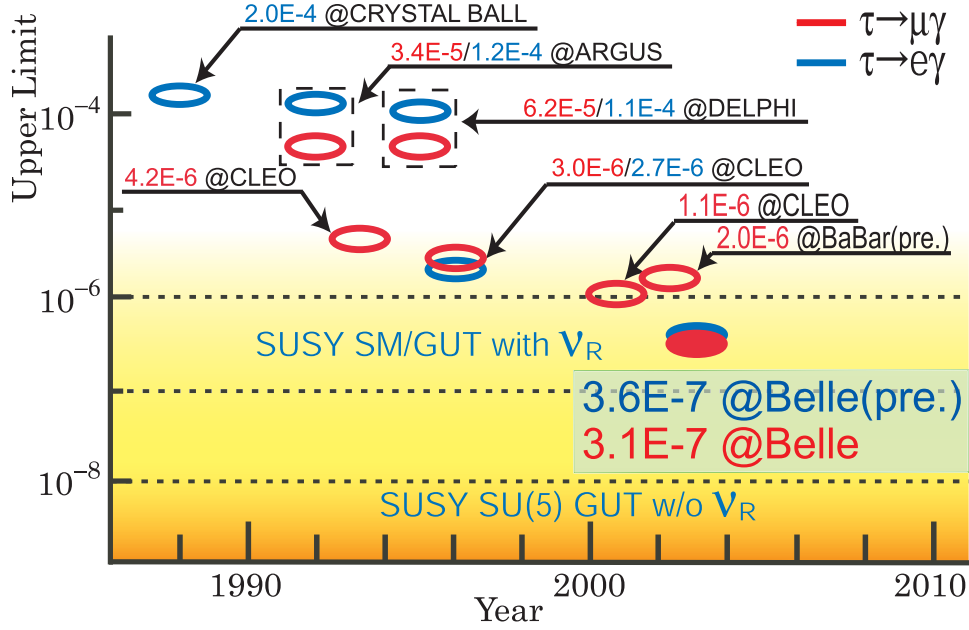


Figure 4.44: Experimental status of the LFV search.

## 4.10 Tau decays

### 4.10.1 Introduction

The  $\tau$  lepton is the only charged lepton that is heavy enough to decay hadronically. Its variety of pure-leptonic and semi-leptonic decay modes makes it possible to study various physics issues. With an anticipated luminosity of  $5 \times 10^{35} \text{ cm}^{-2}\text{sec}^{-1}$ , SuperKEKB is expected to deliver a sample of  $1.5 \times 10^{10}$  tau pairs in three years of data taking. This huge data sample allows us to attain a single event sensitivity of  $3 \times 10^{-10}$  for branching fractions for a 10% detection efficiency with no backgrounds. Research making the best use of such a large data sample can be divided into two categories: the sensitivity frontier and the precision frontier. The sensitivity frontier involves searches for new physics phenomena in rare or forbidden decays, while on the precision frontier one searches for a small inconsistency with the SM in a high precision measurement. Among many possible subjects at the sensitivity frontier, here we discuss the search for Lepton Flavor Violation (LFV) phenomena at SuperKEKB.

A theoretical overview of lepton-flavor-violating process beyond the Standard Model is given in Section 3.6.

### 4.10.2 Present experimental status

So far, tau physics has been carried out mostly at electron-positron collider facilities. Samples of  $e^+e^- \rightarrow \tau^+\tau^-$  reactions are selected based on characteristic properties, such as low multiplicity with a well collimated back-to-back jet-like pattern and missing momentum (energy) due to missing neutrinos. While these requirements will remove  $B\bar{B}$  and a large portion of continuum reactions, an appreciable amount of Bhabha, muon-pair and two-photon processes remain and become severe backgrounds. Since  $\tau$  decays always include neutrinos, the  $\tau$  cannot be exclusively reconstructed. Therefore background contamination cannot be totally avoided. The LFV

processes discussed here are exclusive decays and much higher sensitivity than for other decay modes could be attained.

Belle has so far analyzed  $86 \text{ fb}^{-1}$  of data for  $\tau \rightarrow \mu^-(e^-)\gamma$ ,  $83 \text{ fb}^{-1}$  of data for  $\tau^- \rightarrow \mu^-(e^-)h^0$  (where  $h^0$  denotes either  $h^0 = \eta, \eta'$  or  $\pi^0$ ), and  $87 \text{ fb}^{-1}$  of data for  $\tau^- \rightarrow l^-l^+l^-$ . The current experimental status is summarized in Table 4.21 and the history of  $\tau^- \rightarrow \mu^-(e^-)\gamma$  searches is shown in Figure 4.44. It is seen that the older data, mostly collected by CLEO, are no longer competitive with the best limits from the Belle collaboration. Upper limits for branching fractions go down to the  $10^{-7}$  level and the searches are approaching regions sensitive to new physics.

In this section, we discuss the experience in  $\tau$  physics research that we have acquired during the analysis of the current Belle data.

While the signal side  $\tau$  is exclusively reconstructed for every LFV process, the tag side is required to be composed of a single charged track and any number of photons with neutrinos. The mode  $\tau^- \rightarrow \mu^-(e^-)\gamma$  has the fewest constraints, so that a certain amount of background inevitably remains. The  $\tau^- \rightarrow \mu^-(e^-)h$  mode includes extra constraints that provide additional background rejection power, although there is some decrease of the detection efficiency due to the higher multiplicity. Together with the kinematic constraints for the signal, particle identification, especially for muons and electrons, play an essential role for event selection. The Belle detector provides a  $\mu$ -id efficiency of 90% and an  $e$ -id efficiency of 97-98%: the event selection power is strong and then background contamination is little at the electron accompanying processes. The contamination due to the inefficiency of  $\mu$ -id is 28% for  $\tau^- \rightarrow \mu^-\gamma$ , while the rate due to the inefficiency of  $e$ -id is 6% in  $\tau^- \rightarrow e^-\gamma$ .

We have introduced a new requirement on the relation between the missing momentum and the missing mass-squared in  $\tau^- \rightarrow \mu^-(e^-)\gamma$ , in addition to the conventional requirements. It is quite effective; 98% of generic tau-pairs and 80-90% of radiative Bhabhas, muon-pairs and continuum are removed, while 76% of the signal is retained (See Figure 4.45).

Within the data analyzed, no signal candidates are found in the signal regions for  $\tau^- \rightarrow \mu^-(e^-)h^0$  and  $\tau^- \rightarrow l^-l^+l^-$ . On the other hand,  $\tau^- \rightarrow \mu^-(e^-)\gamma$  suffers from backgrounds as seen in Figure 4.46 (a). The principal background remaining after the selections for  $\tau^- \rightarrow \mu^-(e^-)\gamma$  originates from  $\tau^+\tau^-$ . In particular, the radiative tau-pair process ( $e^-e^- \rightarrow \tau^+\tau^-\gamma$ ) dominates. One of  $\tau$ 's decays semi-leptonically from which the lepton and the radiated photon composes a tau candidate, while the other tau decays leaving one charged track in the detector with a different lepton flavor. Multi-photon radiative muon-pair (and Bhabha events) yield the second largest background: one of leptons and a radiated photon form a tau candidate, and the other lepton is mis-identified. These backgrounds cannot be discriminated from the true signal.

For  $\tau^- \rightarrow \mu^-(e^-)\eta$ ,  $\mu^-(e^-)\eta'$ ,  $\mu^-(e^-)\pi^0$  and  $\tau^- \rightarrow l^-l^+l^-$ , we evaluate the expected backgrounds in the signal region from the sidebands and extract the number of signal candidates. No candidate is found. The upper limits are calculated according to a Bayesian approach. For  $\tau^- \rightarrow \mu^-(e^-)\gamma$  the background distribution was intensively studied using actual data and MC simulations, as is seen in Figure 4.47. A thorough understanding of the background's origin and properties was obtained. Finally, the number of signal events was obtained by means of an unbinned extended maximum likelihood method.

### 4.10.3 Achievable sensitivity at SuperKEKB and physics reaches

Figure 4.48 shows the sensitivities anticipated at SuperKEKB. The sensitivities shown by the triangular symbols are the expected sensitivities obtained by assuming some signal-to-background conditions and applying the unbinned extended maximum likelihood method at

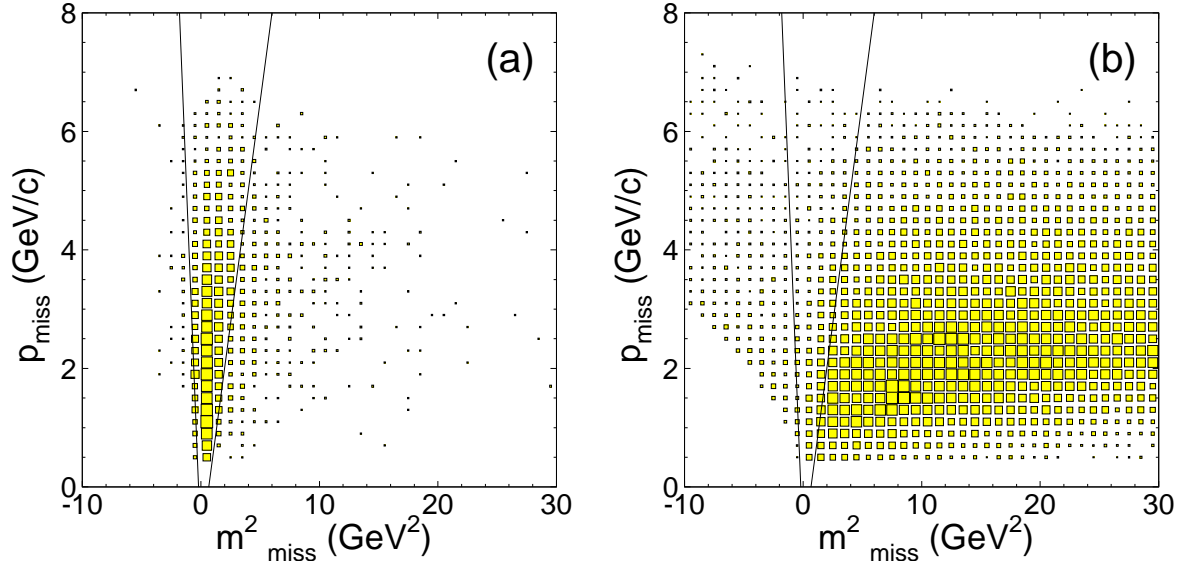


Figure 4.45: A newly introduced selection regarding the missing quantities,  $p_{\text{miss}}$  vs  $m_{\text{miss}}^2$  for (a) signal-MC events, and (b) for generic tau-pair MC. The selected region is the area between the lines.

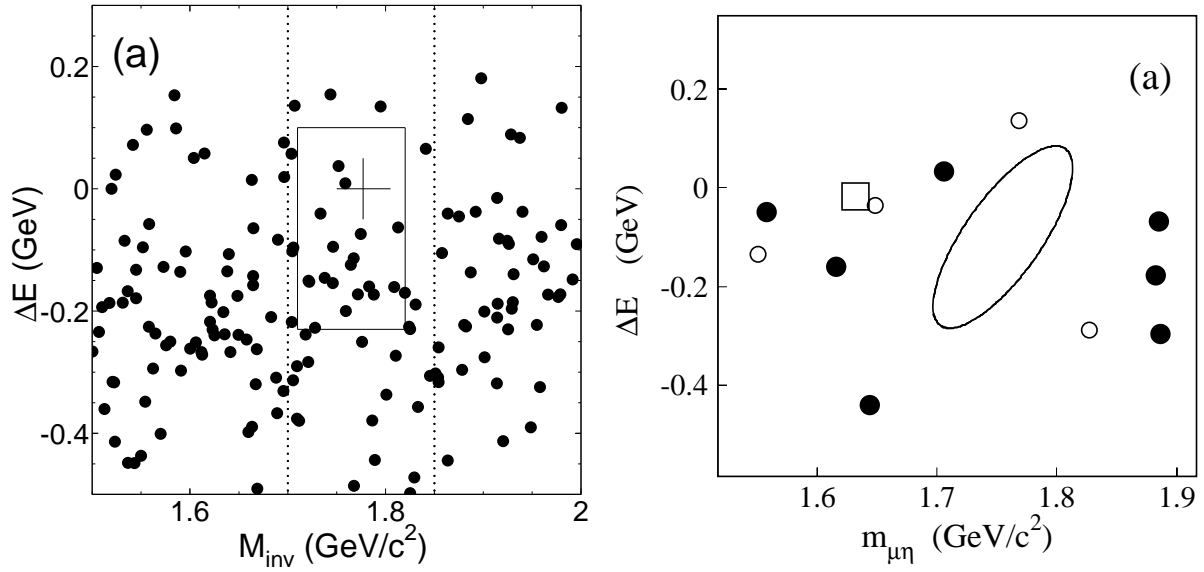


Figure 4.46: Distributions of events after all selection requirements. (a)  $\tau \rightarrow \mu(e)\gamma$  with 86 fb<sup>-1</sup>, (b)  $\tau \rightarrow \mu\gamma$  with 83 fb<sup>-1</sup>.

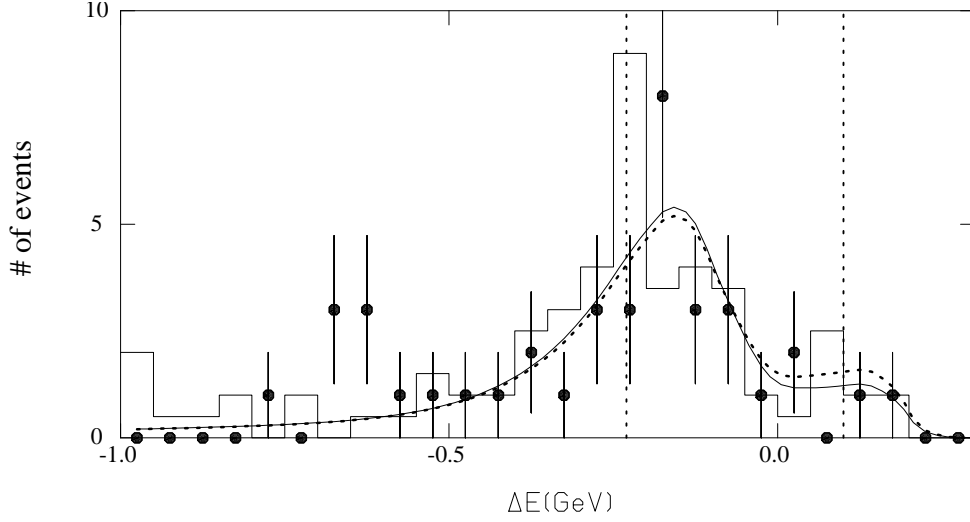


Figure 4.47: Expected background distribution for  $\tau^- \rightarrow \mu^- \gamma$ .

Mode	Limit	Luminosity (fb <sup>-1</sup> )	Refs.	Limit in PDG2000
$\tau^- \rightarrow \mu^- \gamma$	$< 3.1 \times 10^{-7}$	86	[335]	$< 11 \times 10^{-7}$
$\tau^- \rightarrow e^- \gamma$	$< 3.6 \times 10^{-7}$	86		$< 27 \times 10^{-7}$
$\tau^- \rightarrow \mu^- \eta$	$< 3.4 \times 10^{-7}$	83	[336]	$< 96 \times 10^{-7}$
$\tau^- \rightarrow e^- \eta$	$< 6.9 \times 10^{-7}$	83		$< 82 \times 10^{-7}$
$\tau^- \rightarrow e^- e^+ e^-$	$< 3.5 \times 10^{-7}$	87	[337]	$< 29 \times 10^{-7}$
$\tau^- \rightarrow e^- e^+ \mu^-$	$< 1.9 \times 10^{-7}$	87	[337]	$< 17 \times 10^{-7}$
$\tau^- \rightarrow e^- \mu^+ e^-$	$< 1.9 \times 10^{-7}$	87	[337]	$< 15 \times 10^{-7}$
$\tau^- \rightarrow e^- \mu^+ \mu^-$	$< 2.0 \times 10^{-7}$	87	[337]	$< 18 \times 10^{-7}$
$\tau^- \rightarrow \mu^- e^+ \mu^-$	$< 2.0 \times 10^{-7}$	87	[337]	$< 15 \times 10^{-7}$
$\tau^- \rightarrow \mu^- \mu^+ \mu^-$	$< 2.0 \times 10^{-7}$	87	[337]	$< 19 \times 10^{-7}$

Table 4.21: Limits on lepton-flavor-violating decay modes (90% confidence level) obtained so far from Belle data. The last column shows the previous limits from the PDG 2000 compilation.

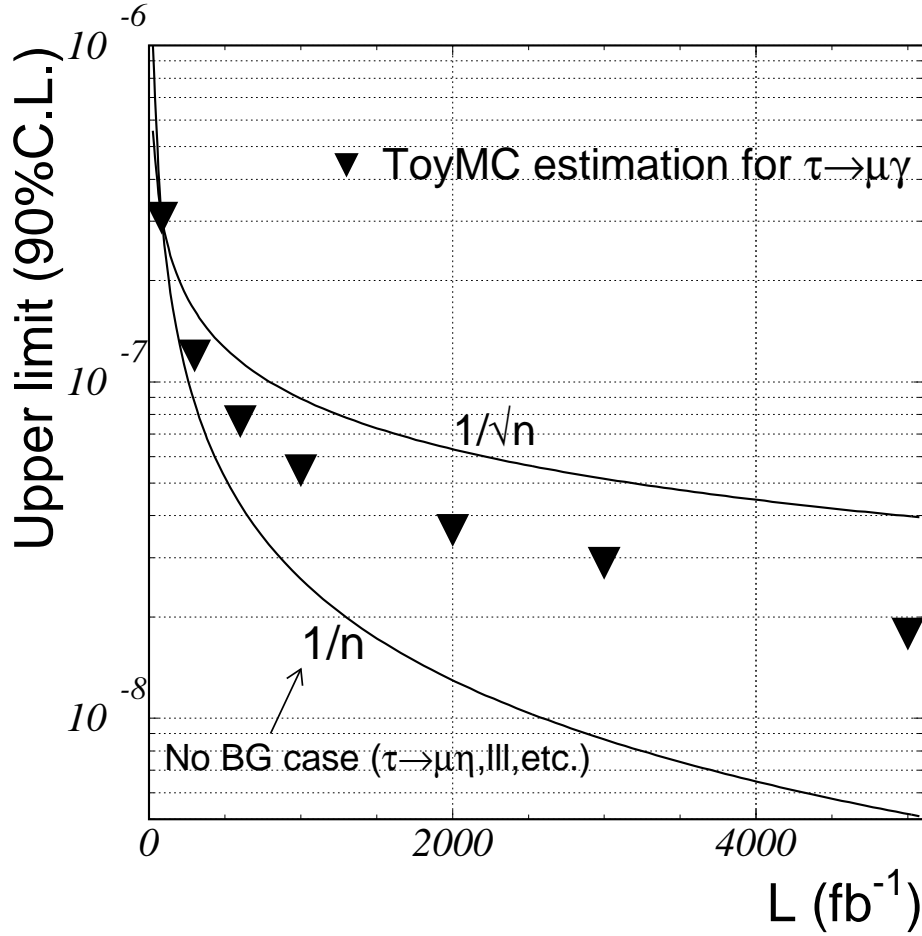


Figure 4.48: Achievable upper limits for LFV decays at SuperKEKB.

SuperKEKB. The lower-solid line are obtained by assuming no candidate events in the signal-region.

The former case corresponds to  $\tau^- \rightarrow \mu^-(e^-)\gamma$ . In the latter case, the upper limit decreases inversely proportional to the total luminosity  $Br \propto 1/N_{\tau^+\tau^-}$ . The  $\tau^- \rightarrow \mu^-(e^-)\eta$ ,  $\mu^-(e^-)\eta'$ ,  $\mu^-(e^-)\pi^0$  and  $\tau^- \rightarrow l^-l^+l^-$  modes would follow a  $\propto 1/N_{\tau^+\tau^-}$  behavior for a short time as up-to a luminosity of a few  $100 \text{ fb}^{-1}$  and then gradually change to a  $\propto 1/\sqrt{N_{\tau^+\tau^-}}$  dependence as candidates begin to appear. Therefore, if the current signal-to-background condition is still maintained, the ultimate goal at  $5,000 \text{ fb}^{-1}$  could be a branching fraction sensitivity of several  $\times 10^{-9}$  for  $\tau^- \rightarrow \mu^-(e^-)\eta$ ,  $\mu^-(e^-)\eta'$ ,  $\mu^-(e^-)\pi^0$  and  $\tau^- \rightarrow l^-l^+l^-$ . The  $\tau^- \rightarrow \mu^-(e^-)\gamma$  mode could be with a branching fraction sensitivity of a few  $\times 10^{-8}$ .

Can we further improve the sensitivity? Experimental sensitivity is in general determined by three key elements: statistics, resolutions, and a signal-to-background ratio; and its experimental reliability depends on how well the systematic uncertainty of these aspects is controlled. We discuss here possible measures for improvements, based on experience from the Belle  $\tau^- \rightarrow \mu^-(e^-)\gamma$  analysis.

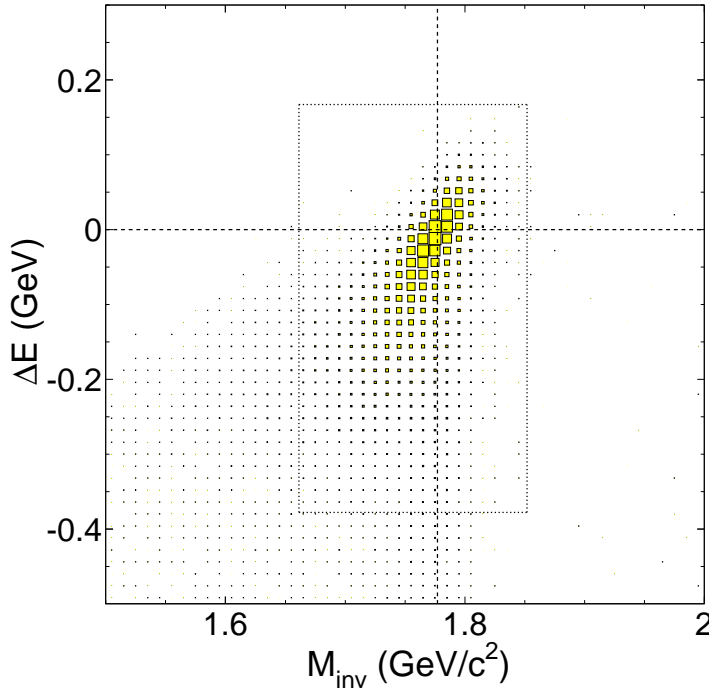


Figure 4.49:  $\Delta E$  vs.  $M_{inv}$  distribution for  $\tau^- \rightarrow \mu^- \gamma$  decay.

**Statistics** Besides accumulating higher luminosity, it is important to the detection efficiency including trigger performance. However, at a SuperKEKB, the selection criteria will become tighter and efficiencies will be lower than the current sizes. There is no way to increase the detection efficiency.

**Resolution** Improvements on the momentum and energy resolution reduce the size of the signal region. The signal-to-background ratio and the resulting sensitivity are enhanced because the background distributes uniformly for a narrow  $\Delta E$  vs.  $M_{inv}$  region. As is seen in Figure 4.49, energy leakage in the calorimeter and initial state radiation yield a long low-energy tail, so that our signal region is defined to be quite large to include a sufficient portion of the signal, say, more than 90%. While the effect of initial state radiation cannot be controlled, the effect of the calorimeter leakage can be improved, for instance, by using a crystal with a longer radiation length and containing less lateral energy leakage in the analysis procedure.

Improvement of particle identification ability is essential for all decay modes. The efficiency of  $e$ -id is already 98% so that further improvement would not be practical. On the other hand, the  $\mu$ -id efficiency is now 90% so that the efficiency increase may reduce background contamination, for example,  $(\mu\gamma)+\text{not}-\mu$  events in the  $\tau^- \rightarrow \mu^- \gamma$  search, and the sensitivity will increase. A KLM counter with finer segmentation in the radial direction might provide a better muon identification.  $K/\pi$  separation is also important in searches for decays into 3 hadrons. The Time-Of-Propagation counter being studied by the Nagoya group could be a very good candidate for improvement here.

**Signal-to-background** A newly introduced requirement for the missing quantities,  $p_{miss} - M_{miss}^2$ , plays an important rule for background as seen in Figure 4.45. It makes it possible to achieve a sensitivity higher than that of the CLEO experiment. We also apply a new selection for  $\tau^- \rightarrow e^- \gamma$ , using the opening angle between the tagged track and missing particle direction; this criterion quite effectively removes the radiative Bhabha background. We have to create this kind of new criteria for future analysis.

## Physics Reach

- Figure 4.50 and 4.51 show a possible exclusion region in the  $m_A - \tan \beta$  parameter space from  $\tau^- \rightarrow \mu^- \eta$ . The region allowed by the current upper bound from the Belle experiment ( $< 3.4 \times 10^{-7}$ ) and the one from non-observation with the  $1000 \text{ fb}^{-1}$  are shown. In Fig. 4.50, the boundary is evaluated by multiplying a factor 8.4 to the formula given by (3.41), *i.e.*

$$\mathcal{B}(\tau^- \rightarrow \mu^- \eta) = 3.2 \times 10^{-6} \times |\delta_{\tau\mu}^L|^2 \times \left( \frac{\tan \beta}{60} \right)^6 \times \left( \frac{M_A}{100 \text{ GeV}} \right)^{-4}, \quad (4.92)$$

where  $|\delta_{\tau\mu}^L| = 1$  is assumed for the evaluation of the boundary. While in Fig.4.51, the same formula is used but the Yukawa coupling and heavy neutrino mass in (3.42) are assumed to be  $(Y^\dagger Y)_{32,33} = 1$  and  $M_N = 10^{14} \text{ GeV}$  instead of the assumption in  $|\delta_{\tau\mu}^L|$ . This is the assumption used by A. Dedes, J. Ellis and M. Raidal in their paper( PRL B549,159(2002)).

Two figures indicate how the branching fraction are sensitive to the value of parameters in the model. All though the allowed region depend on the model parameters, future experiments with 5000-50,000/fb can cover huge parameter space in the model.

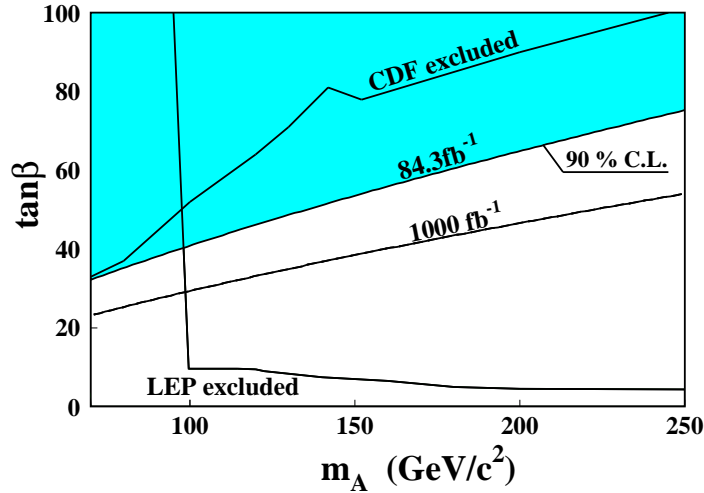


Figure 4.50: Physics reach in  $m_A - \tan \beta$  parameter space at  $1000 \text{ fb}^{-1}$  for the  $\tau^- \rightarrow \mu^- \eta$  decay, together with the regions excluded by direct searches at LEP and in Tevatron experiments [58, 338]. Here,  $m_A$  is the pseudo-scalar Higgs mass in the Higgs mediated model. The boundary is based on the formula Eq.(4.92).



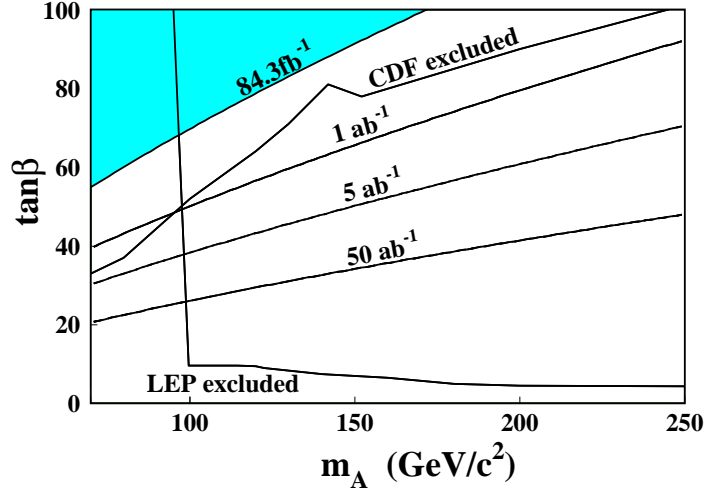


Figure 4.51: Physics reach in  $m_A - \tan\beta$  parameter space at  $1000\text{fb}^{-1}$  for the  $\tau^- \rightarrow \mu^- \eta$  decay, in the Higgs mediated model. the Yukawa coupling and heavy neutrino mass in (3.42) are assumed to be  $(Y^\dagger Y)_{32,33} = 1$  and  $M_N = 10^{14}$  GeV.

- Figure 4.52 and 4.53 show a possible exclusion region in  $m_{SUSY} - \tan\beta$  parameter space for  $\tau^- \rightarrow \mu^- \gamma$ . The excluded regions are from Belle's current upper-bound ( $< 3.1 \times 10^{-7}$ ) and from non-observation at  $1000 \text{ fb}^{-1}$ . In Fig. 4.52, we use the approximate formula for  $Br(\tau^- \rightarrow \mu^- \gamma)$  given as

$$\mathcal{B}(\tau^- \rightarrow \mu^- \gamma) = 3.0 \times 10^{-6} \times \left( \frac{\tan\beta}{60} \right)^2 \times \left( \frac{M_{SUSY}}{1\text{TeV}} \right)^{-4}. \quad (4.93)$$

The formula is obtained from (3.32)–(3.35) by taking that  $|\delta_{\tau\mu}^R| = 1$  and  $|\delta_{\tau\mu}^L| = 1$ .

While in Fig. 4.53, the same formula is used but the Yukawa coupling and heavy neutrino mass in (3.42) are assumed to be  $(Y^\dagger Y)_{32,33} = 1$  and  $M_N = 10^{14}$  GeV.

#### 4.10.4 Summary

Many mechanisms for LFV decays are possible and a wide range of the relevant parameter space is allowed at present. Accordingly, many different models have been proposed as discussed in Section 3.6. Some predict relatively large branching fractions while others give extremely small values. Systematic and extensive investigation of various  $\tau$  decay modes would provide a powerful means to select models, restrict their parameter space, and possibly discover new phenomena beyond the Standard Model. SuperKEKB is the facility best suited to carry out this frontier research.

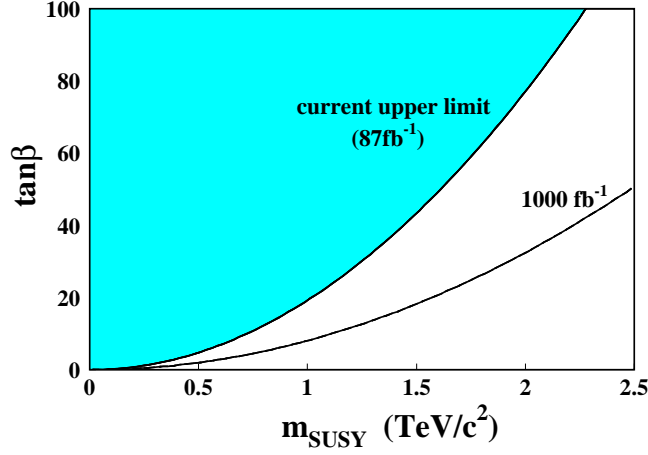


Figure 4.52: Physics reach in  $m_{SUSY} - \tan \beta$  parameter space from Belle's current upper-bound and at  $1000 \text{ fb}^{-1}$  luminosity for  $\tau^- \rightarrow \mu^- \gamma$ . The branching fraction is obtained by taking  $|\delta_{\tau\mu}^R| = |\delta_{\tau\mu}^L| = 1$  in (3.32)–(3.33).

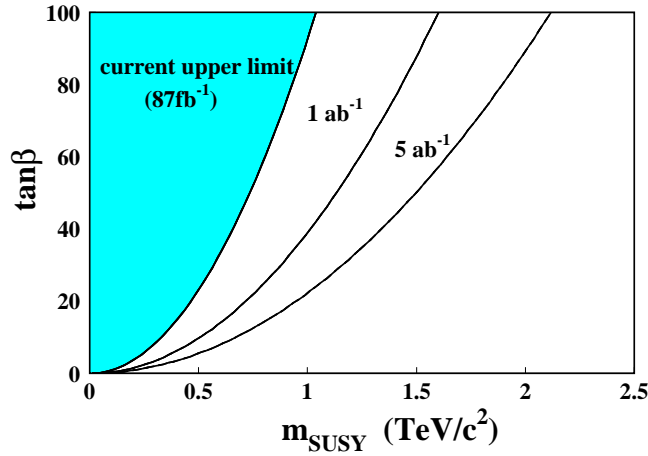


Figure 4.53: Physics reach in  $m_{SUSY} - \tan \beta$  parameter space from Belle's current upper-bound and at  $1000 \text{ fb}^{-1}$  luminosity for  $\tau^- \rightarrow \mu^- \gamma$ . The branching fraction is obtained by taking  $(Y^\dagger Y)_{32,33} = 1$  and  $M_N = 10^{14} \text{ GeV}$  in (3.42).

## 4.11 Diversity of physics at Super-KEKB—other possibilities

### 4.11.1 Charm physics

At a  $B$  factory, a large number of charm mesons are produced from the  $q\bar{q}$  continuum and also from decay products of  $B$  mesons. For example, with  $11.1 \text{ fb}^{-1}$  reconstructs  $10^5 D^0$  ( $\bar{D}^0$ ),  $8 \times 10^3 D^\pm$  and  $6 \times 10^3 D_s^\pm$  mesons in low multiplicity decay modes. We can expect data samples a hundred times larger with a luminosity of  $10^{35} \text{ cm}^{-2}\text{s}^{-1}$ .

Due to the effectiveness of the GIM mechanism, flavor-changing neutral current (FCNC) decays,  $D^0 - \bar{D}^0$  mixing and  $CP$  violation are small in the charm sector. This is in sharp contrast with  $K$  and  $B$  FCNC processes, which are enhanced by the presence of top quarks in loops. In many cases, extensions of the Standard Model (SM) upset this suppression and give contributions sometimes orders of magnitude larger than the SM. As a result, rare charm processes are an excellent place to look for new physics.

The strength of  $D^0 - \bar{D}^0$  mixing is characterized by two parameters  $x = \Delta M/\Gamma$  and  $y = \Delta\Gamma/2\Gamma$ . According to the conventional expectation of the SM,  $x, y \leq 10^{-3}$ . However, in a recent treatment by Falk *et al.*, the possibility of  $y$  (and perhaps  $x$ )  $\sim 10^{-2}$  within the SM is raised [339]. The current experimental limits are at the level of a few times  $10^{-2}$ .

Experimental searches for  $D^0 - \bar{D}^0$  mixing usually involve hadronic decay modes such as  $D^0 \rightarrow K^+\pi^-$ . For such modes, there are contributions from both mixing and doubly Cabibbo suppressed decays (DCSD), which can be distinguished by their time dependences. In the  $CP$  conserving limit, the rate for wrong sign decays is

$$r_{WS}(t) = [R_D + \sqrt{R_D}y't + 1/4(x'^2 + y'^2)t^2]e^{-t},$$

where  $R_D$  is the DCSD rate, and  $y' = y \cos \delta - x \sin \delta$  and  $x' = x \cos \delta + y \sin \delta$  are the mixing parameters  $y$  and  $x$  rotated by  $\delta$ , the relative strong phase between  $D^0 \rightarrow K^+\pi^-$  and  $\bar{D}^0 \rightarrow K^+\pi^-$ . In the absence of interference, mixing has a  $t^2e^{-t}$  dependence which peaks at  $2 D^0$  lifetimes, whereas DCSD follows the usual  $e^{-t}$  dependence. The interference term is proportional to  $te^{-t}$  and dominates the sensitivity to mixing, since  $(x'^2 + y'^2) = (x^2 + y^2) \ll R_D$ . Since the measurement of  $y'$  and  $x'$  requires that these three terms be distinguished from each other, decay-time resolution is crucial: improved vertexing at the Belle upgrade, together with the very large  $D^0$  samples available at  $10^{35} \text{ cm}^{-2}\text{s}^{-1}$ , will lead to an improvement in sensitivity over previous experiments [340] and the existing  $B$ -factories.

Interpretation of  $D^0 \rightarrow K^+\pi^-$  and other hadronic-decay mixing analyses is complicated by the strong phase difference  $\delta$ , which may be large [341,342]: it is important to obtain constraints on this quantity. At a tau-charm facility,  $\delta$  can be determined by using quantum correlations with two fully reconstructed  $D$  decays [343]. At a high luminosity  $B$  factory,  $\delta$  can be determined by measuring related DCSD modes, including modes with  $K_L$  mesons [344].

If  $CP$  is violated in the  $D$  system, then additional  $D^0 - \bar{D}^0$  mixing signals may be seen.  $CP$  violation in the interference of  $D^0$  decays with and without  $D^0 - \bar{D}^0$  mixing is parameterized by the phase  $\phi_D = \arg(q/p)$ : the SM expectation is  $\mathcal{O}(10^{-3} - 10^{-2})$ , whereas in new physics scenarios it can be  $\mathcal{O}(1)$ . This is in contrast with direct  $CP$  violation, which occurs in Cabibbo suppressed decays such as  $D \rightarrow \rho\pi$  at the  $10^{-3}$  level in the SM: new physics scenarios are unlikely to change this expectation.

A time dependent asymmetry

$$\Gamma(D^0(t) - \bar{D}^0(t)) \propto x \sin \phi_D \Gamma t e^{-\Gamma t} \quad (4.94)$$

may be measured by comparing  $D^0 \rightarrow K^+\pi^-$  and  $\bar{D}^0 \rightarrow K^-\pi^+$  decays [345], and would (unlike  $CP$ -conserving mixing) be a clear signal of new physics. The corresponding asymmetry between

$D^0$  and  $\bar{D}^0$  decay rates to  $K^+K^-$ , where the  $D^0$  flavor is tagged by the pion from  $D^{*+} \rightarrow D^0\pi^+$ , allows an especially clean measurement since the final state is identical in both cases, and is only singly Cabibbo suppressed. The analysis of this mode is similar to that used for time dependent  $CP$  violation in  $B$  decays.

There are several classes of rare  $D$  decays where the large data samples available at high luminosity will allow improved measurements. Two body decay modes such as  $D^0 \rightarrow \gamma\gamma, \mu^+\mu^-$  and  $\mu^\pm e^\mp$  are strongly suppressed in the Standard Model: expectations are  $10^{-8}$  for  $D^0 \rightarrow \gamma\gamma$ ,  $10^{-13}$  for  $D^0 \rightarrow \mu^+\mu^-$  and 0 for  $D^0 \rightarrow \mu e$ . In new physics scenarios, the rates can be orders of magnitude larger [346]. For example, in both R-parity violating and leptoquark models, the branching fraction for  $D^0 \rightarrow \mu^+\mu^-$  can be as large as  $3 \times 10^{-6}$  while that for  $D^0 \rightarrow \mu^\pm e^\mp$  could be  $5 \times 10^{-7}$ . The current experimental bounds for  $D^0 \rightarrow \mu^+\mu^-$  and  $D^0 \rightarrow \mu^\pm e^\mp$  are  $3.3 \times 10^{-6}$  and  $8.1 \times 10^{-6}$ , respectively. For 3-body final states such as  $\rho\ell^+\ell^-$ , where SM expectations are similar, orders of magnitude enhancements are expected at low  $\ell^+\ell^-$  invariant masses in some new physics models. In the case of radiative decays such as  $D^0 \rightarrow K^*\gamma, \rho\gamma$ , which are long-distance dominated, measurement at SuperKEKB could constrain long-distance effects in the corresponding modes in the  $B$  sector.

By the time SuperKEKB begins taking data, the tau-charm facility at Cornell will also be operating. Although the design luminosity is relatively low ( $5 \times 10^{32} \text{ cm}^2\text{s}^{-1}$ ), correlated  $D$  meson pairs are produced at threshold from the  $\psi''$  resonance. For measurements where kinematic constraints from production at threshold are essential, such as  $f_D$  and  $D$  absolute branching fractions, the Cornell facility will remain competitive; and a sensitivity to  $D^0 - \bar{D}^0$  mixing at the  $10^{-4}$  level is claimed [343]. SuperKEKB will have the advantage of precision vertexing for measurement of time-dependent decay distributions—especially important if  $CP$  violation is associated with mixing—and very large  $D$  meson samples. Other facilities in the world such as ATLAS/CMS/CDF/D0 cannot do charm physics. LHCb and BTeV may record large charm data samples if they modify their trigger configurations, which are optimized for  $B$  physics. However, these experiments cannot efficiently reconstruct final states with neutrals or  $K_L$  mesons.

#### 4.11.2 Electroweak physics

The standard-electroweak model has two fundamental parameters, which are directly related to measurable quantities: the parameter  $\rho = M_W^2/(M_Z^2 \sin^2 \Theta_W)$ , which is unity in the Standard Model, and the Weinberg angle  $\Theta_W$ , which determines the relative contributions of electromagnetic and weak forces. Both parameters have been measured at the  $e^+e^-$  colliders PETRA and TRISTAN before the high precision measurements at the  $Z$ -pole became available from LEP.

Recently a growing interest is being observed to revisit this type of physics and repeat  $\sin^2 \Theta_W$  and  $\rho$  measurements with high precision. There are two aspects to this renewed interest in a precision determination of the fundamental electro-weak parameters. One is related to a measurement of the NuTeV collaboration at Fermilab [347], who observed values of  $\rho$  and  $\sin^2 \Theta_W$ , which are not in agreement with the Standard Model. The second motivation is that the scale dependence of gauge couplings has been observed for the strong coupling constant  $\alpha_s$  and the electromagnetic coupling  $\alpha$ , however, not yet for the coupling constant of the weak isospin group  $SU(2)$ .

The quantity  $\sin^2 \Theta_W$  is related to the coupling parameters of two gauge groups,  $U(1)$  for the electromagnetic part and  $SU(2)$  for the weak isospin part of the standard electro weak model. Both couplings have a different scale dependence resulting in a scale dependence of a more complicated nature for  $\sin^2 \Theta_W$  [348] as shown in Figure 4.54. To test the scale dependence,

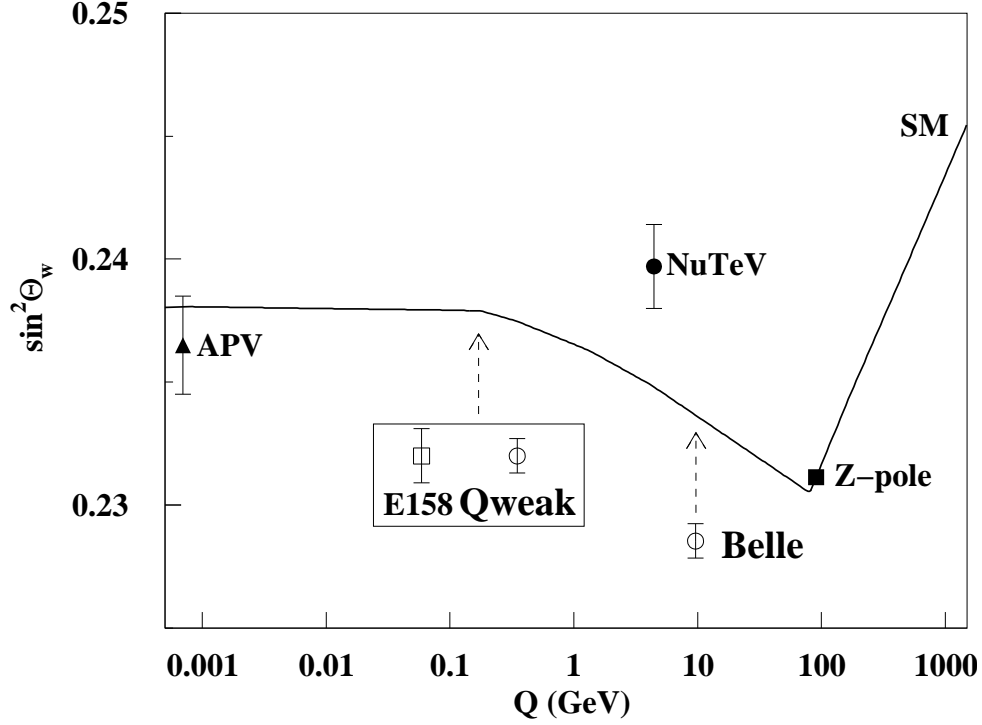


Figure 4.54: Scale dependence of  $\sin^2\Theta_W$ . The full symbols show the current situation, while the open symbols with error bars for the proposed experiments QWEAK, SLAC E-158 and Belle are placed at the correct cm energy with arbitrarily chosen vertical positions. The previous measurements are determinations from atomic parity violation (APV) [349], deep inelastic neutrino scattering (NuTeV), and from Z-pole asymmetries (LEP/SLC).

data below the Z-pole with an accuracy of a few  $10^{-4}$  will serve the purpose.

Two experiments are being proposed to measure  $\sin^2\Theta_W$  at center of mass energies below 1 GeV, QWEAK at the Jefferson Lab in Virginia and one at SLAC, E-158. The QWEAK experiment will deduce  $\sin^2\Theta_W$  from elastic scattering of polarised electrons off protons, while the SLAC experiment measures Møller scattering of polarised electrons.

The NuTeV Detector at Fermilab consists of an 18 m long, 690 ton active steel-scintillator target with drift chambers as tracking devices followed by an iron-toroid spectrometer. High purity  $\nu_\mu$  and  $\bar{\nu}_\mu$  beams resulting from interactions of 800 GeV protons in a BeO target can be directed onto the detector.

In principle  $\sin^2\Theta_W$  can be derived from a measurement of the ratio between neutral current (NC) and charged current interactions (CC) in a nuclear target for just one neutrino species. This approach is, however, subject to large QCD corrections. The corrections can be minimized by a determination of the ratio  $R^-$  with

$$R^- = \frac{\sigma(\nu_\mu N \rightarrow \nu_\mu X) - \sigma(\bar{\nu}_\mu N \rightarrow \bar{\nu}_\mu X)}{\sigma(\nu_\mu N \rightarrow \mu^- X) - \sigma(\bar{\nu}_\mu N \rightarrow \mu^+ X)}. \quad (4.95)$$

NuTeV obtains with this method  $\sin^2\Theta_W = 0.2277 \pm 0.0013 \pm 0.0009$ , a value which is  $3\sigma$  above the value expected for the standard electroweak model. From a two parameter fit to  $\rho$  and  $\sin^2\Theta_W$  they conclude that one of the quantities, but not both of them can be made to agree with the Standard Model value. Their result is sensitive to new physics in the W and Z

sector and suggests a smaller left-handed NC coupling to light quarks than expected. But this result also depends on hadronic corrections and nuclear structure functions, which is the main criticism with respect to an interpretation in terms of deviations from the Standard Model.

In the electro-weak process  $e^+e^- \rightarrow \mu^+\mu^-$  the values for  $\sin^2\Theta_W$  and  $\rho$  are derived from a fit to the angular distribution ( $\Theta^*$ ) of  $\mu$  pairs with respect to the axis of the incoming positron in the  $e^+e^-$  center of mass system [350].

$$\frac{d\sigma}{d\Omega} = \frac{\alpha^2}{4s}(C_1(1 + \cos^2 \Theta^*) + C_2 \cos \Theta^*) \quad (4.96)$$

with the following definitions:

$$C_1 = 1 + 2v_e v_\mu \chi + (v_e^2 + a_e^2)(v_\mu^2 + a_\mu^2)\chi^2, \quad (4.97)$$

$$C_2 = -4a_e a_\mu \chi + 8v_e a_e a_\mu \chi^2, \quad (4.98)$$

$$v_{e,\mu} = -1 + 4 \sin^2 \Theta_W, \quad a_{e,\mu} = -1. \quad (4.99)$$

The quantity  $\chi$  may be written in two different ways, as a function of  $\sin^2\Theta_W$  or as a function of  $\rho$

$$\chi = \frac{1}{16 \sin^2 \Theta_W \cos^2 \Theta_W} \frac{s}{(s - M_Z^2)} \quad (4.100)$$

or

$$\chi = \frac{\rho G_F M_Z^2}{8\pi\alpha\sqrt{2}} \frac{s}{(s - M_Z^2)} \quad (4.101)$$

where  $s$  is the square of the center of mass energy.

For the purpose of estimating statistical errors and significance levels it is sufficient to consider the forward-backward charge asymmetry integrated over all angles  $A_{FB} = (3C_2)/(8C_1) = 1.5\chi$ , while in an actual experiment, one would fit the angular distribution.

A guideline for estimating the significance of a measurement at  $\sqrt{s} = 10$  GeV would be the capability of distinguishing the value of  $\sin^2\Theta_W$  at the  $Z$ -pole from a value it would assume if it were running according to the predictions of the Standard Model. With the  $Z$ -pole value of  $\sin^2\Theta_W = 0.232$  the forward-backward asymmetry assumes a value of  $A_{FB}(\sqrt{s} = 10 \text{ GeV}) = 6.34 \times 10^{-3}$ . For  $\sin^2\Theta_W$  running according to the Standard Model, the asymmetry is  $A_{FB}(\sqrt{s} = 10 \text{ GeV}) = 6.38 \times 10^{-3}$ . The charge asymmetries for a running and a fixed coupling constant thus differ by  $\delta(A_{FB}) = 4 \times 10^{-5}$ .

At 10 GeV center of mass energy, the statistical error on  $\sin^2\Theta_W$  is 30 times larger than the error on the forward-backward asymmetry:  $\sigma(\sin^2 \Theta_W) = 30 \sigma(A_{FB})$ . With a statistical error of  $\sigma(A_{FB}) = \pm 1 \times 10^{-5}$  on the charge asymmetry the corresponding error on  $\sin^2\Theta_W$  is  $\sigma(\sin^2 \Theta_W) = 3 \times 10^{-4}$ .

The number of events required to achieve this accuracy is certainly smaller than  $10^{10}$  events, because when fitting an angular distribution much more efficient use is being made of the experimental data and, thus for an accumulated luminosity of  $1 \text{ ab}^{-1}$  with  $10^9$  events a statistically significant measurement can be made, which is compatible with that of the two dedicated experiments as may be inferred from Figure 4.54.

The  $\mu$ -pairs from the decay of the  $\Upsilon(4S)$  will have a different asymmetry from those of the continuum, as with  $\Upsilon$  as an intermediate state the  $Z$ -boson couples to  $b$ -quarks and the relative weight between  $\gamma$  and  $Z$ -exchange is altered with respect to the continuum. The branching fraction of  $BR(\Upsilon(4S) \rightarrow \mu^+\mu^-) = 3 \times 10^{-5}$  is, however, so small that corrections to the angular dependence will become less important and they can be calculated with sufficient accuracy, as all couplings and weak charges are known. The experiment is thus a continuum experiment.

Radiative corrections are small and can be calculated with sufficient accuracy. Also bin to bin migrations are expected to be small. A potential source of systematic errors are radiative returns of the  $\Upsilon(1S)$  resonance. These events can be removed by a mass cut on the invariant two lepton mass.

The angular distribution of electron pairs is known with high accuracy and therefore electron pairs can be used to check the charge symmetry of the detector and other systematic errors like those, which may be related to the fact that the muon momenta in the forward and backward hemispheres are different due to the asymmetric energies of the colliding electron and positron beams.

Muon identification need not be very restrictive, because there are only very few reactions, which could fake muon pairs, if collinearity of the two tracks is requested. Tau pairs will be rejected by collinearity cuts and invariant mass cuts, the cross section for pion pairs is too small to present a serious background and electron pairs are easily identified by their unique signature in the CsI crystals. As a first guess, a loosely identified muon track would be sufficient for one track, while the second collinear particle need not be identified as a muon, it should be compatible with a muon and incompatible with an electron.

The presence of SU(2) breaking forces could result in a different phenomenological pattern for reactions, where quarks are present or only leptons are involved. Leptoquarks as an example could alter the result of a  $\sin^2\Theta_W$  measurement in neutrino-nucleon scattering without a measurable impact on the charge asymmetry of muon pairs in  $e^+e^-$  annihilation. Therefore one could imagine to face a situation, where purely leptonic experiments do agree with the Standard Model, while reactions involving nucleons don't. In this case one could extend the program at SuperKEKB to a determination of the charge asymmetry of jets. This is a very ambitious measurement, which needs extensive Monte Carlo studies beforehand to investigate the feasibility of such an experiment.

In summary, SuperKEKB will be capable of performing a statistically significant measurement of the Weinberg angle  $\sin^2\Theta_W$  in order to prove the running of the U(1)/SU(2) couplings of the standard electroweak model and set limits on new weak isospin breaking interactions. In order to achieve this, data corresponding to about  $1 \text{ ab}^{-1}$  are needed.

### 4.11.3 Charmonium physics

In the history of physics, many new and important insights have derived from detailed studies of “well understood” systems: precise measurements of the motion of planets in the solar system led to the discovery of an anomalous precession of the perihelion of Mercury's orbit, which provided an important impetus for General relativity; high resolution measurements of atomic spectra were the key to the discovery of fermion spin.

In hadronic physics, the most “well understood” systems are the quarkonium mesons, *i.e.*,  $c\bar{c}$  or  $b\bar{b}$  mesons. Here, because the quarks are massive, they are nearly non-relativistic and ordinary quantum mechanics is applicable. Moreover, lattice calculations are particularly well suited to heavy quark systems. As these improve we can expect reliable first-principle calculations of quarkonium properties with good precision.

In  $B$  meson decays, the  $b \rightarrow c\bar{c}s$  subprocess is CKM-favored and, thus, final states containing charmonium particles are common. A super- $B$  factory would provide *superb* opportunities for precision, high sensitivity measurements of the charmonium system.

Even right at the  $\Upsilon(4S)$  peak, the cross-section for the continuum production of  $c\bar{c}$  quark pairs is higher than that for  $b\bar{b}$  pairs. Thus, a “super- $B$ ” factory is also a “super-charm” factory that will support a variety of interesting studies of charmed particle and charmonium physics.

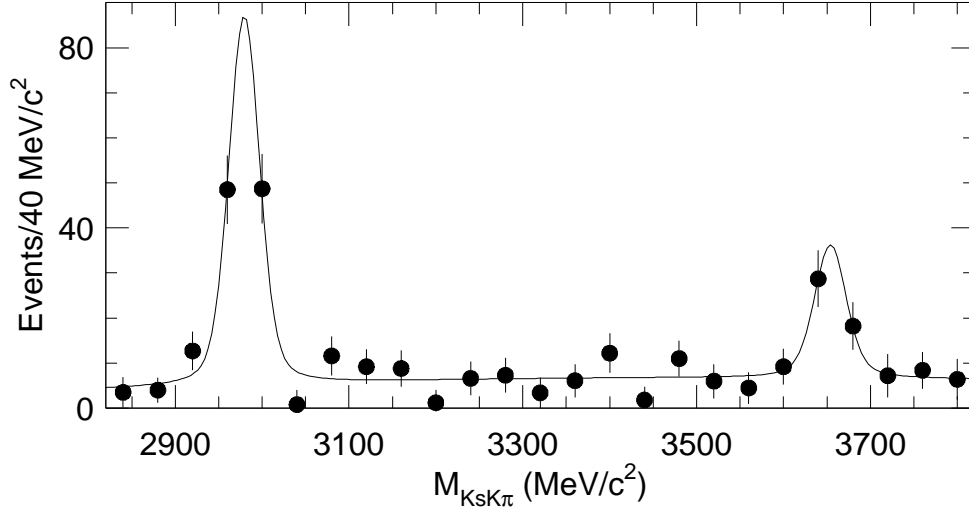


Figure 4.55: The  $K_S K \pi$  invariant mass distribution for  $B^- \rightarrow K^- K_S K \pi$  decays. The large peak near 2980 MeV is the  $\eta_c$ ; the smaller peak near 3650 MeV is attributed to the  $\eta'_c$ .

### New results on charmonium from Belle/KEKB

There are still a few undiscovered charmonium states that are predicted to have masses below the relevant threshold for open charm production and are, thus, expected to be narrow. These include the  $n = 1$  singlet P state, the  $h_c$ , and possibly the  $n = 1$  singlet and triplet spin-2 D states, *i.e.* the  $1^1D_{c2}$  and  $1^3D_{c2}$ . The discovery of these states and the measurements of their properties are important for a number of reasons. First of all, measurements of the masses of these states will pin down unknown parameters of the charmonium model, such as the strength of the fine and hyperfine terms in the inter-quark potential. Second, the properties of these states are highly constrained by theory. Measured variances from theoretical predictions could indicate new and unexpected phenomena. In Belle, modest efforts of studying charmonium production in  $B$  decays and continuum  $e^+e^-$  processes have produced interesting examples of both of these cases.

**Discovery of  $\eta'_c$ :** In 2002, with a  $42 \text{ fb}^{-1}$  data sample, Belle discovered the  $\eta'_c$  via its  $K_S K \pi$  decay mode in exclusive  $B^- \rightarrow K^- K_S K \pi$  decays [351] (see Figure 4.55). This observation was subsequently confirmed by other Belle measurements [352, 353] as well as BaBar [354] and CLEO [355]. Although nobody ever doubted the existence of the  $\eta'_c$ , it had evaded detection for nearly thirty years. A “candidate”  $\eta'_c$ , reported by the Crystal Ball in 1982 [356], indicated an  $\psi' - \eta'_c$  mass splitting ( $92 \pm 7 \text{ MeV}$ ) that is above the range of theoretical expectations ( $43 \sim 75 \text{ MeV}$ ) [357, 358]. The Belle measurement of the  $\eta'_c$  mass indicates that mass splitting ( $32 \pm 10 \text{ MeV}$ ) is, in fact, at the lower end of the theoretically preferred range and has helped pin down the strength of the hyperfine splitting terms in the charmonium potential.

**Discovery of  $X(3872)$ :** In 2003, with a nearly four-times larger data sample, Belle discovered a narrow charmonium-like  $\pi^+\pi^- J/\psi$  state with a mass of 3872 MeV in exclusive  $B \rightarrow K \pi \pi J/\psi$  decays [359] (see Figure 4.56). This state, called the  $X(3872)$ , was originally considered to be the  $^3D_{c2}$ , however a closer examination of its properties indicated problems with this interpretation: the 3872 MeV mass is substantially above model ex-



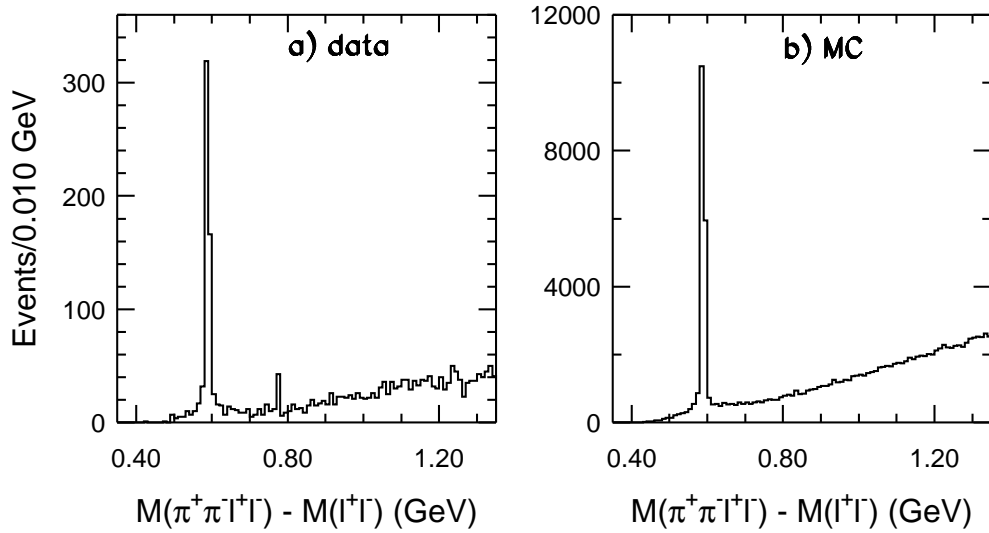


Figure 4.56: Distribution of  $M(\pi^+\pi^-\ell^+\ell^-) - M(\ell^+\ell^-)$  for selected events in the  $\Delta E$ - $M_{bc}$  signal region for (a) Belle data and (b) generic  $\bar{b}$  MC events.

pectations of  $\sim 3815$  MeV; the decay rate to  $\gamma\chi_{c1}$  is too small; the shape of the  $M(\pi\pi)$  distribution is too peaked at high  $\pi\pi$  masses; and the inferred exclusive branching ratio for  $B \rightarrow K(^3D_{c2})$  is too large. As a result, a number of theorists have speculated that this particle may not be a  $c\bar{c}$  charmonium state, but, instead, a new type of four-quark meson [360, 361, 362]. Either the standard charmonium model has to be modified, or the  $X(3872)$  is a first example of an altogether new type of particle. More data will help sort this out.

**Discovery of the large rate for the continuum process  $e^+e^- \rightarrow c\bar{c}c\bar{c}$ :** A major problem for QCD are calculations of the production of physical hadrons. This is because the long-range, low- $q^2$  processes that are involved, can not be dealt with perturbatively. Charmonium is an exception. Since charmonium is formed at relatively short distances, perturbation theory should be applicable. An elegant effective theory called Non-relativistic QCD (NRQCD) has been developed to deal with various aspects of charmonium production [363, 364]. In Belle, studies of  $J/\psi$  production in continuum  $e^+e^-$  annihilation processes were started as a way to test the predictions of NRQCD. This led to the remarkable, and totally unexpected discovery that continuum-produced  $J/\psi$ s are almost always accompanied by another  $c\bar{c}$  system; As can be seen in Figure 4.57, the recoil system appears to be totally saturated by either other charmonium states such as  $\eta_c$ ,  $\chi_{c0}$  or  $\eta'_c$ , or by pairs of charmed particles [352, 353]. There is no evidence in the spectrum for low recoil masses that NRQCD predicts should dominate; the measured cross-sections for exclusive and inclusive  $e^+e^- \rightarrow c\bar{c}c\bar{c}$  processes are an order-of-magnitude larger than NRQCD predictions. Theorists have not been able to modify the model to accommodate the Belle experimental results. NRQCD specialist Bodwin has said that explaining these results “either requires the invention of charmonium production mechanisms within the Standard Model that have not yet been recognized, or physics beyond the Standard Model” [365].

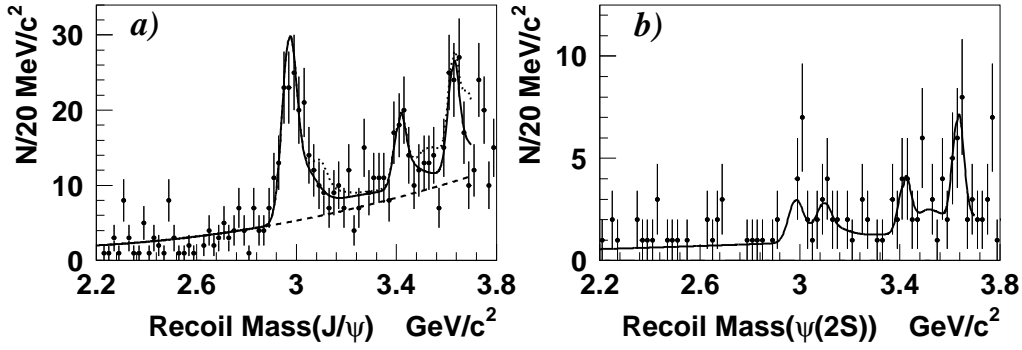


Figure 4.57: Distribution of recoil masses from inclusive (a)  $J/\psi$  and (b)  $\psi(2S)$  mesons produced in continuum  $e^+e^-$  annihilation processes near  $\sqrt{s} = 10.6$  GeV. The three peaks in the  $J/\psi$  recoil mass spectrum are the  $\eta_c$ , the  $\chi_{c0}$  and the  $\eta'_c$ . There is no evidence for events with recoil masses below the  $\eta_c$ ; there the observed level of events is consistent with background.

### Strategies for a Super-B factory

These examples demonstrate that when data samples containing a significantly larger number of  $B$  mesons becomes available, we can reasonably expect that, as a bonus, charmonium studies might produce important new discoveries. As the  $X(3872)$  and continuum  $e^+e^- \rightarrow c\bar{c}c\bar{c}$  discoveries demonstrate, these could provide new insights into hadronic physics.

The  $e^+e^-$  environment is well suited for these investigations. The  $X(3872) \rightarrow \pi^+\pi^-J/\psi$  has an especially distinct signature that makes it observable at hadron colliders [366]. However, understanding the nature of the particle requires sensitivity to other, less distinct modes such as  $\gamma\chi_{c1}$ , and also  $\pi^0\pi^0J/\psi$ ,  $\pi^+\pi^-\pi^0J/\psi$  and  $D^0\bar{D}^0\pi^0$  [367,368]; these are only accessible in the  $e^+e^-$  environment. Likewise, the recoil-mass technique that was used to discover  $e^+e^- \rightarrow c\bar{c}c\bar{c}$  is also only possible in the  $e^+e^-$  environment.

**Search for the  $h_c$ :** The  $h_c$  has proven to be the most elusive of the low-lying charmonium states. A signal for an  $h_c$  candidate in E760 at Fermilab [369] was not reproduced in the subsequent experiment E835 [370]. The  $h_c$  is expected to decay predominantly into final states that include an  $\eta_c$ ; these are experimentally not very distinct. Searches in  $B$  meson decays are also hampered by the fact that the exclusive decay process  $B \rightarrow Kh_c$ , which violates factorization, is expected to be small. Using a technique based on a suggestion by Suzuki [371], Belle is looking for the  $h_c$  via the  $B \rightarrow Kh_c$ :  $h_c \rightarrow \gamma\eta_c$  decay chain. Here the hope is that the large expected decay branching ratio for  $h_c \rightarrow \gamma\eta - c$  ( $\sim 60\%$ ) might compensate for the small, factorization-suppressed rate for  $B \rightarrow Kh_c$ .

So far, no signal is seen, but the branching ratio limit (of  $\sim 1 \times 10^{-4}$ ) is not very restrictive. This is because of the low efficiency for reconstructing the  $\eta_c$  in low-background channels. Future searches at higher luminosity will improve this limit, but only by a factor that goes as the square-root of the increase in luminosity.

The process  $e^+e^- \rightarrow \eta_ch_c$  is allowed by  $C$ -parity conservation. Thus, another approach for  $h_c$  searches would be to use experimentally distinct  $\eta_c$  decay final states, such as  $p\bar{p}$  and  $4K$  modes, to study states recoiling against continuum  $\eta_c$ s in  $e^+e^- \rightarrow c\bar{c}c\bar{c}$  processes. Since the useful  $\eta_c$  modes have branching fractions ( $\sim 10^{-3}$ ) that are  $\sim 10^{-2}$

smaller than those for the  $J/\psi$  this method will require a large data sample. If we assume that the  $\sigma(e^+e^- \rightarrow \eta_c h_c) \simeq \sigma(e^+e^- \rightarrow J/\psi \chi_{c0})$ , about  $10 \text{ ab}^{-1}$  of data would be needed to uncover the  $h_c$  by this method.

**Search for the  $^3D_{c2}$ :** Since it looks more-and-more unlikely that the  $X(3872)$  is the  $^3D_{c2}$ , the discovery of the  $^3D_{c2}$  remains an open experimental question. Since the exclusive decay  $B \rightarrow K^3D_{c2}$  is expected to be strongly suppressed by factorization, here also searches in exclusive decays are not promising. Since the  $\gamma\chi_{c1}$  and  $\pi^+\pi^-J/\psi$  modes are expected to be strong and are experimentally distinct, inclusive searches are feasible. (Belle has reported a strong signal for the inclusive process  $B \rightarrow \chi_{c2}X$  [372], even though no evidence has been seen for it in exclusive two-body decays.)

## Summary

A super- $B$  factory will provide opportunities for unprecedented studies of the properties of charmonium systems and to search for the missing charmonium states. These measurements will provide stringent tests of hadronic models where they are supposed to be most reliable.

Taking history as our guide, we are confident that new and surprising discoveries will be made.

### 4.11.4 Physics potential at $\Upsilon(5S)$

The physics potential of the Super KEKB collider can be extended significantly by running at the energy of the  $\Upsilon(10860)$  resonance, usually denoted as the  $\Upsilon(5S)$ . The advantage is that at this center-of-mass energy it is possible to produce pairs of  $B_s/\bar{B}_s$  mesons, which are kinematically forbidden when running at the  $\Upsilon(4S)$  resonance. This would provide an opportunity to study  $B_s$  decays in a relatively low background environment as compared to that at a hadron collider. In order to operate the KEKB accelerator in the  $\Upsilon(5S)$  mass range, the electron and positron beam energies would need to be increased by 2.7% relative to their energies at the  $\Upsilon(4S)$  resonance; this increase would result in the same Lorentz boost factor of  $\beta\gamma = 0.425$ .

The production ratio of  $B_s$  mesons at the  $\Upsilon(5S)$  resonance to  $B_d$  mesons at the  $\Upsilon(4S)$  resonance is conservatively estimated to be  $1/10$  [373,374,375]. Thus for an integrated luminosity of  $1 \text{ ab}^{-1}$ , which is equivalent to about  $10^9 \Upsilon(4S) \rightarrow B\bar{B}$  decays, a total of  $10^8 B_s$  decays would be recorded. A reconstruction efficiency of 10% would therefore allow one to measure branching fractions down to the level of  $10^{-7}$ .

The  $\Upsilon(5S)$  can decay to  $B\bar{B}$ ,  $B\bar{B}^*$ ,  $B^*\bar{B}^*$ ,  $B_s\bar{B}_s$ ,  $B_s\bar{B}_s^*$  or  $B_s^*\bar{B}_s^*$  final states. The excited  $B$  mesons decay to ground states via  $B^* \rightarrow B\gamma$  and  $B_s^* \rightarrow B_s\gamma$  radiative decays. A detailed Monte Carlo simulation shows that, using the full reconstruction technique,  $B_s$  signals for these states are well-identified using the variables  $E_B^* - E_{beam}$  and  $P_B^*$ , where  $E_B^*$  and  $P_B^*$  are the reconstructed energy and momentum of the  $B_s$  candidate in the  $e^+e^-$  center-of-mass frame, and  $E_{beam}$  is the beam energy in this frame. The number of low energy photons from  $B_s^* \rightarrow B_s\gamma$  decays can also be determined, providing a measurement of the total numbers of  $B_s\bar{B}_s^*$  and  $B_s^*\bar{B}_s^*$  final states produced. Knowing this total yield would allow one to measure absolute (rather than relative) branching fractions, which are very difficult to measure at a hadron machine.

Many  $B_s$  decay modes can be observed and studied at an  $e^+e^-$  Super  $B$  Factory. The strange “partners” of topical  $B_d$  decays can be reconstructed, such as Cabibbo-favored  $B_s \rightarrow D_s^-\pi^+$  and  $B_s \rightarrow D_s^-D_s^+$  decays, color-suppressed  $B_s \rightarrow DK$  and  $B_s \rightarrow J/\Psi\phi$  decays, Cabibbo-suppressed  $B_s \rightarrow D_s^-K^+$  and  $B_s \rightarrow J/\Psi K^0$  decays, the electroweak penguin decay  $B_s \rightarrow \phi\gamma$ , and the  $b$  to  $u$  transition  $B_s \rightarrow K\pi$ . Final states containing  $\pi^0$ 's, which are difficult

Decay	Branching fraction	Efficiency	Super $B$ ( $4 \text{ ab}^{-1}$ )	LHCB (per year)	BTeV (per year)
$D_s^+ \pi^-$	$5 \cdot 10^{-3}$	$2 \cdot 10^{-2}$	40000	80000	120000
$J/\Psi \phi$	$1 \cdot 10^{-3}$	$1.5 \cdot 10^{-2}$	6000	120000	$\sim 90000$
$D_s^{(*)+} D_s^{(*)-}$	$5 \cdot 10^{-2}$	$5 \cdot 10^{-4}$	10000		

Table 4.22: The number of fully-reconstructed  $B_s$  mesons expected from  $\Upsilon(5S)$  decays with  $L_{int} = 4 \text{ ab}^{-1}$ , and by the LHCB and BTeV hadron collider experiments per year of running.

to separate from background in a hadron collider environment, would be well-identified at an  $e^+e^-$  machine. In addition,  $\Upsilon(5S)$  decays are well-suited for studying large multiplicity  $B_s$  decays due to the lower particle momenta, the  $\sim 100\%$  trigger efficiency, and the excellent  $\pi/K$  discrimination. Inclusive  $B_s$  branching fractions can also be measured, in particular the inclusive leptonic branching fraction. Such inclusive measurements are easier to compare with theoretical predictions. Partial-reconstruction techniques can also be used, for example, to measure the exclusive decay  $B_s \rightarrow D_s^+ l^- \nu$ . The numbers of  $B_s$  decays reconstructed in several topical decay modes are listed in Table 4.22, along with the corresponding numbers of events (when available) for the LHCB [23, 376] and BTeV [377] hadron collider experiments. The event yields listed correspond to one year of running; the corresponding luminosity at the Super  $B$  Factory would be  $4 \text{ ab}^{-1}$ .

An important measurement in  $B_s$  physics is that of the lifetime or decay width difference  $\Delta\Gamma$  between the two mass eigenstates of the  $B_s$ - $\bar{B}_s$  system [378, 379, 380]. The ratio of the difference to the mean value is theoretically predicted to be  $\Delta\Gamma/\Gamma \approx 15\%$ , where  $\Delta\Gamma \equiv \Gamma_{light} - \Gamma_{heavy}$  [381, 382, 383, 384, 385, 386, 387, 388]. Such a difference could be measured at an asymmetric  $e^+e^-$  collider. Assuming  $CP$  conservation, the mass eigenstates are  $CP$  eigenstates, and one could compare the lifetime distributions of a  $B_s/\bar{B}_s$  decaying to  $CP$ -even and  $CP$ -odd final states. In practice, one would plot the time difference  $\Delta t = t_{heavy} - t_{light}$  between the decay vertices for  $\Upsilon(5S) \rightarrow B_s \bar{B}_s$  decays, in which one  $B_s$  decays to a  $CP$ -even final state and the other decays to a  $CP$ -odd final state. This distribution is proportional to  $e^{-(\Gamma_{heavy} \Delta t)}$  for  $\Delta t > 0$  and  $e^{+(\Gamma_{light} \Delta t)}$  for  $\Delta t < 0$ ; thus, fitting to this distribution yields both  $\Gamma_{heavy}$  and  $\Gamma_{light}$ . For  $\Upsilon(5S) \rightarrow B_s \bar{B}_s^*$  decays, both  $B_s$  mesons decay to  $CP$ -even or  $CP$ -odd final states (i.e., no mixture of  $CP$ -even and  $CP$ -odd), so the  $\Delta t$  distribution is symmetrical and would yield an independent measurement of  $\Gamma_{heavy}$  or  $\Gamma_{light}$ . Some  $CP$ -definite final states with measurable branching fractions are  $D_s^{(*)+} D_s^{(*)-}$ ,  $K^+ K^-$ , and  $\phi\phi$ . Using the above methods, it is estimated that an accuracy for  $\Delta\Gamma/\Gamma$  of  $\sim 2\%$  would be obtained with an integrated luminosity of  $4 \text{ ab}^{-1}$ .

If these  $\Delta t$  distributions show deviations from pure exponential behavior, that would indicate  $CP$  violation. In particular, if the mass eigenstates were not  $CP$  eigenstates, then the  $\Delta t$  distribution (i.e., for  $\Delta t > 0$  or  $\Delta t < 0$ ) would be the sum of two exponentials. Thus, looking for a deviation from a single exponential allows one to search for  $CP$  violation in the  $B_s$ - $\bar{B}_s$  system. Some theoretical models predict a very large  $B_s$ - $\bar{B}_s$  mass difference  $\Delta m_s$  (i.e.,  $\Delta m_s > 100 \text{ ps}^{-1}$ ); in this case it would be very difficult to observe  $B_s$ - $\bar{B}_s$  mixing at a hadron collider, and consequently,  $CP$  violation due to interference between mixed and unmixed decay amplitudes. Thus, an  $e^+e^-$  machine (and the quantum correlations inherent in production via the  $\Upsilon(5S)$ ) may provide the best opportunity to observe  $CP$ -violation in this system.

The time-integrated  $CP$  asymmetry  $A \equiv (N_{\bar{B}_s \rightarrow f} - N_{B_s \rightarrow \bar{f}})/(N_{\bar{B}_s \rightarrow f} + N_{B_s \rightarrow \bar{f}})$  would allow one to measure *direct*  $CP$  violation in  $B_s$  decays. A good candidate for this measurement is

$B_s \rightarrow K^- \pi^+$ : assuming a branching fraction of  $10^{-5}$  and an asymmetry of  $-6\%$  [389], one would observe a  $3\sigma$  effect with  $4 \text{ ab}^{-1}$  of data. The penguin diagram causing the direct  $CP$ -violation is very sensitive to nonstandard contributions (some of which can give asymmetries much larger than  $6\%$ ), and measuring a direct  $CP$  asymmetry could probe physics beyond the Standard Model.

Observable	Belle 2003 (0.14ab <sup>-1</sup> )	SuperKEKB (5 ab <sup>-1</sup> ) (50 ab <sup>-1</sup> )		LHCb (0.002ab <sup>-1</sup> )
$\Delta\mathcal{S}_{\phi K_S^0}$	0.51	0.079	0.031	0.2 [390]
$\Delta\mathcal{S}_{K^+K^-K_S^0}$	+0.32 -0.26	0.056	0.026	
$\Delta\mathcal{S}_{\eta'K_S^0}$	0.27	0.049	0.024	×
$\Delta\mathcal{S}_{K_S^0K_S^0K_S^0}$	NA	0.14	0.04	×
$\Delta\mathcal{S}_{\pi^0K_S^0}$	NA	0.10	0.03	×
$\sin 2\chi (B_s \rightarrow J/\psi\phi)$	×	×	×	0.058
$\mathcal{S}_{K^{*0}\gamma}$	NA	0.14	0.04	×
$\mathcal{B}(B \rightarrow X_s\gamma)$	26% (5.8 fb <sup>-1</sup> )	5%	5%	×
$A_{CP}(B \rightarrow X_s\gamma)$	0.064	0.011	5×10 <sup>-3</sup>	×
$C_9$ from $\overline{A}_{\text{FB}}(B \rightarrow K^*\ell^+\ell^-)$	NA	32%	10%	
$C_{10}$ from $\overline{A}_{\text{FB}}(B \rightarrow K^*\ell^+\ell^-)$	NA	44%	14%	
$\mathcal{B}(B_s \rightarrow \mu^+\mu^-)$	×	×	×	4σ (3 years) [392]
$\mathcal{B}(B^+ \rightarrow K^+\nu\nu)$	NA		5.1σ	×
$\mathcal{B}(B^+ \rightarrow D\tau\nu)$	NA	12.7σ	40.3σ	×
$\mathcal{B}(B^0 \rightarrow D\tau\nu)$	NA	3.5σ	11.0σ	×
$\sin 2\phi_1$	0.06	0.019	0.014	0.022
$\phi_2$ ( $\pi\pi$ isospin)	NA	3.9°	1.2°	×
$\phi_2$ ( $\rho\pi$ )	NA	2.9°	0.9°	×
$\phi_3$ ( $DK^{(*)}$ )	20°	4°	1.2°	8°
$\phi_3$ ( $B_s \rightarrow KK$ )	×	×	×	5°
$\phi_3$ ( $B_s \rightarrow D_sK$ )	×	×	×	14°
$ V_{ub} $ (inclusive)	16%	5.8%	4.4%	×
$\mathcal{B}(\tau \rightarrow \mu\gamma)$	< 3.1 × 10 <sup>-7</sup>	< 1.8 × 10 <sup>-8</sup>		
$\mathcal{B}(\tau \rightarrow \mu(e)\eta)$	< 3.4(6.9) × 10 <sup>-7</sup>	< 5 × 10 <sup>-9</sup>		
$\mathcal{B}(\tau \rightarrow \ell\ell\ell)$	< 1.4-3.1 × 10 <sup>-7</sup>	< 5 × 10 <sup>-9</sup>		

Table 4.23: Summary of sensitivity studies. Values for LHCb are taken from [391] unless otherwise stated.

## 4.12 Summary

Table 4.23 summarizes the sensitivities for some of key observables described in the previous sections. As a comparison, we also list expected sensitivities at LHCb whenever available. It is seen that most of key observables are accessible only at the  $e^+e^-$   $B$  factories. The advantage of the clean environment at SuperKEKB is thus clear. Note that the  $B$  physics program at hadron colliders has its own unique measurements that are not accessible at  $e^+e^-$   $B$  factories. Examples include rare  $B_s$  decays such as  $B_s \rightarrow \mu^+\mu^-$ . Thus  $B$  physics programs at hadron colliders also help scrutinize the rich phenomenologies of  $B$  meson decays.

## Chapter 5

# Study of New Physics Scenarios at SuperKEKB

### 5.1 New physics case study

As discussed in the previous sections, there are a number of processes in which one may find observable effects of physics beyond the Standard Model (BSM). In particular, processes induced by loop diagrams can be sensitive to new particles at the TeV energy scale, as the Standard Model contribution is relatively suppressed. Such processes include  $\mathcal{S}_{\phi K_S^0}$ ,  $A_{CP}^{\text{dir}}(b \rightarrow s\gamma)$ ,  $A_{CP}^{\text{mix}}(b \rightarrow s\gamma)$ ,  $Br(b \rightarrow s\ell^+\ell^-)$ ,  $A_{FB}(b \rightarrow s\ell^+\ell^-)$ , and  $Br(\tau \rightarrow \mu\gamma)$ . In this section we consider some specific new physics models in the context of supersymmetry (SUSY) and investigate how their effects could be seen in these processes.

The hierarchy problem of the Higgs mass suggests that the physics beyond the Standard Model most likely exists at the TeV energy scale, and hence the LHC has a good chance of discovering some new particles. However, the flavor structure of the BSM will still remain to be investigated, as hadron collider experiments are largely insensitive to flavor-violating processes. In SUSY models, for example, flavor physics is the key to investigating the mechanism of SUSY breaking, which is expected to lie at a higher energy scale.

As discussed in Section 3.3, even in the minimal supersymmetric extension of the SM (MSSM), most of the parameter space is already excluded by the present FCNC constraints, and hence one has to consider some structure in the soft SUSY breaking terms such that the FCNC processes are naturally suppressed. In this study we consider the following three models according to refs. [173, 174].

- *Minimal supergravity model (mSUGRA)*

In this model one assumes that supersymmetry is broken in some invisible (hidden) sector and its effect is mediated to the visible (observable) world only through the gravitational interaction. Since gravity is insensitive to flavor, the induced soft breaking terms are flavor blind at the scale where they are generated. Namely, all sfermions have degenerate mass  $m_0^2$ ; trilinear couplings of scalars are proportional to Yukawa couplings; all gauginos are degenerate with mass  $M_{1/2}$ . Even though the soft breaking terms are flavor blind, they could induce flavor violation as they evolve from the SUSY breaking scale (assumed here to be  $M_X \simeq 2 \times 10^{16}$  GeV for simplicity) to the electroweak scale by the renormalization group equations, since the Yukawa couplings are flavor dependent. In general, FCNC effects are small for this model.

- *SU(5) SUSY GUT with right-handed neutrinos*

Grand Unification (GUT) is one of the motivations to consider supersymmetric models, as they naturally lead to the unification of the gauge couplings. In GUT models quarks and leptons belong to the same multiplet at the GUT scale. Therefore the flavor mixings of the quark and lepton sectors are related to each other. In particular, large neutrino mixing can induce large squark mixing for right-handed down-type squarks [244, 393, 170, 171, 172, 175]. In this class of models we consider two cases where the masses of the right-handed neutrinos are *degenerate* or *non-degenerate*. Because of the large neutrino mixing, the bulk of the parameter space is excluded in the degenerate case due to the  $\mathcal{B}(\mu \rightarrow e\gamma)$  constraint, and as a result the effect on other FCNC processes is limited. On the other hand, for the non-degenerate case one can expect larger FCNC effects.

- *U(2) flavor symmetry*

The family structure of the quarks and leptons could be explained by some flavor symmetry among generations. Although  $U(3)$  is a natural candidate for such a symmetry, it is badly broken by the top quark Yukawa coupling. Therefore, here we consider a  $U(2)$  flavor symmetry among the first two generations in the context of SUSY. We assume some breaking structure of the  $U(2)$  symmetry for the Yukawa couplings, squark mass matrices, and the scalar trilinear couplings.

These models still contain many parameters. We randomly choose a number of points from the multi-dimensional parameter space, while fixing the gluino mass at  $600 \text{ GeV}/c^2$  and  $\tan\beta = 30$ . Among these points, those that are already excluded from existing mass bounds and FCNC constraints, such as  $\epsilon_K$ ,  $b \rightarrow s\gamma$  branching fraction, and  $\mu \rightarrow e\gamma$  branching ratio, are eliminated. The results for several quantities are then shown in the following scatter plots.

First of all, the expectations from these models for two interesting FCNC processes  $\mathcal{S}_{\phi K_S^0}$  and  $\mathcal{S}_{b \rightarrow s\gamma}$  are shown in Fig. 5.1, together with the expected sensitivity at SuperKEKB. Each dot in the plots shows a randomly chosen parameter point of the model. One can observe a significant deviation from the SM for the  $SU(5)$  SUSY GUT with a right-handed neutrino (non-degenerate case) while the mSUGRA model gives comparatively small deviations from the SM for these FCNC processes. We emphasize that these different models could have almost an identical mass spectrum of SUSY particles as shown on the bottom panels in the figure. This means that the flavor structure of BSM models is barely probed by measurements at high energy collider experiments.

Correlations for other interesting FCNC processes are shown in Figs. 5.2–5.5 for the above four SUSY models. Also shown in the figures are expected errors at  $50 \text{ ab}^{-1}$ . With these additional correlations, we can further narrow down possible scenarios; for instance, large direct  $CP$  violation in  $b \rightarrow s\gamma$  would imply that the  $U(2)$  model was favored. On the other hand, observation of  $\tau \rightarrow \mu\gamma$  decays would strongly suggest the non-degenerate  $SU(5)$  model. Even if the deviation from the mSUGRA in  $\mathcal{S}_{\phi K_S^0}$  and  $\mathcal{S}_{b \rightarrow s\gamma}$  turns out to be too small to distinguish among different scenarios, there are many other possibilities that can be pursued at SuperKEKB.

## 5.2 Model independent approaches

At SuperKEKB, there are a number of processes from which we can measure the fundamental parameters of the Standard Model (SM), *i.e.* quark mixing angles and phases. In this section we discuss how these measurements at SuperKEKB may be used to gain insight into the flavor structure of new physics without assuming some particular model.



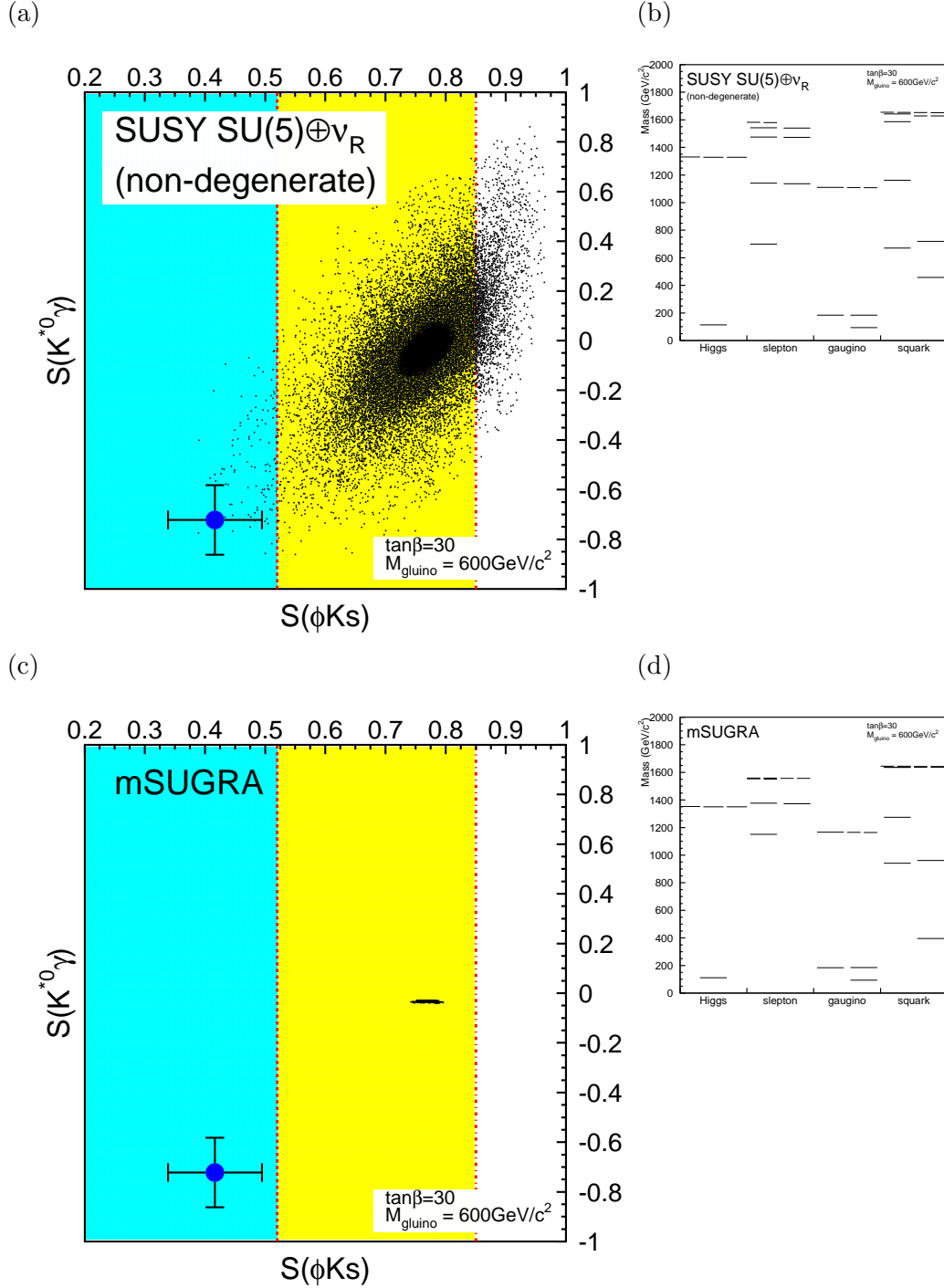


Figure 5.1:  $\mathcal{S}_{K^{*0}\gamma}$  and  $\mathcal{S}_{\phi K_S^0}$  for various parameters in (a) SUSY  $SU(5)$  with right-handed neutrinos (the non-degenerate case), and (c) mSUGRA. Circles with error bars indicate an expected result from a certain parameter set in the  $SU(5)$  SUSY GUT, where the errors are obtained at  $5 \text{ ab}^{-1}$ . A present experimental bound at  $2\sigma$  ( $3\sigma$ ) level is also shown by the dashed (dot-dashed) vertical line. Associated small figures show examples of mass spectra of SUSY particles for (b) the SUSY  $SU(5)$  and (d) mSUGRA.

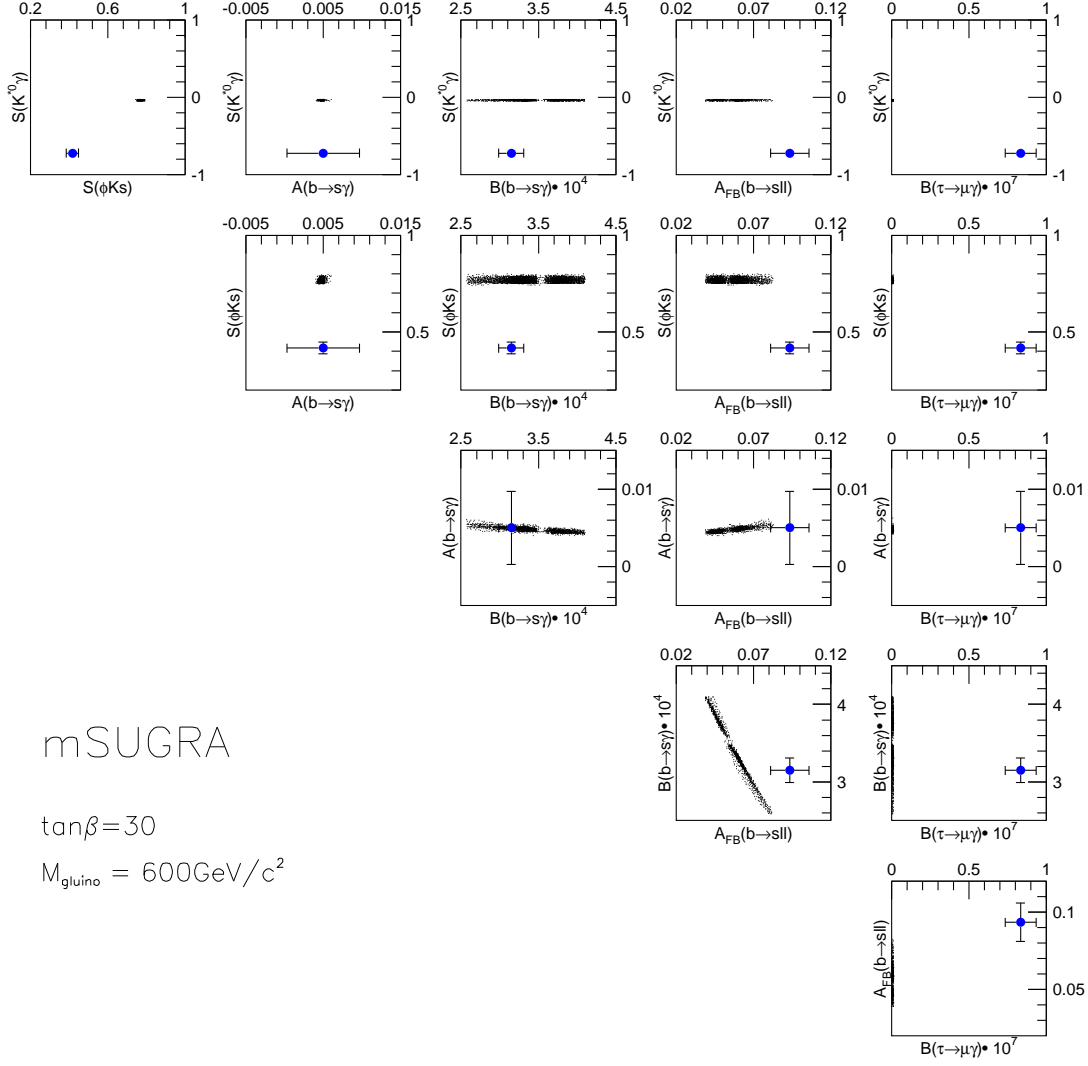


Figure 5.2: Correlations between key observables in the case of mSUGRA. Dots show the possible range in mSUGRA. The circles correspond to a certain parameter set of non-degenerate SUSY SU(5) GUT model with  $\nu_R$ . Expected errors with an integrated luminosity of  $50 \text{ ab}^{-1}$  are shown by bars associated with the circles.

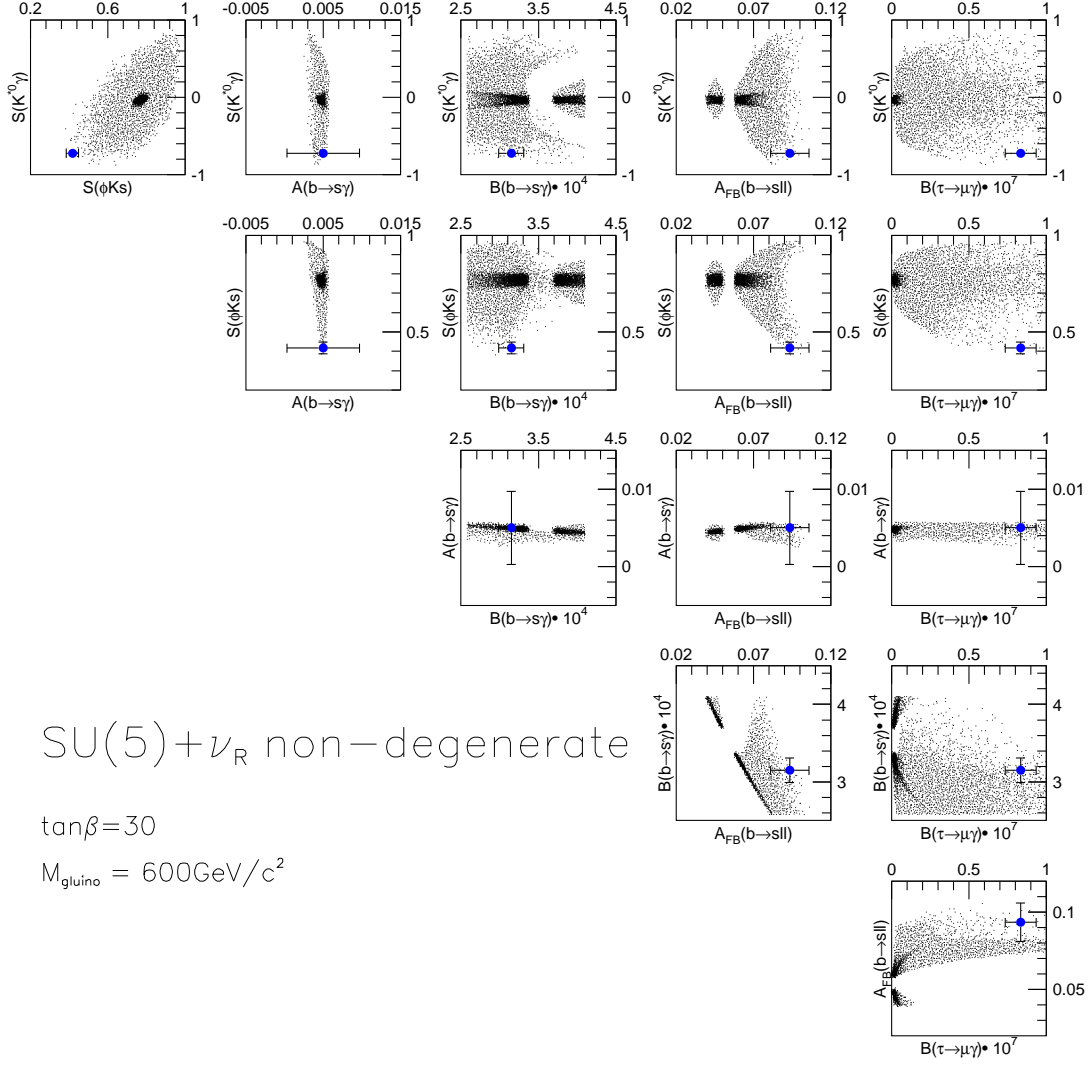


Figure 5.3: Correlations between key observables in the case of the non-degenerate SUSY  $SU(5)$  GUT model with  $\nu_R$ . Dots show the possible range in the model. The circles correspond to a certain parameter set in this model. Expected errors with an integrated luminosity of  $50 \text{ ab}^{-1}$  are shown by bars associated with the circles.

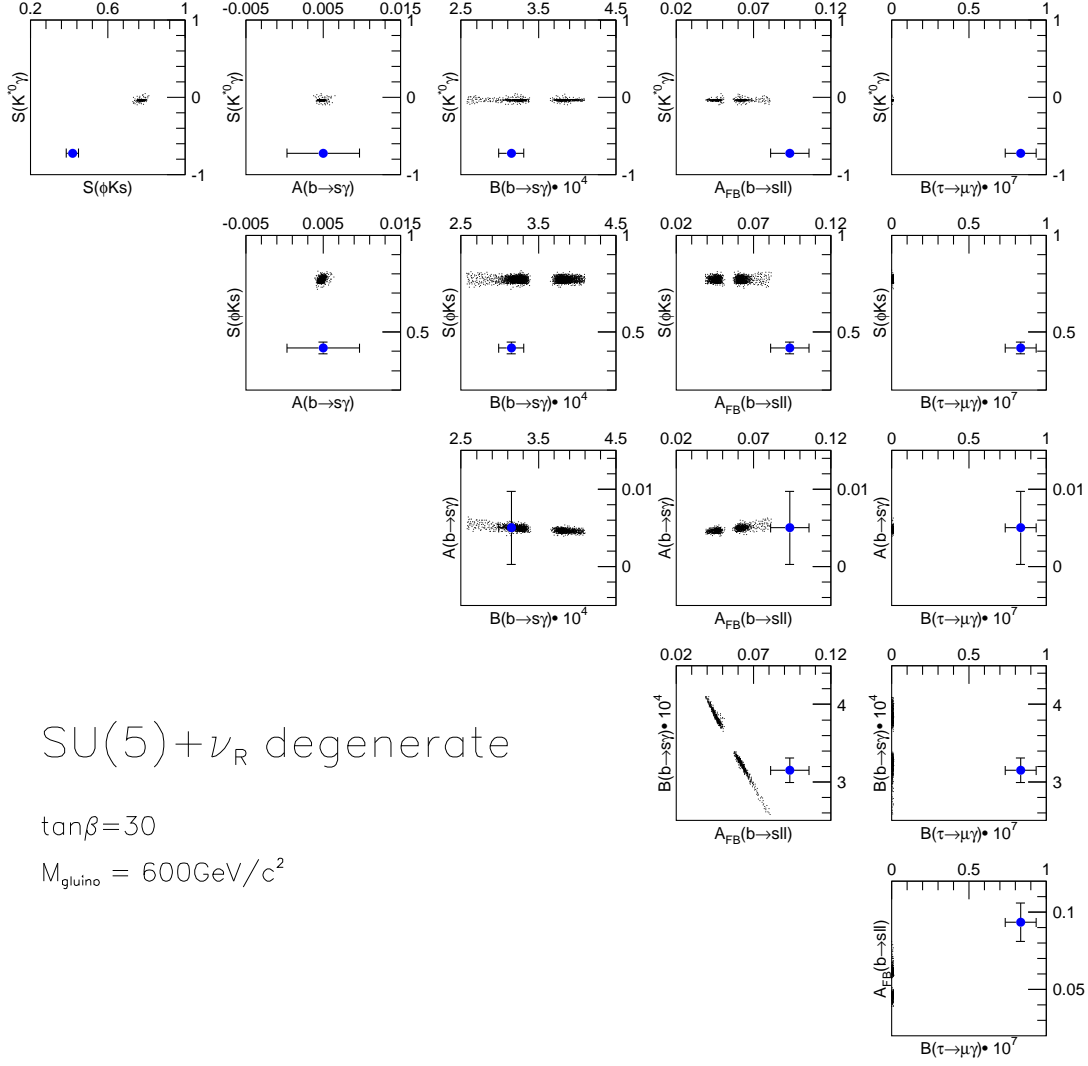


Figure 5.4: Correlations between key observables in the case of the degenerate SUSY SU(5) GUT model. Dots show the possible range in the model. The circles correspond to a certain parameter set of the non-degenerate SUSY SU(5) GUT model with  $\nu_R$ . Expected errors with an integrated luminosity of  $50 \text{ ab}^{-1}$  are shown by bars associated with the circles.

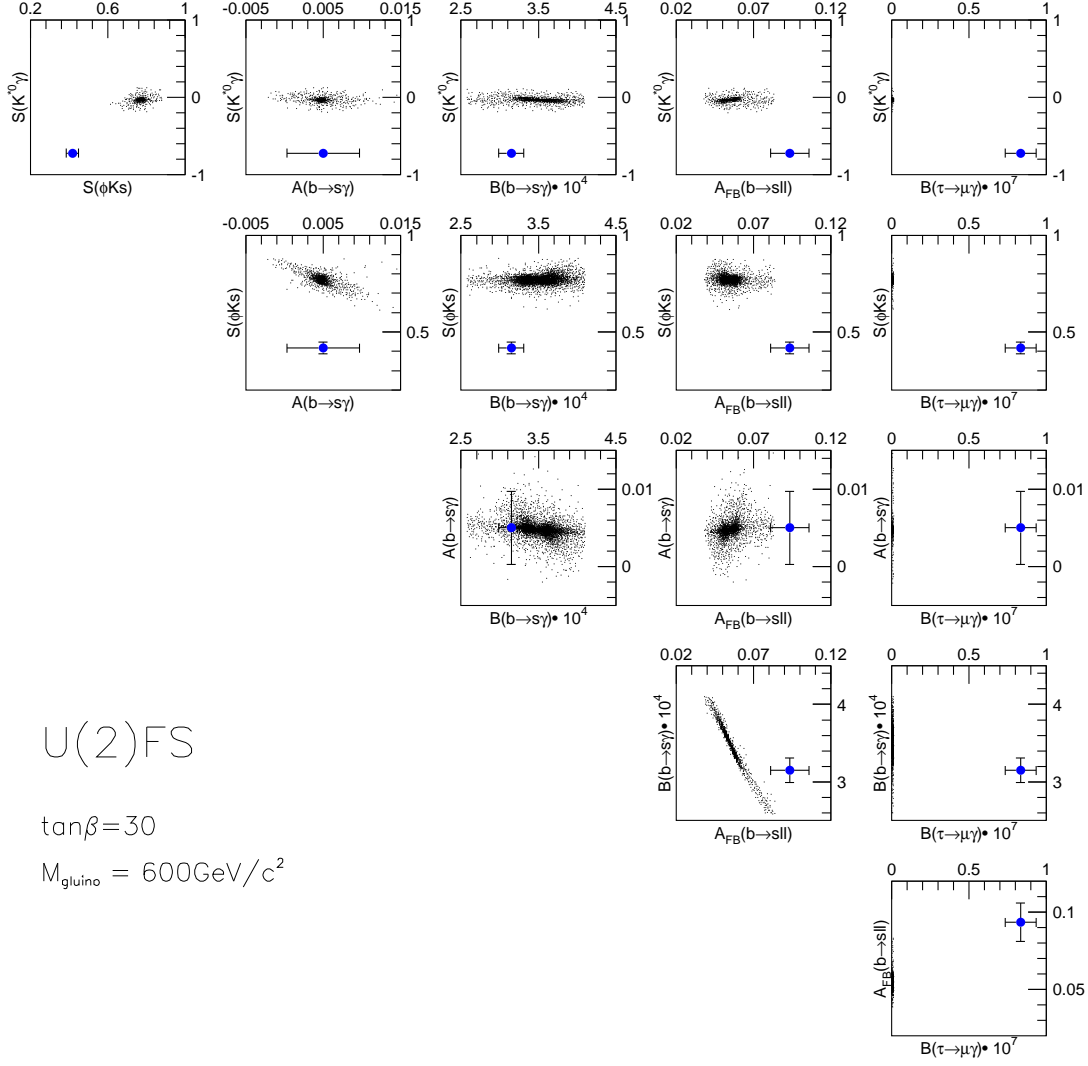


Figure 5.5: Correlations between key observables in the case of the  $U(2)$  flavor symmetry model. Dots show the possible range in the model. The circles correspond to a certain parameter set of the non-degenerate SUSY  $SU(5)$  GUT model with  $\nu_R$ . Expected errors with an integrated luminosity of  $50 \text{ ab}^{-1}$  are shown by bars associated with the circles.

Fitting the CKM parameters using the available data is a common practice. One draws the constraints obtained from several measurements in the parameter space of  $(\bar{\rho}, \bar{\eta})$ , which are the least known parameters in the usual parametrization of the CKM matrix. If one found an inconsistency among the different input quantities, it would indicate the existence of a new physics effect for some quantities. We investigate how SuperKEKB can contribute to narrowing down the allowed region from each measurement.

Once deviations from the SM are established, the next question is which quantities are affected by the new physics and how. To consider such questions, it is natural to assume that tree-level processes are not affected much by the new physics. If the Standard Model is a low energy effective theory of some more fundamental theory, the new physics effects will manifest themselves as non-renormalizable higher dimensional operators. In tree-level processes such operators are relatively suppressed, while in loop-induced FCNC processes the higher dimensional operators could compete with the loop effects of the Standard Model.

Therefore, we may proceed in three steps. Firstly, we obtain a constraint on  $(\bar{\rho}, \bar{\eta})$  using only tree-level processes, *i.e.*  $|V_{ub}|$  from the semileptonic decay  $b \rightarrow u\ell\bar{\nu}$  and  $\phi_3$  from the  $DK$  asymmetry. The result can be considered as the SM value of  $(\bar{\rho}, \bar{\eta})$  even in the presence of the new physics. Secondly, the allowed region for  $(\bar{\rho}, \bar{\eta})$  is compared with the determination through  $B^0 - \bar{B}^0$  mixing, *i.e.*  $\Delta m_d$  and  $\sin 2\phi_1$  from  $B \rightarrow J/\psi K_S^0$ . If we assume that the decay amplitude for  $B \rightarrow J/\psi K_S^0$  is dominated by the tree-level contribution, this region of  $(\bar{\rho}, \bar{\eta})$  contains loop effects from  $\Delta B = 2$  processes. Finally, we consider a parametrization of new physics contributions to  $B^0 - \bar{B}^0$  mixing with the amplitude  $M_{12}$  expressed as  $M_{12} = M_{12}^{\text{SM}} + M_{12}^{\text{new}}$ , and obtain a constraint on  $M_{12}^{\text{new}}$  [394, 395, 396]. Such a study of the CKM parameter fit is described in the next section.

The separation of the Standard Model and new physics contributions can also be formulated for radiative and semileptonic  $B$  decays:  $b \rightarrow s\gamma$  and  $b \rightarrow s\ell^+\ell^-$ . As discussed in Section 3.4, in the language of the effective Hamiltonian the new physics contribution can be expressed in terms of Wilson coefficients.

A similar strategy can be applied to hadronic decay amplitudes. For instance, the difference between the values of  $\sin 2\phi_1$  measured by  $J/\psi K_S^0$  and  $\phi K_S^0$  implies some new physics effect in the  $b \rightarrow s\bar{s}s$  penguin process. One can parametrize the  $b \rightarrow s\bar{s}s$  amplitude in terms of SM and new physics amplitudes. In this case, however, the calculation of the decay amplitudes from the fundamental theory is much more difficult and the utility of the parametrization is limited.

### 5.3 The CKM fit

We perform a global fit to the CKM parameters  $(\bar{\rho}, \bar{\eta})$  using the CKMfitter package [24]<sup>1</sup>. If no new physics effect exists, all the measurements should agree with each other in the  $(\bar{\rho}, \bar{\eta})$  plane and can be combined to obtain the constraint on them. On the other hand, the effect of new physics may cause discrepancies among these measurements.

The strategy is to look for the new physics effects from only one source at a time, in order to quantitatively identify the new physics contribution. Assuming that the tree-level processes are insensitive to new physics effects, we determine the SM value of  $(\bar{\rho}, \bar{\eta})$  using  $|V_{ub}|$  from  $B \rightarrow X_u \ell \nu$  decays and  $\phi_3$  from  $B^\pm \rightarrow D^0 [\rightarrow K_S^0 \pi^+ \pi^-] K^\pm$ <sup>2</sup>. We then examine the  $b \rightarrow d$  box diagram, *i.e.*

<sup>1</sup>We use the CKMfitter package with the *R*-fit option. The parameter values are the default values used in the package if not mentioned explicitly.

<sup>2</sup>There is a possible effect of new physics on the Dalitz distributions through  $D^0 - \bar{D}^0$  mixing or  $CP$  violation in  $D^0$ . However, we can check and measure the effect from the data using soft-pion tagged  $D^0$  decays ( $D^{*+} \rightarrow D^0 \pi_s^+$ ) [397], and verify whether its effect to the  $\phi_3$  measurement is small enough.

parameters	central values	errors		
		0.5 ab <sup>-1</sup>	5 ab <sup>-1</sup>	50 ab <sup>-1</sup>
$\sin 2\phi_1$	0.753	$\pm 4.4\%$	$\pm 2.5\%$	$\pm 1.9\%$
$\phi_3$ (Dalitz)	65°	$\pm 23\%$	$\pm 7.2\%$	$\pm 2.3\%$
$ V_{ub} $	$3.79 \times 10^{-3}$	$\pm 6.9\% \pm 8\%$	$\pm 3.7\% \pm 4.5\%$	$\pm 3.2\% \pm 3\%$
$\Delta m_d$	0.496 ps <sup>-1</sup>	$\pm 0.8\%$	$\pm 0.5\%$	$\pm 0.4\%$
$f_{B_d} \sqrt{B_{B_d}}$	0.230 GeV	$\pm 0.011 \pm 0.026$	$\pm 0.011 \pm 0.026$	$\pm 0.005 \pm 0.015$
$\phi_2$	91°	$\pm 9^\circ$	$\pm 2.9^\circ$	$\pm 0.9^\circ$

Table 5.1: Summary of inputs to in the CKM-fit. If two errors are given, the second error is treated as flat in the fit [24]. Otherwise, errors are taken to be Gaussian.  $|V_{cb}|$  is fixed at  $4.04 \times 10^{-3}$  in the fit. Central values correspond to  $\bar{\rho} = 0.176$  and  $\bar{\eta} = 0.376$ .

$B^0 - \bar{B}^0$  oscillations, for which the available measurements are  $\sin 2\phi_1$  from  $B^0 \rightarrow c\bar{c}K^0$  and  $\Delta m_d$ .

The input parameters used in the fit are listed in Table 5.1, where the errors are based on the sensitivity studies in the previous sections. The errors for  $\Delta m_d$  are extrapolated from the current measurements with an irreducible systematic error of 0.4% [398]. The current value of  $f_{B_d} \sqrt{B_{B_d}}$  is from a recent unquenched lattice calculation  $215(11)(^{+0}_{-23})(15)$  MeV [127], where the first error is statistical, the second is the uncertainty from the chiral extrapolation and the third is due to other systematic errors. In Table 5.1 the two systematic errors are combined and the error is symmetrized. To improve the accuracy of the lattice calculation, simulations at significantly smaller sea quark masses will be required. With the staggered fermion formulation for sea quarks this is possible, albeit with additional complications, by introducing more flavors (or tastes) of fictitious quarks [129]. Within several years it will also become possible to perform unquenched simulations using lattice fermions with an exact chiral symmetry, such as overlap or domain-wall fermions. The reduction of errors down to a level of several percent is feasible within the time scale of the construction of SuperKEKB.

The constraint on  $(\bar{\rho}, \bar{\eta})$  using all these measurements for the SM case is shown in Figure 5.6. The plots are shown for (a) 500 fb<sup>-1</sup>, (b) 5 ab<sup>-1</sup>, and (c) 50 ab<sup>-1</sup>. Drastic improvements are expected with the statistical power of the SuperKEKB. The error in the determination of  $(\rho, \eta)$  will be eventually reduced to a  $\pm 0.03$  level with 50 ab<sup>-1</sup>.

Among those input parameters the measurement of the angle  $\phi_3$  is not yet precise at present. Therefore, despite the good agreement of  $(\bar{\rho}, \bar{\eta})$  from different measurements, there is a possibility that  $\phi_3$  does not agree with the current world average obtained with the CKM fit. It means that the SM value of  $(\bar{\rho}, \bar{\eta})$  could still be significantly different from the current central values, if other loop-induced processes contain large new physics effects. To see what could be observed at SuperKEKB, here we show a plot assuming that the central value of the  $\phi_3$  measurement is 120° instead of the current average 65° (Figure 5.7). The CKM fits are independently done for tree-level processes ( $|V_{ub}|$  and  $\phi_3$ ) and for  $b \rightarrow d$  mixing processes ( $\sin 2\phi_1$ ,  $\Delta m_d$  and  $\phi_2$ ). Clear separation of these two regions is achieved with the integrated luminosity of 5 ab<sup>-1</sup>, while the deviation is not significant at 0.5 ab<sup>-1</sup> that can be achieved at the present KEKB/Belle.

Measurements of  $\phi_2$  using  $B^0 \rightarrow \pi^+\pi^-$  or  $B^0 \rightarrow \rho\pi$  decay modes are contaminated by the  $b \rightarrow d$  penguin diagram, which can be eliminated using the isospin relations within the Standard Model. However, the spin and flavor structure of new physics contribution to the  $b \rightarrow d$  box and penguin amplitudes is model-dependent, and the isospin relations could be violated for some class

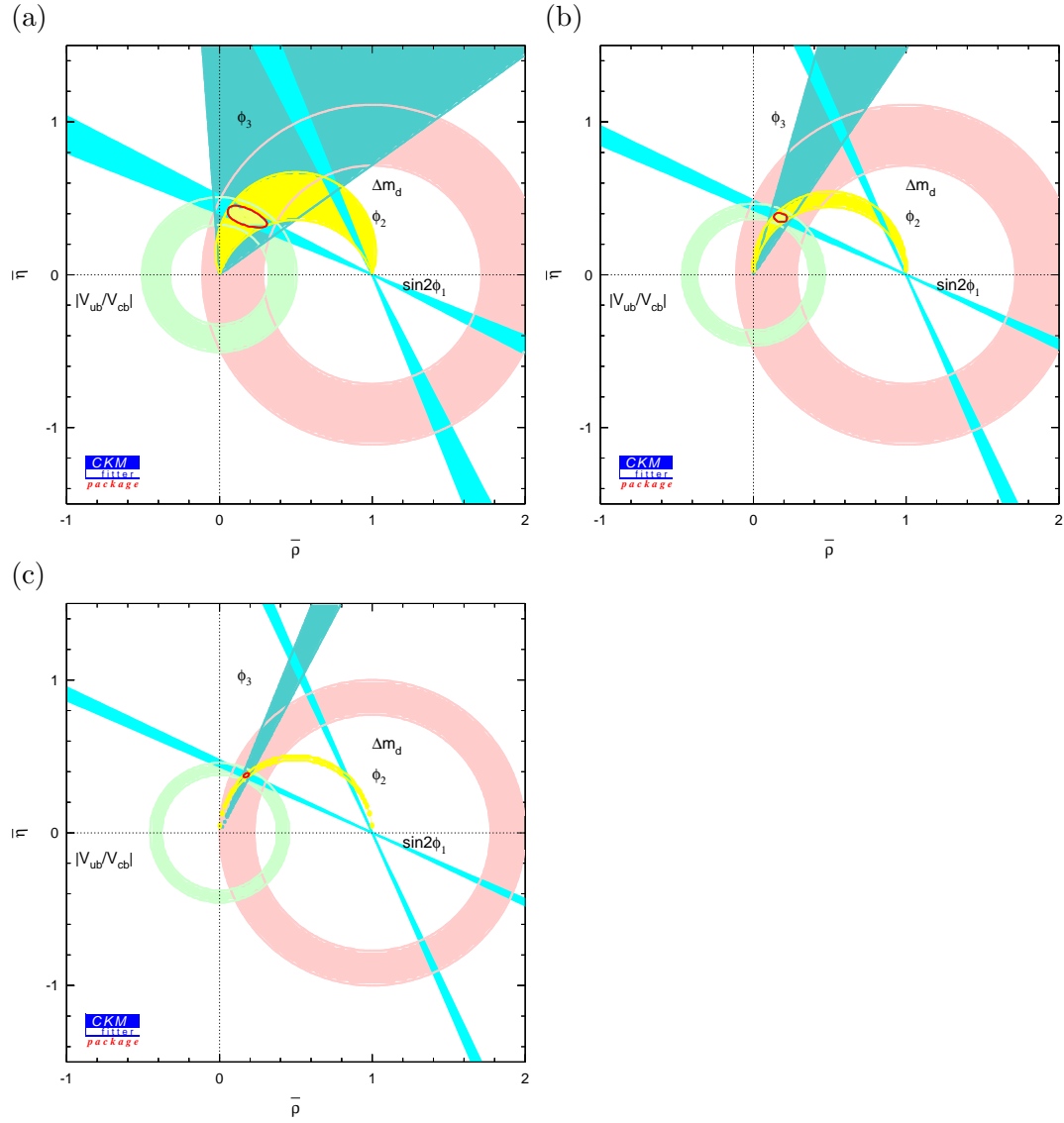


Figure 5.6: Constraints on the CKM unitarity triangle at (a)  $0.5 \text{ ab}^{-1}$ , (b)  $5 \text{ ab}^{-1}$ , and (c)  $50 \text{ ab}^{-1}$ .



of new physics models. Here, for simplicity we assume that the “penguin trapping” technique based on the isospin relation is not affected by the new physics contribution in the penguin-loop, which is satisfied if the new physics diagrams only contribute to  $\Delta I = 1/2$  amplitudes. In this case, the sum of the SM penguin and new physics penguin amplitudes is treated as a penguin amplitude to be trapped out.

The effect of new physics on the  $b \rightarrow d$  box diagram can be expressed as

$$M_{12} = M_{12}^{\text{SM}} + M_{12}^{\text{new}}, \quad (5.1)$$

where  $M_{12}^{\text{SM}}$  ( $M_{12}^{\text{new}}$ ) is the contribution of the amplitude to the  $b \rightarrow d$  box diagram from the SM (new physics particles) [394,395,396]. The fit result for the constraints in the  $(\text{Re } M_{12}^{\text{new}}, \text{Im } M_{12}^{\text{new}})$  plane is shown in Figure 5.8.

For the SUSY models discussed in Section 5.1, the  $M_{12}^{\text{new}}$  is tiny and the details of the models could not be distinguished from the fit on the  $(\text{Re } M_{12}^{\text{new}}, \text{Im } M_{12}^{\text{new}})$  plane. However, it implies that if one finds a significant deviation of  $(\text{Re } M_{12}^{\text{new}}, \text{Im } M_{12}^{\text{new}})$  from the origin, those specific SUSY models are excluded. Thus, this analysis provides another method to probe different kinds of new physics models that are sensitive to the  $b \rightarrow d$  transitions.

The method we described above can be extended to the  $b \rightarrow s$  box diagram ( $\Delta m_s$ ) and time dependent  $CP$  violation using  $B_s^0 \rightarrow J\psi\phi$  *etc.*,  $s \rightarrow d$  box diagram ( $\epsilon_K$ ), and  $b \rightarrow d$  penguin diagram ( $b \rightarrow d\gamma$  *etc.*). The exploration of new physics effects in flavor physics will be most powerful from a combination of these many different directions.

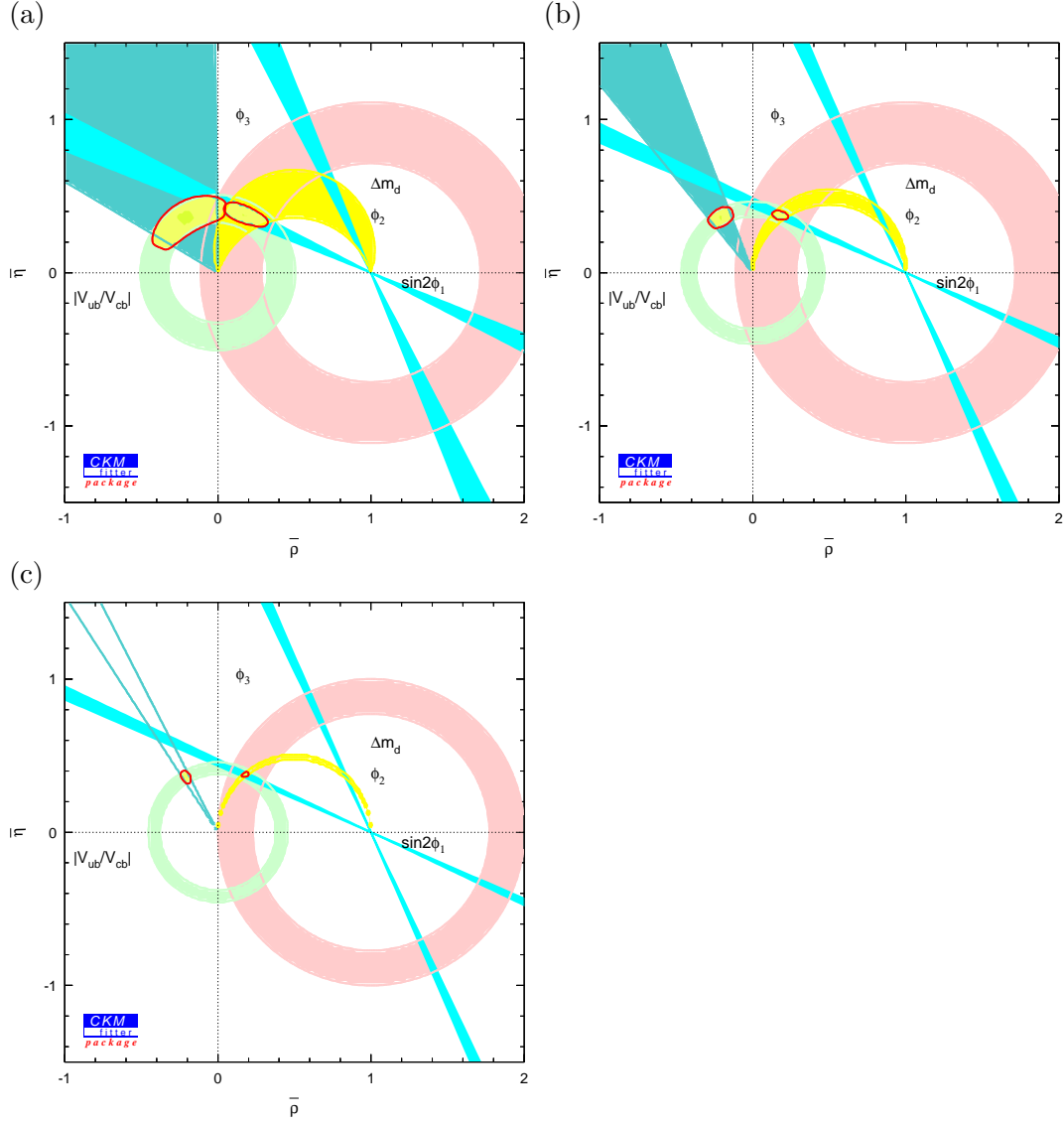


Figure 5.7: Constraints on the CKM unitarity triangle assuming  $\phi_3 = 120^\circ$  at (a)  $0.5 \text{ ab}^{-1}$ , (b)  $5 \text{ ab}^{-1}$ , and (c)  $50 \text{ ab}^{-1}$ . Independent constraints are shown for tree-level processes ( $|V_{ub}|$  and  $\phi_3$ ) and for  $b \rightarrow d$  mixing processes ( $\sin 2\phi_1$ ,  $\Delta m_d$  and  $\phi_2$ ).

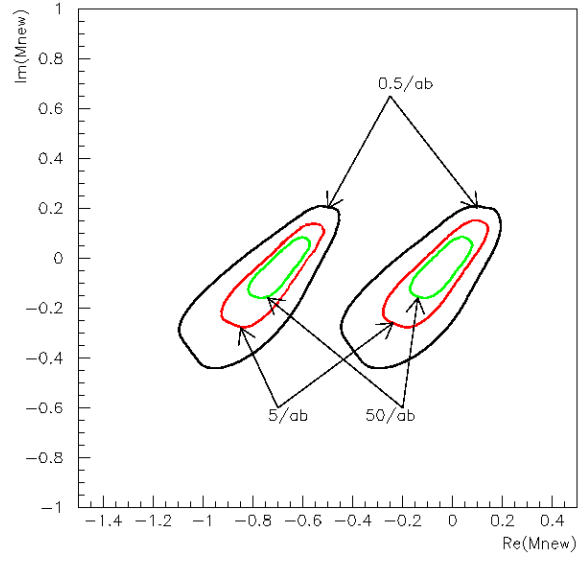


Figure 5.8: Constraints on the new physics contribution to the  $b \rightarrow d$  box amplitude  $M_{12}^{\text{new}}$ . Contours correspond to  $0.5 \text{ ab}^{-1}$  (black),  $5 \text{ ab}^{-1}$  (red) and  $50 \text{ ab}^{-1}$  (green).

## Chapter 6

# Summary

The grand challenge of elementary particle physics is to identify the fundamental elements of Nature and uncover the ultimate theory of their creation, interactions and annihilation. To this end, all elementary particles and the forces between them should be described in a unified picture. Such unification naturally requires a deep understanding of physical laws at a very high-energy scale; for instance the unification of electroweak and strong forces is expected to occur at around  $10^{16}$  GeV, which is often called the GUT scale.

It is unlikely that the GUT scale will be realized at any accelerator-based experiment even in the distant future. However, there are a few very promising ways to promote our grand challenge. One such approach is to elucidate the nature of quantum loop effects by producing as many particles as possible. This provides the rationale to pursue the luminosity frontier.

There is no doubt that past experiments at the luminosity (or intensity) frontier of the age have yielded epoch-making results. This good tradition has been followed by Belle and BaBar, experiments at energy-asymmetric  $e^+e^-$   $B$  factories KEKB and PEP-II, which have observed  $CP$  violation in the neutral  $B$  meson system. The result is in good agreement with the constraints from the Kobayashi-Maskawa (KM) model of  $CP$  violation. We are now confident that the KM phase is the dominant source of  $CP$  violation. In 2003 the KEKB collider achieved its design luminosity of  $1 \times 10^{34} \text{ cm}^{-2}\text{s}^{-1}$ . The Belle experiment will accumulate an integrated luminosity of  $500 \text{ fb}^{-1}$  within a few years. This will suffice to determine the Unitarity Triangle with a precision of  $\mathcal{O}(10)\%$ . Various other quantities in  $B$  meson decays will also become accessible. In particular, the first observation of direct  $CP$  violation in charmless  $B$  decays is anticipated.

Over the past thirty years, the success of the Standard Model, which incorporates the KM mechanism, has become increasingly firm. This strongly indicates that the Standard Model is *the* effective low-energy description of Nature. Yet there are several reasons to believe that physics beyond the Standard Model should exist. One of the most outstanding problems is the quadratically divergent radiative correction to the Higgs mass, which requires a fine tuning of the bare Higgs mass unless the cutoff scale is  $\mathcal{O}(1)$  TeV. This suggests that the new physics lies at the energy scale of  $\mathcal{O}(1)$  TeV. There is a good chance that LHC will discover new elementary particles such as supersymmetric (SUSY) particles. With this vision in mind, we raise an important question “what should be a role of the luminosity frontier in the LHC era?”

To answer the question, we note that the flavor sector of the Standard Model is quite successful in spite of the problem in the Higgs sector. This is connected to the observation that Flavor-Changing-Neutral-Currents (FCNCs) are highly suppressed. Indeed, if one considers a general new physics model without any mechanism to suppress FCNC processes, present experimental results on  $B$  physics imply that the new physics energy scale should be larger than  $\mathcal{O}(10^3)$  TeV. This apparent mismatch is called *the new physics flavor problem*. To overcome

the problem, any new physics at the TeV scale should have a mechanism to suppress FCNC processes, which often results in a distinctive flavor structure at low energy. Therefore, the indispensable roles of the luminosity frontier are to observe deviations from the Standard Model in flavor physics, and more importantly, to distinguish between different new physics models by a close examination of the flavor structure. Comprehensive studies of  $B$  meson decays in the clean  $e^+e^-$  environment provide the ideal solution for this purpose, which is not possible at LHC nor even at the future linear collider.

These provide the primary motivation for SuperKEKB, a major upgrade of KEKB. Its design luminosity is  $5 \times 10^{35} \text{ cm}^{-2}\text{s}^{-1}$ , which is 50 times as large as the peak luminosity achieved by KEKB. Various FCNC processes, such as the radiative decay  $b \rightarrow s\gamma$ , the semileptonic decay  $b \rightarrow sl^+l^-$ , and the hadronic decays  $b \rightarrow s\bar{q}q$  and  $b \rightarrow d\bar{q}q$ , can be studied with unprecedented precision. All of these processes are suppressed in the Standard Model by the GIM mechanism, and therefore the effect of new physics is relatively enhanced. New observables that are currently out of reach will also become accessible. In addition to  $B$  meson decays, FCNC processes in  $\tau$  and charm decays will also be studied at SuperKEKB.

The Belle detector will be upgraded to take full advantage of the high luminosity of SuperKEKB. In spite of harsh beam backgrounds, the detector performance will be at least as good as the present Belle detector and improvements in several aspects are envisaged. Table 6.1 summarizes the physics reach at SuperKEKB. As a reference, measurements expected at LHCb are also listed. One of the big advantages of SuperKEKB is the capability to reconstruct rare decays that have  $\gamma$ 's,  $\pi^0$ 's,  $K_L^0$ 's or neutrinos in the final states. There are several key observables in Table 6.1 that require this capability. Also important are time-dependent  $CP$  asymmetry measurements using only a  $K_S^0$  and a constraint from the interaction point to determine the  $B$  decay vertices. Examples include  $B^0 \rightarrow K^{*0}(\rightarrow K_S^0\pi^0)\gamma$ ,  $\pi^0 K_S^0$  and  $K_S^0 K_S^0 K_S^0$ . These fundamental measurements cannot be carried out at hadron colliders.

Figure 6.1(a) shows a comparison between time-dependent  $CP$  asymmetries in  $B^0 \rightarrow J/\psi K_S^0$ , which is dominated by the  $b \rightarrow c\bar{c}s$  tree process, and  $B^0 \rightarrow \phi K_S^0$ , which is governed by the  $b \rightarrow s\bar{s}s$  FCNC (penguin) process. It demonstrates how well a possible new  $CP$ -violating phase can be measured. Such a new source of  $CP$  violation may revolutionize the understanding of the origin of the matter-dominated Universe, which is one of the major unresolved issues in cosmology. Figure 6.1(b) shows correlations between time-dependent  $CP$  asymmetries in  $B^0 \rightarrow K^{*0}\gamma$  and  $B^0 \rightarrow \phi K_S^0$  decays in two representative new physics models with different SUSY breaking scenarios; the SU(5) SUSY GUT with right-handed neutrinos and the minimal supergravity model. The two can be clearly distinguished. This demonstrates that SuperKEKB is sensitive to a quantum phase even at the GUT scale. Note that these two models may have rather similar mass spectra. It will therefore be very difficult to distinguish one from the other at LHC. If SUSY particles are discovered at LHC, the origin of SUSY breaking will become one of the primary themes in elementary particle physics. SuperKEKB will play a leading role in such studies.

We emphasize that the example above is just one of several useful correlations that can be measured only at SuperKEKB. The true value of SuperKEKB is a capability to observe the pattern as a whole, which allows us to differentiate a variety of new physics scenarios. It is so to speak “*DNA identification of new physics*”, in that each measurement does not yield a basic physical parameter of the new physics but provides an essential piece of the overall flavor structure. This strategy works better when we accumulate more data. Thus the target annual integrated luminosity of  $5 \text{ ab}^{-1}$  is not a luxury but necessity, and stable long-term operation of SuperKEKB is necessary to meet the requirements.

Determination of the Unitarity Triangle will also be pushed forward and will be incorporated

Observable	SuperKEKB		LHCb
	(5 ab <sup>-1</sup> )	(50 ab <sup>-1</sup> )	(0.002ab <sup>-1</sup> )
$\Delta\mathcal{S}_{\phi K_S^0}$	0.079	0.031	0.2
$\Delta\mathcal{S}_{K^+K^-K_S^0}$	0.056	0.026	
$\Delta\mathcal{S}_{\eta'K_S^0}$	0.049	0.024	×
$\Delta\mathcal{S}_{K_S^0K_S^0K_S^0}$	0.14	0.04	×
$\Delta\mathcal{S}_{\pi^0K_S^0}$	0.10	0.03	×
$\sin 2\chi (B_s \rightarrow J/\psi\phi)$	×	×	0.058
$\mathcal{S}_{K^{*0}\gamma}$	0.14	0.04	×
$\mathcal{B}(B \rightarrow X_s\gamma)$	5%	5%	×
$A_{CP}(B \rightarrow X_s\gamma)$	0.011	$5 \times 10^{-3}$	×
$C_9$ from $\overline{A}_{\text{FB}}(B \rightarrow K^*\ell^+\ell^-)$	32%	10%	
$C_{10}$ from $\overline{A}_{\text{FB}}(B \rightarrow K^*\ell^+\ell^-)$	44%	14%	
$\mathcal{B}(B_s \rightarrow \mu^+\mu^-)$	×	×	$4\sigma$ (3 years)
$\mathcal{B}(B^+ \rightarrow K^+\nu\nu)$		$5.1\sigma$	×
$\mathcal{B}(B^+ \rightarrow D\tau\nu)$	8%	2.5%	×
$\mathcal{B}(B^0 \rightarrow D\tau\nu)$	$3.5\sigma$	9%	×
$\sin 2\phi_1$	0.019	0.014	0.022
$\phi_2$ ( $\pi\pi$ isospin)	$3.9^\circ$	$1.2^\circ$	×
$\phi_2$ ( $\rho\pi$ )	$2.9^\circ$	$0.9^\circ$	×
$\phi_3$ ( $DK^{(*)}$ )	$4^\circ$	$1.2^\circ$	$8^\circ$
$\phi_3$ ( $B_s \rightarrow KK$ )	×	×	$5^\circ$
$\phi_3$ ( $B_s \rightarrow D_sK$ )	×	×	$14^\circ$
$ V_{ub} $ (inclusive)	5.8%	4.4%	×
$\mathcal{B}(\tau \rightarrow \mu\gamma)$	$< 1.8 \times 10^{-8}$		

Table 6.1: Summary of the physics reach at SuperKEKB. Expected errors for the key observables are listed for an integrated luminosity of 5 ab<sup>-1</sup>, which corresponds to one year of operation, and with 50 ab<sup>-1</sup>.  $\Delta\mathcal{S}_f$  is defined by  $\Delta\mathcal{S}_f \equiv (-\xi_f)\mathcal{S}_f - \mathcal{S}_{J/\psi K_S^0}$ , where  $\xi_f$  is the  $CP$  eigenvalue of the final state  $f$ . For comparison, expected sensitivities at LHCb with one year of operation are also listed if available. The × marks indicate measurements that are very difficult or impossible.

in the global pattern mentioned above. This can be done at SuperKEKB using redundant measurements of all three angles and all three sides of the Unitarity Triangle. In particular,  $\phi_2$  measurements and  $V_{ub}$  measurements require the reconstruction of  $\pi^0$  mesons and neutrinos and are thus unique to a Super  $B$ -Factory. An inconsistency among these measurements implies new physics. Figure 6.2(a) and (b) show the expected constraints at 50 ab<sup>-1</sup> in two cases that are both allowed with the present experimental constraints. The clear difference between two figures demonstrates the power of the ultimate precision of  $\mathcal{O}(1)\%$ , which will be obtained at SuperKEKB.

We thus conclude that the physics case at SuperKEKB is compelling. It will be the place to elucidate *the new physics flavor problem* in the LHC era. The physics program at SuperKEKB is not only complementary to the next-generation energy frontier programme, but is an essential element of the grand challenge in elementary particle physics.

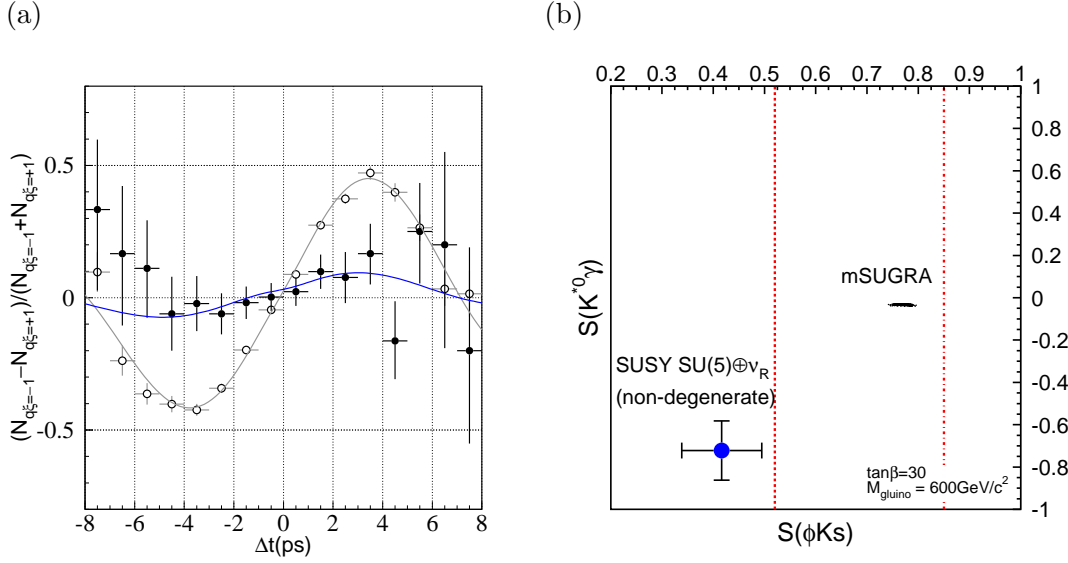


Figure 6.1: (a) Time-dependent  $CP$  asymmetries in  $B^0 \rightarrow \phi K_S^0$  and  $B^0 \rightarrow J/\psi K_S^0$  decays expected with one year of operation at SuperKEKB ( $5 \text{ ab}^{-1}$ ). The world average values (as of August 2003) for the modes governed by the  $b \rightarrow s$  transition are used as the input values of  $\mathcal{S}_{\phi K_S^0} = +0.24$  and  $\mathcal{A}_{\phi K_S^0} = +0.07$ . (b) A correlation between time-dependent  $CP$  asymmetries in  $B^0 \rightarrow K^{*0} \gamma$  and  $B^0 \rightarrow \phi K_S^0$ . The dots show the range in the minimal supergravity model (mSUGRA). The circle corresponds to a possible point of supersymmetric SU(5) GUT model with right-handed neutrinos. Error bars associated with the circle indicate expected errors with one year of operation at SuperKEKB. The present experimental bound of  $\mathcal{S}_{\phi K_S^0} < +0.52$  ( $\mathcal{S}_{\phi K_S^0} < +0.85$ ) at the  $2\sigma$  ( $3\sigma$ ) level is also shown by the dashed (dot-dashed) vertical line.

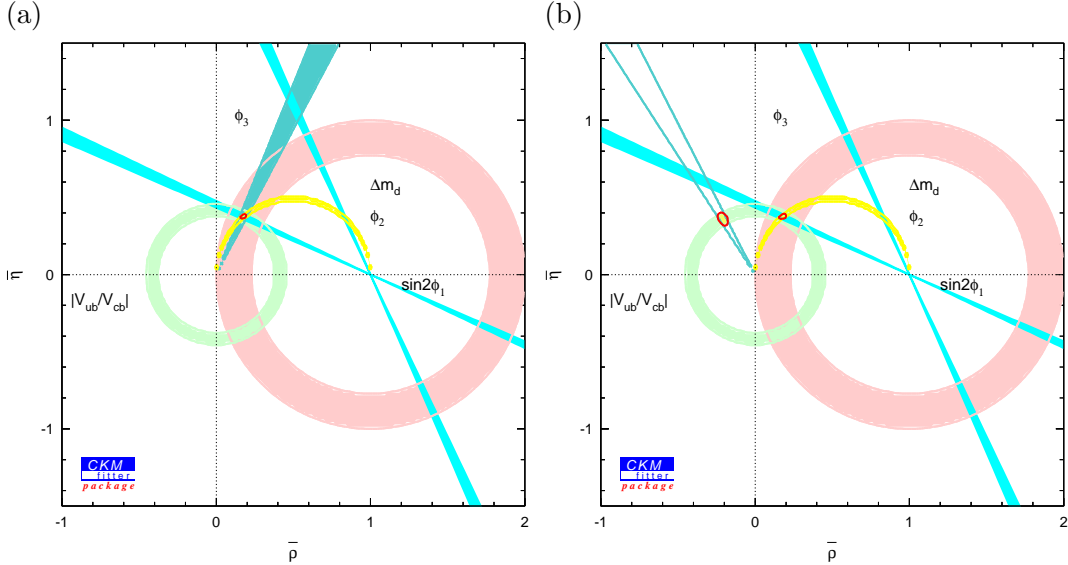


Figure 6.2: Constraints on the CKM unitarity triangle at  $50 \text{ ab}^{-1}$  (a) in the case consistent with the SM, and (b) with a large deviation from the SM. Both cases are within present experimental constraints.

# References

- [1] S. L. Glashow, J. Iliopoulos and L. Maiani, “Weak Interactions With Lepton – Hadron Symmetry,” *Phys. Rev. D* **2**, 1285 (1970).
- [2] M. Kobayashi and T. Maskawa, “CP Violation In The Renormalizable Theory Of Weak Interaction,” *Prog. Theor. Phys.* **49**, 652 (1973).
- [3] A. Abashian *et al.* [BELLE Collaboration], “Measurement of the CP violation parameter  $\sin(2\phi_1)$  in  $B_d^0$  meson decays,” *Phys. Rev. Lett.* **86**, 2509 (2001) [arXiv:hep-ex/0102018].
- [4] K. Abe *et al.* [Belle Collaboration], “Observation of large CP violation in the neutral B meson system,” *Phys. Rev. Lett.* **87**, 091802 (2001) [arXiv:hep-ex/0107061].
- [5] K. Abe *et al.* [Belle Collaboration], “Observation of mixing-induced CP violation in the neutral B meson system,” *Phys. Rev. D* **66**, 032007 (2002) [arXiv:hep-ex/0202027].
- [6] K. Abe *et al.* [Belle Collaboration], “An improved measurement of mixing-induced CP violation in the neutral B meson system. ((B)),” *Phys. Rev. D* **66**, 071102 (2002) [arXiv:hep-ex/0208025].
- [7] B. Aubert *et al.* [BABAR Collaboration], “Measurement of CP violating asymmetries in  $B^0$  decays to CP eigenstates,” *Phys. Rev. Lett.* **86**, 2515 (2001) [arXiv:hep-ex/0102030].
- [8] B. Aubert *et al.* [BABAR Collaboration], “A study of time dependent CP-violating asymmetries and flavor oscillations in neutral B decays at the  $\Upsilon(4S)$ ,” *Phys. Rev. D* **66**, 032003 (2002) [arXiv:hep-ex/0201020].
- [9] B. Aubert *et al.* [BABAR Collaboration], “Observation of CP violation in the  $B^0$  meson system,” *Phys. Rev. Lett.* **87**, 091801 (2001) [arXiv:hep-ex/0107013].
- [10] B. Aubert *et al.* [BABAR Collaboration], “Measurement of the CP-violating asymmetry amplitude  $\sin 2\beta$ . ((B)),” *Phys. Rev. Lett.* **89**, 201802 (2002) [arXiv:hep-ex/0207042].
- [11] K. Abe *et al.* [Belle Collaboration], “Measurement of CP-violation parameter  $\sin(2\phi_1)$  with 152 million  $B\bar{B}$  pairs,” arXiv:hep-ex/0308036.
- [12] K. Abe *et al.* [Belle Collaboration], “Measurement of CP-violating asymmetries in  $B^0 \rightarrow \pi^+\pi^-$  decays,” *Phys. Rev. Lett.* **89**, 071801 (2002) [arXiv:hep-ex/0204002].
- [13] K. Abe *et al.* [Belle Collaboration], “Evidence for CP-violating asymmetries  $B^0 \rightarrow \pi^+\pi^-$  decays and constraints on the CKM angle  $\phi_2$ ,” *Phys. Rev. D* **68**, 012001 (2003) [arXiv:hep-ex/0301032].



- [14] K. Abe *et al.* [Belle Collaboration], “Observation of large CP violation and evidence for direct CP violation in  $B^0 \rightarrow \pi^+\pi^-$  decays,” [arXiv:hep-ex/0401029].
- [15] S. K. Swain *et al.* [Belle Collaboration], “Measurement of branching fraction ratios and CP asymmetries in  $B^\pm \rightarrow D_{CP}K^\pm$ ,” Phys. Rev. D **68**, 051101 (2003) [arXiv:hep-ex/0304032].
- [16] K. Abe *et al.* [Belle Collaboration], “Measurement of the angle  $\phi_3$  with Dalitz analysis of three-body  $D^0$  decay from  $B \rightarrow D^0K$  process,” arXiv:hep-ex/0308043.
- [17] K. Abe *et al.* [BELLE Collaboration], “Study of CP violating effects in time dependent  $B^0(\bar{B}^0) \rightarrow D^{(*)\mp}\pi^\pm$  decays,” arXiv:hep-ex/0308048.
- [18] K. Abe *et al.* [BELLE Collaboration], “Observation of the decay  $B \rightarrow K\mu^+\mu^-$ ,” Phys. Rev. Lett. **88**, 021801 (2002) [arXiv:hep-ex/0109026].
- [19] A. Ishikawa *et al.* [Belle Collaboration], “Observation of the electroweak penguin decay  $B \rightarrow K^*\ell^+\ell^-$ ,” Phys. Rev. Lett. **91**, 261601 (2003) [arXiv:hep-ex/0308044].
- [20] J. Kaneko *et al.* [Belle Collaboration], Phys. Rev. Lett. **90**, 021801 (2003) [arXiv:hep-ex/0208029].
- [21] K. Abe *et al.* [Belle Collaboration], “Measurement of time-dependent CP-violating asymmetries in  $B^0 \rightarrow \phi K_S^0$ ,  $K^+K^-K_S^0$ , and  $\eta'K_S^0$  decays,” Phys. Rev. Lett. **91**, 261602 (2003) [arXiv:hep-ex/0308035].
- [22] K. Anikeev *et al.*, “B physics at the Tevatron: Run II and beyond,” arXiv:hep-ph/0201071.
- [23] P. Ball *et al.*, “B decays at the LHC,” arXiv:hep-ph/0003238.
- [24] A. Hocker, H. Lacker, S. Laplace and F. Le Diberder, “A new approach to a global fit of the CKM matrix,” Eur. Phys. J. C **21**, 225 (2001) [arXiv:hep-ph/0104062].
- [25] Y. Grossman and M. P. Worah, “CP asymmetries in B decays with new physics in decay amplitudes,” Phys. Lett. B **395**, 241 (1997) [arXiv:hep-ph/9612269].
- [26] D. London and A. Soni, “Measuring the CP angle  $\beta$  in hadronic  $b \rightarrow s$  penguin decays,” Phys. Lett. B **407**, 61 (1997) [arXiv:hep-ph/9704277].
- [27] Y. Grossman, G. Isidori and M. P. Worah, “CP asymmetry in  $B_d \rightarrow \phi K_S$ : Standard model pollution,” Phys. Rev. D **58**, 057504 (1998) [arXiv:hep-ph/9708305].
- [28] Y. Grossman, Z. Ligeti, Y. Nir and H. Quinn, “SU(3) relations and the CP asymmetries in B decays to  $\eta'K_S$ ,  $\phi K_S$  and  $K^+K^-K_S$ ,” Phys. Rev. D **68**, 015004 (2003) [arXiv:hep-ph/0303171].
- [29] BaBar Collaboration, B. Aubert *et al.*, BABAR-PLOT-0053; BABAR-PLOT-0056.
- [30] A. Garmash *et al.* [Belle Collaboration], “Study of B meson decays to three-body charmless hadronic final states,” Phys. Rev. D **69**, 012001 (2004) [arXiv:hep-ex/0307082].
- [31] K. F. Chen *et al.* [Belle Collaboration], “Measurement of CP-violating parameters in  $B \rightarrow \eta'K$  decays. ((B)),” Phys. Lett. B **546**, 196 (2002) [arXiv:hep-ex/0207033].

- [32] B. Aubert *et al.* [BABAR Collaboration], “Measurements of CP-violating asymmetries and branching fractions in  $B$  meson decays to  $\eta'K$ ,” Phys. Rev. Lett. **91**, 161801 (2003) [arXiv:hep-ex/0303046].
- [33] T. E. Coan *et al.* [CLEO Collaboration], “Study of exclusive radiative  $B$  meson decays,” Phys. Rev. Lett. **84**, 5283 (2000) [arXiv:hep-ex/9912057].
- [34] B. Aubert *et al.* [BABAR Collaboration], “Measurement of  $B \rightarrow K^*\gamma$  branching fractions and charge asymmetries,” Phys. Rev. Lett. **88**, 101805 (2002) [arXiv:hep-ex/0110065].
- [35] Belle Collaboration, K. Abe *et al.*, Belle-CONF-0319.
- [36] A. Ali and A. Y. Parkhomenko, “Branching ratios for  $B \rightarrow \rho\gamma$  decays in next-to-leading order in  $\alpha_s$  including hard spectator corrections,” Eur. Phys. J. C **23**, 89 (2002) [arXiv:hep-ph/0105302].
- [37] S. W. Bosch and G. Buchalla, “The radiative decays  $B \rightarrow V\gamma$  at next-to-leading order in QCD,” Nucl. Phys. B **621**, 459 (2002) [arXiv:hep-ph/0106081].
- [38] Y. Y. Keum, M. Matsumori, and A.I. Sanda, “ $CP$  asymmetry, branching ratios and isospin breaking effects of  $B \rightarrow K^*\gamma$  with perturbative QCD approach,” arXiv:hep-ph/0406055.
- [39] A. L. Kagan and M. Neubert, “Isospin breaking in  $B \rightarrow K^*\gamma$  decays,” Phys. Lett. B **539**, 227 (2002) [arXiv:hep-ph/0110078].
- [40] S. Nishida *et al.* [Belle Collaboration], “Radiative  $B$  meson decays into  $K\pi\gamma$  and  $K\pi\pi\gamma$  final states,” Phys. Rev. Lett. **89**, 231801 (2002) [arXiv:hep-ex/0205025].
- [41] A. Drutskoy *et al.* [BELLE Collaboration], “Observation of radiative  $B \rightarrow \phi K\gamma$  decays,” Phys. Rev. Lett. **92**, 051801 (2004) [arXiv:hep-ex/0309006].
- [42] J. M. Soares, “CP violation in radiative  $b$  decays,” Nucl. Phys. B **367**, 575 (1991).
- [43] A. L. Kagan and M. Neubert, “Direct CP violation in  $B \rightarrow X_s\gamma$  decays as a signature of new physics,” Phys. Rev. D **58**, 094012 (1998) [arXiv:hep-ph/9803368].
- [44] K. Abe *et al.* [BELLE Collaboration], “Measurement of the CP asymmetry in  $B \rightarrow X_s\gamma$ ,” arXiv:hep-ex/0308038.
- [45] B. Aubert *et al.* [BABAR Collaboration], “Search for the radiative decays  $B \rightarrow \rho\gamma$  and  $B^0 \rightarrow \omega\gamma$ ,” arXiv:hep-ex/0306038.
- [46] M. Nakao for the Belle Collaboration, talk given at 2nd Workshop on the CKM Unitarity Triangle, Durham, England, Apr. 2003, “Belle results on  $b \rightarrow sl^+l^-$  and  $b \rightarrow \gamma$ ,” eConf **C0304052**, WG208 (2003) [arXiv:hep-ex/0307031].
- [47] B. Aubert *et al.* [BABAR Collaboration], “Evidence for the flavor changing neutral current decays  $B \rightarrow Kl^+l^-$  and  $B \rightarrow K^*l^+l^-$ . ((B)),” arXiv:hep-ex/0207082.
- [48] B. Aubert *et al.* [BABAR Collaboration], “Evidence for the rare decay  $B \rightarrow K^*l^+l^-$  and measurement of the  $B \rightarrow Kl^+l^-$  branching fraction,” Phys. Rev. Lett. **91**, 221802 (2003) [arXiv:hep-ex/0308042].

- [49] A. Ali, E. Lunghi, C. Greub and G. Hiller, “Improved model-independent analysis of semileptonic and radiative rare  $B$  decays,” Phys. Rev. D **66**, 034002 (2002) [arXiv:hep-ph/0112300].
- [50] E. Lunghi, “Improved model-independent analysis of semileptonic and radiative rare  $B$  decays,” arXiv:hep-ph/0210379.
- [51] W. Jaus and D. Wyler, “The Rare Decays Of  $B \rightarrow K l \bar{l}$  And  $B \rightarrow K^* l \bar{l}$ ,” Phys. Rev. D **41**, 3405 (1990).
- [52] D. Melikhov, N. Nikitin and S. Simula, “Rare decays  $B \rightarrow (K, K^*)(l^+ l^-, \nu \bar{\nu})$  in the quark model,” Phys. Lett. B **410**, 290 (1997) [arXiv:hep-ph/9704268].
- [53] P. Colangelo, F. De Fazio, P. Santorelli and E. Scrimieri, “QCD Sum Rule Analysis of the Decays  $B \rightarrow K \ell + \ell -$  and  $B \rightarrow K^* \ell + \ell -$ ,” Phys. Rev. D **53**, 3672 (1996) [Erratum-ibid. D **57**, 3186 (1998)] [arXiv:hep-ph/9510403].
- [54] T. M. Aliev, C. S. Kim and Y. G. Kim, “A systematic analysis of the exclusive  $B \rightarrow K^* l^+ l^-$  decay,” Phys. Rev. D **62**, 014026 (2000) [arXiv:hep-ph/9910501].
- [55] M. Zhong, Y. L. Wu and W. Y. Wang, “Exclusive B meson rare decays and new relations of form factors in effective field theory of heavy quarks,” Int. J. Mod. Phys. A **18**, 1959 (2003) [arXiv:hep-ph/0206013].
- [56] B. Aubert *et al.* [BABAR Collaboration], “Measurement of the  $B \rightarrow X_s l^+ l^-$  branching fraction using a sum over exclusive modes,” arXiv:hep-ex/0308016.
- [57] N. Cabibbo, “Unitary Symmetry And Leptonic Decays,” Phys. Rev. Lett. **10** (1963) 531.
- [58] K. Hagiwara *et al.* [Particle Data Group Collaboration], “Review Of Particle Physics,” Phys. Rev. D **66**, 010001 (2002).
- [59] L. Wolfenstein, “Parametrization Of The Kobayashi-Maskawa Matrix,” Phys. Rev. Lett. **51**, 1945 (1983).
- [60] M. Battaglia *et al.*, “The CKM matrix and the unitarity triangle,” Proceedings of the First Workshop on the CKM Unitarity Triangle, CERN 13-16 February 2002; arXiv:hep-ph/0304132.
- [61] K. G. Wilson, “Nonlagrangian Models Of Current Algebra,” Phys. Rev. **179** (1969) 1499.
- [62] T. Inami and C. S. Lim, “Effects Of Superheavy Quarks And Leptons In Low-Energy Weak Processes  $K_L \rightarrow \mu \bar{\mu}$ ,  $K^+ \rightarrow \pi^+ \nu \bar{\nu}$  and  $K^0 \leftrightarrow \bar{K}^0$ ,” Prog. Theor. Phys. **65**, 297 (1981) [Erratum-ibid. **65**, 1772 (1981)].
- [63] G. Altarelli, G. Curci, G. Martinelli and S. Petrarca, “QCD Nonleading Corrections To Weak Decays As An Application Of Regularization By Dimensional Reduction,” Nucl. Phys. B **187**, 461 (1981).
- [64] A. J. Buras and P. H. Weisz, “QCD Nonleading Corrections To Weak Decays In Dimensional Regularization and 't Hooft-Veltman Schemes,” Nucl. Phys. B **333**, 66 (1990).
- [65] A. J. Buras, M. Jamin, M. E. Lautenbacher and P. H. Weisz, “Effective Hamiltonians for  $\Delta S = 1$  and  $\Delta B = 1$  nonleptonic decays beyond the leading logarithmic approximation,” Nucl. Phys. B **370**, 69 (1992) [Addendum-ibid. B **375**, 501 (1992)].

- [66] A. J. Buras, M. Jamin, M. E. Lautenbacher and P. H. Weisz, “Two loop anomalous dimension matrix for  $\Delta S = 1$  weak nonleptonic decays. 1.  $O(\alpha_s^2)$ ,” Nucl. Phys. B **400**, 37 (1993) [arXiv:hep-ph/9211304].
- [67] A. B. Carter and A. I. Sanda, “CP Violation In Cascade Decays Of B Mesons,” Phys. Rev. Lett. **45**, 952 (1980).
- [68] A. B. Carter and A. I. Sanda, “CP Violation In B Meson Decays,” Phys. Rev. D **23**, 1567 (1981).
- [69] I. I. Y. Bigi and A. I. Sanda, “Notes On The Observability Of CP Violations In B Decays,” Nucl. Phys. B **193**, 85 (1981).
- [70] M. Gronau and D. London, “Isospin Analysis Of CP Asymmetries In B Decays,” Phys. Rev. Lett. **65**, 3381 (1990).
- [71] A. E. Snyder and H. R. Quinn, “Measuring CP asymmetry in  $B \rightarrow \rho\pi$  decays without ambiguities,” Phys. Rev. D **48**, 2139 (1993).
- [72] N. G. Deshpande and X. G. He, “Isospin structure of penguins and their consequences in B physics,” Phys. Rev. Lett. **74**, 26 (1995) [Erratum-ibid. **74**, 4099 (1995)] [arXiv:hep-ph/9408404].
- [73] M. Gronau, O. F. Hernandez, D. London and J. L. Rosner, “Electroweak penguins and two-body B decays,” Phys. Rev. D **52**, 6374 (1995) [arXiv:hep-ph/9504327].
- [74] M. Neubert, “Model-independent analysis of  $B \rightarrow \pi K$  decays and bounds on the weak phase gamma,” JHEP **9902**, 014 (1999) [arXiv:hep-ph/9812396].
- [75] T. Yoshikawa, “A possibility of large electro-weak penguin contribution in  $B \rightarrow K\pi$  modes,” Phys. Rev. D **68**, 054023 (2003) [arXiv:hep-ph/0306147].
- [76] M. Gronau and J. L. Rosner, “Rates and asymmetries in  $B \rightarrow K\pi$  decays,” Phys. Lett. B **572**, 43 (2003) [arXiv:hep-ph/0307095].
- [77] A. J. Buras, R. Fleischer, S. Recksiegel and F. Schwab, “The  $B \rightarrow \pi K$  puzzle and its relation to rare B and K decays,” arXiv:hep-ph/0309012.
- [78] N. Isgur and M. B. Wise, “Weak Decays Of Heavy Mesons In The Static Quark Approximation,” Phys. Lett. B **232**, 113 (1989).
- [79] N. Isgur and M. B. Wise, “Weak Transition Form-Factors Between Heavy Mesons,” Phys. Lett. B **237**, 527 (1990).
- [80] E. Eichten and B. Hill, “An Effective Field Theory For The Calculation Of Matrix Elements Involving Heavy Quarks,” Phys. Lett. B **234**, 511 (1990).
- [81] H. Georgi, “An Effective Field Theory For Heavy Quarks At Low-Energies,” Phys. Lett. B **240**, 447 (1990).
- [82] B. Grinstein, “The Static Quark Effective Theory,” Nucl. Phys. B **339**, 253 (1990).
- [83] J. Chay, H. Georgi and B. Grinstein, “Lepton Energy Distributions In Heavy Meson Decays From QCD,” Phys. Lett. B **247**, 399 (1990).

- [84] I. I. Y. Bigi, N. G. Uraltsev and A. I. Vainshtein, “Nonperturbative corrections to inclusive beauty and charm decays: QCD versus phenomenological models,” *Phys. Lett. B* **293**, 430 (1992) [Erratum-ibid. *B* **297**, 477 (1993)] [arXiv:hep-ph/9207214].
- [85] I. I. Y. Bigi, M. A. Shifman, N. G. Uraltsev and A. I. Vainshtein, “QCD predictions for lepton spectra in inclusive heavy flavor decays,” *Phys. Rev. Lett.* **71**, 496 (1993) [arXiv:hep-ph/9304225].
- [86] A. V. Manohar and M. B. Wise, “Inclusive semileptonic B and polarized Lambda(b) decays from QCD,” *Phys. Rev. D* **49**, 1310 (1994) [arXiv:hep-ph/9308246].
- [87] B. Blok, L. Koyrakh, M. A. Shifman and A. I. Vainshtein, “Differential distributions in semileptonic decays of the heavy flavors in QCD,” *Phys. Rev. D* **49**, 3356 (1994) [Erratum-ibid. *D* **50**, 3572 (1994)] [arXiv:hep-ph/9307247].
- [88] P. Ball and V. M. Braun, “Next-to-leading order corrections to meson masses in the heavy quark effective theory,” *Phys. Rev. D* **49**, 2472 (1994) [arXiv:hep-ph/9307291].
- [89] M. Neubert, “QCD sum-rule calculation of the kinetic energy and chromo-interaction of heavy quarks inside mesons,” *Phys. Lett. B* **389**, 727 (1996) [arXiv:hep-ph/9608211].
- [90] M. Crisafulli, V. Gimenez, G. Martinelli and C. T. Sachrajda, “First lattice calculation of the  $B$  meson binding and kinetic energies,” *Nucl. Phys. B* **457**, 594 (1995) [arXiv:hep-ph/9506210].
- [91] V. Gimenez, G. Martinelli and C. T. Sachrajda, “A high-statistics lattice calculation of  $\lambda_1$  and  $\lambda_2$  in the  $B$  meson,” *Nucl. Phys. B* **486**, 227 (1997) [arXiv:hep-lat/9607055].
- [92] A. S. Kronfeld and J. N. Simone, “Computation of  $\bar{\Lambda}$  and  $\lambda_1$  with lattice QCD,” *Phys. Lett. B* **490**, 228 (2000) [Erratum-ibid. *B* **495**, 441 (2000)] [arXiv:hep-ph/0006345].
- [93] S. Aoki *et al.* [JLQCD Collaboration], “Heavy quark expansion parameters from lattice NRQCD,” arXiv:hep-lat/0305024.
- [94] R. D. Dikeman, M. A. Shifman and N. G. Uraltsev, “ $b \rightarrow s + \gamma$ : A QCD consistent analysis of the photon energy distribution,” *Int. J. Mod. Phys. A* **11**, 571 (1996) [arXiv:hep-ph/9505397].
- [95] A. Kapustin and Z. Ligeti, “Moments of the photon spectrum in the inclusive  $B \rightarrow X_s \gamma$  decay,” *Phys. Lett. B* **355**, 318 (1995) [arXiv:hep-ph/9506201].
- [96] A. F. Falk, M. E. Luke and M. J. Savage, “Hadron spectra for semileptonic heavy quark decay,” *Phys. Rev. D* **53**, 2491 (1996) [arXiv:hep-ph/9507284].
- [97] A. F. Falk, M. E. Luke and M. J. Savage, “Phenomenology of the  $1/m_Q$  Expansion in Inclusive  $B$  and  $D$  Meson Phys. Rev. D **53**, 6316 (1996) [arXiv:hep-ph/9511454].
- [98] M. Gremm, A. Kapustin, Z. Ligeti and M. B. Wise, “Implications of the  $B \rightarrow X \ell \bar{\nu}_\ell$  lepton spectrum for heavy quark theory,” *Phys. Rev. Lett.* **77**, 20 (1996) [arXiv:hep-ph/9603314].
- [99] J. D. Bjorken, “Topics In B Physics,” *Nucl. Phys. Proc. Suppl.* **11**, 325 (1989).
- [100] M. Beneke, G. Buchalla, M. Neubert and C. T. Sachrajda, “QCD factorization for  $B \rightarrow \pi\pi$  decays: Strong phases and CP violation in the heavy quark limit,” *Phys. Rev. Lett.* **83**, 1914 (1999) [arXiv:hep-ph/9905312].

- [101] M. Beneke, G. Buchalla, M. Neubert and C. T. Sachrajda, “QCD factorization for exclusive, non-leptonic  $B$  meson decays: General arguments and the case of heavy-light final states,” Nucl. Phys. B **591**, 313 (2000) [arXiv:hep-ph/0006124].
- [102] M. Beneke, G. Buchalla, M. Neubert and C. T. Sachrajda, “QCD factorization in  $B \rightarrow \pi K$ ,  $\pi\pi$  decays and extraction of Wolfenstein parameters,” Nucl. Phys. B **606**, 245 (2001) [arXiv:hep-ph/0104110].
- [103] C. W. Bauer, S. Fleming and M. E. Luke, “Summing Sudakov logarithms in  $B \rightarrow X/s$  gamma in effective field theory,” Phys. Rev. D **63**, 014006 (2001) [arXiv:hep-ph/0005275].
- [104] C. W. Bauer, S. Fleming, D. Pirjol and I. W. Stewart, “An effective field theory for collinear and soft gluons: Heavy to light decays,” Phys. Rev. D **63**, 114020 (2001) [arXiv:hep-ph/0011336].
- [105] C. W. Bauer and I. W. Stewart, “Invariant operators in collinear effective theory,” Phys. Lett. B **516**, 134 (2001) [arXiv:hep-ph/0107001].
- [106] C. W. Bauer, D. Pirjol and I. W. Stewart, Phys. Rev. D **65**, 054022 (2002) [arXiv:hep-ph/0109045].
- [107] H-n. Li and H. L. Yu, “Extraction of  $V(\text{ub})$  from decay  $B \rightarrow \pi l \nu$ ,” Phys. Rev. Lett. **74**, 4388 (1995) [arXiv:hep-ph/9409313].
- [108] H-n. Li and H. L. Yu, “PQCD Analysis Of Exclusive Charmless B Meson Decay Spectra,” Phys. Lett. B **353** (1995) 301.
- [109] H-n. Li and H. L. Yu, “Perturbative QCD analysis of B meson decays,” Phys. Rev. D **53**, 2480 (1996) [arXiv:hep-ph/9411308].
- [110] Y. Y. Keum, H-n. Li and A. I. Sanda, “Fat penguins and imaginary penguins in perturbative QCD,” Phys. Lett. B **504**, 6 (2001) [arXiv:hep-ph/0004004].
- [111] Y. Y. Keum, H-n. Li and A. I. Sanda, “Penguin enhancement and  $B \rightarrow K\pi$  decays in perturbative QCD,” Phys. Rev. D **63**, 054008 (2001) [arXiv:hep-ph/0004173].
- [112] Y. Y. Keum and H-n. Li, “Nonleptonic charmless B decays: Factorization vs. perturbative QCD,” Phys. Rev. D **63**, 074006 (2001) [arXiv:hep-ph/0006001].
- [113] K. G. Wilson, “Confinement Of Quarks,” Phys. Rev. D **10**, 2445 (1974).
- [114] W. E. Caswell and G. P. Lepage, “Effective Lagrangians For Bound State Problems In QED, QCD, And Other Field Theories,” Phys. Lett. B **167**, 437 (1986).
- [115] B. A. Thacker and G. P. Lepage, “Heavy Quark Bound States In Lattice QCD,” Phys. Rev. D **43**, 196 (1991).
- [116] G. P. Lepage, L. Magnea, C. Nakhleh, U. Magnea and K. Hornbostel, “Improved non-relativistic QCD for heavy quark physics,” Phys. Rev. D **46**, 4052 (1992) [arXiv:hep-lat/9205007].
- [117] A. X. El-Khadra, A. S. Kronfeld and P. B. Mackenzie, “Massive Fermions in Lattice Gauge Theory,” Phys. Rev. D **55**, 3933 (1997) [arXiv:hep-lat/9604004].

- [118] A. S. Kronfeld, “Application of heavy-quark effective theory to lattice QCD. I: Power corrections,” Phys. Rev. D **62**, 014505 (2000) [arXiv:hep-lat/0002008].
- [119] K. I. Ishikawa, H. Matsufuru, T. Onogi, N. Yamada and S. Hashimoto, “ $f_B$  with lattice NRQCD including  $O(1/m_Q^2)$  corrections,” Phys. Rev. D **56**, 7028 (1997) [arXiv:hep-lat/9706008].
- [120] K. Symanzik, “Continuum Limit And Improved Action In Lattice Theories. 1. Principles And  $\Phi^4$  Theory,” Nucl. Phys. B **226**, 187 (1983).
- [121] K. Symanzik, “Continuum Limit And Improved Action In Lattice Theories. 2.  $O(N)$  Nonlinear Sigma Model In Perturbation Theory,” Nucl. Phys. B **226**, 205 (1983).
- [122] B. Sheikholeslami and R. Wohlert, “Improved Continuum Limit Lattice Action For QCD With Wilson Fermions,” Nucl. Phys. B **259**, 572 (1985).
- [123] K. Jansen *et al.*, “Non-perturbative renormalization of lattice QCD at all scales,” Phys. Lett. B **372**, 275 (1996) [arXiv:hep-lat/9512009].
- [124] M. Luscher, S. Sint, R. Sommer, P. Weisz and U. Wolff, “Non-perturbative  $O(a)$  improvement of lattice QCD,” Nucl. Phys. B **491**, 323 (1997) [arXiv:hep-lat/9609035].
- [125] G. P. Lepage and P. B. Mackenzie, “On the viability of lattice perturbation theory,” Phys. Rev. D **48**, 2250 (1993) [arXiv:hep-lat/9209022].
- [126] N. Yamada, “Heavy quark physics and lattice QCD,” Nucl. Phys. Proc. Suppl. **119**, 93 (2003) [arXiv:hep-lat/0210035].
- [127] S. Aoki *et al.* [JLQCD Collaboration], “ $B^0 - \bar{B}^0$  mixing in unquenched lattice QCD,” Phys. Rev. Lett. **91**, 212001 (2003) [arXiv:hep-ph/0307039].
- [128] B. Grinstein, E. Jenkins, A. V. Manohar, M. J. Savage and M. B. Wise, Nucl. Phys. B **380**, 369 (1992) [arXiv:hep-ph/9204207].
- [129] C. T. H. Davies *et al.* [HPQCD Collaboration], “High-precision lattice QCD confronts experiment,” arXiv:hep-lat/0304004.
- [130] S. Hashimoto, A. X. El-Khadra, A. S. Kronfeld, P. B. Mackenzie, S. M. Ryan and J. N. Simone, “Lattice QCD calculation of  $\bar{B} \rightarrow D l \bar{\nu}$  decay form factors at zero recoil,” Phys. Rev. D **61**, 014502 (2000) [arXiv:hep-ph/9906376].
- [131] S. Hashimoto, A. S. Kronfeld, P. B. Mackenzie, S. M. Ryan and J. N. Simone, “Lattice calculation of the zero recoil form factor of  $\bar{B} \rightarrow D^* l \bar{\nu}$ : Toward a model independent determination of  $|V_{cb}|$ ,” Phys. Rev. D **66**, 014503 (2002) [arXiv:hep-ph/0110253].
- [132] K. C. Bowler *et al.* [UKQCD Collaboration], “Improved  $B \rightarrow \pi l \nu_l$  form factors from the lattice,” Phys. Lett. B **486** (2000) 111 [arXiv:hep-lat/9911011].
- [133] A. Abada, D. Becirevic, P. Boucaud, J. P. Leroy, V. Lubicz and F. Mescia, “Heavy  $\rightarrow$  light semileptonic decays of pseudoscalar mesons from lattice QCD,” Nucl. Phys. B **619** (2001) 565 [arXiv:hep-lat/0011065].
- [134] A. X. El-Khadra, A. S. Kronfeld, P. B. Mackenzie, S. M. Ryan and J. N. Simone, “The semileptonic decays  $B \rightarrow \pi l \nu$  and  $D \rightarrow \pi l \nu$  from lattice QCD,” Phys. Rev. D **64** (2001) 014502 [arXiv:hep-ph/0101023].

- [135] S. Aoki *et al.* [JLQCD Collaboration], “Differential decay rate of  $B \rightarrow \pi l \nu$  semileptonic decay with lattice NRQCD,” *Phys. Rev. D* **64** (2001) 114505 [arXiv:hep-lat/0106024].
- [136] L. Lellouch, “Phenomenology from lattice QCD,” *Nucl. Phys. Proc. Suppl.* **117**, 127 (2003) [arXiv:hep-ph/0211359].
- [137] D. Becirevic, “Lattice results relevant to the CKM matrix determination,” arXiv:hep-ph/0211340.
- [138] A. S. Kronfeld, “Heavy quarks and lattice QCD,” arXiv:hep-lat/0310063.
- [139] S. Weinberg, “Implications Of Dynamical Symmetry Breaking,” *Phys. Rev. D* **13**, 974 (1976).
- [140] S. Weinberg, “Implications Of Dynamical Symmetry Breaking: An Addendum,” *Phys. Rev. D* **19** (1979) 1277.
- [141] L. Susskind, “Dynamics Of Spontaneous Symmetry Breaking In The Weinberg-Salam Theory,” *Phys. Rev. D* **20**, 2619 (1979).
- [142] A. G. Cohen, D. B. Kaplan and A. E. Nelson, “Progress in electroweak baryogenesis,” *Ann. Rev. Nucl. Part. Sci.* **43**, 27 (1993) [arXiv:hep-ph/9302210].
- [143] H. P. Nilles, “Supersymmetry, Supergravity And Particle Physics,” *Phys. Rept.* **110**, 1 (1984).
- [144] H. E. Haber and G. L. Kane, “The Search For Supersymmetry: Probing Physics Beyond The Standard Model,” *Phys. Rept.* **117**, 75 (1985).
- [145] C. T. Hill and E. H. Simmons, “Strong dynamics and electroweak symmetry breaking,” *Phys. Rept.* **381**, 235 (2003) [arXiv:hep-ph/0203079].
- [146] N. Arkani-Hamed, S. Dimopoulos and G. R. Dvali, “The hierarchy problem and new dimensions at a millimeter,” *Phys. Lett. B* **429**, 263 (1998) [arXiv:hep-ph/9803315].
- [147] L. Randall and R. Sundrum, “A large mass hierarchy from a small extra dimension,” *Phys. Rev. Lett.* **83**, 3370 (1999) [arXiv:hep-ph/9905221].
- [148] J. Hewett and M. Spiropulu, “Particle physics probes of extra spacetime dimensions,” *Ann. Rev. Nucl. Part. Sci.* **52**, 397 (2002) [arXiv:hep-ph/0205106].
- [149] N. Arkani-Hamed, A. G. Cohen and H. Georgi, “Electroweak symmetry breaking from dimensional deconstruction,” *Phys. Lett. B* **513**, 232 (2001) [arXiv:hep-ph/0105239].
- [150] H. Georgi and S. L. Glashow, “Unity Of All Elementary Particle Forces,” *Phys. Rev. Lett.* **32**, 438 (1974).
- [151] J. C. Pati and A. Salam, “Lepton Number As The Fourth Color,” *Phys. Rev. D* **10**, 275 (1974).
- [152] M. Dine, A. E. Nelson and Y. Shirman, “Low-energy dynamical supersymmetry breaking simplified,” *Phys. Rev. D* **51**, 1362 (1995) [arXiv:hep-ph/9408384].
- [153] M. Dine, A. E. Nelson, Y. Nir and Y. Shirman, “New tools for low-energy dynamical supersymmetry breaking,” *Phys. Rev. D* **53**, 2658 (1996) [arXiv:hep-ph/9507378].



- [154] M. Dine, Y. Nir and Y. Shirman, “Variations on minimal gauge mediated supersymmetry breaking,” *Phys. Rev. D* **55**, 1501 (1997) [arXiv:hep-ph/9607397].
- [155] D. E. Kaplan, G. D. Kribs and M. Schmaltz, “Supersymmetry breaking through transparent extra dimensions,” *Phys. Rev. D* **62**, 035010 (2000) [arXiv:hep-ph/9911293].
- [156] Z. Chacko, M. A. Luty, A. E. Nelson and E. Ponton, “Gaugino mediated supersymmetry breaking,” *JHEP* **0001**, 003 (2000) [arXiv:hep-ph/9911323].
- [157] M. Schmaltz and W. Skiba, “Minimal gaugino mediation,” *Phys. Rev. D* **62**, 095005 (2000) [arXiv:hep-ph/0001172].
- [158] L. Randall and R. Sundrum, “Out of this world supersymmetry breaking,” *Nucl. Phys. B* **557**, 79 (1999) [arXiv:hep-th/9810155].
- [159] G. F. Giudice, M. A. Luty, H. Murayama and R. Rattazzi, “Gaugino mass without singlets,” *JHEP* **9812**, 027 (1998) [arXiv:hep-ph/9810442].
- [160] L. J. Hall, V. A. Kostelecky and S. Raby, “New Flavor Violations In Supergravity Models,” *Nucl. Phys. B* **267**, 415 (1986).
- [161] Y. Nir and N. Seiberg, “Should squarks be degenerate?,” *Phys. Lett. B* **309**, 337 (1993) [arXiv:hep-ph/9304307].
- [162] M. Leurer, Y. Nir and N. Seiberg, “Mass matrix models: The Sequel,” *Nucl. Phys. B* **420**, 468 (1994) [arXiv:hep-ph/9310320].
- [163] M. Dine, A. Kagan and S. Samuel, “Naturalness In Supersymmetry, Or Raising The Supersymmetry Breaking Scale,” *Phys. Lett. B* **243**, 250 (1990).
- [164] M. Dine, R. G. Leigh and A. Kagan, “Flavor symmetries and the problem of squark degeneracy,” *Phys. Rev. D* **48**, 4269 (1993) [arXiv:hep-ph/9304299].
- [165] S. Dimopoulos and G. F. Giudice, “Naturalness constraints in supersymmetric theories with nonuniversal soft terms,” *Phys. Lett. B* **357**, 573 (1995) [arXiv:hep-ph/9507282].
- [166] A. Pomarol and D. Tommasini, “Horizontal symmetries for the supersymmetric flavor problem,” *Nucl. Phys. B* **466**, 3 (1996) [arXiv:hep-ph/9507462].
- [167] A. G. Cohen, D. B. Kaplan and A. E. Nelson, “The more minimal supersymmetric standard model,” *Phys. Lett. B* **388**, 588 (1996) [arXiv:hep-ph/9607394].
- [168] J. Hisano, K. Kurosawa and Y. Nomura, “Large squark and slepton masses for the first-two generations in the anomalous U(1) SUSY breaking models,” *Phys. Lett. B* **445**, 316 (1999) [arXiv:hep-ph/9810411].
- [169] J. Hisano, K. Kurosawa and Y. Nomura, “Natural effective supersymmetry,” *Nucl. Phys. B* **584**, 3 (2000) [arXiv:hep-ph/0002286].
- [170] T. Moroi, “CP violation in  $B_d \rightarrow \phi K_S$  in SUSY GUT with right-handed neutrinos,” *Phys. Lett. B* **493**, 366 (2000) [arXiv:hep-ph/0007328].
- [171] N. Akama, Y. Kiyo, S. Komine and T. Moroi, “CP violation in kaon system in supersymmetric SU(5) model with seesaw-induced neutrino masses,” *Phys. Rev. D* **64**, 095012 (2001) [arXiv:hep-ph/0104263].

- [172] S. Baek, T. Goto, Y. Okada and K. i. Okumura, “Muon anomalous magnetic moment, lepton flavor violation, and flavor changing neutral current processes in SUSY GUT with right-handed neutrino,” *Phys. Rev. D* **64**, 095001 (2001) [arXiv:hep-ph/0104146].
- [173] T. Goto, Y. Okada, Y. Shimizu, T. Shindou and M. Tanaka, “Exploring flavor structure of supersymmetry breaking at B factories,” *Phys. Rev. D* **66**, 035009 (2002) [arXiv:hep-ph/0204081].
- [174] T. Goto, Y. Okada, Y. Shimizu, T. Shindou and M. Tanaka, “Exploring flavor structure of supersymmetry breaking from rare B decays and unitarity triangle,” arXiv:hep-ph/0306093.
- [175] D. Chang, A. Masiero and H. Murayama, *Phys. Rev. D* **67**, 075013 (2003) [arXiv:hep-ph/0205111].
- [176] M. Ciuchini, E. Franco, A. Masiero and L. Silvestrini, *Phys. Rev. D* **67**, 075016 (2003) [Erratum-ibid. *D* **68**, 079901 (2003)] [arXiv:hep-ph/0212397].
- [177] J. Hisano and Y. Shimizu, “GUT relation in neutrino induced flavor physics in SUSY SU(5) GUT,” *Phys. Lett. B* **565**, 183 (2003) [arXiv:hep-ph/0303071].
- [178] M. Ciuchini, A. Masiero, L. Silvestrini, S. K. Vempati and O. Vives, “Grand unification of quark and lepton FCNCs,” arXiv:hep-ph/0307191.
- [179] F. Gabbiani, E. Gabrielli, A. Masiero and L. Silvestrini, “A complete analysis of FCNC and CP constraints in general SUSY extensions of the standard model,” *Nucl. Phys. B* **477**, 321 (1996) [arXiv:hep-ph/9604387].
- [180] M. Ciuchini *et al.*, “ $\Delta M_K$  and  $\epsilon_K$  in SUSY at the next-to-leading order,” *JHEP* **9810**, 008 (1998) [arXiv:hep-ph/9808328].
- [181] M. B. Causse and J. Orloff, “Supersymmetric penguin contributions to the decay  $b \rightarrow s\gamma$  with non-universal squarks masses,” *Eur. Phys. J. C* **23**, 749 (2002) [arXiv:hep-ph/0012113].
- [182] A. Masiero and O. Vives, “Flavour And CP Violation In Supersymmetry,” *New J. Phys.* **4**, 4 (2002).
- [183] G.L. Kane, P. Ko, H.B. Wang, C. Kolda, J.H. Park and L.T. Wang, “ $B_d \rightarrow \phi K_S$  CP asymmetries as an important probe of supersymmetry,” *Phys. Rev. Lett.* **90** (2003) 141803; [arXiv:hep-ph/0304239].
- [184] S. Mishima and A. I. Sanda, “An analysis of supersymmetric effects on  $B \rightarrow \phi K$  decays in PQCD approach,” arXiv:hep-ph/0311068.
- [185] S. Khalil and E. Kou, “On supersymmetric contributions to the CP asymmetry of the  $B \rightarrow \phi K_S$ ,” *Phys. Rev. D* **67** (2003) 055009 [arXiv:hep-ph/0212023].
- [186] A. Ali and C. Greub, “An analysis of two-body non-leptonic B decays involving light mesons in the standard model,” *Phys. Rev. D* **57** (1998) 2996; [arXiv:hep-ph/9707251].
- [187] B. Aubert *et al.* [BABAR Collaboration], “Observation of B meson decays to  $\eta\pi$  and  $\eta K$ ,” arXiv:hep-ex/0303039.
- [188] S. Khalil and E. Kou, “A possible supersymmetric solution to the discrepancy between  $B \rightarrow \phi K_S$  and  $B \rightarrow \eta' K_S$  CP asymmetries,” *Phys. Rev. Lett.* **91**, 241602 (2003) [arXiv:hep-ph/0303214].

- [189] A. Ali, G. F. Giudice and T. Mannel, “Towards a model independent analysis of rare  $B$  decays,” *Z. Phys. C* **67**, 417 (1995) [arXiv:hep-ph/9408213].
- [190] S. Fukae, C. S. Kim, T. Morozumi and T. Yoshikawa, “A model independent analysis of the rare  $B$  decay  $B \rightarrow X_s l^+ l^-$ ,” *Phys. Rev. D* **59**, 074013 (1999) [arXiv:hep-ph/9807254].
- [191] S. Fukae, C. S. Kim and T. Yoshikawa, “The effects of non-local operators in rare  $B$  decays,  $B \rightarrow X_s l^+ l^-$ ,” *Int. J. Mod. Phys. A* **16**, 1703 (2001) [arXiv:hep-ph/0003053].
- [192] G. Hiller and F. Kruger, “More model-independent analysis of  $b \rightarrow s$  processes,” arXiv:hep-ph/0310219.
- [193] G. Senjanovic and R. N. Mohapatra, “Exact Left-Right Symmetry And Spontaneous Violation Of Parity,” *Phys. Rev. D* **12**, 1502 (1975).
- [194] K. Fujikawa and A. Yamada, “Test of the chiral structure of the top – bottom charged current by the process  $b \rightarrow s\gamma$ ,” *Phys. Rev. D* **49**, 5890 (1994).
- [195] K. S. Babu, K. Fujikawa and A. Yamada, “Constraints on left-right symmetric models from the process  $b \rightarrow s\gamma$ ,” *Phys. Lett. B* **333**, 196 (1994) [arXiv:hep-ph/9312315].
- [196] P. L. Cho and M. Misiak, “ $b \rightarrow s\gamma$  Decay In  $SU(2)_L \times SU(2)_R \times U(1)$  Extensions Of The Standard Model,” *Phys. Rev. D* **49**, 5894 (1994) [arXiv:hep-ph/9310332].
- [197] D. Atwood, M. Gronau and A. Soni, “Mixing-induced CP asymmetries in radiative  $B$  decays in and beyond the standard model,” *Phys. Rev. Lett.* **79**, 185 (1997) [arXiv:hep-ph/9704272].
- [198] D. Melikhov, N. Nikitin and S. Simula, “Probing right-handed currents in  $B \rightarrow K^* l^+ l^-$  transitions,” *Phys. Lett. B* **442**, 381 (1998) [arXiv:hep-ph/9807464].
- [199] F. Kruger, L. M. Sehgal, N. Sinha and R. Sinha, “Angular distribution and CP asymmetries in the decays  $\bar{B} \rightarrow K^- \pi^+ e^- e^+$  and  $\bar{B} \rightarrow \pi^- \pi^+ e^- e^+$ ,” *Phys. Rev. D* **61**, 114028 (2000) [Erratum-ibid. *D* **63**, 019901 (2001)] [arXiv:hep-ph/9907386].
- [200] C. S. Kim, Y. G. Kim, C. D. Lu and T. Morozumi, “Azimuthal angle distribution in  $B \rightarrow K^*(\rightarrow K\pi) l^+ l^-$  at low invariant  $m_{l^+ l^-}$  region,” *Phys. Rev. D* **62**, 034013 (2000) [arXiv:hep-ph/0001151].
- [201] M. Gronau, Y. Grossman, D. Pirjol and A. Ryd, “Measuring the photon helicity in radiative  $B$  decays,” *Phys. Rev. Lett.* **88**, 051802 (2002) [arXiv:hep-ph/0107254].
- [202] M. Gronau and D. Pirjol, “Photon polarization in radiative  $B$  decays,” *Phys. Rev. D* **66**, 054008 (2002) [arXiv:hep-ph/0205065].
- [203] C. Bobeth, M. Misiak and J. Urban, “Photonic penguins at two loops and  $m_t$ -dependence of  $BR(B \rightarrow X_s l^+ l^-)$ ,” *Nucl. Phys. B* **574**, 291 (2000) [arXiv:hep-ph/9910220].
- [204] H. H. Asatrian, H. M. Asatrian, C. Greub and M. Walker, “Two-loop virtual corrections to  $B \rightarrow X_s l^+ l^-$  in the standard model,” *Phys. Lett. B* **507**, 162 (2001) [arXiv:hep-ph/0103087].
- [205] Z. Xiong and J. M. Yang, “Rare  $B$ -Meson Dileptonic Decays In Minimal Supersymmetric Model,” *Nucl. Phys. B* **628**, 193 (2002) [arXiv:hep-ph/0105260].

- [206] T. Goto, Y. Okada, Y. Shimizu and M. Tanaka, “ $b \rightarrow s\bar{l}l$  in the minimal supergravity model,” Phys. Rev. D **55**, 4273 (1997) [Erratum-ibid. D **66**, 019901 (2002)] [arXiv:hep-ph/9609512].
- [207] G. Buchalla, G. Hiller and G. Isidori, “Phenomenology of non-standard  $Z$  couplings in exclusive semileptonic  $b \rightarrow s$  transitions,” Phys. Rev. D **63**, 014015 (2001) [arXiv:hep-ph/0006136].
- [208] Y. Fukuda *et al.* [Super-Kamiokande Collaboration], “Evidence for oscillation of atmospheric neutrinos,” Phys. Rev. Lett. **81**, 1562 (1998) [arXiv:hep-ex/9807003].
- [209] M. H. Ahn *et al.* [K2K Collaboration], “Indications of neutrino oscillation in a 250-km long-baseline experiment,” Phys. Rev. Lett. **90**, 041801 (2003) [arXiv:hep-ex/0212007].
- [210] S. Fukuda *et al.* [Super-Kamiokande Collaboration], Phys. Rev. Lett. **86**, 5651 (2001) [arXiv:hep-ex/0103032].
- [211] Q. R. Ahmad *et al.* [SNO Collaboration], “Direct evidence for neutrino flavor transformation from neutral-current interactions in the Sudbury Neutrino Observatory,” Phys. Rev. Lett. **89**, 011301 (2002) [arXiv:nucl-ex/0204008].
- [212] Q. R. Ahmad *et al.* [SNO Collaboration], “Measurement of day and night neutrino energy spectra at SNO and constraints on neutrino mixing parameters,” Phys. Rev. Lett. **89**, 011302 (2002) [arXiv:nucl-ex/0204009].
- [213] K. Eguchi *et al.* [KamLAND Collaboration], “First results from KamLAND: Evidence for reactor anti-neutrino disappearance,” Phys. Rev. Lett. **90**, 021802 (2003) [arXiv:hep-ex/0212021].
- [214] K. S. Babu and C. Kolda, “Higgs-mediated  $\tau \rightarrow 3\mu$  in the supersymmetric seesaw model,” Phys. Rev. Lett. **89**, 241802 (2002) [arXiv:hep-ph/0206310].
- [215] A. Dedes, J. R. Ellis and M. Raidal, “Higgs mediated  $B_{s,d}^0 \rightarrow \mu\tau$ ,  $e\tau$  and  $\tau \rightarrow 3\mu$ ,  $e\mu\mu$  decays in supersymmetric seesaw models,” Phys. Lett. B **549** (2002) 159 [arXiv:hep-ph/0209207].
- [216] M. Sher, “ $\tau \rightarrow \mu\eta$  in supersymmetric models,” Phys. Rev. D **66**, 057301 (2002) [arXiv:hep-ph/0207136].
- [217] J. Hisano and Y. Shimizu, in preparation.
- [218] R. Barbieri and L. J. Hall, “Signals for supersymmetric unification,” Phys. Lett. B **338**, 212 (1994) [arXiv:hep-ph/9408406].
- [219] R. Barbieri, L. J. Hall and A. Strumia, “Violations of lepton flavor and CP in supersymmetric unified theories,” Nucl. Phys. B **445**, 219 (1995) [arXiv:hep-ph/9501334].
- [220] J. Hisano, T. Moroi, K. Tobe and M. Yamaguchi, “Exact event rates of lepton flavor violating processes in supersymmetric SU(5) model,” Phys. Lett. B **391**, 341 (1997) [Erratum-ibid. B **397**, 357 (1997)] [arXiv:hep-ph/9605296].
- [221] F. Borzumati and A. Masiero, “Large Muon And Electron Number Violations In Supergravity Theories,” Phys. Rev. Lett. **57**, 961 (1986).

- [222] J. Hisano, T. Moroi, K. Tobe, M. Yamaguchi and T. Yanagida, “Lepton flavor violation in the supersymmetric standard model with seesaw induced neutrino masses,” *Phys. Lett. B* **357**, 579 (1995) [arXiv:hep-ph/9501407].
- [223] J. Hisano, T. Moroi, K. Tobe and M. Yamaguchi, “Lepton-Flavor Violation via Right-Handed Neutrino Yukawa Couplings in Supersymmetric Standard Model,” *Phys. Rev. D* **53**, 2442 (1996) [arXiv:hep-ph/9510309].
- [224] J. A. Casas and A. Ibarra, “Oscillating neutrinos and  $\mu \rightarrow e\gamma$ ,” *Nucl. Phys. B* **618**, 171 (2001) [arXiv:hep-ph/0103065].
- [225] J. R. Ellis, J. Hisano, M. Raidal and Y. Shimizu, “A new parametrization of the seesaw mechanism and applications in supersymmetric models,” *Phys. Rev. D* **66**, 115013 (2002) [arXiv:hep-ph/0206110].
- [226] N. Arkani-Hamed, H. C. Cheng and L. J. Hall, “Flavor mixing signals for realistic supersymmetric unification,” *Phys. Rev. D* **53**, 413 (1996) [arXiv:hep-ph/9508288].
- [227] J. Hisano, D. Nomura, Y. Okada, Y. Shimizu and M. Tanaka, “Enhancement of  $\mu \rightarrow e\gamma$  in the supersymmetric SU(5) GUT at large  $\tan\beta$ ,” *Phys. Rev. D* **58**, 116010 (1998) [arXiv:hep-ph/9805367].
- [228] N. Arkani-Hamed, S. Dimopoulos, G. R. Dvali and J. March-Russell, “Neutrino masses from large extra dimensions,” *Phys. Rev. D* **65**, 024032 (2002) [arXiv:hep-ph/9811448].
- [229] K. R. Dienes, E. Dudas and T. Gherghetta, “Light neutrinos without heavy mass scales: A higher-dimensional seesaw mechanism,” *Nucl. Phys. B* **557**, 25 (1999) [arXiv:hep-ph/9811428].
- [230] Y. Grossman and M. Neubert, “Neutrino masses and mixings in non-factorizable geometry,” *Phys. Lett. B* **474**, 361 (2000) [arXiv:hep-ph/9912408].
- [231] A. E. Faraggi and M. Pospelov, “Phenomenological issues in TeV scale gravity with light neutrino masses,” *Phys. Lett. B* **458**, 237 (1999) [arXiv:hep-ph/9901299].
- [232] A. De Gouvea, G. F. Giudice, A. Strumia and K. Tobe, “Phenomenological implications of neutrinos in extra dimensions,” *Nucl. Phys. B* **623**, 395 (2002) [arXiv:hep-ph/0107156].
- [233] J. P. Saha and A. Kundu, “Constraints on R-parity violating supersymmetry from leptonic and semileptonic  $\tau$ ,  $B_d$  and  $B_s$  decays,” *Phys. Rev. D* **66**, 054021 (2002) [arXiv:hep-ph/0205046].
- [234] A. Ilakovac and A. Pilaftsis, “Flavor violating charged lepton decays in a GUT and superstring inspired standard model,” *Nucl. Phys. B* **437** (1995) 491 [arXiv:hep-ph/9403398].
- [235] G. Cvetič, C. Dib, C. S. Kim and J. D. Kim, “On lepton flavor violation in tau decays,” *Phys. Rev. D* **66**, 034008 (2002) [Erratum-ibid. *D* **68**, 059901 (2003)] [arXiv:hep-ph/0202212].
- [236] H. Tajima *et al.*, “Proper-time resolution function for measurement of time evolution of  $B$  mesons at the KEK B-factory,” arXiv:hep-ex/0301026.
- [237] T. Matsumoto, “Tagging with fully reconstructed  $B$ ’s in  $B$ -factory experiments,” ACAT03 conference, Dec. 1-5, 2003, KEK, Japan.

- [238] B. Aubert *et al.* [BABAR Collaboration], “Measurement of the inclusive charmless semileptonic branching ratio of  $B$  mesons and determination of  $|V_{ub}|$ ,” Phys. Rev. Lett. **92**, 071802 (2004) [arXiv:hep-ex/0307062].
- [239] del Re, Daniele, “Measurement of  $V_{ub}$  studying inclusive semileptonic decays on the recoil of fully reconstructed  $B$ ’s with the BaBar experiment Ph.D. thesis, Dec. 5, 2002.
- [240] A. Sugiyama, “ $B \rightarrow X_u l \nu$  measurement using the pseudo full reconstruction of  $\Upsilon(4s)$  at BELLE,” Belle Note No. 509.
- [241] B. Aubert *et al.* [BABAR Collaboration], “A search for  $B^+ \rightarrow K^+ \nu \bar{\nu}$ . ((B)),” arXiv:hep-ex/0207069.
- [242] B. Aubert *et al.* [BABAR Collaboration], “A search for  $B^+ \rightarrow^t a u^+ \nu_\tau$  recoiling against  $B^- \rightarrow D^0 l^- \nu_l X$ ,” arXiv:hep-ex/0303034.
- [243] For a recent review, see for example, Y. Nir, “CP violation: The CKM matrix and new physics,” Nucl. Phys. Proc. Suppl. **117**, 111 (2003) [arXiv:hep-ph/0208080].
- [244] S. Baek, T. Goto, Y. Okada and K. i. Okumura, “Neutrino oscillation, SUSY GUT and B decay,” Phys. Rev. D **63**, 051701 (2001) [arXiv:hep-ph/0002141].
- [245] For a recent review, see for example, W. Bernreuther, “CP violation and baryogenesis,” Lect. Notes Phys. **591**, 237 (2002) [arXiv:hep-ph/0205279].
- [246] Heavy Flavor Averaging Group, <http://www.slac.stanford.edu/xorg/hfag/>.
- [247] T. E. Browder, “Results on the CKM angle  $\phi_1$  ( $\beta$ ),” arXiv:hep-ex/0312024; B. Aubert *et al.* (BaBar Collaboration), BABAR-PLOT-0053; A. Farbin (BaBar Collaboration), poster presented at Lepton Photon 2003.
- [248] T. Gershon and M. Hazumi, “Time-dependent CP violation in  $B^0 \rightarrow P^0 P^0 X^0$  decays,” arXiv:hep-ph/0402097.
- [249] M. Ciuchini, E. Franco, G. Martinelli, A. Masiero and L. Silvestrini, “CP violating B decays in the standard model and supersymmetry,” Phys. Rev. Lett. **79**, 978 (1997) [arXiv:hep-ph/9704274].
- [250] Y. Chao *et al.* [Belle Collaboration], “Improved measurements of branching fractions for  $B \rightarrow K\pi$ ,  $\pi\pi$  and  $K\bar{K}$  decays,” arXiv:hep-ex/0311061.
- [251] M. Hazumi, “Large direct CP violation in  $B \rightarrow \phi\phi X_s$  decays,” Phys. Lett. B **583**, 285 (2004) [arXiv:hep-ph/0303089].
- [252] F. Fang *et al.* [Belle Collaboration], “Measurement of branching fractions for  $B \rightarrow \eta_c K^*$  decays,” Phys. Rev. Lett. **90**, 071801 (2003) [arXiv:hep-ex/0208047].
- [253] H. C. Huang *et al.* [Belle Collaboration], Phys. Rev. Lett. **91**, 241802 (2003).
- [254] N. G. Deshpande and J. Trampetic, “Exclusive and semiinclusive  $B$  decays based on  $b \rightarrow s\eta_c$  transition,” Phys. Lett. B **339**, 270 (1994) [arXiv:hep-ph/9406393].
- [255] M. Gourdin, Y. Y. Keum and X. Y. Pham, “Testing factorization in color suppressed beauty decays with the  $B \rightarrow \eta_c + K(K^*)$  modes,” Phys. Rev. D **51**, 3510 (1995) [arXiv:hep-ph/9409221].

- [256] M. R. Ahmady and E. Kou, “Combined  $B \rightarrow X_s \psi$  and  $B \rightarrow X_s \eta_c$  decays as a test of factorization,” *Eur. Phys. J. C* **1**, 243 (1998) [arXiv:hep-ph/9701224].
- [257] “The Belle detector,” *Nucl. Instrum. Meth. A* **479**, 117 (2002).
- [258] H. M. Asatrian, K. Bieri, C. Greub and A. Hovhannisyan, “NNLL corrections to the angular distribution and to the forward-backward asymmetries in  $b \rightarrow X_s l^+ l^-$ ,” *Phys. Rev. D* **66**, 094013 (2002) [arXiv:hep-ph/0209006].
- [259] A. Ali, G. Hiller, L. T. Handoko and T. Morozumi, “Power corrections in the decay rate and distributions in  $B \rightarrow X_s l^+ l^-$  in the standard model,” *Phys. Rev. D* **55**, 4105 (1997) [arXiv:hep-ph/9609449].
- [260] C. S. Lim, T. Morozumi and A. I. Sanda, “A Prediction For  $d\Gamma(B \rightarrow sl\bar{l})/dQ^2$  Including The Long Distance Effects,” *Phys. Lett. B* **218**, 343 (1989).
- [261] Y. Wang and D. Atwood, “Rate difference between  $b \rightarrow s\mu^+\mu^-$  and  $b \rightarrow se^+e^-$  in SUSY with large  $\tan\beta$ ,” *Phys. Rev. D* **68**, 094016 (2003) [arXiv:hep-ph/0304248].
- [262] T. Hurth, E. Lunghi and W. Porod, “Untagged  $B \rightarrow X_s \gamma$  CP asymmetry as a probe for new physics,” arXiv:hep-ph/0312260.
- [263] A. G. Akeroyd, Y. Y. Keum and S. Recksiegel, “Effect of supersymmetric phases on the direct CP asymmetry of  $B \rightarrow X_d \gamma$ ,” *Phys. Lett. B* **507**, 252 (2001) [arXiv:hep-ph/0103008].
- [264] A. G. Akeroyd and S. Recksiegel, “Direct CP asymmetry of  $B \rightarrow X_{d,s} \gamma$  in a model with vector quarks,” *Phys. Lett. B* **525**, 81 (2002) [arXiv:hep-ph/0109091].
- [265] L. T. Handoko and T. Morozumi, “ $b \rightarrow s(d)\gamma$  with a vector - like quark as fourth generation,” *Mod. Phys. Lett. A* **10**, 309 (1995) [Erratum-ibid. A **10**, 1733 (1995)] [arXiv:hep-ph/9409240].
- [266] A. Arhrib, C. K. Chua and W. S. Hou, “Supersymmetric model contributions to  $B_d^0 - \bar{B}_d^0$  mixing and  $B \rightarrow \pi\pi, \rho\gamma$  decays,” *Eur. Phys. J. C* **21**, 567 (2001) [arXiv:hep-ph/0104122].
- [267] G. Buchalla and A. J. Buras, “QCD corrections to rare K and B decays for arbitrary top quark mass,” *Nucl. Phys. B* **400**, 225 (1993).
- [268] Y. Grossman, Z. Ligeti and E. Nardi, “First limit on inclusive  $B \rightarrow X_s \nu \bar{\nu}$  decay and constraints on new physics,” *Nucl. Phys. B* **465**, 369 (1996) [Erratum-ibid. B **480**, 753 (1996)] [arXiv:hep-ph/9510378].
- [269] P. Colangelo, F. De Fazio, P. Santorelli and E. Scrimieri, “Rare  $B \rightarrow K^{(*)} \nu \bar{\nu}$  decays at B factories,” *Phys. Lett. B* **395**, 339 (1997) [arXiv:hep-ph/9610297].
- [270] R. Barate *et al.* [ALEPH Collaboration], “Measurements of  $BR(b \rightarrow \tau^- \bar{\nu}_\tau X)$  and  $BR(b \rightarrow \tau^- \bar{\nu}_\tau D^{*\pm} X)$  and upper limits on  $BR(B^- \rightarrow \tau^- \bar{\nu}_\tau)$  and  $BR(b \rightarrow s \nu \bar{n} u)$ ,” *Eur. Phys. J. C* **19**, 213 (2001) [arXiv:hep-ex/0010022].
- [271] T. E. Browder *et al.* [CLEO Collaboration], *Phys. Rev. Lett.* **86**, 2950 (2001) [arXiv:hep-ex/0007057].
- [272] B. Aubert *et al.* [BABAR Collaboration], “A Search for the decay  $B^- \rightarrow K^- \nu \bar{\nu}$ ,” arXiv:hep-ex/0304020.

- [273] W. S. Hou, Phys. Rev. D **48**, 2342 (1993)
- [274] A. G. Akeroyd and S. Recksiegel, J. Phys. G **29**, 2311 (2003)
- [275] D. Guetta and E. Nardi, Phys. Rev. D **58**, 012001 (1998) S. Baek and Y. G. Kim, Phys. Rev. D **60**, 077701 (1999) A. G. Akeroyd and S. Recksiegel, Phys. Lett. B **541**, 121 (2002)
- [276] M. Tanaka, “Charged Higgs effects on exclusive semitauonic  $B$  decays,” Z. Phys. C **67**, 321 (1995) [arXiv:hep-ph/9411405].
- [277] T. Miki, T. Miura and M. Tanaka, “Effects of charged Higgs boson and QCD corrections in  $\bar{B} \rightarrow D\tau\bar{\nu}_\tau$ ,” arXiv:hep-ph/0210051.
- [278] I. Caprini, L. Lellouch and M. Neubert, “Dispersive bounds on the shape of  $\bar{B} \rightarrow D^{(*)}l\nu$  form factors,” Nucl. Phys. B **530**, 153 (1998) [arXiv:hep-ph/9712417].
- [279] K. Abe *et al.* [Belle Collaboration], “Determination of  $|V_{cb}|$  from the semileptonic decay  $\bar{B}^0 \rightarrow D^{*+}l^-\bar{\nu}$ ,” KEK-PREPRINT-2001-82 *Prepared for 20th International Symposium on Lepton and Photon Interactions at High Energies (LP 01), Rome, Italy, 23-28 Jul 2001.*
- [280] O. Long, M. Baak, R. N. Cahn and D. Kirkby, “Impact of tag-side interference on time dependent CP asymmetry measurements using coherent  $B^0\bar{B}^0$  pairs,” Phys. Rev. D **68**, 034010 (2003) [arXiv:hep-ex/0303030].
- [281] K. Abe *et al.* [Belle Collaboration], “Observation of large CP violation and evidence for direct CP violation in  $B^0 \rightarrow \pi^+\pi^-\pi^0$  decays,” [arXiv:hep-ex/0401029].
- [282] B. Aubert *et al.* [BABAR Collaboration], “Measurements of branching fractions and CP-violating asymmetries in  $B^0 \rightarrow \pi^+\pi^-, K^+\pi^-, K^+K^-$  decays. ((B)),” Phys. Rev. Lett. **89**, 281802 (2002) [arXiv:hep-ex/0207055];
- [283] Y. Y. Keum and A. I. Sanda, “Possible large direct CP violations in charmless B decays: Summary report on the pQCD method. ((U)),” Phys. Rev. D **67**, 054009 (2003) [arXiv:hep-ph/0209014]; Y.-Y. Keum, private communication.
- [284] The CKMfitter site on the web: <http://ckmfitter.in2p3.fr/>.
- [285] C. Lü, K. Ukai and M. Yang, “Branching ratio and CP violation of  $B \rightarrow \pi\pi$  decays in the perturbative QCD approach,” Phys. Rev. D **63**, 074009 (2001) [arXiv:hep-ph/0004213].
- [286] B. Aubert *et al.* [BABAR Collaboration], “Measurements of branching fractions and CP-violating asymmetries in  $B^0 \rightarrow \rho^\pm h^\mp$  decays,” Phys. Rev. Lett. **91**, 201802 (2003) [arXiv:hep-ex/0306030].
- [287] H. J. Lipkin, Y. Nir, H. R. Quinn and A. Snyder, “Penguin trapping with isospin analysis and CP asymmetries in B decays,” Phys. Rev. D **44**, 1454 (1991).
- [288] J. Stark, “ $B^0 \rightarrow \pi^+\pi^-\pi^0$  feasibility studies,” eConf **C0304052**, WG423 (2003) [arXiv:hep-ph/0307032].
- [289] T. R. Sarangi, K. Abe *et al.* [Belle Collaboration], “Study of CP violating effects in time dependent  $B^0(\bar{B}^0) \rightarrow D^{(*)\mp}\pi^\pm$  decays,” [arXiv:hep-ex/0308048].
- [290] M. Gronau and D. London., “How To Determine All The Angles Of The Unitarity Triangle From  $B_d^0 \rightarrow DK_S$  And  $B_s^0 \rightarrow D^0$ ,” Phys. Lett. B **253**, 483 (1991).



- [291] M. Gronau and D. Wyler, “On determining a weak phase from CP asymmetries in charged  $B$  decays,” Phys. Lett. B **265**, 172 (1991).
- [292] D. Atwood, I. Dunietz and A. Soni, “Enhanced CP violation with  $B \rightarrow KD^0(\bar{D}^0)$  modes and extraction of the CKM angle  $\gamma$ ,” Phys. Rev. Lett. **78**, 3257 (1997) [arXiv:hep-ph/9612433].
- [293] D. Atwood, I. Dunietz and A. Soni, “Improved methods for observing CP violation in  $B^\pm \rightarrow KD$  and measuring the CKM phase  $\gamma$ ,” Phys. Rev. D **63**, 036005 (2001) [arXiv:hep-ph/0008090].
- [294] A. Giri, Y. Grossman, A. Soffer and J. Zupan, “Determining  $\gamma$  using  $B^\pm \rightarrow DK^\pm$  with multibody  $D$  decays,” Phys. Rev. D **68**, 054018 (2003) [arXiv:hep-ph/0303187].
- [295] H. Muramatsu *et al.* [CLEO Collaboration], “Dalitz analysis of  $D^0 \rightarrow K_S^0 \pi^+ \pi^-$ . ((B)),” Phys. Rev. Lett. **89**, 251802 (2002) [Erratum-ibid. **90**, 059901 (2003)] [arXiv:hep-ex/0207067].
- [296] M. Neubert, “QCD based interpretation of the lepton spectrum in inclusive  $\bar{B} \rightarrow X_u l \bar{\nu}$  decays,” Phys. Rev. D **49**, 3392 (1994) [arXiv:hep-ph/9311325].
- [297] T. Mannel and M. Neubert, “Resummation of nonperturbative corrections to the lepton spectrum in inclusive  $B \rightarrow X l \bar{\nu}$  decays,” Phys. Rev. D **50**, 2037 (1994) [arXiv:hep-ph/9402288].
- [298] I. I. Y. Bigi, M. A. Shifman, N. G. Uraltsev and A. I. Vainshtein, “On the motion of heavy quarks inside hadrons: Universal distributions and inclusive decays,” Int. J. Mod. Phys. A **9**, 2467 (1994) [arXiv:hep-ph/9312359].
- [299] M. Neubert, “Analysis of the photon spectrum in inclusive  $B \rightarrow X_s \gamma$  decays,” Phys. Rev. D **49**, 4623 (1994) [arXiv:hep-ph/9312311].
- [300] A. K. Leibovich, I. Low and I. Z. Rothstein, “Extracting  $V_{ub}$  without recourse to structure functions,” Phys. Rev. D **61**, 053006 (2000) [arXiv:hep-ph/9909404].
- [301] M. Neubert, “Note on the extraction of  $|V_{ub}|$  using radiative B decays,” Phys. Lett. B **513**, 88 (2001) [arXiv:hep-ph/0104280].
- [302] C. W. Bauer, M. E. Luke and T. Mannel, “Light-cone distribution functions for  $B$  decays at subleading order in  $1/m_b$ ,” Phys. Rev. D **68**, 094001 (2003) [arXiv:hep-ph/0102089].
- [303] C. W. Bauer, M. Luke and T. Mannel, “Subleading shape functions in  $B \rightarrow X_u l \bar{n} u$  and the determination of  $|V_{ub}|$ ,” Phys. Lett. B **543**, 261 (2002) [arXiv:hep-ph/0205150].
- [304] A. K. Leibovich, Z. Ligeti and M. B. Wise, “Enhanced subleading structure functions in semileptonic  $B$  decay,” Phys. Lett. B **539**, 242 (2002) [arXiv:hep-ph/0205148].
- [305] M. Neubert, “Subleading shape functions and the determination of  $|V_{ub}|$ ,” Phys. Lett. B **543**, 269 (2002) [arXiv:hep-ph/0207002].
- [306] I. I. Y. Bigi and N. G. Uraltsev, “Weak annihilation and the endpoint spectrum in semileptonic  $B$  decays,” Nucl. Phys. B **423**, 33 (1994) [arXiv:hep-ph/9310285].

- [307] M. B. Voloshin, “Nonfactorization effects in heavy mesons and determination of  $|V_{ub}|$  from inclusive semileptonic  $B$  decays,” Phys. Lett. B **515**, 74 (2001) [arXiv:hep-ph/0106040].
- [308] A. F. Falk, Z. Ligeti and M. B. Wise, “ $V_{ub}$  from the hadronic invariant mass spectrum in semileptonic  $B$  decay,” Phys. Lett. B **406**, 225 (1997) [arXiv:hep-ph/9705235].
- [309] R. D. Dikeman and N. G. Uraltsev, “Key distributions for charmless semileptonic  $B$  decay,” Nucl. Phys. B **509**, 378 (1998) [arXiv:hep-ph/9703437].
- [310] I. I. Y. Bigi, R. D. Dikeman and N. Uraltsev, “The hadronic recoil mass spectrum in semileptonic  $B$  decays and extracting  $|V_{ub}|$  in a model-insensitive way,” Eur. Phys. J. C **4**, 453 (1998) [arXiv:hep-ph/9706520].
- [311] A. K. Leibovich, I. Low and I. Z. Rothstein, “On the resummed hadronic spectra of inclusive  $B$  decays,” Phys. Rev. D **62**, 014010 (2000) [arXiv:hep-ph/0001028].
- [312] A. K. Leibovich, I. Low and I. Z. Rothstein, “Extracting  $|V_{ub}|$  from the hadronic mass spectrum of inclusive  $B$  decays,” Phys. Lett. B **486**, 86 (2000) [arXiv:hep-ph/0005124].
- [313] C. W. Bauer, Z. Ligeti and M. E. Luke, “A model independent determination of  $|V_{ub}|$ ,” Phys. Lett. B **479**, 395 (2000) [arXiv:hep-ph/0002161].
- [314] M. Neubert, “On the inclusive determination of  $|V_{ub}|$  from the lepton invariant mass spectrum,” JHEP **0007**, 022 (2000) [arXiv:hep-ph/0006068].
- [315] C. W. Bauer, Z. Ligeti and M. E. Luke, “Precision determination of  $|V_{ub}|$  from inclusive decays,” Phys. Rev. D **64**, 113004 (2001) [arXiv:hep-ph/0107074].
- [316] G. Burdman, Z. Ligeti, M. Neubert and Y. Nir, “The Decay  $B \rightarrow \pi l \nu$  in heavy quark effective theory,” Phys. Rev. D **49**, 2331 (1994) [arXiv:hep-ph/9309272].
- [317] J. Shigemitsu, S. Collins, C. T. H. Davies, J. Hein, R. R. Horgan and G. P. Lepage, “Semileptonic  $B$  decays from an NRQCD/D234 action,” Phys. Rev. D **66**, 074506 (2002) [arXiv:hep-lat/0207011].
- [318] S. Aoki *et al.* [JLQCD Collaboration], “Light hadron spectroscopy with two flavors of  $O(a)$ -improved dynamical quarks,” Phys. Rev. D **68**, 054502 (2003) [arXiv:hep-lat/0212039].
- [319] A. Khodjamirian and R. Ruckl, “QCD sum rules for exclusive decays of heavy mesons,” Adv. Ser. Direct. High Energy Phys. **15**, 345 (1998) [arXiv:hep-ph/9801443].
- [320] P. Ball, “ $B \rightarrow \pi$  and  $B \rightarrow K$  transitions from QCD sum rules on the light-cone,” JHEP **9809**, 005 (1998) [arXiv:hep-ph/9802394].
- [321] A. Khodjamirian, R. Ruckl, S. Weinzierl, C. W. Winhart and O. I. Yakovlev, “Predictions on  $B \rightarrow \pi l \nu_l$ ,  $D \rightarrow \pi l \nu_l$  and  $D \rightarrow K l \nu_l$  from QCD light-cone sum rules,” Phys. Rev. D **62**, 114002 (2000) [arXiv:hep-ph/0001297].
- [322] P. Ball and R. Zwicky, “Improved analysis of  $B \rightarrow \pi e \nu$  from QCD sum rules on the light-cone,” JHEP **0110**, 019 (2001) [arXiv:hep-ph/0110115].
- [323] L. Lellouch, “Lattice-Constrained Unitarity Bounds for  $\bar{B}^0 \rightarrow \pi^+ \ell^- \bar{\nu}_\ell$  Decays,” Nucl. Phys. B **479**, 353 (1996) [arXiv:hep-ph/9509358].

- [324] K. C. Bowler, J. F. Gill, C. M. Maynard and J. M. Flynn, “ $B \rightarrow \rho l \nu$  form factors in lattice QCD,” arXiv:hep-lat/0402023.
- [325] A. Abada, D. Becirevic, P. Boucaud, . M. Flynn, . P. Leroy, V. Lubicz and F. Mescia [SPQcdR collaboration], “Heavy to light vector meson semileptonic decays,” Nucl. Phys. Proc. Suppl. **119**, 625 (2003) [arXiv:hep-lat/0209116].
- [326] H. Kakuno *et al.* [BELLE Collaboration], “Measurement of  $|V_{ub}|$  using inclusive  $B \rightarrow X_u l \nu$  decays with a novel X/u reconstruction method,” arXiv:hep-ex/0311048.
- [327] C. W. Bauer, Z. Ligeti, M. Luke and A. V. Manohar, “ $B$  decay shape variables and the precision determination of  $|V_{cb}|$  and  $m_b$ ,” Phys. Rev. D **67**, 054012 (2003) [arXiv:hep-ph/0210027].
- [328] J. P. Alexander *et al.* [CLEO Collaboration], “First measurement of the  $B \rightarrow \pi l \nu$  and  $B \rightarrow \rho(\omega) l \nu$  branching fractions,” Phys. Rev. Lett. **77**, 5000 (1996).
- [329] B. H. Behrens *et al.* [CLEO Collaboration], “Measurement of  $B \rightarrow \rho l \nu$  decay and  $|V_{ub}|$ ,” Phys. Rev. D **61**, 052001 (2000) [arXiv:hep-ex/9905056].
- [330] B. Aubert *et al.* [BABAR Collaboration], “Measurement of the CKM matrix element  $|V_{ub}|$  with  $B \rightarrow \rho e \nu$  decays. ((B)),” Phys. Rev. Lett. **90**, 181801 (2003) [arXiv:hep-ex/0301001].
- [331] S. B. Athar *et al.* [CLEO Collaboration], Phys. Rev. D **68**, 072003 (2003) [arXiv:hep-ex/0304019].
- [332] C. Schwanda [BELLE Collaboration], “Evidence for  $B^+ \rightarrow \omega l^+ \nu$ ,” eConf **C0304052**, WG116 (2003) [arXiv:hep-ex/0306059].
- [333] K. Abe *et al.* [Belle Collaboration], “Evidence for  $B^+ \rightarrow \omega l^+ \nu$ ,” arXiv:hep-ex/0307075.
- [334] A. Sugiyama [BELLE Collaboration], “Measurements of  $|V_{ub}|$  at BELLE,” arXiv:hep-ex/0306020.
- [335] K. Abe *et al.* [Belle Collaboration], arXiv:hep-ex/0310029.
- [336] Belle Collaboration, Y. Enari, “Search for the lepton-flavor-violating  $\tau^- \rightarrow \mu^- \eta$  decay at Belle”, Contributed paper for 2003 summer conference, BELLE-CONF-0330.
- [337] Y. Yusa, H. Hayashii, T. Nagamine and A. Yamaguchi [BELLE Collaboration], eConf **C0209101**, TU13 (2002) [Nucl. Phys. Proc. Suppl. **123**, 95 (2003)] [arXiv:hep-ex/0211017].
- [338] T. Affolder *et al.* [CDF Collaboration], “Search for neutral supersymmetric Higgs bosons in  $p\bar{p}$  collisions at  $\sqrt{s} = 1.8$  TeV,” Phys. Rev. Lett. **86**, 4472 (2001) [arXiv:hep-ex/0010052].
- [339] A. F. Falk, Y. Grossman, Z. Ligeti and A. A. Petrov, “SU(3) breaking and  $D^0 - \bar{D}^0$  mixing,” Phys. Rev. D **65**, 054034 (2002) [arXiv:hep-ph/0110317].
- [340] R. Godang *et al.* [CLEO Collaboration], “Search for  $D^0 - \bar{D}^0$  mixing,” Phys. Rev. Lett. **84**, 5038 (2000) [arXiv:hep-ex/0001060].
- [341] G. Blaylock, A. Seiden and Y. Nir, “The Role of CP violation in  $D^0 - \bar{D}^0$  mixing,” Phys. Lett. B **355**, 555 (1995) [arXiv:hep-ph/9504306].

- [342] S. Bergmann, Y. Grossman, Z. Ligeti, Y. Nir and A. A. Petrov, “Lessons from CLEO and FOCUS measurements of  $D^0 - \bar{D}^0$  mixing parameters,” Phys. Lett. B **486**, 418 (2000) [arXiv:hep-ph/0005181].
- [343] M. Gronau, Y. Grossman and J. L. Rosner, “Measuring  $D^0 - \bar{D}^0$  mixing and relative strong phases at a charm factory,” Phys. Lett. B **508**, 37 (2001) [arXiv:hep-ph/0103110].
- [344] E. Golowich and S. Pakvasa, “Phenomenological issues in the determination of  $\Delta(\Gamma(D))$ ,” Phys. Lett. B **505**, 94 (2001) [arXiv:hep-ph/0102068].
- [345] L. Wolfenstein, “CP violation in  $D^0 - \bar{D}^0$  mixing,” Phys. Rev. Lett. **75**, 2460 (1995) [arXiv:hep-ph/9505285].
- [346] G. Burdman, E. Golowich, J. Hewett and S. Pakvasa, “Rare charm decays in the standard model and beyond,” Phys. Rev. D **66**, 014009 (2002) [arXiv:hep-ph/0112235].
- [347] G. P. Zeller *et al.* [NuTeV Collaboration], “A precise determination of electroweak parameters in neutrino nucleon scattering,” Phys. Rev. Lett. **88**, 091802 (2002) [Erratum-ibid. **90**, 239902 (2003)] [arXiv:hep-ex/0110059].
- [348] M. J. Ramsey-Musolf, “Low-energy parity violation and new physics,” Phys. Rev. C **60**, 015501 (1999) [arXiv:hep-ph/9903264].
- [349] C. S. Wood, S. C. Bennett, D. Cho, B. P. Masterson, J. L. Roberts, C. E. Tanner and C. E. Wieman, “Measurement Of Parity Nonconservation And An Anapole Moment In Cesium,” Science **275**, 1759 (1997).
- [350] R. Marshall, “A Determination Of  $\sin^2 \Theta_W$  And The Lepton And Quark Electroweak Couplings From  $e^+e^-$  Data,” Z. Phys. C **43**, 607 (1989).
- [351] S. K. Choi *et al.* [BELLE collaboration], “Observation of the  $\eta_c(2S)$  in exclusive  $B \rightarrow KK_S K^- \pi^+$  decays,” Phys. Rev. Lett. **89**, 102001 (2002) [Erratum-ibid. **89**, 129901 (2002)] [arXiv:hep-ex/0206002].
- [352] K. Abe *et al.* [Belle Collaboration], “Observation of double  $c\bar{c}$  production in  $e^+e^-$  annihilation at  $\sqrt{s} \simeq 10.6$  GeV,” Phys. Rev. Lett. **89**, 142001 (2002) [arXiv:hep-ex/0205104].
- [353] K. Abe *et al.* [Belle Collaboration], “Comment on ‘ $e^+e^-$  annihilation into  $J/\psi + J/\psi$ ,’” arXiv:hep-ex/0306015.
- [354] B. Aubert *et al.* [BABAR Collaboration], “Measurements of the mass and width of the  $\eta_c$  meson and of an  $\eta_c(2S)$  candidate,” arXiv:hep-ex/0311038.
- [355] D. M. Asner *et al.* [CLEO Collaboration], “Observation of  $\eta'_c$  production in  $\gamma\gamma$  fusion at CLEO,” arXiv:hep-ex/0312058.
- [356] C. Edwards *et al.*, “Observation Of An  $\eta'_c$  Candidate State With Mass  $3592 \text{ MeV} \pm 5 \text{ MeV}$ ,” Phys. Rev. Lett. **48**, 70 (1982).
- [357] W. Buchmuller and S. H. H. Tye, “Quarkonia And Quantum Chromodynamics,” Phys. Rev. D **24**, 132 (1981).
- [358] T. A. Lahde and D. O. Riska, “Pion rescattering in two-pion decay of heavy quarkonia,” Nucl. Phys. A **707**, 425 (2002) [arXiv:hep-ph/0112131].

- [359] S. K. Choi *et al.* [Belle Collaboration], “Observation of a new narrow charmonium state in exclusive  $B^\pm \rightarrow K^\pm \pi^+ \pi^- J/\psi$  decays,” *Phys. Rev. Lett.* **91**, 262001 (2003) [arXiv:hep-ex/0309032].
- [360] M. B. Voloshin and L. B. Okun, “Hadron Molecules And Charmonium Atom,” *JETP Lett.* **23**, 333 (1976) [*Pisma Zh. Eksp. Teor. Fiz.* **23**, 369 (1976)].
- [361] A. De Rujula, H. Georgi and S. L. Glashow, “Molecular Charmonium: A New Spectroscopy?,” *Phys. Rev. Lett.* **38**, 317 (1977).
- [362] N. A. Tornqvist, “From The Deuteron To Deusons, An Analysis Of Deuteron - Like Meson Meson Bound States,” *Z. Phys. C* **61**, 525 (1994) [arXiv:hep-ph/9310247].
- [363] V. V. Kiselev, A. K. Likhoded and M. V. Shevlyagin, “Double charmed baryon production at B factory,” *Phys. Lett. B* **332**, 411 (1994) [arXiv:hep-ph/9408407].
- [364] G. T. Bodwin, J. Lee and E. Braaten, “Exclusive double-charmonium production from  $e^+e^-$  annihilation into two virtual photons,” *Phys. Rev. D* **67**, 054023 (2003) [arXiv:hep-ph/0212352].
- [365] G. T. Bodwin, “Inclusive quarkonium production and the NRQCD-factorization approach,” arXiv:hep-ph/0312173.
- [366] D. Acosta *et al.* [CDF II Collaboration], “Observation of the narrow state  $X(3872) \rightarrow J/\psi \pi^+ \pi^-$  in  $\bar{p}p$  collisions at  $\sqrt{s} = 1.96$  TeV,” arXiv:hep-ex/0312021.
- [367] M. B. Voloshin, “Interference and binding effects in decays of possible molecular component of  $X(3872)$ ,” *Phys. Lett. B* **579**, 316 (2004) [arXiv:hep-ph/0309307].
- [368] E. S. Swanson, “Short range structure in the  $X(3872)$ ,” arXiv:hep-ph/0311229.
- [369] T. A. Armstrong *et al.*, “Observation of the p wave singlet state of charmonium,” *Phys. Rev. Lett.* **69**, 2337 (1992).
- [370] A. Tomaradze, Talk presented at Hadron 2001, Prodvino, Russia, Aug. 25 - Sept. 1, 2001.
- [371] M. Suzuki, “Search of  $^1P_1$  charmonium in  $B$  decay,” *Phys. Rev. D* **66**, 037503 (2002) [arXiv:hep-ph/0204043].
- [372] K. Abe *et al.* [Belle Collaboration], “Observation of  $\chi_{c2}$  production in  $B$  meson decay,” *Phys. Rev. Lett.* **89**, 011803 (2002) [arXiv:hep-ex/0202028].
- [373] D. Besson *et al.* [CLEO Collaboration], “Observation Of New Structure In The  $e^+e^-$  Annihilation Cross-Section Above  $B\bar{B}$  Threshold,” *Phys. Rev. Lett.* **54**, 381 (1985).
- [374] D. M. J. Lovelock *et al.*, “Masses, Widths, And Leptonic Widths Of The Higher Upsilon Resonances,” *Phys. Rev. Lett.* **54**, 377 (1985).
- [375] J. Lee-Franzini *et al.*, “Hyperfine Splitting Of  $B$  Mesons And  $B_s$  Production At The  $\Upsilon(5s)$ ,” *Phys. Rev. Lett.* **65**, 2947 (1990).
- [376] U. Egede, Physics at LHCb, Second workshop on the discovery potential of an asymmetric B factory at  $10^{36}$  luminosity, SLAC, Stanford, October 22-24, 2003.

- [377] L. Moroni [BTeV Collaboration], “BTeV: Strategy and sensitivity,” eConf **C0304052**, FO004 (2003) [arXiv:hep-ph/0307157].
- [378] M. Beneke, G. Buchalla and I. Dunietz, “Width Difference in the  $B_s - \bar{B}_s$  System,” Phys. Rev. D **54**, 4419 (1996) [arXiv:hep-ph/9605259].
- [379] K. Hartkorn and H. G. Moser, “A New Method Of Measuring  $\Delta\Gamma/\Gamma$  In The  $B_S^0 - \bar{B}_S^0$  System,” Eur. Phys. J. C **8**, 381 (1999).
- [380] R. Barate *et al.* [ALEPH Collaboration], “A study of the decay width difference in the  $B_s^0 - \bar{B}_s^0$  system using  $\phi\phi$  correlations,” Phys. Lett. B **486**, 286 (2000).
- [381] M. Beneke, G. Buchalla, C. Greub, A. Lenz and U. Nierste, “Next-to-leading order QCD corrections to the lifetime difference of  $B_s$  mesons,” Phys. Lett. B **459**, 631 (1999) [arXiv:hep-ph/9808385].
- [382] M. Ciuchini, E. Franco, V. Lubicz, F. Mescia and C. Tarantino, JHEP **0308**, 031 (2003) [arXiv:hep-ph/0308029].
- [383] S. Hashimoto, K. I. Ishikawa, T. Onogi and N. Yamada, “Width difference in the  $B_s - \bar{B}_s$  system with lattice NRQCD,” Phys. Rev. D **62**, 034504 (2000) [arXiv:hep-ph/9912318].
- [384] S. Hashimoto, K. I. Ishikawa, T. Onogi, M. Sakamoto, N. Tsutsui and N. Yamada, “Renormalization of the  $\Delta B = 2$  four-quark operators in lattice NRQCD,” Phys. Rev. D **62**, 114502 (2000) [arXiv:hep-lat/0004022].
- [385] D. Becirevic, D. Meloni, A. Retico, V. Gimenez, V. Lubicz and G. Martinelli, “A theoretical prediction of the  $B_s$  meson lifetime difference,” Eur. Phys. J. C **18**, 157 (2000) [arXiv:hep-ph/0006135].
- [386] J. Flynn and C. J. D. Lin, “ $B_s^0\bar{B}_s^0$  mixing and  $b$  hadron lifetimes from lattice QCD,” J. Phys. G **27**, 1245 (2001) [arXiv:hep-ph/0012154].
- [387] S. Aoki *et al.* [JLQCD Collaboration], “ $B^0 - \bar{B}^0$  mixing in quenched lattice QCD. ((U)) ((W)),” Phys. Rev. D **67**, 014506 (2003) [arXiv:hep-lat/0208038].
- [388] M. Beneke and A. Lenz, “Lifetime difference of  $B_s$  mesons: Theory status,” J. Phys. G **27**, 1219 (2001) [arXiv:hep-ph/0012222].
- [389] J. f. Sun, G. h. Zhu and D. s. Du, “Phenomenological analysis of charmless decays  $B_s \rightarrow PP, PV$  with QCD factorization. ((U)),” Phys. Rev. D **68**, 054003 (2003) [arXiv:hep-ph/0211154].
- [390] Round table discussions at 19th International Workshop on Weak Interactions and Neutrinos (WIN03), Oct. 6-11, 2003, Lake Geneva, Wisconsin, USA, <http://conferences.fnal.gov/win03/Talks/CKM/SecIX+X/ROUNDTABLE.doc>.
- [391] T. Nakada, talk given at the 5th workshop on higher luminosity  $B$  factory, Sep. 24-26, 2003, Izu, Japan, <http://belle.kek.jp/superb/workshop/2003/HL05/slide/H/Nakada.ppt>.
- [392] R. Forty, talk given at Eighth workshop on high energy physics phenomenology (WHEPP-8), January 5-16, 2004, Bombay, India, <http://lhcb-doc.web.cern.ch/lhcb-doc/presentations/conferencetalks/postscript/2004presentations/FortyBombay04.ppt>.

- [393] T. Moroi, “Effects of the right-handed neutrinos on  $\Delta S = 2$  and  $\Delta B = 2$  processes in supersymmetric SU(5) model,” JHEP **0003**, 019 (2000) [arXiv:hep-ph/0002208].
- [394] J. M. Soares and L. Wolfenstein, “CP violation in the decays  $B^0 \rightarrow \psi K_S$  and  $B^0 \rightarrow \pi^+ \pi^-$ : A Probe for new physics,” Phys. Rev. D **47**, 1021 (1993).
- [395] T. Goto, N. Kitazawa, Y. Okada and M. Tanaka, “Model independent analysis of  $B - \bar{B}$  mixing and CP violation in  $B$  decays,” Phys. Rev. D **53**, 6662 (1996) [arXiv:hep-ph/9506311].
- [396] R. N. Cahn and M. P. Worah, “Constraining the CKM parameters using CP violation in semi-leptonic B decays,” Phys. Rev. D **60**, 076006 (1999) [arXiv:hep-ph/9904480].
- [397] D. M. Asner *et al.* [CLEO Collaboration], “Search for CP violation in  $D^0 \rightarrow K_S^0 \pi^+ \pi^-$ ,” arXiv:hep-ex/0311033.
- [398] F. J. Ronga, “Advances in  $\Delta m_d$  measurements,” eConf **C0304052**, WG210 (2003) [arXiv:hep-ex/0306061].